



HAL
open science

Study of the application of pulsed electric fields (PEF) on microalgae for the extraction of neutral lipids.

Pierre Bodenes

► **To cite this version:**

Pierre Bodenes. Study of the application of pulsed electric fields (PEF) on microalgae for the extraction of neutral lipids.. Physics [physics]. Université Paris Saclay (COmUE), 2017. English. NNT : 2017SACLN017 . tel-01540436

HAL Id: tel-01540436

<https://theses.hal.science/tel-01540436v1>

Submitted on 16 Jun 2017

HAL is a multi-disciplinary open access archive for the deposit and dissemination of scientific research documents, whether they are published or not. The documents may come from teaching and research institutions in France or abroad, or from public or private research centers.

L'archive ouverte pluridisciplinaire **HAL**, est destinée au dépôt et à la diffusion de documents scientifiques de niveau recherche, publiés ou non, émanant des établissements d'enseignement et de recherche français ou étrangers, des laboratoires publics ou privés.

2017SACLN017



CentraleSupélec

THESE DE DOCTORAT
DE
L'UNIVERSITE PARIS-SACLAY
PREPAREE À
L'ECOLE NORMALE SUPERIEURE DE CACHAN
(ECOLE NORMALE SUPERIEURE PARIS-SACLAY)

ECOLE DOCTORALE N° (575)
ELECTRICAL, OPTICAL, BIO-PHYSICS AND ENGINEERING

Spécialité de doctorat : Physique

Par

Mr Pierre Bodénès

Etude de l'application de champs électriques pulsés sur des microalgues en vue de
l'extraction de lipides neutres

Thèse présentée et soutenue à Cachan, le mercredi 10 Mai 2017 :

Composition du Jury :

Mme Marie-Pierre Rols	Directeur de recherche, IPBS, Toulouse	Rapporteur
Mr Luc Marchal	Maître de conférences, GEPEA, Université de Nantes	Rapporteur
Mme Elisabeth Dufour-Gergam	Professeur des Universités, C2N, Université Paris Sud	Présidente du Jury
Mme Filipa Lopes	Maître de conférences, LGPM, CentraleSupélec	Encadrante
Mr Olivier Français	Professeur, ESIEE Paris	Encadrant
Mr Bruno Le Pioufle	Professeur des Universités, SATIE, ENS Paris Saclay	Directeur de thèse
Mme Dominique Pareau	Professeur émérite, LGPM, CentraleSupélec	Co-directrice (invitée)

Sommaire général – Summary

Preface

Remerciements – Acknowledgments	7
Résumé du travail de thèse	12
Introduction.....	12
Matériel et méthodes.....	13
Résultats et perspectives.....	15
Thesis outline (objectif et plan)	22

Chapter 1: The future of algae-derived biodiesel

I. Global outlook on energy supply and demand	28
II. Review on crude oil production and future alternative	29
III. Current biofuel production and future technologies	32
IV. From algae culture to oil harvesting. Review of existing technologies and constraints	37
V. Key points for future viability of algae-derived biodiesel	53
Chapter 1 conclusion	60
Chapter 1 references	62

Chapter 2: Inducing lipid accumulation in green microalgae and developing characterization methods

Chapter 2: Introduction	75
I. Morphology, composition and metabolism of green micro-algae	76
I.1) Cell structure	76
I.2) Respiration activity.....	80
I.3) Photosynthetic activity.....	81
II. Lipid biosynthesis and composition	85
II.1) Lipid synthesis in microalgae: from light to TAGs	85
II.2) Lipid classes	87

II.3) Culture conditions and cell composition	90
III. Review of analytical methods	95
III.1) Biomass growth	95
III.2) Lipid content	99
III.3) Cell size	107
IV. Procedure to induce lipid accumulation developed in this work	108
V. Development and validation of the methods	111
VI. Results	118
VI.1) Biomass growth	119
VI.2) Chlorophyll content	121
VI.3) Dry weight (stress condition)	123
VI.4) Lipid content	125
VI.5) Monitoring cell size	135
Chapter 2: conclusion	137
Chapter 2: references	139

Chapter 3: The use of Pulsed Electric Fields for the extraction of lipids from *Chlamydomonas reinhardtii*: study in microdevice and electroporation cuvettes

Chapter 3: Introduction	165
I. State of the art	166
I.1) Principle and interests of Pulsed Electric Field (PEF)	166
I.2) Use of PEF in biotechnology.....	175
I.3) Use of bio-micro-devices to monitor algae cells <i>in situ</i>	178
II. Material and methods	181
II.1) Micro-device for studying the <i>in situ</i> permeabilization and characterization of <i>Chlamydomonas reinhardtii</i>	181
II.2) Electroporation in cuvettes.....	183
II.3) Viability/permeability measurements.....	184
II.4) Measurement of lipid extraction with/without PEF	196
III. Results.....	200

III.1) Electroporation in the micro-device	200
III.2) Electroporation in cuvettes	209
III.2) Association of PEF to solvent for lipid extraction	216
Chapter 3: conclusions	224
Chapter 3: references	226

Discussion

Discussion	235
------------------	------------

Abstract / Résumé

Remerciements – Acknowledgments

Je tiens tout d'abord à remercier les structures d'accueil qui ont permis à cette thèse pluridisciplinaire de se réaliser dans des conditions remarquables. Je remercie donc Pascal Larzabal, directeur du laboratoire SATIE (Systèmes et Applications des Technologies de l'Information et de l'Energie) pour ces entrevues toujours très chaleureuses et son accueil dans ce laboratoire de l'ENS Cachan. Je remercie également Patrick Perré pour m'avoir permis de réaliser une grande partie de mon travail au sein du laboratoire LGPM (Laboratoire de Génie des Procédés et Matériaux) de l'école CentraleSupélec. Enfin, je remercie également Eric Deprez, directeur de l'institut d'Alembert, l'entité pluridisciplinaire de l'ENS Cachan où de multiples équipes de recherche variées se côtoient et profitent de l'équipement mis à disposition par l'institut. Je ne peux que remercier l'ENS Cachan pour l'attribution de cette bourse de thèse en 2013. Les bourses IDA ont été un gros coup de pouce également pour acheter l'équipement nécessaire lors de cette thèse. Enfin les bourses Labex LaSIPS ont également été d'une grande aide, en effet les recherches expérimentales sont très coûteuses en matériel et consommables ! Enfin, un contrat CNRS m'a donné quelques mois de plus pour prolonger légèrement mon contrat doctoral et réaliser des expériences supplémentaires présentées dans le chapitre 3 de ce manuscrit. Trois ans c'est malheureusement extrêmement court lorsque le projet nécessite la mise en place du matériel et des méthodes expérimentales et analytiques.

Je ne peux que remercier le personnel administratif des structures citées précédemment : Sophie Abriet, Aurore Gracia, Béatrice Bacquet, Gaëlle Callouard, Marjolaine Vernier, Brigitte Dudon, Véronique Mathet, Catherine Kruch et Sandra Julien-Anchier. Je sais que les doctorants qui sont sur plusieurs sites donnent beaucoup de fil à retordre d'un point de vue administratif... et ce n'est pas encore fini pour moi. Je remercie également le personnel administratif qui m'a suivi au cours de ce cursus universitaire, à l'école doctorale administrative (EDSP ENS Cachan) ou scientifique (ED EOBE Université Paris Saclay) : Christine Rose, Sophie Garus, Laurence Stephen, et finalement Eric Cassan, le directeur de mon école doctorale.

Je n'aurais jamais eu ce goût prononcé pour la biotechnologie des microalgues sans les enseignements sur cette thématique à Saint Nazaire, je pense notamment à Jeremy Pruvost et son cours sur les photo-bioréacteurs, qui mine de rien a lancé plusieurs vocations (les personnes visées se reconnaîtront) ! Mes deux stages de 6 mois ont fortement contribué à accroître ma curiosité scientifique et à donner du sens à toutes ces années d'études. Je remercie donc grandement le docteur Stéphane Le Floch, et Matthieu Dussauze pour la transmission de leur expertise dans le domaine de l'écotoxicologie marine. Que de bons moments à pêcher des crevettes pour nos expériences ! Finally, I have earned an infinite quantity of knowledge in the bioprocess group of Wageningen University being supervised by Dirk Martens, Packo Lamers and Kim Mulders: so much things to learn from you whether in

your management or in the way you conduct your researchs. The quantity of interactions with this first generation of young algaeers have not fallen on deaf ears. I continue to read your publications with a big pleasure. Also I did my best to continue to improve my English and share my work to you by writing this manuscript in English.

Merci au personnel technique pour leur aide lors de la fabrication de pièces, la réparation d'éléments électriques, ou l'enregistrement d'images en microscopie : Etienne Henry, Thierry Martin, Cyril Breton, Joel Casalinho, Jean Trubuil, Patrice Vallade, Gerard Chaplier, Jeff Audibert et les toutes les autres personnes qui ont apporté leur pierre à l'édifice.

J'ai beaucoup apprécié les discussions que j'ai pu avoir avec tous les permanents, je pense notamment à Hervé Duval, avec qui nous avons pu partager nos goûts musicaux, Bertrand David, toujours là pour me donner des conseils, Moncef Stambouli, toujours très sympathique et Touhami Smaoui pour nos discussions variées. Sans oublier Jean-Pierre Lefevre qui a eu la malchance de se sentir petit trop régulièrement, mais avec qui j'ai appris beaucoup de choses sur des sujets variés. Je remercie également tout le personnel de SATIE et du LGPM qui ont enrichi mon savoir et adouci certaines journées difficiles.

Merci aux membres du jury de m'avoir fait l'honneur d'examiner et d'évaluer mon travail. C'est une chance d'avoir la possibilité d'avoir un retour sur ce travail complexe par des acteurs majeurs des disciplines approchées au cours de ce doctorat en Physique : Elisabeth Dufour-Gergam pour l'aspect micro-technologies, Marie-Pierre Rols pour son expérience sur l'étude de l'électroporation *in situ*, et Luc Marchal sur la thématique extraction de composés d'intérêts de microalgues.

J'exprime tous mes remerciements à Dominique Pareau, qui a eu le courage et la motivation d'encadrer officiellement une énième et peut-être sa dernière thèse après une longue et riche carrière scientifique. Je la remercie vivement pour son expérience et sa tempérance (l'arcane 14 du tarot de Marseille donne tout le sens que Dominique a pu apporter), et malgré tout elle a su garder une grande curiosité et un enthousiasme de jeunesse lorsque des résultats prometteurs se sont dévoilés.

Filipa Lopes a été d'une grande sagesse et s'est souvent fait l'avocat du diable pour canaliser ma curiosité et la diriger vers un travail rigoureux et le plus irréprochable possible. Nous avons pu avancer très vite dans l'exploration de méthodologies nouvelles et adaptés à nos conditions expérimentales. Je te remercie pour ton encadrement mais aussi tes efforts à faire vivre l'équipe bioprocédés en étant toujours à la recherche de financements : on y croit à cette ANR !

Je crois que je ne peux que faire un remerciement groupé à Olivier Français et Bruno Le Pioufle tant votre « duo » parait inséparable. Comme l'a déjà évoqué Olivier, notre première

rencontre dans la cafeteria de l'institut pour me présenter le sujet a été un moment de révélation, j'ai immédiatement eu envie de travailler avec vous et de découvrir vos recherches, et de vous partager mes connaissances et mon enthousiasme pour la biotechnologie des micro algues. A cette époque, Claudia Tranito et Ferial Hamdi étaient encore en thèse et j'ai pu être formé aux Bio-MEMS grâce à votre travail conjoint. C'était toujours un moment de bonheur d'aller au restaurant japonais tous ensemble et de commander les traditionnels oeufs de poulets, algues et même saké pour les grandes occasions. Enfin c'était un plaisir d'observer avec vous tout ce que l'on a fait subir à ces pauvres cellules pour leur faire cracher ces maudites gouttelettes !

I would like to thank Maria Antonia Correira and Madhumidha MURUGAN for their very harsh work during their respective 6 month internships. Your work was precious to help me at the intensive moments of my PhD, when I was struggling to develop the methodology using fluorescent dyes such as Bodipy and Nile Red. I hope that you have learnt the capacity to face the numerous difficulties of the experimental research, and I wish you the best in your future careers.

Après avoir parlé de Biomis et des étudiants en stage qui m'ont aidé, mes remerciements se tournent naturellement vers Sakina Bensalem, tu as eu la chance de prolonger ton aventure de stage vers la thèse pour le meilleur et pour le pire ! C'est un immense plaisir de partager ces nombreux moments avec toi que ce soit pour ton dynamisme, ta joie de vivre, et ta générosité. A deux on a parfois pu rendre les expériences bien plus joyeuses et efficaces... mais dans certains cas la joie l'a emporté sur l'efficacité ! Et je te souhaite le meilleur pour continuer cette recherche, sur des terrains de plus en plus innovants mais délicats à maîtriser.

Je remercie tous les doctorants et post-doctorants que j'ai croisé au sein des différentes structures... Je n'ai pas toujours eu le temps de bien tous vous connaître. Je voudrais saluer les nombreuses personnes qui ont partagé mon bureau : Hela, Vanessa, Claudia, Ferial, Li, Abdellatif, Yu-Sheng, Jean, Tieying, Timothée. Je voudrais saluer également Marine qui a aussi débuté sa thèse dans des conditions similaires au miennes, c'est-à-dire à cheval entre le laboratoire LGPM et l'institut d'Alembert, avec qui j'ai partagé cette aventure parfois difficile. Un merci à Cedric pour ses conseils avisés et son expérience pour les montages expérimentaux et l'utilisation de marqueurs fluorescents. Salutations également à Armelle, toujours de bonne humeur et bienveillante. J'adresse enfin ma gratitude envers Jordan, aka Dr No ou El Principe, pour les nombreux moments où nous avons confronté nos visions de la vie.

J'adresse finalement mes remerciements à mes amis qui me voient évoluer et grandir depuis plusieurs années. Comme vous pouvez le voir je peux me montrer un peu plus bavard à l'écrit qu'à l'oral comme l'atteste les nombreuses pages de ce manuscrit. Je remercie donc mes potes de Pen Bellec : Romain, Fred, Thomas. Je suis bien heureux que Plougastel démarre la production de microalgues. Je remercie mes amis d'IUT de Pontivy, Pierro, Coco, Val, Tutur,

les bledar du Galsen. Mes profs et amis de Saint Nazaire, notamment les surics que je revois régulièrement : Maruiie, Chatuss, Rombouv, DamsD, Denis&Quentin, et tous les autres qui me connaissent principalement sous le nom de GrandPierre. Un grand merci à Kenzui qui nous accueille toujours les bras ouverts à Saint Nazaire, et à Arnaud Artu pour toutes les aventures que nous continuons à partager tous ensemble.

J'adresse mes remerciements à ma famille. La famille de Traouidan : Philippe, Françoise, Gaël, Rozenn et Antoine. Toute la famille du Finistère Nord, du côté de ma mère. Un gros bisou à ma grande sœur Lucille qui a eu le courage de démarrer une carrière fantasque dans le milieu de la mode après un doctorat en chimie. Je ne peux que terminer ces remerciements en remerciant ma mère, Monique Bodénès, pour la force qu'elle au travers de son parcours de vie semé d'embuches, et pour sa générosité infinie envers ses proches.

Je voudrais enfin adresser un dernier au revoir à tous ceux qui nous ont quitté récemment : Jean Yves Kervella, qui pour moi fait partie de mon enfance avec qui nous avons visité les îles bretonnes sur le Salsa. Ma Grand-Mère, pleine de fantaisie et d'originalité, toujours très généreuse envers ses 5 petits-enfants. Et bien sûr mon père Jaques Bodénès qui a toujours clamé haut et fort sa malice, sa liberté, et qui a transmis à moi et ma sœur un certain goût pour la prise de risques et la volonté de sortir des sentiers battus. Je suis heureux qu'il puisse être fier du parcours de ses deux enfants.

Résumé du travail de thèse

Introduction

Les microalgues, tout comme les plantes supérieures, ont la capacité de fixer l'énergie lumineuse sous la forme de chaînes carbonées (sucre/huile) qui peuvent être ensuite converties par fermentation/transestérification en bioéthanol/biodiesel. Ces molécules bio-sourcées renouvelables ont le potentiel de se substituer aux molécules issues du pétrole, de plus en plus rares et onéreuses à extraire. La faisabilité technologique du procédé de culture de microalgues en bioréacteur solaire et d'extraction des lipides pour une valorisation en biodiesel a été démontrée ; cependant ses importants coûts (notamment énergétiques) l'empêchent pour l'instant d'être viable d'un point de vue économique, mais surtout d'un point de vue énergétique. L'utilisation industrielle des microalgues est donc aujourd'hui restreinte à la production de molécules à haute valeur ajoutée pour des applications nutraceutiques, cosmétiques, biomédicales.

Ce travail de thèse s'inscrit donc dans la problématique de réduction des coûts énergétiques d'un tel procédé, et en particulier de l'étape d'extraction des lipides des microalgues (plus particulièrement des lipides neutres, ciblés pour la production de biodiesel) ; le but est en effet de développer à terme un procédé industriel de production de biocarburant à rendement énergétique positif (énergie produite/énergie dépensée). Dans le cadre de cette thèse nous avons choisi d'étudier en particulier l'extraction de ces lipides piégés au sein du cytoplasme, par l'utilisation de champs électriques pulsés.

Pour la plupart des microalgues vertes (« chlorophytes »), les conditions de croissance en conditions phototrophes diffèrent des conditions entraînant une haute teneur en lipides intracellulaires. Ces dernières conditions sont généralement appelées « stress » puisqu'elles entraînent une réponse métabolique non optimale du point de vue de la croissance. En effet, en photo-autotrophie (régime de croissance associé à l'apport de lumière et de CO₂), l'apport de lumière devra être contrôlé de façon à éviter la photo-inhibition (excès de lumière) ou la photo-limitation (manque de lumière) ; de plus l'apport de nutriments (majoritairement N, P, K) permet une croissance très rapide. Lors du stress induisant l'accumulation de lipides, l'azote est absent du milieu de culture et la lumière est apportée en excès de façon à entraîner un déséquilibre énergétique au sein de la cellule : sans azote la cellule ne peut plus se diviser et le flux d'électrons vers cette voie métabolique est donc bloqué. Ce déséquilibre énergétique est dangereux pour la cellule et sa solution pour se maintenir en vie est de stocker en énergie carbonée sous forme de sucres ou de lipides non fonctionnels.

Les champs électriques pulsés (PEF, Pulsed Electric Fields en anglais) agissent par l'application répétée d'une différence de potentiel entre deux électrodes et entraînent un gradient ionique au sein du cytoplasme de la cellule ainsi que dans le milieu externe. Ce gradient augmente artificiellement le potentiel transmembranaire au niveau de la membrane cytoplasmique faisant face aux électrodes et se traduit par l'apparition de pores dans la bicouche lipidique de celle-ci. Selon les paramètres de traitement (principalement la durée des impulsions et l'amplitude du champ électrique appliqué), l'apparition de pores sous l'effet du champ électrique (électroporation) peut être irréversible (conduisant à la mort cellulaire) ou réversible (fermeture des pores après arrêt du champ électrique, permettant, en principe, le maintien de la viabilité). Les applications de ce traitement sont

nombreuses, notamment dans le domaine biomédical (traitement du cancer par lyse non thermique, insertion de molécules anti-cancéreuses) ou agroalimentaire (extraction de jus de fruit, stérilisation, etc...). C'est donc tout naturellement que ce procédé est envisagé ?? dans le cas des microalgues où l'étape d'extraction des composés d'intérêt est souvent réalisée par des procédés très énergivores et peu respectueux de l'environnement (centrifugation, broyage mécanique, utilisation de solvants toxiques...); il est donc important de trouver des alternatives et le procédé PEF semble très prometteur en ce sens.

Le projet s'inscrit dans le cadre d'une collaboration entre l'équipe BIOMIS (Bio-micro-systèmes) du Laboratoire des Systèmes et Applications des Technologies de l'Information et de l'Energie (SATIE ; UMR CNRS 8029) de l'ENS Paris Saclay et l'équipe Bioprocédés du Laboratoire Génie des Procédés et Matériaux (LGPM,EA 4038) de CentraleSupélec. Ce travail de thèse étant un projet nouveau pour les deux équipes (culture d'algues pour la production lipidique au sein du LGPM, étude de micro-algues en micro-systèmes au sein de SATIE), une partie importante du projet a été consacrée au développement de méthodes ainsi qu'à la mise en place d'outils de caractérisation des microalgues.

Matériel et méthodes

Un certain nombre de d'espèces de microalgues ont été étudiées afin de sélectionner la souche modèle pour ce travail. Dans le cas du procédé PEF, il est primordial d'utiliser une espèce d'eau douce afin de pouvoir traiter les cellules dans un milieu faiblement conducteur et ainsi réduire l'effet Joule. L'utilisation de *Chlorella vulgaris*, étudiée en premier lieu, a conduit à diverses difficultés expérimentales. Nous nous sommes ensuite tournés vers des espèces de taille plus importante qui sont plus sensibles à l'application d'un champ électrique (sensibilité proportionnelle au rayon selon l'équation de Schwan) et plus faciles à observer/caractériser à l'aide de la microscopie. Parmi plusieurs souches étudiées, ***Chlamydomonas reinhardtii* wild type a finalement été retenue** pour la majorité des essais ; sa souche mutante déficiente en paroi (cw15) a permis par comparaison d'évaluer l'effet de la paroi sur le niveau d'électroporation.

Il était ensuite important de pouvoir caractériser les cellules avant et après traitement PEF : leur nombre et leur état (taille, contenu en lipides, morphologie des gouttelettes de lipides, perméabilisation de la membrane, viabilité etc). **Des techniques de caractérisation ont été ainsi développées et optimisées.**

Une grande partie du suivi de la concentration cellulaire et de la caractérisation des cellules a été réalisée à l'aide de la cytométrie en flux permettant, notamment, des mesures plus rapides que le comptage cellulaire par cellule de Malassez; nous avons corrélé les résultats obtenus par les deux méthodes en phases de croissance et de stress des cellules.

Différents marqueurs fluorescents ont été également utilisés pour caractériser la viabilité cellulaire et permettre de visualiser les gouttelettes lipidiques et la paroi cellulaire : Bodipy marqueur spécifique aux lipides neutres, Concanavaleine marqueur de la paroi, Propidium Iodide (PI) et Sytox Green marqueurs de perméabilisation de la membrane, Fluorescein diacetate (FDA) marqueur d'activité enzymatique. Les conditions de marquage (quantité de marqueur vs biomasse, temps d'incubation...) ont été optimisées dans chaque cas. Des mesures d'autofluorescence ont permis de suivre les pigments photosynthétiques de la cellule (chlorophylle a/chlorophylle b).

Les cellules marquées ont été également observées à l'aide de la microscopie à épifluorescence (équipé d'une caméra à haute sensibilité photonique) ou de la microscopie confocale (Confocal Laser Scanning Microscopy). Les paramètres d'acquisition des images ont été optimisés.

L'imagerie confocale permet notamment de réaliser un scan en 3 dimensions d'une cellule et d'estimer la taille des gouttelettes de lipides, leur nombre par cellule ainsi que leur volume après une reconstruction 3D (avec déconvolution permettant de corriger les déformations de l'image).

Le marquage conjoint de la cellule par la Concanavoline et le Bodipy permet d'observer en microscopie confocale les gouttelettes de lipides et la paroi cellulaire. Les pigments sont également visualisés par autofluorescence. Cependant cette observation se fait à l'échelle de la cellule ; le résultat n'est pas extrapolable à l'ensemble de la population cellulaire, la morphologie cellulaire et le contenu lipidique étant très disparates chez des cellules en stress.

L'intensité moyenne de fluorescence par cellule marquée au Bodipy peut par contre être mesurée en cytométrie en flux. L'appareil mesure l'intensité émise par chaque cellule et estime ensuite la moyenne de l'échantillon analysé (1000 - 5000 cellules). Etant donné la qualité des images acquises qui montrent une affinité très spécifique du Bodipy avec les lipides neutres, l'idée de faire de cette technique une méthode d'analyse quantitative des lipides a été testée (voir ci-dessous).

Pour évaluer la viabilité et la perméabilité de la membrane, les cellules sont marquées et leur fluorescence mesurée : vert pour la FDA (indicateur d'activité enzymatique, donc de viabilité) et jaune pour le sytox green (indicateur de perméabilité). Au dessus d'un certain seuil de fluorescence la cellule est comptée comme marquée et l'appareil calcule la proportion de cellules marquées, donnant pour la FDA le taux de viabilité et pour le SG ou le PI le pourcentage de cellules perméabilisées.

En ce qui concerne la taille des cellules, nous avons testé deux méthodes permettant de déterminer leur diamètre : une estimation directe par microscopie et une mesure par granulométrie laser. La mesure par granulométrie laser est extrêmement sensible aux paramètres optiques des particules analysées, ce qui complique l'interprétation des résultats et les rend sujets à caution, à moins d'une étude exhaustive très longue de mise au point que nous n'avons pas réalisée. Nous avons donc préféré les mesures directes par microscopie qui sont fiables.

L'analyse des lipides a été bien sûr un point important de notre travail.

Les méthodes classiques de mesure des lipides sont la méthode gravimétrique (extraction des lipides totaux par chloroforme/méthanol, puis pesée du résidu après évaporation) et ? la chromatographie gazeuse ; cependant elles nécessitent une quantité assez importante de biomasse (plusieurs milligrammes d'algues sèches par analyse) et sont incompatibles avec l'échelle de nos essais. Nous avons donc testé deux autres méthodes ne nécessitant que des quantités faibles de biomasse (quelques millions de cellule dans 100 µL).

Dans un premier temps nous avons réalisé des essais afin de vérifier si la méthode de marquage au Bodipy (et mesure de la fluorescence par cytométrie à flux) pouvait être utilisée pour quantifier les lipides neutres. Nous avons en particulier étudié l'influence de la quantité de Bodipy (rapport bodipy/cellule) utilisée et de la présence ou non d'un lavage à la suite du marquage ; les résultats en terme d'intensité moyenne de fluorescence sont extrêmement sensibles au rapport lipides/Bodipy et

au lavage. Mais le plus préjudiciable est que, malgré une optimisation du protocole, la perméabilité de la membrane, étant fortement modifiée suite à un traitement PEF, influence le marquage, toutes choses égales par ailleurs ; en effet à quantités de lipides égales, un traitement des cellules par PEF peut augmenter d'un facteur deux l'intensité de fluorescence des cellules par rapport aux cellules non traitées. Cette technique n'est pas donc utilisable pour quantifier précisément les lipides neutres dans nos conditions de travail. Des résultats montrent de plus qu'il n'est pas possible de corrélérer de manière fiable l'intensité moyenne de fluorescence associée au Bodipy avec la quantité de lipides neutres intracellulaires, mesurée par chromatographie gazeuse (mesure faite par un laboratoire externe). Il n'en reste pas moins que cette méthode peut être un outil intéressant et rapide d'estimation qualitative des lipides.

Nous avons finalement employé une méthode colorimétrique dite SPV (Sulpho-Phospho-Vanillin)). Les réactifs chimiques employés réagissent avec les acides gras insaturés des lipides neutres, mais aussi polaires (lipides membranaires). Cette méthode doit donc être utilisée avec précaution pour quantifier les lipides neutres ; elle nécessite en effet d'effectuer des corrélations préalables entre l'absorbance obtenue et les quantités de lipides neutres et polaires, mesurées par ailleurs par chromatographie gazeuse. Elle semble également pouvoir être employée directement sur des phases solvant contenant des lipides extraits, ce qui est un autre avantage. Même si elle est imparfaite en absolu, elle a été utilisée pour comparer les teneurs en lipides des microalgues avant et après traitements (PEF et/ou solvant). Les résultats sont présentés en équivalents trioléine, le lipide témoin employé dans cette étude, et il a été vérifié que ces résultats étaient du même ordre de grandeur que ceux obtenus par chromatographie gazeuse.

Après la mise au point des diverses méthodes d'analyse et caractérisation, **nous avons étudié et optimisé le procédé de culture des cellules en deux phases** : une phase de croissance et une phase d'accumulation des lipides.

Dans un premier temps les microalgues ont été cultivées dans des conditions propices à leur croissance afin d'obtenir une biomasse relativement concentrée. Ensuite les conditions ont été changées lors de la deuxième phase afin que les cellules accumulent des lipides. La mise en place de ces deux phases a nécessité une optimisation des conditions : principalement l'apport de lumière, la durée des phases et la concentration cellulaire au sein des cultures au cours des deux phases. Pour ce faire nous avons suivi **la concentration cellulaire et caractérisé les cellules** en termes de teneur en lipides des cellules, viabilité et perméabilité de la membrane et taille des cellules.

Résultats et perspectives

Nous avons pu mesurer une très forte réduction de l'autofluorescence associée à des pigments cellulaires (chlorophylle) chez *Chlamydomonas reinhardtii* en période de stress par rapport à la phase de croissance. Il s'agit d'une réaction de la cellule en réponse au stress azoté.

La durée de la deuxième phase (stress) à la fin de laquelle le traitement d'extraction de lipides doit être effectuée a été choisie ensuite de façon à maximiser la productivité en lipides.

Les résultats ont montré que le contenu lipidique des cellules atteint un maximum après 4 à 7 jours de stress ; nous avons donc choisi une durée de 7 jours pour la durée du stress azoté. A l'issue de cette phase, les teneurs en lipides ont été estimées ; nous avons trouvé 39 pg/cellule en équivalent trioléin (SPV, acides gras insaturés) et 27 pg/cellule en lipides neutres (chromatographie). La teneur en lipides neutres des cellules peut cependant varier selon les cultures ; les cellules de certaines d'entre elles continuent à croître en début de stress et accumulent donc moins de lipides, ceci associé à une dilution des photons compte tenu d'un phénomène de photo-ombrage lié à une forte densité cellulaire.

Par ailleurs, à 7 jours de stress azoté, le taux de perméabilité membranaire est inférieur à 5 % et le taux de viabilité est de l'ordre de 90 à 95% : les cellules sont donc en excellent état à ce moment. Par contre, leur viabilité se dégrade significativement si la période de stress est prolongée au delà de 7 jours.

Enfin les cellules grossissent en période de stress par suite de l'accumulation de lipides ; elles restent ovoïdales, mais leur dimension maximale moyenne passe de 7 μm en phase de croissance à 10 μm en phase de stress. Cette différence de taille indiquerait que les cellules seraient légèrement plus sensibles au traitement électrique en phase de stress.

Le système de traitement PEF a ensuite été développé. Les impulsions électriques ont tout d'abord été produites avec un générateur électrique de paillasse couplé à un amplificateur ; les cellules étaient observées au microscope optique. L'emploi d'un marqueur fluorescent de perméabilisation membranaire tel que PI ou SG a ensuite permis d'évaluer l'effet des champs électriques sur les cellules avec le microscope à épifluorescence.

Un générateur d'impulsions bipolaires a été acquis au cours du projet afin de pouvoir réaliser une étude des paramètres sur une large gamme de temps d'impulsions (temps de pulse minimal théorique, 1 μs) et de champs électriques (impulsions bipolaires de $-1\,000\text{ V}$ à $+1\,000\text{ V}$). **Un microsystème** comportant un grand nombre de chambres parallèles permettant de piéger des cellules de microalgues (environ 30 - 150 cellules par chambre) dans un réseau d'électrodes en or, **couplé à la microscopie** a été conçu et réalisé en salle blanche ; il permet de plus de caractériser les effets des PEF sur des populations d'algues relativement importantes afin d'en déduire des comportements globaux. La distance réduite entre les électrodes a permis de pouvoir appliquer un champ électrique très élevé, jusqu'à 50 kV/cm.

Ce dispositif optimisé a permis ensuite de réaliser une première étude sur la consommation d'énergie du traitement PEF mettant en lumière le lien crucial entre la durée des impulsions et l'intensité du champ électrique. Cette relation est connue dans le domaine de l'électroporation, mais de manière empirique ; en effet aucune équation théorique ne permet de faire le lien entre le temps d'impulsion et le champ électrique. **Nos résultats ont montré que pour un même taux de perméabilisation des cellules, la dépense énergétique du traitement est réduite lors de l'utilisation d'impulsions courtes couplées à un champ électrique élevé.** En effet, par exemple pour perméabiliser 50 % des cellules de *Chlamydomonas reinhardtii wt* en phase d'accumulation de lipides, un traitement avec des impulsions de 5 μs et un champ électrique de 3,56 kV/cm résulte en une dépense énergétique 10 fois plus faible que celle d'un traitement avec des impulsions de 500 μs et un champ électrique de 1,12 kV/cm. Par ailleurs, l'utilisation d'impulsions très courtes, de quelques micro-secondes, permet également de **limiter l'échauffement thermique réduisant ainsi la dégradation des molécules lipidiques ;**

l'échauffement est même négligeable dans nos essais car la température dans la chambre d'électroporation retombe à son niveau initial entre chaque impulsion (durée entre chaque impulsion : 100 ms) grâce à la diffusion thermique vers l'extérieur de la chambre.

En parallèle de ces aspects purement énergétiques, **nous avons étudié l'effet des PEF sur les cellules**. Plusieurs **effets ont pu être observés *in situ* et en temps** réel grâce à l'utilisation de la microscopie d'épifluorescence couplée à une caméra permettant d'enregistrer des effets dynamiques avec une haute résolution.

En premier lieu la **pénétration du marqueur fluorescent PI dans des cellules a été observée *in situ***. Les résultats ont montré **que le traitement par champ électriques pulsés seul ne permet pas d'extraire l'huile des cellules** quelles que soient les conditions utilisées, même les plus énergétiques. **Ce résultat important prouve que la membrane n'est pas la seule barrière à l'extraction de l'huile, la paroi jouant également un rôle majeur dans le maintien de la structure cellulaire**, sur laquelle le traitement PEF à effet thermique réduit a peu d'effets. De plus le caractère hydrophobe des lipides neutres peut freiner leur transfert vers l'extérieur hydrophile de la cellule. **Le procédé par champs électriques pulsés peut donc être utilisé comme pré-traitement de la biomasse algale, associé par exemple à l'extraction par solvant. Un autre résultat très intéressant démontre une coalescence des gouttelettes de lipides à l'intérieur de la cellule (traitement électrique appliqué de 5 μ s, 6 kV/cm). Les PEF ont donc des effets intracellulaires, en plus de la perméabilisation membranaire. Ces observations de coalescence en direct des gouttelettes de lipides sont totalement inédites dans la communauté de l'électroporation.**

Troisièmement des essais avec la souche mutante *Chlamydomonas reinhardtii* cw15 qui a une paroi beaucoup plus fine ont montré une lyse des cellules après traitement, résultant en un déversement du contenu intracellulaire dans le milieu. La résistance mécanique de la paroi de la souche mutante ne permet donc pas de maintenir l'intégrité cellulaire, au contraire de la souche non mutée (wild type). **Ces résultats montrent bien l'effet important de la paroi et ont donné lieu à un premier article publié dans le journal Algal Research (Juin 2016).**

Après les deux premières phases décrites précédemment que sont le développement des techniques de culture et de caractérisation des algues et le développement du microsystème PEF dédié, **des essais d'électroporation à une échelle supérieure à celle du microsystème** (en microcuvettes) ont été réalisés de façon à mieux comprendre les mécanismes d'électroporation et à quantifier l'impact des PEF sur l'extraction des lipides.

Les conditions de champ entraînant les deux types de perméabilisation (réversible ou irréversible) ont été déterminées grâce à un marquage conjoint FDA et SG pour des durées d'impulsions de 5, 50 et 500 μ s. On retrouve les limites correspondant à la perméabilisation réversible que nous avons déterminées au préalable dans le microsystème. Il a été nécessaire d'ajouter le marqueur à différents moments pour atteindre les deux types de perméabilisation. Le marqueur est ajouté pendant le traitement d'électroporation et les cellules marquées correspondent alors aux deux types de perméabilisation. Si le marqueur est mis en contact avec les cellules 1h après traitement, il ne peut pénétrer que dans les cellules perméabilisées de façon irréversible. Les champs nécessaires pour obtenir une perméabilisation irréversible sont légèrement plus élevés que les conditions réversibles.

Les résultats montrent qu'il est possible d'obtenir jusqu'à 80 % de cellules en phase de stress perméabilisées de façon réversible. Dans le cas des impulsions de 5 μ s, le champ électrique doit être égal à 4.5 kV/cm pour obtenir ce résultat. Des expériences supplémentaires (mise en contact des cellules avec le marqueur de perméabilité quelques secondes après perméabilisation) ont permis de déterminer la dynamique de fermeture des pores et de montrer que les **pores réversibles ont une durée de vie extrêmement courte, de l'ordre de quelques secondes. La viabilité des cellules reste élevée, supérieure à 80 %.**

Il semble donc possible d'utiliser les impulsions électriques dans une perspective de « milking », c'est-à-dire l'extraction de composés d'intérêt des microalgues par l'ouverture de pores réversibles tout en maintenant la viabilité cellulaire. Cette pratique serait donc envisageable pour l'extraction de petites molécules hydrosolubles, la taille des pores réversibles étant de l'ordre du nano-mètre.

En ce qui concerne l'extraction des lipides neutres hydrophobes, les résultats ont montré qu'il est nécessaire d'associer le traitement électrique à une autre méthode d'extraction pour obtenir une extraction significative.

Nous avons donc associé le **traitement électrique à l'extraction par solvant**. Le choix du solvant est délicat ; il doit être « doux » vis-à-vis des microalgues, c'est à dire ne pas entraîner de lyse cellulaire ou affecter la viabilité, et il doit être le plus spécifique possible des lipides neutres (peu d'interactions avec les lipides polaires).

Le coefficient de partage du solvant entre l'octanol et l'eau, noté LogP, a été le critère principal de choix. Les solvants à LogP faible sont les plus hydrophiles tandis que ceux à logP élevés sont fortement hydrophobes et ont donc une forte affinité avec les lipides neutres ; il est cependant difficile de réaliser un bon contact entre eux et les algues qui évoluent dans un environnement aqueux. Les solvants à LogP élevé (supérieur à 5,5) sont généralement considérés comme biocompatibles, notamment car ils sont peu en contact direct avec les cellules ; ils ont en effet du mal à franchir les têtes polaires des bicouches lipidiques de la membrane cytoplasmique.

Nous avons commencé donc par évaluer l'impact sur la lyse cellulaire de trois solvants de diverses hydrophobicités : l'acétate d'éthyle (LogP = 0,73), l'hexane (LogP = 4,00), et le dodécane (LogP = 6,6). Mis en contact avec les cellules, l'acétate d'éthyle relativement hydrophile a provoqué une lyse cellulaire. Les deux autres solvants n'ont pas montré d'effet significatif sur la lyse, même après 2 heures de mise en contact avec les cellules.

Après contact de cellules non traitées par PEF avec le solvant, les observations au microscope confocal ont montré la libération des lipides du cytoplasme par l'acétate d'éthyle, alors que le dodécane a une très faible capacité d'extraction. Le solvant intermédiaire, l'hexane, montre une certaine capacité à extraire les lipides neutres. Nous avons donc décidé de l'utiliser.

En mettant en contact 100 μ L de solution d'algues (7 jours d'accumulation, $2 \cdot 10^7$ cellules/mL) et 200 μ L d'hexane sous une agitation modérée (effectué à l'aide d'un arbre mécanique), l'extraction des lipides est totale en deux heures. On obtient un système pluri-phasique après centrifugation : le culot d'algues épuisées en lipides neutres, le milieu aqueux, une couche jaune interfaciale contenant les lipides et la phase supérieure (hexane pur). Ceci pourrait être dû à l'insolubilité des lipides dans

l'hexane, ce qui est étonnant car la trioléine est elle-même très soluble dans ce dernier. L'explication pourrait plutôt être liée à la co-extraction de phospholipides de la membrane qui entoure les gouttelettes lipidiques et libérés en même temps que les lipides neutres ; ces phospholipides joueraient le rôle de surfactants et interagiraient avec les lipides, créant une barrière entre ceux-ci et l'hexane. L'ajout d'un solvant polaire tel que l'isopropanol l'éthanol permet de faire migrer les lipides extraits dans la phase supérieure en détruisant cette barrière, les lipides polaires pouvant certainement être re-solubilisés dans la phase aqueuse à l'aide du solvant polaire. Cet effet devra être confirmé par l'analyse des diverses phases en chromatographie gazeuse ; la méthode SPV permettrait quant à elle d'évaluer le contenu en lipides insaturés de réserve (neutres) et membranaires (polaires) des deux phases séparées.

Afin de comparer l'impact des différents traitements (solvant seul, PEF seul ou combinaison des deux) sur l'extraction de lipides, nous avons simplement dosé la phase aqueuse contenant les microalgues avant et après traitement, ce qui permet d'évaluer par différence le taux d'extraction des lipides. Des résultats préliminaires des essais PEF couplés à l'hexane semblent indiquer une extraction accrue de lipides en présence des champs électriques de durées d'impulsion très élevés, entraînant à côté des effets d'électroporation, des effets secondaires liés à l'effet Joule, à l'apparition de bulles (électrolyse de l'eau) et certainement une lyse cellulaire. Une étude plus poussée sera prochainement réalisée afin de déterminer dans quelles conditions de traitement PEF, l'extraction par solvant peut être améliorée (extraction plus rapide, quantité moindre de solvant nécessaire etc). Le but reste bien sûr de réduire le coût énergétique du procédé global d'extraction par rapport aux procédés actuels. Notons tout de même un avantage très important de ce procédé ; il permet en effet de réaliser l'extraction des lipides directement sur les algues humides, ce qui élimine l'étape de séchage, très gourmande en énergie. La principale consommation énergétique est, outre le traitement PEF, l'étape de mélange des algues avec le solvant car pour assurer un bon transfert, celui-ci doit être efficace et développer une aire interfaciale importante entre les phases.

Les apports de ce travail de thèse sont multiples :

- Un large éventail de méthodes de caractérisation des microalgues en périodes de croissance et de stress : perméabilité de la membrane, viabilité, teneur en lipides, taille des cellules... grâce à la mise au point de nombreuses méthodes (marquages fluorescents, observations microscopiques, mesures plus globales par cytométrie de flux, méthodes chimiques) et leur combinaison raisonnée et optimisée.
- Des conditions optimisées de culture des algues en période de croissance et d'accumulation de lipides.
- La mise au point d'un système microfluidique de champs électriques pulsés pour l'observation, *in situ* et en temps réel, à l'échelle de la cellule, des effets du traitement électrique et une étude plus globale sur ses besoins énergétiques. Ce système peut être employé pour de nombreuses autres applications, nécessitant une connaissance fine à l'échelle de la cellule. Ce

travail a donné lieu à la publication d'un article dans une revue internationale.

- L'étude à plus grande échelle, avec des combinaisons pertinentes de marqueurs, de l'électroporation réversible et irréversible. Ce travail réalisé en microcuvettes d'électroporation a permis de mesurer les taux de perméabilité réversible et irréversible à différents champs électriques pour différentes durées d'impulsions ; il a également conduit à une estimation du temps de fermeture des pores, un couplage électroporation/extraction par solvant et une caractérisation cellulaire après extraction par solvant.
- Le couplage de l'électroporation à l'extraction par solvant et la caractérisation cellulaire fine après la combinaison des traitements (perméabilité membranaire, activité enzymatique, reprise de croissance, lyse cellulaire, imagerie) ; les premiers résultats sont prometteurs pour pouvoir envisager la mise au point d'un procédé couplant ces deux traitements, applicable directement sur les algues humides et moins gourmand en énergie que les procédés actuels d'extraction. Des nouveaux essais sont prévus pour aller plus loin et quantifier l'impact du pré-traitement PEF sur l'extraction des lipides de *Chlamydomonas reinhardtii*.

Ce travail bien sûr soulève encore de nombreuses questions et ouvre donc la voie à quelques perspectives très intéressantes :

- L'évaluation du contenu lipidique marqué au Bodipy par reconstitution 3D avec les images acquises au microscope confocal est une méthode peu exploitée dans la littérature et qu'il serait intéressant de développer. Accompagner cette reconstitution 3D des gouttelettes de lipides, de la visualisation de la chlorophylle par autofluorescence et de la reconstitution des différentes couches de la paroi marquée par la concanavalin permettrait de mieux caractériser les cellules, notamment à la suite des traitements multiples (PEF, PEF avec solvant, etc). La fixation des cellules à un substrat pour un scan 3D pourrait se révéler nécessaire.
- La mise au point et l'optimisation d'un procédé couplant PEF à l'extraction par solvant devraient être étudiées plus en détail à la suite des résultats obtenus. Par ailleurs, ce procédé pourrait être inséré dans un contexte de fractionnement de la biomasse algale de façon à récupérer différents produits d'intérêt des microalgues, dont les lipides en intégrant une étape de recyclage du solvant.
- Une autre voie explorée à la suite de cette thèse est d'associer au traitement PEF, un système permettant de soumettre les algues à des sollicitations mécaniques (notamment par ondes acoustiques), en couplage ou non à l'extraction par solvant et d'évaluer l'intérêt du couplage de procédés pour l'extraction de molécules des microalgues.
- Un autre cas intéressant serait d'évaluer l'intérêt du procédé PEF pour l'extraction de molécules à haute valeur ajoutée, comme par exemple, des caroténoïdes.

Thesis outline

Among the 21st century challenges that the humanity has to face, the energetic transition towards sustainable and environmentally-friendly productions and the increasing nutritional demand due to a rise in the worldwide population, open the gate towards innovative bio-based processes.

Microalgae, with their high growth rate and diversity, have a great potential to produce a variety of chemicals in multiple environments. However, this industry is still very young and the current high production costs limit the use of microalgae to very specific markets and high valued products.

The biofuel production using microalgae, highly needed due to the declining reserves of fossil fuels, requires a reduction of the energy consumption at the different steps of this process. Indeed, one of the main issues which jeopardize the economic and energetic viability of algae-derived biodiesel is the high energetic cost involved in the extraction of oils produced by algae cells.

As a consequence, the objective of this work is to propose an innovative extraction technique which may replace the current mechanical or chemical processes used to extract lipids trapped in algae cytoplasm. Pulsed Electric Field (PEF), an electrical treatment used to permeate cells or tissues in various applications, can be a good candidate. Indeed, it destabilizes the cell membrane and thus, by creating pores, foster insertion of exogenous molecules into the cell or extraction of endogenous ones from it. PEF actions on lipid accumulated cells will then be investigated in the context of this thesis.

The developed approach aims at studying the PEF process at the scale of a single algae cell using a miniaturized electroporation device and to monitor, *in situ*, the effect of PEF on the potential lipid extraction from microalgae. Afterwards, the goal is to optimize the parameters of electroporation to reduce energy consumption while permeabilizing the cell membrane. Preliminary solvent extraction experiments are thereafter carried out in order to evaluate how PEF could be used in a lipid extraction process.

The work is a first collaboration between two laboratories (SATIE of ENS Cachan and LGPM of CentraleSupélec) having different expertise and this to tackle the subject with a multidisciplinary approach. In the particular field of process engineering, algae are mainly considered, at macroscopic scale, as biomass. However, when one wants to develop innovative processes, studies at microscopic scale must be carried out. This kind of study is performed in this thesis. In addition, understanding interactions between microalgae and electric fields requires a deep knowledge in both biology and electrical engineering, which is only possible through collaboration between specialists of these domains. Finally, many equipment and expertise were needed in various fields such as chemistry, microscopy, and microtechnology to develop the tools and methods required for this multidisciplinary approach.

The work is presented in three distinct chapters. In chapter 1, the state of the art is presented in order to introduce the context of algae biofuel. The Chapter 2 is devoted to the cultivation of oleaginous algae and their characterization. The Chapter 3 is focused on the study of PEF effects on oleaginous algae and on lipid recovery.

The **Chapter 1** aims to offer a global view of the complexity of algae-derived biodiesel. The first part presents the current state of global energy uses with a particular emphasis on the future of crude oil supply and the alternative fuel sources. Afterwards, the current and future biofuels are briefly reviewed with a comparison of first and second generations of biodiesel with the potential third generation: microalgae. Microalgae require specific cultivation technologies and downstream

processes whose advantages and disadvantages are presented. Finally, the principle keys for a future feasibility of algae-derived biodiesel are introduced.

The **Chapter 2** details more specifically the biological aspects, such as the different classes of lipids of the cell and the metabolism of lipid accumulation. Then a literature review of different methods to produce algae with a high oil content and to characterize the biomass is presented. As algae cultures and PEF treatments are performed in very low volumes, several specific cultivation and analytical methods are developed and described. A suitable algae strain was identified for this study: *Chlamydomonas reinhardtii*.

The **Chapter 3** is focused on the application of PEF on *Chlamydomonas reinhardtii* towards the extraction of lipids. The first part presents the theory and applications of PEF in general and in algal technologies. Afterwards, the micro-system designed and built in a clean room to study, *in situ*, the electroporation of microalgae is presented. Complementary analyses are performed with another electroporation system (electroporation cuvette) in order to study PEF association with solvent extraction. The development and optimization of methods to estimate cell viability and permeability at micro and macroscales is then presented. The outputs of the study are the following: 1) analysis of PEF energy consumption under several electrical field conditions, 2) characterization of PEF effects on lipid bodies, the cell membrane and the cell wall. Finally, a method was also developed to evaluate the effect of PEF as a pre-treatment for lipid extraction with a solvent.

Chapter 1

The future of algae-derived biodiesel

List of abbreviations:	27
I. Global outlook on energy supply and demand.....	28
II. Review on crude oil production and future alternatives	29
II1) Crude oil production and consumption	29
II2) Hydrocarbon production.....	30
III. Current biofuel production and future technologies	32
III1) Current production.....	32
III2) Future technologies.....	34
IV. From algae culture to oil harvesting. Review of existing technologies and constraints...	37
IV1) Birth of algae biotechnology and discovery of the biodiversity.....	37
IV2) Culture constraints.....	38
IV2a) Light supply.....	38
IV2b) Temperature and pH	40
IV2c) Nutrients.....	41
IV2d) Mixing	42
IV3) Culture systems	42
IV3a) Open illuminated systems.....	42
IV3b) Closed photobioreactors	44
IV3c) Heterotrophic and mixotrophic cultures.....	47
IV3d) Biofilm cultures.....	48
IV4) Harvesting/Extraction methods in suspension cultures	48
IV4a) Harvesting.....	48
IV4b) Physical processes of extraction.....	50
IV4c) Chemical processes of extraction.....	52
V. Key points for future viability of algae-derived biodiesel	53
V1) Current economic review	53
V2) Biorefinery concept	57
V3) Bioengineering algae	59
Chapter 1 conclusion	60
Chapter 1 references	62
II. Appendix I.1: Additional information about oil production.....	66

List of abbreviations:

- toe: tons of oil equivalent (11.63 MWh)
- OECD: Organization for Economic Co-operation and Development countries
- NGLs Natural Gas liquids
- CTLs Coal-to-liquids
- GTLs Gas-to-liquids
- IEA International Energy Agency (<https://www.iea.org/>)
- US\$/bbl US dollar per barrel of crude oil
- mb Million barrels of crude oil
- NO_x Nitrogen oxides
- BtL Biomass to liquids
- FT Fischer-Tropsch process
- Syngas Synthetic gas
- DME Dimethylether
- Bio-SG Bio-synthetic gas
- HVO Hydrotreated vegetable oil
- HMV Hydroxymethyl furfural
- ASP Aquatic Species Program
- ATP Adenosine Triphosphate
- NADPH Nicotinamide adenine dinucleotide phosphate
- $h\nu$ Photon energy flow (Planck constant multiplied by frequency)
- G_c Critical irradiance ($\mu\text{mol}/\text{m}^2/\text{s}$)
- G_z Irradiance at a certain depth z of a photobioreactor ($\mu\text{mol}/\text{m}^2/\text{s}$)
- NPQ Non-Photochemical Quenching
- DIC Dissolved Inorganic Carbon
- FAMES Fatty Acids Methyl Esters
- I Light irradiance supplied ($\mu\text{mol}/\text{m}^2/\text{s}$)
- NER Net Energy Ratio (Energy input/Energy output)
- RP Raceway Ponds
- OP Open Ponds
- PBR Photobioreactors
- PEF Pulsed Electric Fields
- MSN Mesoporous Silica Nanoparticles
- FFAs Free Fatty Acids
- PLE Pressurized Liquid Extraction
- UAE Ultrasound Assisted Extraction
- ASE Accelerated Solvent Extraction
- BaU Business as Usual
- HRJ Hydrotreated Renewable Jet fuel
- TAGs Triacylglyceride
- HVP High Value Compounds
- FCCS Flow Cytometry and Cell Sorting

I. Global outlook on energy supply and demand

The world global energy consumption (Figure 1.a) was estimated at 8,978 million tons of oil equivalent (toe) in 2012 (1 toe represents 11.63 MWh). About 40% of this energy is used by OECD (Organisation for Economic Co-operation and Development) countries. The energy demand of these countries tends to stabilize after a strong increase due to industrial development (+11% from 2012 to 2050). However the energy demand of other regions will keep increasing strongly [1]. By 2050, the final energy demand may rise by 74% in China, 120% in Asia, 160% in Africa and 90% in South America. Therefore, according to these estimations, the energy consumption may increase up to 14,000 Mtoe in 2050.

Before being used to produce heat, electricity or other products primary energy must be transformed. All the energies resulting from human-made transformations are called secondary energies. These transformations are indeed necessary to make energy available for trade and use. The main primary energy sources (Figure 1.b) are oil, coal and gas, representing 81.7% of the total supply. The renewable sources, biofuels and biogas, earth (geothermal energy), wind, sun and water (hydroelectricity) represent only 13.5% of the total primary energy supply. Nuclear energy only counts for 4.8%.

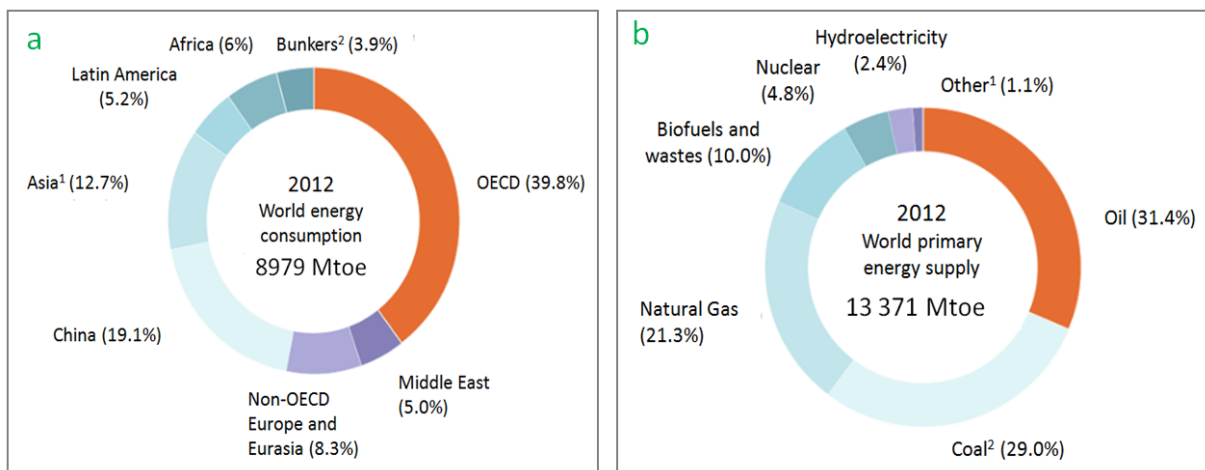


Figure 1: a) 2012 World final energy consumption by region adapted from [2,3]. 1 Asia excludes China. 2 Includes international aviation and international marine bunkers. b) World primary energy supply in 2012 adapted from [2,3]. 1 Includes geothermal, solar, wind, heat, etc. 2 peat and oil shale are aggregated with coal.

Energy consumption is globally divided into three sectors: industry, transport and services* (*agriculture, residential, commercial and public services etc...) as illustrated in Figure 2. But the source used can depend on the sector type; for example, the transport sector is highly dependent on crude oil and industry on coal.

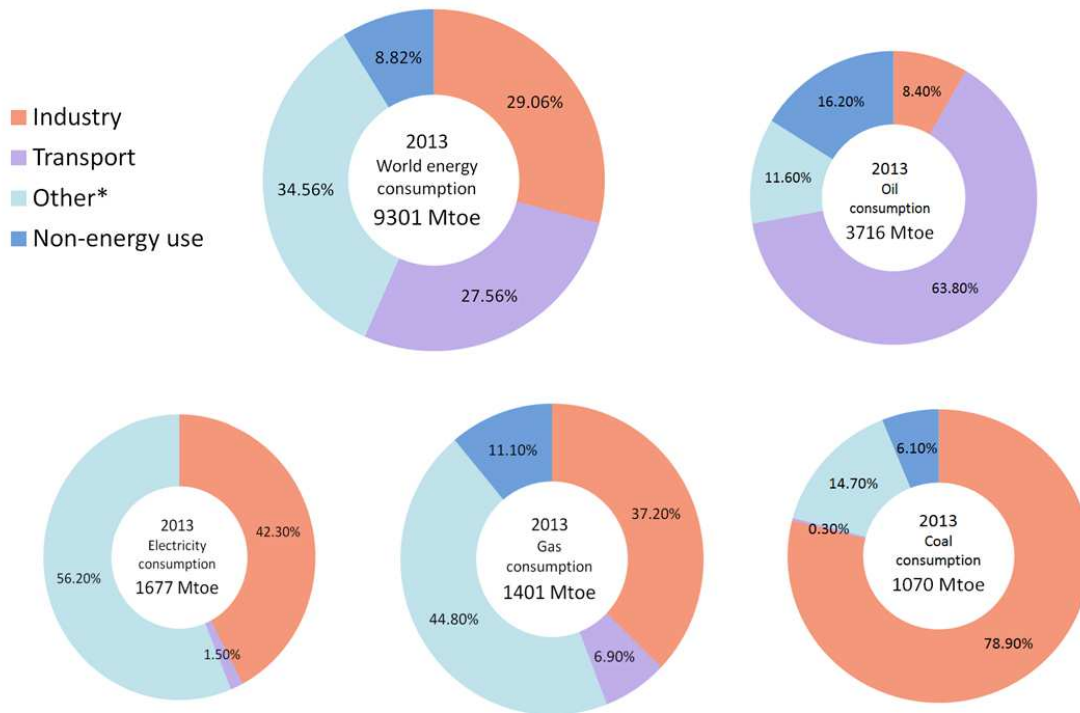


Figure 2: World energy consumption by sector, adapted from [3]. *Other includes agriculture, commercial and public services, residential and non-specified... Renewable energy sources not presented in this Figure.

II. Review on crude oil production and future alternatives

II.1) Crude oil production and consumption

Crude oil, or petroleum or petrol, which was used as a source of energy at a rate of 85 millions of barrels per day in 2013 [4] (one barrel is equivalent to 158 L, *i.e.* 0.12 to 0.16 toe) is a natural and renewable resource at a geological time scale. Crude oil is a fossil fuel which origins started 20 to 350 million years ago. The natural production of petrol has started millions years ago with the sedimentation of non-assimilated organic material in the sedimentary basin of oceans, lakes and deltas. Carbon is incorporated into sedimentary sludges with mineral matter (sand, clay). During a dozen millions of years, the matter will migrate to a deeper level of the terrestrial crust and beyond 1,000 meters be converted into an insoluble mixture of extremely large organic molecules called 'kerogen', trapped in the source rock. Generation of liquid oil starts at around 60 to 70°C (1,500 to 2,000 meters) and continues until 120 to 160°C through a phenomenon called pyrolysis [5]. Crude oil and gas, under high pressure constraints, can be expelled through permeable rocks toward upper layers. Expelled oil can leak to the surface and emerge as a 'seep'. Most of the oil is trapped under non permeable sub-surface rocks in storage spaces named 'reservoir rocks' and forms a pool. The oil remaining in the source rocks or in impermeable rocks is named 'tight oil'. The rate of current oil generation has been estimated to be no more than few million barrels per year [4].

The well-known natural origins of crude oil were however rapidly forgotten behind the economic constraints which make this rare and precious resource a predominant tool to human development. The main world producers are Saudi Arabia, Russia and United States which represent more than 35% of the total world production [3]. A map of the world oil production is presented in appendix 1, Figure 1. The world demands, of some 30 billion barrels per year, increase constantly by a rate of 1 to 2 % per

year. It is clear that at an entropic time scale, natural petrol reserves can be considered as finite and then petrol is a rapidly depleting fossil resource.

112) Hydrocarbon production

Crude oil extracted from reservoir pools out of the ground is a complex mixture of hydrocarbons that remains in liquid phase when extracted to the surface. The nature and relative abundance of the components, described in Figure 3, vary with the petroleum source. Petroleum is converted to refined products in three steps: distillation, cracking and reforming. Petroleum is first heated to approximately 400°C, temperature at which it is a mixture of liquid and vapor. This mixture, called the feedstock, is introduced into the refining tower. The most volatile components are recovered at the top of the column where temperature is lower while the less volatile condense at its bottom. The composition of the fraction obtained at each level of the column, called petroleum fraction, varies; each fraction is indeed a mixture of compounds of nearby volatilities (*i.e.* with a similar number of carbon atoms) and presents various final uses [6].

	Number of carbons	Boiling point range	Uses
Gases	1–4	0–30°C	Bottled and natural gas
Naphthas	5–10	30–180°C	Gasoline
Kerosenes	10–16	180–260°C	Kerosene for home heaters, jet fuel
Gas oils	16–60	260–350°C	Diesel fuel, feedstock for cracking
Lubricants	>60	350–575°C	Motor oil, feedstock for cracking
Fuel oil	>70	>490°C	Candles, fuel oil for ships and power stations
Asphalt	>80	>580°C	Roofing tar, road tar

Figure 3: Petroleum fractions condense at different temperatures, depending on the number of carbons atoms in the molecules, and are drawn of the column. The most volatile components (those with the lowest boiling points) condense at the top of the column, and the least volatile (those with the highest boiling points) condense at the bottom [6].

In addition to crude oil and condensates, many liquid hydrocarbons can be extracted or produced, and are a substantial complement in the liquid fuel supply (Figure 4).

While crude oil and condensates represent 68.5 million barrels per year in 2011 [4], natural gas liquids (NGLs) count for 12.1 million barrels. Crude oil and NGLs are named 'conventional petrol resources'. 'Non-conventional hydrocarbon resources' include oil sands, biofuels, tight oil, extra-heavy oil, Gas-to-Liquids (GTLs) and Coal-to-Liquids (CTLs).

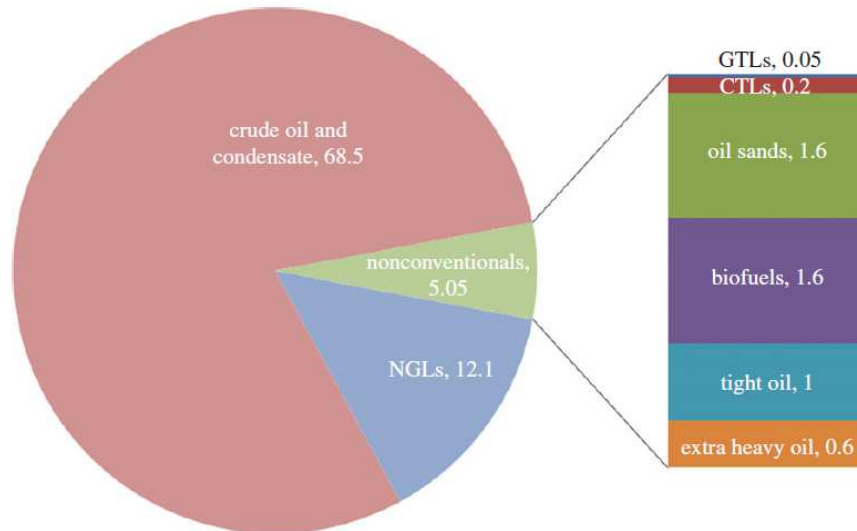


Figure 4: global hydrocarbons liquids production in 2011 (million barrels per year) [4].

Natural Gas liquids (NGLs) are the liquid fractions of natural gas, mostly ethane and pentane. Oil sands are extremely viscous forms of petroleum referred to as bitumen. Biofuels are transport fuels derived from biological sources. Tight oil is crude oil contained in shale or carbonate rocks that can be obtained using horizontal wells with multi-stage hydraulic fracturing (fracking). Extra-heavy oil is very dense crude oil with a viscosity higher than 10,000 centipoises. Gas-to-liquids (GTLs) and Coal-to-liquids (CTLs) are obtained using Fischer-Tropsch process to convert gas or coals to synthetic fuels (synfuels).

The major part of liquid hydrocarbons production is crude oil and NGLs, referred as conventional hydrocarbons feedstocks. The non-conventional feedstocks represent a minor part of this production (6 % in 2011). The global production (crude oil, condensats, and NGLs) will need to increase by 1 to 2 % every year to meet the future demand. The future evolution in the energy supply and demand is influenced by 5 main factors: (i) world population (+1.5 % per year), (ii) globalization which rapidly increases the energy needed per inhabitant in the developing countries (+1.5 % per year), (iii) energy price fluctuations, (iv) improvements in the energy uses (-1 % per year) and (v) willingness to reduce gas emissions by 2025-2030 in order to mitigate global warming [7]. Tremendous amounts of greenhouse gases are indeed released from fossil fuel consumption; consequently the atmospheric CO₂ concentration was increased from a pre-industrial level of 280 ppm to 401 ppm in september 2016 [8,9]. The aim is to reduce CO₂ emissions by 40 to 70 % by 2050 in order to limit its atmospheric concentration to 450-500 ppm and then the temperature increase to a maximum of 2°C above pre-industrial temperatures. If no effort is made, the atmospheric CO₂ concentration may increase to 750 to 1300 ppm leading to a temperature increase up to 3.7 to 4.8°C at the end of the century [10].

Crude oil price is extremely unstable. The barrel price has varied from 30 to 150 US\$/bbl (US\$ price of one barrel) during the last decade (for more details, see Figure 2, appendix 1). A sharp decrease of the demand (due to financial crisis which reduced global activity in 2009), or, on the contrary, an excess of production (due to the strong development of fracking sources and an excess of production in Saudi Arabia and Iran in 2015) lead to a collapsing oil price, below 40 US\$/bbl.

In parallel to the offer/demand rule, the different crude oil feedstocks possess inherent extraction costs (illustrated Figure 3 of appendix 1) which vary between 20 and 180 US\$/bbl. A depletion of the

low cost feedstocks and a need to meet the increasing world demand by extracting more and more expensive sources lead to a slow and irremediable crude oil price increase. The barrel price is expected to increase chaotically within the range of 120 to 200 US\$/bbl by 2035 [11].

A future increase of the demand, in parallel with the reduction in the production capacities of the current sources, must be supported by expanding the diversity of supply sources : crude oil including tight oil, NGLs and unconventional oils including sands gas, coal to liquids and biofuels [4] as illustrated in Figure 5.

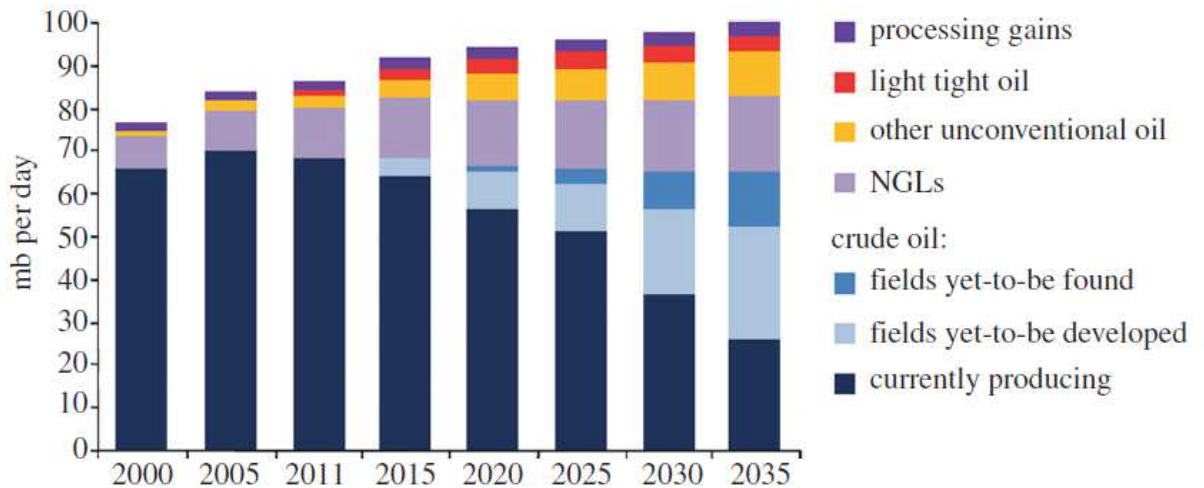


Figure 5: Projection of global all-liquids production to 2035 [4]

III. Current biofuel production and future technologies

III1) Current production

Biofuels are predominantly produced from a variety of bio-feedstocks. Bio-feedstocks or biomass refer to all vegetable matters that can be obtained by photosynthesis. Biomass is currently the only renewable feedstock to produce liquid fuel.

Biofuels have a massive potential to represent a significant part of future sustainable energy. IEA (International Energy Agency) indeed estimates that biofuels will provide 27 % of the transport consumption by 2050 [2]. Globally, the annual biodiesel production increased from 15 thousand barrels per day in 2000 to 289 in 2008 [12], but this is still very low in comparison with the 85 millions of barrels consumed.

The biomass feedstock for biofuels production should fulfill two main requirements: low production costs and large production volume to be able to compete with crude oil supplies. On the other hand, this feedstock is strongly dependent on climate conditions, geographical location, local soil nature and agricultural practices.

The main advantage of biofuels over crude oil, besides their sustainability, is their very low carbon footprint. Indeed, despite carbon dioxide is released during fuel combustion, it is roughly counterbalanced by the CO₂ absorption by plants during their culture. But the impact analysis of biofuels must also take into account the footprint of farming operations and transports [13]. This results in a negative carbon balance, rising skepticism among scientists about the industrial scale up of biofuel production. Biofuels combustion nevertheless releases less sulfur dioxide and particules (87.7 % reduction) than diesel fuel [14]. When considering nitrogen oxides (NO_x), the emission may however be increased up to 70 % [15] when using current engine technologies. A modification of the combustion process (injection, ignition temperature) is then necessary for biodiesel engines [16], as conventional engines were optimized over a century to work with petroleum carbon fuels.

The biofuel worldwide production is illustrated in Figure 6.

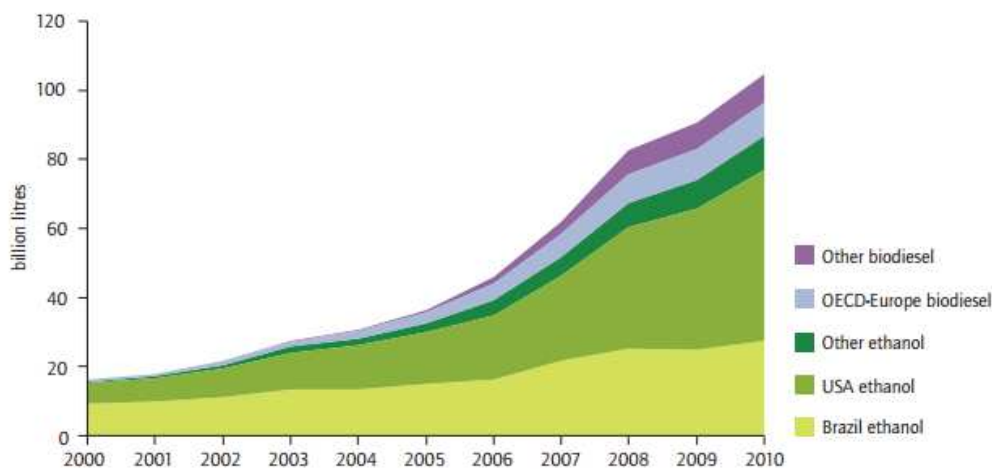


Figure 6: 2000-2010 liquid biofuels production [17].

In 2012, the USA were responsible of 45.5 % of the global production with 27.4 Mtep thanks to the program 'Renewable Fuel Standard', with two main axes developed : increase of ethanol production and expanding development of second generation biofuels technologies. Brazil started a program in 1970 called 'Proalcool' and positions itself as the historical leader of biofuel production. In 2012 Brazil represented 22.5 % of the worldwide production while Europe contributed only to 16.6 % with Germany and France as the dominant actors.

The development of biofuels during the last decades was mainly focused on three axes : conversion of sugar to ethanol, production of biodiesel, production of biogas (not illustrated in Figure 6).

In the classic **sugar-to-ethanol** process, sucrose is obtained from sugar crops. The main industrial steps of the process include press milling, liquefaction, saccharification, fermentation, distillation, drying and denaturing [9]. The conversion of starch crops to ethanol requires a pre-transformation step: the hydrolysis of starch into glucose, which requires more energy than the sugar-to-ethanol route. The cost of production from sugar and starch is very sensitive to the highly volatile feedstock prices. Commercial bioethanol is currently produced from starch and sugar-based crops including sugar cane, wheat, sugar beet, sweet sorghum, corn, barley, potato, yam and cassava [9]. In 2012, 42 % of the U.S. corn grains were used to produce 49 billion liters of bioethanol replacing then 10 % of gasoline fuel used in the whole country [9]. Sugar cane is the predominant feedstock to produce bioethanol in Brazil.

Biodiesel is a mixture of mono-alkyl esters of long chain fatty acids derived from raw edible or non-edible vegetable oils, animal fats and used cooking oil [12][17]. These oils and fats are converted to biodiesel thanks to a trans-esterification process by addition of alcohol (mostly methanol or ethanol).

Currently, more than 95 % of the worldwide biodiesel is produced from edible oils coming from rapeseed (84 %), sunflower (13 %), palm (1 %), soybean and others (2 %).

Biogas is produced through anaerobic digestion of feedstocks such as animal manure, organic waste (compost), sewage sludge or dedicated green energy crops. Biogas is often used to generate heat and electricity. It can be also upgraded to biomethane CH₄ by removing CO₂ and hydrogen sulfide (H₂S).

Biodiesel and biofuels produced from food crops are generally referred as 'first-generation biofuels'. Their use raises some concerns, in particular the competition with food and feed crop exploitation... Indeed, by 2050 the expected worldwide population of 9 billion inhabitants will result in a huge food supply demand. Consequently, this will increase the price of vegetable oils which indirectly will affect the economical viability of the first generation biodiesel industry.

III2) Future technologies

Because of the constraints of current biofuels, many studies are performed on advanced biofuel technologies; several are already deployed at early commercial scale, as illustrated in Figure 7.

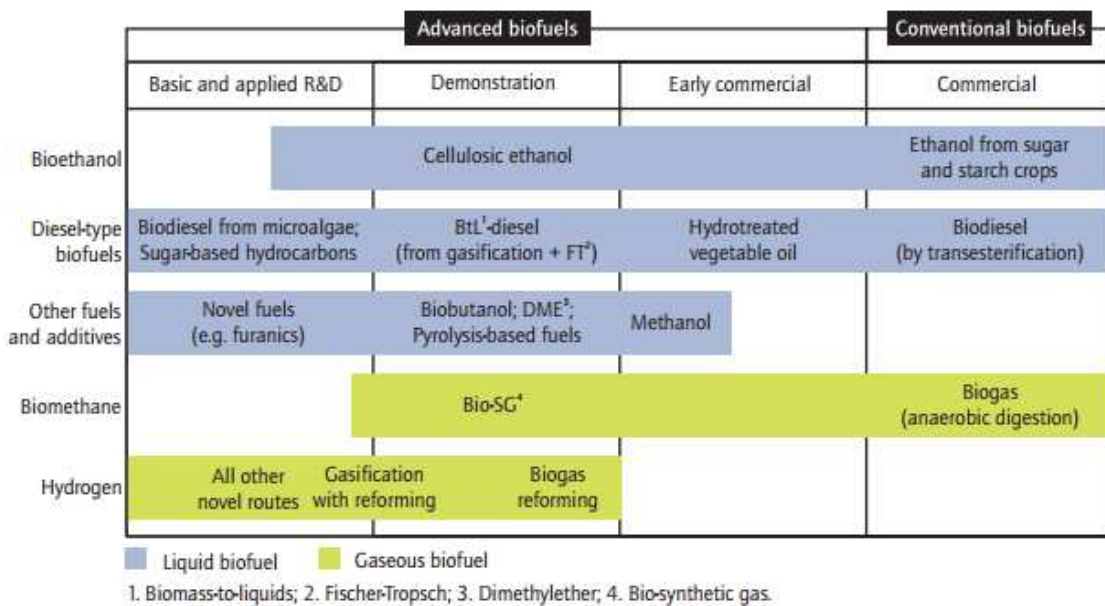


Figure 7: Biofuel commercialization stage [17]. Conventional biofuel technologies include well-established processes that are already producing biofuels on a commercial scale, commonly referred to as first-generation. Advanced biofuel technologies are conversion processes which are still in research and development, pilot or demonstration phase, they are commonly referred to as a second- or third-generation.

In comparison with the first generation of oil feedstocks, non-edible oil resources are gaining increased attention because they can be cultivated on wastelands, not suitable for food crops, and are more economical than edible oils. Non edible oils as well as animal fats and waste oils are considered as the **second generation of biodiesel** feedstocks.

This so-called second generation of biodiesel is the future of biodiesel supply for the next decades.

Yet, the second generation feedstocks may not fulfill the global oil demand increase because of the surface productivity limitations. Moreover, in the case of many types of animal fats, the transesterification process is difficult due to the high amount of saturated fatty acids.

Many other advanced biofuels are on development stage and represent the future of energy supply at longer term. They are listed below.

Hydrotreated vegetable oil (HVO) is produced by hydrogenation of vegetable oils or animal fats instead of their transesterification [18]. This reaction consists in the catalytic reduction of unsaturated fatty acids with a hydrogen source.

Biomass-to-liquid (BtL) diesel, similarly to coal to liquid (CtL), is produced by a two-step process; first the biomass is converted into syngas (synthetic gas) rich in hydrogen and carbon monoxide; then, the syngas is catalytically converted through Fisher-Tropsch synthesis into various hydrocarbon liquids, including synthetic diesel and bio-kerosene.

Bio-synthetic gas (Bio-SG) corresponds to biomethane derived from biomass *via* thermal processes.

Bio-methanol can be produced from a wide range of biomass feedstocks *via* a thermochemical route which is similar to Biomass-to-liquid (BtL). It can be blended with petrol at 10 to 20 %.

Biobutanol is traditionally produced by ABE fermentation - the anaerobic conversion of carbohydrates by strains of *Clostridium* into Acetone, Butanol and Ethanol. 85 % Butanol/gasoline blends can be used in unmodified petrol engines [19]. Biobutanol can be used as a transport fuel.

Furanics are “furan-based organic liquids” with biofuel potential. Furans are heterocyclic organic compounds containing rings of one oxygen and four carbon atoms. 5-Hydroxymethylfurfural (HMF), a main building-block of Furanics, can be produced by the acid catalyzed dehydration of hexoses, such as glucose and fructose from biological feedstocks [20–22].

Biohydrogen for use as a transport fuel can be produced from fossil fuels as well as renewable sources: biogas reforming, fermentation of renewable materials, cell-free enzymatic process, production from microbial fuel cells and from algae [19].

Microalgae are considered as the third generation of biodiesel feedstock. Microalgae are photosynthetic microorganisms that convert sunlight, water and CO₂ to algal biomass, more efficiently than conventional crop plants. They are a very promising feedstock because of their high capacity to produce biomass containing high oil contents, with higher growth rate and productivity than edible and non-edible feedstocks (Table 1) [12,23].

Table 1: Estimated oil productivity of different biodiesel feedstocks [12,23]

Plant source	Biodiesel (L/ha/year)	Area to satisfy global oil demand (10 ⁶ ha)
Cotton	325	15 002
Soybean	446	10 932
Mustard seed	572	8 524
Sunflower	952	5 121
Rapeseed/canola	1 190	4 097
Jatropha	1 892	2 577
Oil palm	5 950	819
Algae	12 000 - 136 900	35 - 406

Microalgae oil yields can be up to 25 and 250 times higher than those of palm and soybean respectively. Among all the sources of renewable biodiesel feedstocks, microalgae seem the only one capable of meeting the global demand for transport [12,24] regarding the arable area available (5,000 Mha arable land with 1,400 Mha are used for agriculture [25] in 2016). In addition to this productivity advantage, algae, thanks to their high diversity, can grow in multiple conditions even when traditional crops cannot be farmed.

The algae biodiversity, culture systems and energetic costs associated are presented in the next section.

IV. From algae culture to oil harvesting. Review of existing technologies and constraints

IV1) Birth of algae biotechnology and discovery of the biodiversity

The idea of using algae to produce lipids emerged in 1942 with Richard Harder and Hans von Witsch's works [26]; in the following decades, many biologists underlined the high capacity of algae to convert efficiently solar energy into lipids [27,28]. Specific culture and engineering systems were developed then to cultivate this new biological feedstock at larger scales. In 1970s, the United States started a program named Aquatic Species Program (ASP) which aim was to produce biodiesel from microalgae. During more than 30 years, 3,000 algal strains were collected and screened for properties such as high growth rate, high lipid content and resistance to the environmental conditions. Japan started a program in 1990 focused on 'biological CO₂ fixation and utilization' which underlined the capability of algae to grow on flue gas as a CO₂ source. These first programs were successful - promising lipid production strains were obtained, new photobioreactors for algae culture were designed, processes at large scale were studied. The increasing interest of microalgae biotechnology was also driven by their potential to produce feed and food.

Research on algae for the mass-production of oil is mainly focused on so-called 'microalgae'; they are microorganisms capable of photosynthesis with diameters lower than 0.4 mm and including diatoms and cyanobacteria, as opposed to macroalgae such as seaweed. In April 2016, the algae base contained 4,516 prokaryotic and 42,582 eukaryotic species [29].

The tree of life presented in Figure 8 illustrates the 9 domains of life in bold (e.g. Bacteria) divided in kingdoms (e.g. Cyanobacteria). The kingdoms of photosynthetic algae (in white characters in the tree) are located in 6 of the 9 existing life domains. According to the phylogenetic evolution, primates (kingdom Metazoa) are surprisingly closer to sponges (same kingdom) than two different microalgae between themselves, for example *Chlamydomonas* (kingdom *Viridi plantae*) and *Nannochloropsis* (kingdom *Heterokontophytes*). The symbiosis represented with a blue-green arrow is at the origin of the chloroplasts of red algae, blue algae, green algae and plants which evolved from an endosymbiotic cyanobacteria living in an eukaryotic host cell [30] (mitochondria may also come from an endosymbiosis, illustrated with a blue arrow). Photosynthetic cells have spread to other domains of life with various symbiosis represented with green, yellow or red arrows. Some of the organisms are known to be toxic and are indicated with a red star.

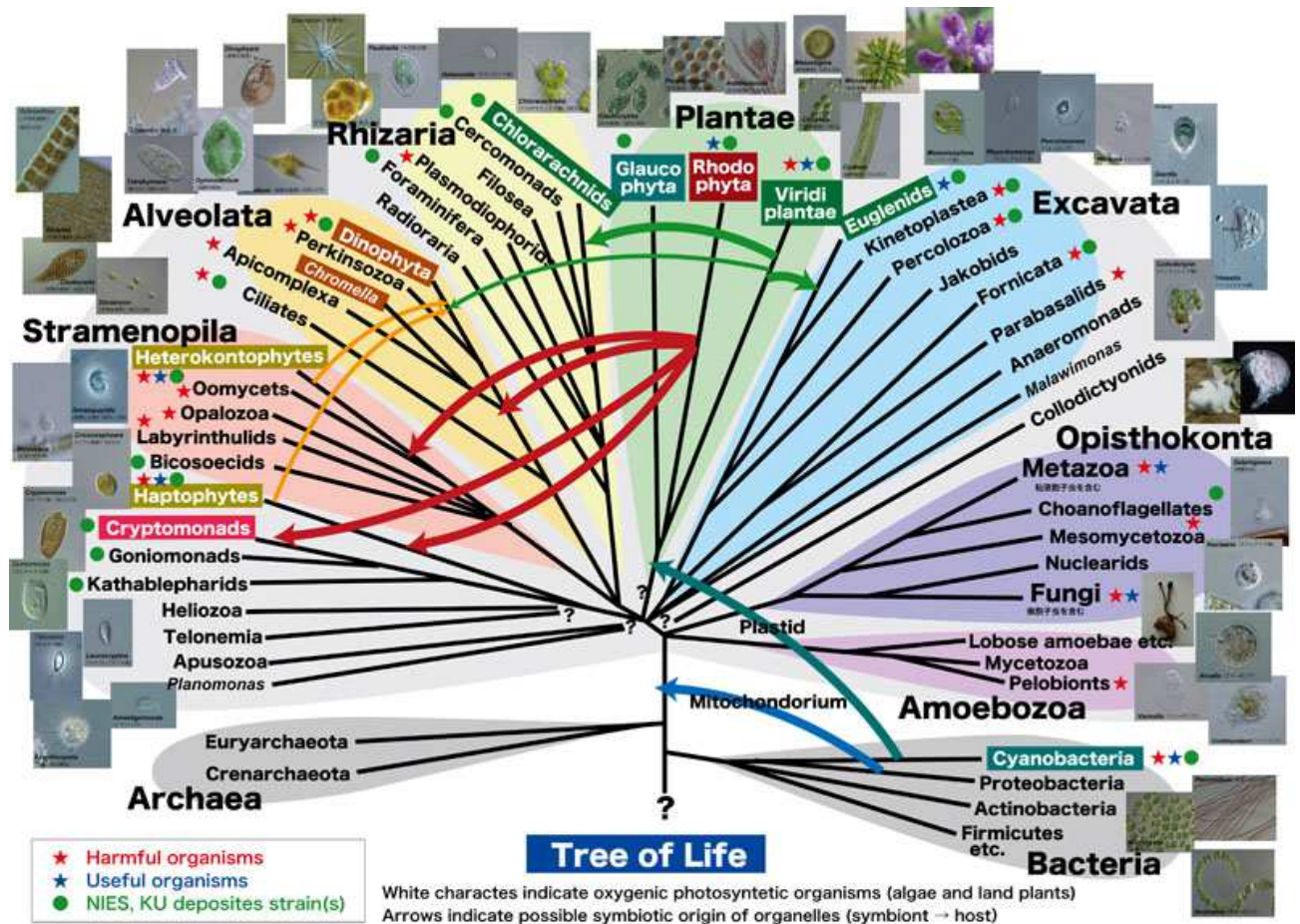


Figure 8 : Photosynthetic species in the tree of life represented in white Characters [31].

This amazing diversity is very hard to perceive and to estimate; we are still in the infancy in the field of microalgae phylogeny. But this high diversity is promising for the microalgae biotechnology. However, each strain has its own specificities and the technology associated must be adapted to the strain used.

IV2) Culture constraints

In algae and plants, carbon assimilation into cells is performed by photosynthesis. This complex process enables the conversion of light energy (photons) to chemical energy (ATP and NADPH), further used by the cell to synthesize organic carbon from inorganic carbon (CO₂). CO₂ and light supplies are thus paramount during the autotrophic growth of algae. The reactions involved in photosynthesis are further explained in Chapter 2.

IV2a) Light supply

Microalgae growth strongly depends on light supply; one of the main concerns is that the light distribution in the culture is not homogeneous, light is indeed self-attenuated by the biomass. Therefore the light collected during a given period by a cell depends on many parameters: light irradiance at the surface of the reactor (μmol/m²/s), culture density (number of cell/mL), cell optical parameters [32] (optical section, refraction/absorption index, etc...), cell position in the reactor, degree of mixing, as illustrated in Figure 9. The critical irradiance G_c is the value under which the light supply is insufficient for prokaryotic cells to grow [33]; respiration then exceeds photosynthesis, leading to a reduction of the organic content of the medium (if any) and of the cells.

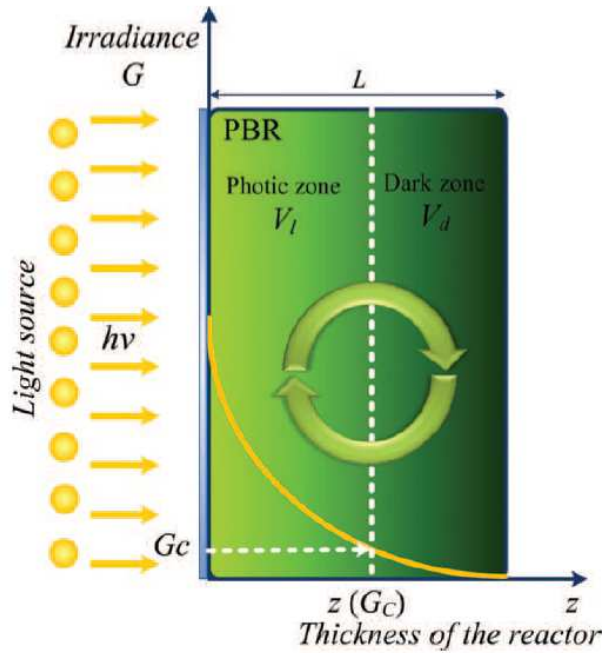


Figure 9: Irradiance distribution in a reactor [33]

Individual algae cells develop large antenna pigment complexes to absorb a maximum of photons [34–36], as illustrated in Figure 10. Consequently, most of the available light is absorbed by the cells close to the illuminated surface that can then easily absorb energy beyond their photochemical capacity. This phenomenon leads to three problems (i) an excess of excitation in the superficial cells leading to oxidative damage and photo-inhibition (mortality, growth rate reduction, degradation of sensitive compounds), (ii) a photoprotective mechanism, Non-Photochemical Quenching (NPQ), in these cells, resulting in energy dissipation into heat (up to 80 %) [37,38] and (iii) a shading effect to the cells far away from the light source, photo-limitation.

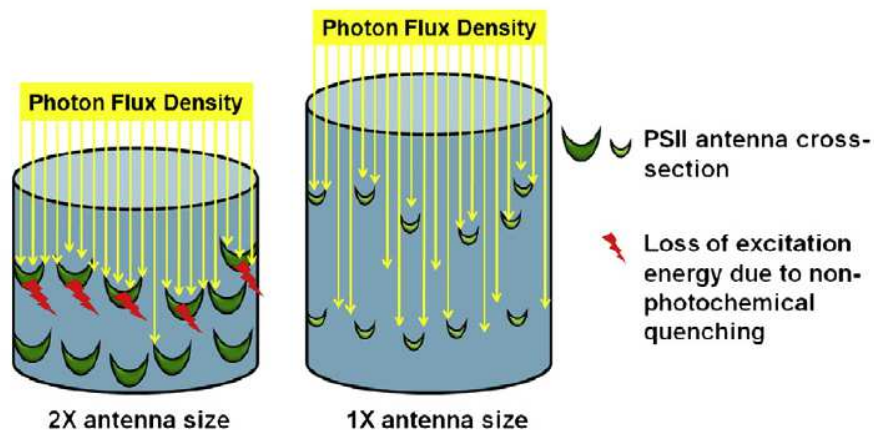


Figure 10: Antenna size influence on light transfer, and problem associated [36]

As a result of light distribution in the volume, the culture can be divided into different zones according to the light regime of the cells: light inhibition, light saturation (maximum growth rate), light limitation and no cell growth (Figure 11).

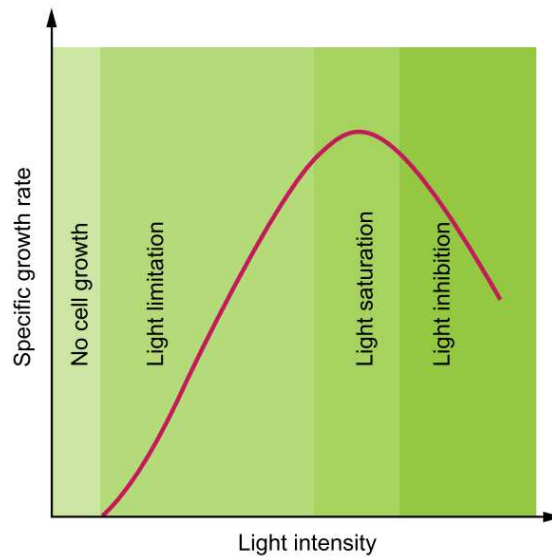


Figure 11: Effect of light intensity on photoautotrophic growth of photosynthetic cells [39]

During a batch culture, a dark zone appears at a certain distance z to the illuminated surface when the cell concentration is too high (Figure 9); in this zone the irradiance is lower than its critical value $G_z < G_c$. This leads to a reduction in the biomass productivity in the reactor and thus requires a periodic harvest of the cells to maintain a reasonable biomass concentration and then a high productivity. For a continuous culture, a good solution is to harvest continuously the biomass produced when the light regime is optimal (no dark zone and low light inhibition), to maintain an optimal cell concentration in the bioreactor.

In addition to this difficulty concerning the crucial relation between light regime and biomass productivity, daily and seasonal irradiance variations in natural conditions must be considered. These unavoidable variations increase the difficulty to manage both photo-inhibition and photo-limitation efficiently in order to optimize the biomass productivity.

IV2b) Temperature and pH

As mentioned previously, the light saturation regime leads to a significant dissipation of energy in the culture; in addition, water strongly absorbs infrared waves [40], also leading to heat dissipation. Temperature can then highly increase leading to undesirable effects; it is thus important to control and maintain this parameter at the optimal value of the cultivated strain (Figure 12). In the case of natural conditions, the strain must therefore be carefully selected according to the geographical position of the cultivation system in order to limit energy consumptions (cooling down or heating the culture). Most of algae strains are mesophiles, *i.e.* growing at temperatures within the range of 15 to 50°C. Psychrophiles optimally grow below 15°C; some snow and ice algae even grow at 1°C, for example *Chlamydomonas nivalis* in Figure 13. As for thermophiles the culture temperature must be higher than 50°C and for hyperthermophiles above 80°C. Microalgae may live in very high or low pHs media (Figure 14), in fresh and salty waters, even in high saline conditions as *Dunaliella salina* (up to 3 M NaCl) (Figure 15) [41].

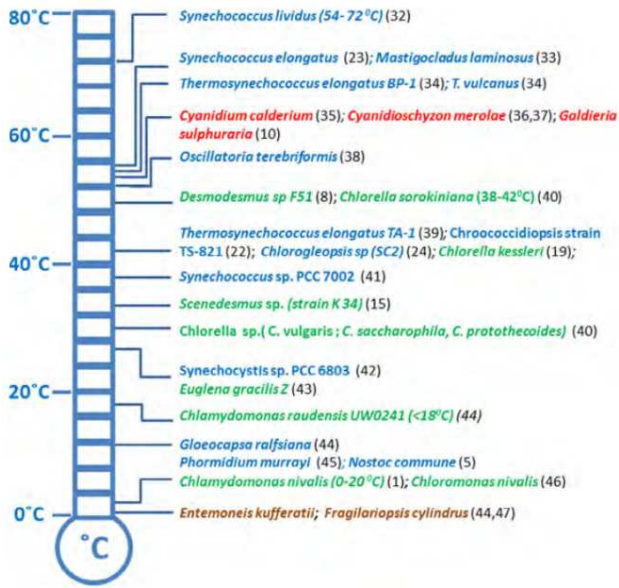


Figure 12: Optimal growth temperatures for representative microalgae. Red algae are indicated in red, green algae in green, cyanobacteria in blue, and diatoms in brown. (The number inside parenthesis indicates the reference number from the original article [41]).



Figure 13: *Chlamydomonas nivalis*, a green algae that can grow in ice and snow. When subjected to high light, the algae produces high contents of carotenoids (astaxanthin)[42]. Also commonly referred as 'watermelon snow' or 'blood snow'.

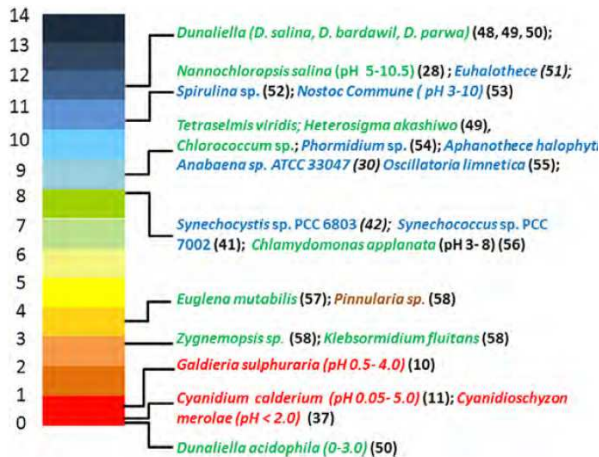


Figure 14: Example of known pH limits for representative acidophilic, mesophilic and alkaliphilic algae and cyanobacteria [41].



Figure 15: Algae bloom of a halophilic, alkaline green algae: *Dunaliella salina* [43]

A strain already adapted to the specific environmental conditions, temperature, pH and salinity, can be cultivated in open conditions. In addition, using extremophilic strains prevents contaminations as few species are able to grow in these conditions.

IV2c) Nutrients

Dissolved inorganic carbon (DIC) must be present in the medium for microalgae growth. The production of 1 kg of dry algal biomass requires 1.83 kg CO₂, which can readily be obtained from industrial flue gases *via* bio-fixation [44]. Carbon is indeed the main element of the biomass,

representing approximately 50 % of the dry weight. In autotrophic cultures, it can be provided as soluble inorganic salts (HCO_3^- or CO_3^{2-}) or as gaseous CO_2 .

In an open culture, the liquid culture is generally in equilibrium with the atmospheric air containing approximately 400 ppm CO_2 [8]. The nature of the soluble carbon species depends on pH: mostly CO_2 between pH 0 and 6, HCO_3^- between pH 6 and 10 and CO_3^{2-} above pH 10. If the culture is fed with inorganic carbon, a desorption of CO_2 from the medium to the atmosphere could occur depending on pH; covering the culture system and/or maintaining a high pH can limit this phenomenon.

The second most important nutrient is nitrogen representing from 1 to 10% of the dry weight and particularly needed for the biosynthesis of proteins and photosynthetic pigments. It is mostly provided as mineral salts: ammonium, nitrate or nitrite ions, which are easily assimilated by a majority of algae strains. Some cyanobacteria are also able to use gaseous N_2 as nitrogen source.

Moreover, many other macronutrients must also be supplied to the culture medium: Na, K, Ca, P, S, Mg, Cl as well as micronutrients: Fe, Si, Zn, Mn, Br, B, Mo, V, Sr, Al, Rb, Li, Cu, Co; I, Se and vitamins.

As mentioned previously, each strain has its own optimal pH. But photosynthesis leads to an increase in pH due to CO_2 consumption; gaseous CO_2 can be added to the culture to maintain its pH at the optimal value.

IV2d) **Mixing**

An efficient mixing of the culture is generally paramount to meet the requirements mentioned above (easy transfer of micro and macronutrients, homogeneity in pH...) and limit the negative phenomena (thermal stratification, dark zones for some microalgae...). But mixing generally requires high energy amounts and the shear stress induced by agitation can affect the cells viability [45].

For choosing the mixing system (mechanical agitation, gas spraying, pumping system), different parameters must be taken into account: (1) the shear stress sensitivity of the strain, (2) the mixing efficiency (residence time, dead zones) and (3) the energy cost.

IV3) **Culture systems**

IV3a) **Open illuminated systems**

The largest (considering the surface) culture systems nowadays are extensive open systems (also referred as open ponds). Temperature is regulated by natural evaporation; CO_2 is supplied by atmospheric air and there is no agitation (Figure 16). The investment costs are then minimal and the energy cost negligible. They generally can only be used for extremophilic algae strains, able to grow in harsh conditions (e.g. *Dunaliella Salina* which can grow in high salinity cultures).



Figure 16 Hutt Lagoon in Australia is a natural salty lake, with 250 ha of artificial ponds used to farm *Dunaliella Salina*, a carotenoid producing algae.

Many other open artificial bioreactors for algae culture are available but the most commonly used is the "raceway reactor" also called "raceway pond", in which agitation is generally ensured by a paddlewheel. Examples of raceways are illustrated in Figure 17 and Figure 18. Aside from open ponds this technology is the easiest and cheapest to cultivate algae cells. The reactor is either excavated in the ground, the bottom being covered by an impermeable material, or built in plastic or cement above the ground. The most common values for the pond depth are between 0.1 and 0.5 m [46]. Mixing is performed by a mechanical rotating device, usually a paddlewheel, giving a liquid velocity between 0.15 and 0.25 m·s⁻¹, which prevents cells sedimentation. To optimize gas-liquid transfer and satisfy the CO₂ requirements, the raceway is generally equipped with submerged aerators.

Raceways



Figure 17: *Dunaliella salina* and *Spirulina platensis* cultivated in raceways, Cyanotech Hawaii[47]



Figure 18 Partially covered raceways for microalgae cultivation at Ourofino Agronegocio, Brazil [48]

However open cultivation technologies lead to serious problems, such as lower volumetric productivities compared to closed systems (0.1 compared to 1.5 kg·m⁻³·day⁻¹), water evaporation through the open surface and contaminations [49]. Many studies were performed to model and/or to follow the productivity of an algae during a given season [50–52] and to optimize the pond design in terms of hydrodynamics [53–56], thermal behavior, solubilization of CO₂, nutrient supply, etc... As

shown in Figure 18, raceway reactors may be partially covered with a transparent plastic material to limit evaporation and contaminations.

IV3b) Closed photobioreactors

Multiple reactor designs were developed to face the drawbacks of the raceways: low productivity, high contamination risks, high evaporation. The diversity of design is so large that it cannot be listed exhaustively in this report, but for a large scale production, two main designs are encountered: flat panels reactors and tubular reactors (vertical or horizontal).

Panel photobioreactors are flat, transparent vessels made of glass, plexiglass, plastic or other transparent materials. The mixing of the culture is carried out directly by air bubbling; air is introduced *via* a perforated tube at the bottom of the reactor [49]. Flat panels are never thicker than 5-6 cm, otherwise the light entering the panel would not penetrate into the heart of the culture. Vertical reactors result in the dilution of direct sunlight and a reduced illumination *via* shading effects, as illustrated in Figure 19.

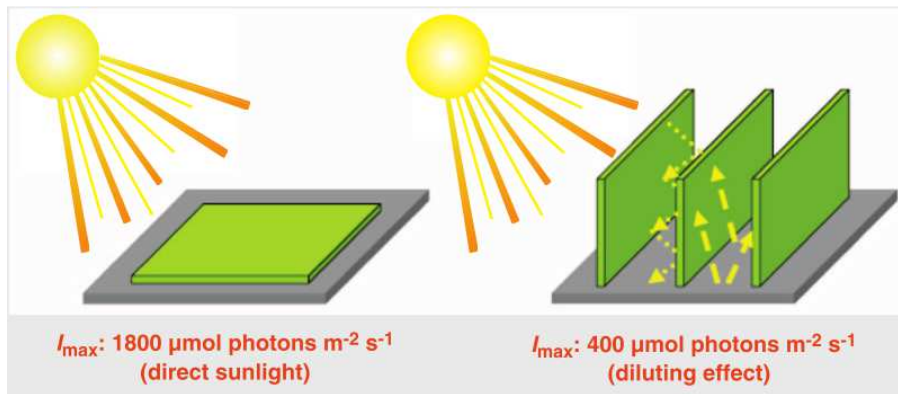


Figure 19 Shading effect of vertical panels[27]

Tubular reactors, as flat panels, are made of transparent material with a limited diameter in order to reduce light gradients. Agitation is provided by an air pump.

The main advantage of these closed systems, compared to raceways ponds, is the large surface to volume ratio which enables a better control of the light intensity supplied to the culture. Contaminations are also minimized and the cultivation conditions (pH, temperature, CO₂ concentration, mixing intensity and nutrient level) can be more easily controlled to suit the optimal growing conditions of microalgae strains, in contrast with open systems.

An example of a vertical tubular reactor is illustrated in Figure 20; the shading effect between the vertical structures can be seen. A large production facility of carotenoid pigments in horizontal tubular reactors is presented in Figure 21. In this case, the high illumination from direct sunlight is aimed to induce accumulation of carotenoid pigments in *Haematococcus pluvialis* cells in response to a light stress. The energy required for the agitation in this system is high because of the great length and small radius of the tubes. In addition, cooling is performed by spraying demineralized water on the tubes. The important cost of the process is however counterbalanced by the high value of the pigments extracted from the algae.

Among the various possibilities, some examples of flat panels are presented in Figure 22 and Figure 23. Like a photovoltaic panel, the reactor of example 22 can be inclined to face the sun all along the day or in some cases be positioned at particular angles to get an optimal irradiance. The Figure 23 presents a system of vertical flat panels surrounded by water in a plastic bag. This original solution enables to control the algae culture temperature night and day.

Tubular reactors



Figure 20 Vertical photobioreactors for microalgae cultivation [57]



Figure 21 *Haematococcus pluvialis* cultivation via horizontal tubular reactors in Israel [58] for astaxantin production (red pigment)

Flat panels



Figure 22 Flat panel reactor on the roof of a building in Saint Nazaire, France [59]



Figure 23 Flat panels immersed in water in Algae parc, Wageningen University, Netherlands. [60]

For the production of large market scale and low cost products such as oil for biofuel, the choice of the bioreactor type must be focused on a single criterion: the balance between the energy consumption for production and the potential energy production associated with biomass. This criterion is generally estimated via the NER indicator: Net Energy Ratio, defined as the ratio of total energy input and output, where a ratio lower than 1 denotes a positive energy balance and vice versa [48] (in some articles the Energy Efficiency Ratio is defined as the inverse: total energy output vs total energy input).

It is interesting to compare NERs for oil produced by crops and by microalgae. For oil bearing crops, despite their low surface productivity, NER is always significantly lower than 1 (between 0.7 and 0.2) for the whole process: feedstock cultivation, harvesting, seeds drying, oil extraction (mechanical pressing/enzymatic extraction/solvent extraction) and generally transesterification to obtain Fatty Acids Methyl Esters (FAMES) and glycerol [12]. For algae production however, NER is hardly below 1 (Figure 24). On current knowledge, raceway ponds are more energy efficient than closed systems [61]. Even if closed systems exhibit lipid surface productivities 10 to 20 times higher than raceways [62], the energy consumption for agitation in closed systems drastically increases the NER indicator. Indeed, decreasing the light path of photobioreactors while increasing mixing (turbulence) in high cell density cultures requires a high energy input; this bioreactor type is therefore not recommended for large-scale production of biofuels from microalgae [44,48].

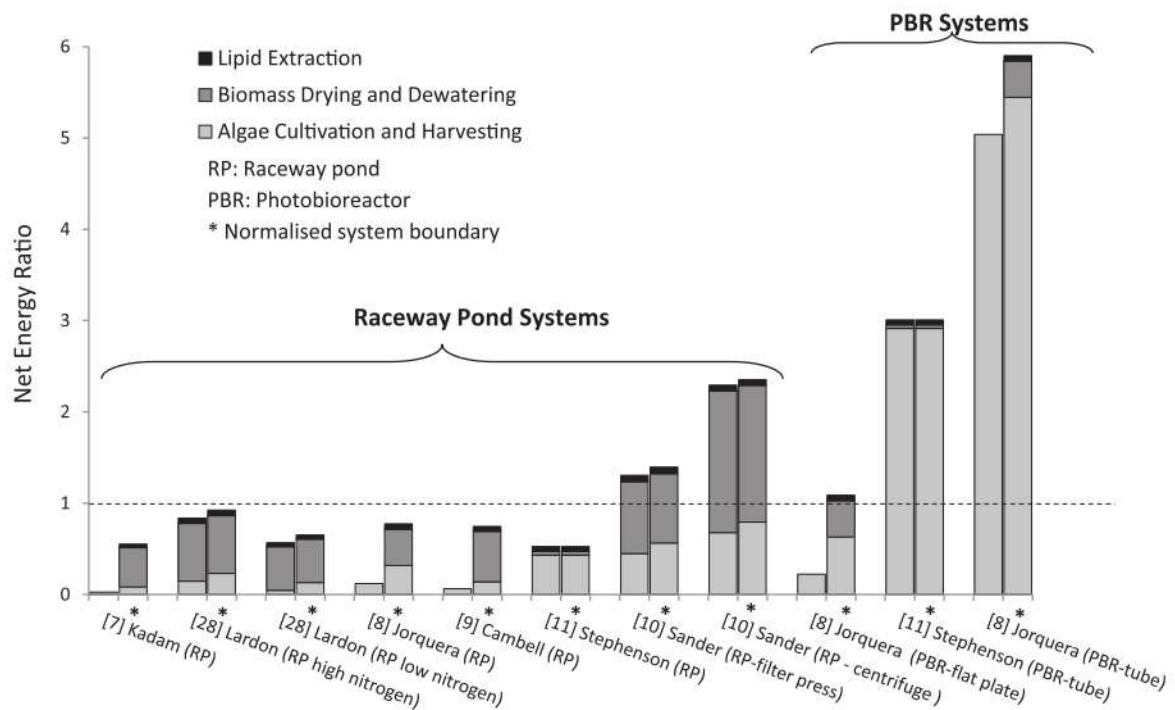


Figure 24: Net energy ratio for micro-algae biomass production (The NER is defined as the sum of the energy used for cultivation, harvesting and drying, divided by the energy content of the dry biomass) [61]

But when the biomass lipid content increases, along with its energetic value, the NER indicator is decreased [63]. Finally an additional valorization of biomass wastes after lipid extraction by other energetic processes (*e.g.* anaerobic digestion of microalgae residue) may drastically reduce the NER value [64]. But thanks to many active researches, future technological progresses in managing energy consumptions in closed photo-bioreactors will without any doubt improve the energy efficiency of these systems.

As illustrated in Figure 24, for raceway systems, algae harvesting and dewatering/drying steps represent the major part of the process energetic cost; this is due to the generally low biomass concentrations of the cultures (less than 1 g/L), leading to the elimination of huge water amounts. On the contrary, for very intensive PBR systems in which the biomass concentration can reach up to 10 to

20 g/L (thanks to a high illuminated surface to volume ratio, an optimized cooling system, a good mixing, a satisfactory CO₂ supply etc...), the dewatering step represents a minor part of the high production cost.

Two alternative algae growth systems must also be covered in this report: (i) **heterotrophic cultures** and (ii) **biofilms cultures**.

IV3c) **Heterotrophic and mixotrophic cultures**

In heterotrophic systems, algae grow in the absence of light, using their respiration metabolism (Figure 25). The fixation of gaseous CO₂ in the case of autotrophic cultures is replaced by external organic carbon sources (e.g. glucose, acetate, glycerol, fructose, sucrose, lactose, galactose, mannose) [65].

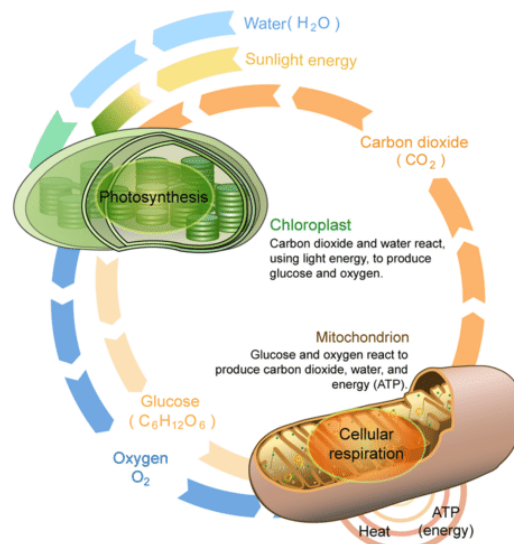


Figure 25 Photosynthesis and cellular respiration [66]

Even in autotrophic cultures (no organic carbon supplied to the culture), respiration occurs during night and even in day light for highly concentrated cultures. Mitochondria enable the cell to create ATP energy from the degradation of organic carbon stored in the cytoplasm (carbohydrates or lipids) [67]. The reactions involved in respiration and photosynthesis are further detailed in Chapter 2.

Mixotrophy is a combination of autotrophic and heterotrophic cultures, in which CO₂ and external organic carbon are simultaneously assimilated. This provides two important advantages: (i) it leads to much higher biomass concentrations compared to autotrophic cultures (ii) existing technologies (fermenters and centrifuges) can be used [65].

These hetero or mixotrophic culture systems however exhibit many major drawbacks: (i) increasing costs with the use of organic carbon as nutrient, (ii) high risk of contamination and competition with other organisms, (iii) limitation to specific algae strains, (iv) inability to produce light-induced metabolites [65] and (v) production of CO₂.

IV3d) **Biofilm cultures**

Biofilm cultures are alternatives to suspension-based culture systems; they are characterized by an accumulation of biomass on a solid surface. This mode of cultivation has a strong advantage in comparison with suspended cultures, as the harvesting step is greatly facilitated; the biofilm attached to the surface has indeed a high solid content of 10 to 20 % and can be easily harvested by scraping [68,69]. An example of biofilm culture is illustrated in Figure 26.

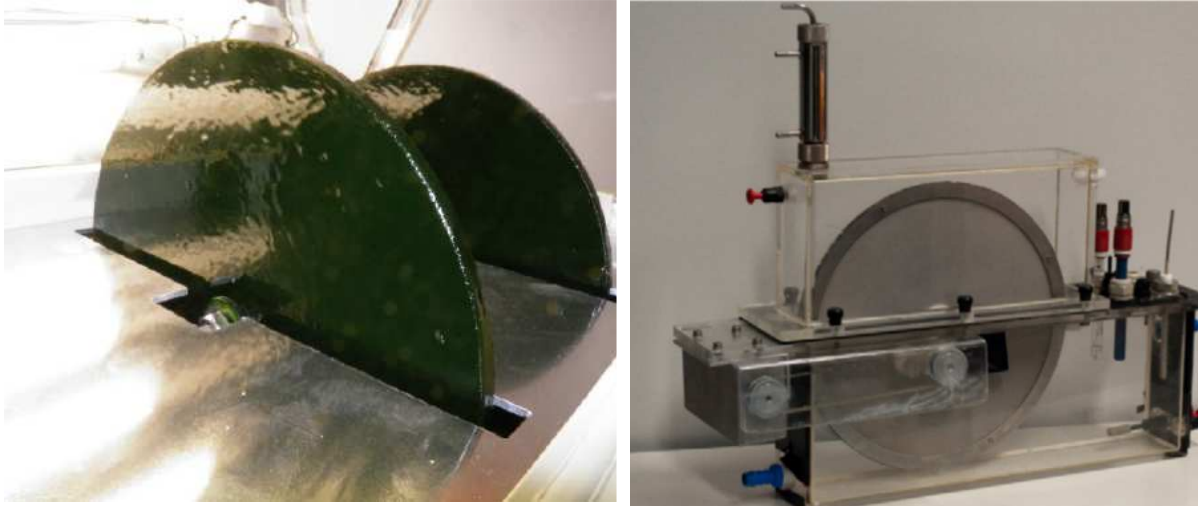


Figure 26 Biofilm growth on a rotating disk. Disks are partially submerged in a medium [69,70]

In addition, in this type of culture, the amount of water required is strongly reduced. But there is still a significant lack of understanding of CO₂ transfer and light penetration across the biofilm [68]. However, a few recent projects showed promising results of this process as an alternative to classic suspended cultures. Further researches however need to be carried out to test different attachment materials and strains, and to estimate the economic feasibility of this process at large scale [68].

IV4) **Harvesting/Extraction methods in suspension cultures**

IV4a) **Harvesting**

Harvesting, also referred as dewatering or drying, is the separation of the biomass from the culture medium. The cost is significant because microalgae grown in open cultivation systems are relatively diluted (*ca.* 0.1 to 3 g.L⁻¹) [71]. In addition, unicellular microalgal cells are very small, with a diameter usually lower than 20 µm, sometimes even under 5 µm.

The different harvesting methods are summarized in table 2.

Table 2: Algal biomass harvesting methods (modified from [48]).

Harvesting Method	Process description	Advantages	Disadvantages
Centrifugation [72]	Governed by Stokes' Law: Sedimentation of suspended solids is determined by density and radius of algal cells. Concentrated algal biomass can be obtained. Centrifugation force: 5,000 - 10,000 g with 95% removal efficiency.	Rapid and efficient	Energy intensive and high maintenance cost
Flocculation [73–79]	To aggregate the algal biomass to a larger size and hence ease sedimentation. Coagulants used: ferric chloride (FeCl ₃), aluminium sulfate (Al ₂ (SO ₄) ₃ , alun) and ferric sulfate (Fe ₂ (SO ₄) ₃). Normally used as a pretreatment step to centrifugation, gravity sedimentation, or filtration.	Cost effective	The algal biomass cannot be used for some downstream applications such as animal feed or anaerobic digestion because of flocculants toxicity. Some bio-based flocculants/coagulants may be used as an alternative but are more expensive.
Dissolved air Flotation [80]	Trapping algal biomass by dispersing micro air bubbles. The fine bubbles (less than 10 µm) adhere to the biomass (after flocculation process) and lift them to the surface.	Applicable to large volumes of biomass	Toxicity of flocculants may reduce algal biomass value. Flocculation is indeed necessary to apply this method. Some bio-based flocculants/coagulants may be used as an alternative but are more expensive.
Filtration [81–86]	Press and membrane filters are operated under pressured or vacuum conditions.	Filter press: Effective in recovering algae of relatively large size (e.g., <i>Spirulina platensis</i>) Micro/ultrafiltration (membrane filters) : Effective in recovering both large and small algae.	Filter press: Ineffective to recover small algae (e.g., <i>Scenedesmus</i> and <i>Chlorella</i>) Micro/ultrafiltration: High cost due to membrane replacement (membrane clogging), and maintenance.
Gravity sedimentation	Governed by Stokes' law: Sedimentation of suspended solids is determined by density and radius of algal cells. Algae are left to settle naturally by means of gravity. The cell density evolves with its content: a high lipid content reduces cells density.	Low cost because no additional chemicals or physical treatment needed, no energy consumption.	Requires relatively high settling times Not effective for small algae
Drying (solar drying, roller drying (Figure 27), spray drying, freeze drying) [87]	Thermal process to induce water evaporation facilitated by an increased surface to volume ratio.	Low moisture content in the final product	Denaturation of organic compounds for high temperature conditions.

<p>Electrophoresis techniques [88]</p>	<p>Form aggregates induced by an electric field generated by two or more electrodes. The negatively charged microalgal cells are attracted to positive electrodes where upon contact, they are neutralized and form aggregates (electrolytic flocculation). This phenomenon can be used as "Electrolytic coagulation" with reactive electrodes that releases coagulants (iron or aluminium hydroxide). Electrolytic flotation performed via cathodes of inactive metal that generate hydrogen bubbles from water electrolysis.</p>	<p>Low energy and no release of contaminating flocculants [89] in the case of electrolytic flocculation.</p>	<p>Electrodes need to be replaced periodically.</p> <p>High energy (in the case of electrolytic flotation)</p>
---	--	--	--

Centrifugation is broadly used, it is the most rapid and reliable method of harvesting suspended algae. However, as stated by the U.S. Department of Energy, at the current state of the centrifugation technology, this method is cost-prohibitive for large scale uses [90].

Lower energy consuming processes (0.1 to 1 kWh/t of water evaporated) are generally used to make a first concentration to 1 to 5 % w/w; a second concentration step (centrifugation, filtration or drying) allows to obtain an algal paste/powder of above 15 % w/w by [71].

Some systems are especially developed to face the problematic of algae dewatering. An exemple among the solutions is presented in Figure 27, referred as "roller drying". At the entrance of the system, algae are pre-concentrated before being spread on a large surface and rolled to dry them to a powder with a reduced energy consumption.



Figure 27: Solid liquid Separation pilot model dewatering microalgae from Algaeventure systems (roller drying)

After harvesting the biomass, a disruption step is generally needed to separate the intracellular valuable compounds (lipids, pigments, proteins) from the cell wall. Many methods are used and are usually classified between physical and bio-chemical processes.

IV4b) Physical processes of extraction

The physical processes aim to break the wall of the cells and/or permeabilize their membrane: different types of technology are described below:

Expeller pressing is a classical method used to extract oil from raw materials, which are squeezed under high pressure. In the case of algae, it is highly recommended to dry the cells before this type of process.

Bead milling (or mixer milling) [91,92] uses a homogenizer containing beads, originally designed for size reduction of paint or lacquer particles [92]. It was proved to be a powerful technique for the mild disintegration of microbial cells and microalgae by frequent collisions or frictions with the beads. The dispersion system consists of a milling chamber and a mechanical agitator; the milling chamber is filled with grinding beads (glass, zircon oxide, steel...) and the product to be fractionated. This method requires an expensive cooling system to prevent the thermal degradation of the target products [93], increasing the global cost.

High pressure homogenization also known as French pressing is a cell disruption process in which a flow is sprayed at a high hydrostatic pressure (at least 100 MPa) into a restriction tube. At this high pressure, shear stress, cavitation, turbulence, impingement and temperature increases are observed [94] leading to a very high disruption efficiency.

Microwaves: A dielectric or polar material placed in a rapidly oscillating electric field, such as that produced by microwaves (approximately 2450 MHz [95]), generates heat because of the frictional forces arising from molecular movements [96]. Intracellular heating results in the formation of water vapor, leading to permeabilization of the membranes and micro-cracks in the cell walls. The drawbacks of microwave processes are the degradation of thermo-sensitive chemicals and the high energy cost.

Ultrasonication: when ultrasounds radiate in a liquid medium, two main mechanisms lead to the impairment of the cells or other structures: cavitation and acoustic streaming [97]. Cavitation is the production of microbubbles due to the applied ultrasounds. As the microbubbles continue to expand, they eventually become unstable and implode violently. Bubbles explosion is sending shock waves that disrupt surrounding materials such as cells. Cavitation effects are more intense at low frequencies (18 to 40 kHz) than at high (400 to 800 kHz). Ultrasonic cavitation is affected by the liquid viscosity and its temperature. Because temperature rapidly increases with heat dissipation, the medium must be cooled down continuously for a maximal efficiency. In addition, the release of free radicals from the breakdown of water molecules may degrade the oil quality. Ultrasound can also be used in the presence of an organic solvent, the process is named **ultrasound-assisted extraction (UAE)** [98–100]; ultrasounds enhance the solvent transfer through the cell wall thanks to the collapses produced by cavitation.

Pulsed electric fields (PEF), also referred as electroporation or permeabilization, is a process using short or high voltage pulses generated by two electrodes placed in the medium. The generated electric field leads to a displacement of charges in and outside the cells. This phenomenon indirectly increases the charge gradient across the cell membrane (trans-membrane potential) which leads to the spontaneous formation of aqueous pores in the membrane lipid bilayer [101]. According to the treatment parameters, the pores can either reseal in several milliseconds or be irreversible. The process can generate heat in the medium depending on its parameters. The effects on cell wall is still very few studied but works suggest that it may be weakly affected by non-thermal electroporation [102] (treatment leading to a low temperature increase).

Mesoporous Silica Nanoparticles (MSN) is a novel technology using mesoporous nanoparticles to selectively extract and sequester target fuel-relevant and high value compounds within the algae

mixture. These 10 nm particles present pores with various surface functional groups and are used for example for sequestration of FFAs [103,104].

IV4c) **Chemical processes of extraction**

The chemical processes aim to dissolve the microalgae cell wall and/or permeabilize the cell membrane by addition of chemicals, to separate polar and non-polar contents by hydrophilic/hydrophobic affinities.

Osmotic shock or osmotic stress: leads to cell disruption through a sudden increase or decrease in the salt concentration of the liquid medium, which disturbs the balance of osmotic pressures between the interior and the exterior of the cell [93]. This effect causes the creation of numerous pores and a rapid change in the movement of water across the cell membrane leading to a permanent cell disruption. Most of the studies are performed with hyper-osmotic shocks by increasing salt concentration in the medium. When coupled with solvent extraction, it allows increased extraction yields, especially for wall deficient strains [105].

Enzymatic treatment: consists in using various enzymes to digest and thus weaken the microalgae cell wall. As the algae wall is composed of a complex polysaccharide and glycoprotein matrix [106], specific enzymes able to degrade its components are available, without damaging the sensitive chemicals inside the cytoplasm. The critical drawback of this method is the high cost of these enzymes [93].

Solvent extraction: extraction of algal oil by organic chemicals. Benzene and ether have been widely used, along with hexane which is relatively cheap. In a Soxhlet extractor, the algal sample is continuously in contact with fresh solvent, but the solvent amount is still limited thanks to recycling (successive evaporation and condensation); the extraction of lipids can be then highly efficient [93]. However, this process is energy consuming and its scale up is difficult. And the principal downside of solvents is the potential hazard related to their use: the majority of them are indeed highly flammable, harmful and dangerous for environment.

Pressurized liquid extraction (PLE), also known as accelerated solvent extraction (ASE), is a method that enhances extraction by using compressed supercritical solvents at high temperature: lipid recovery increased from 37.6 % to 69.6 % when heating a mixture of limonene and ethanol (1:1, v/v) from 50°C to 200°C at 20.7 MPa [107]. In comparison with the Soxhlet method, PLE exhibits a higher yield, a higher extraction rate and a lower solvent consumption [93]. Carbon dioxide (CO₂) is the most common solvent used to extract bioactive compounds from natural sources; it indeed has interesting properties for bioactive extraction: (i) cost efficiency, (ii) critical conditions easily attainable, (iii) environmentally friendly solvent [108].

Conclusion: Determining the most efficient and cost effective extraction method is paramount to maximize the ratio “lipids recovered per spent energy”. The high elasticity of cell walls and membranes reduces the efficiency of pure mechanical methods. Besides, even when free water is removed, the wet biomass retains interstitial water which hinders lipid extraction by organic solvents and, acting as a lubricant, decreases the effectiveness of mechanical methods. It seems then to be interesting to couple different methods to favor lipid extraction.

V. Key points for future viability of algae-derived biodiesel

The current autotrophic production of algae for biofuel is still clearly at pilot - early demonstration scale. Companies are not yet able to commercialize algae derived biofuel because of high costs associated with culture, harvesting and extraction steps and with the variability of productivities due to weather variations [109,110] and contamination issues. Several steps of the process must be improved before large scale production of algal oil: algae culture, mixing and thermal regulation (to reduce energy demands), gas supply, harvesting and extraction.

v1) Current economic review

Several universities are developing in the frame of public-private partnerships research platforms to compare and optimize different processes at pilot scale. We can mention as an example the R&D Algosolis platform in Saint-Nazaire, France (Figure 28), Algae park in Wageningen University, Netherlands (Figure 29), or the platform of Arizona State University (Figure 30). In addition sustainability and economic feasibility of algae-derived biodiesel production using current technologies are evaluated by numerous research programs.



Figure 28 Algosolis platform, Saint-Nazaire, France [111]



Figure 29 Algae park facility, Wageningen, Netherlands [112]



Figure 30 Arizona Center for Algae Technology, Arizona state, USA [113]

The production of such facilities remains negligible in term of volume and the processes are not yet economical for biofuel production. The current state of productivities, costs and large scale requirements of water and nutrients is detailed below.

In a photosynthetic system, 8 photons of photosynthetically active radiation (*ca.* 48% of the incident solar flux) are required to fix one molecule of CO₂ into carbohydrate form - thus resulting in a maximum photosynthetic efficiency of 12 % (fraction of light converted to chemical energy). However, under real and essentially favorable conditions (*i.e.* low to moderate light levels), **the photosynthetic efficiency reported actually ranges of 4.5 to 7 % in ponds and close photobioreactors**, respectively; in the former case, this corresponds to a **yield of 30-40 g_{dry biomass} m⁻² d⁻¹** [44].

Finally, the annual yield of algal crops generally ranges from 50 to 150 tons of dry biomass per hectare [63]. However, because a high lipid content and a high growth rate correspond to significantly different culture conditions (see Chapter 2), the **inverse relationship between the lipid content and the cell growth rate reduces the total amount of oil produced annually**. The sensitivity of the biodiesel production cost to key input parameters decreases in the following order: algae oil content > algae annual productivity per unit area > plant production capacity > carbon price increase rate [63]. **Despite the higher surface productivities of algae in comparison with food crops, the cost of oil production from algae (in the range of 2.4 to 6 US\$/L [114], illustrated in Figure 31) greatly exceeds the price of biodiesel, which was below 1 US\$/L beginning 2015.**

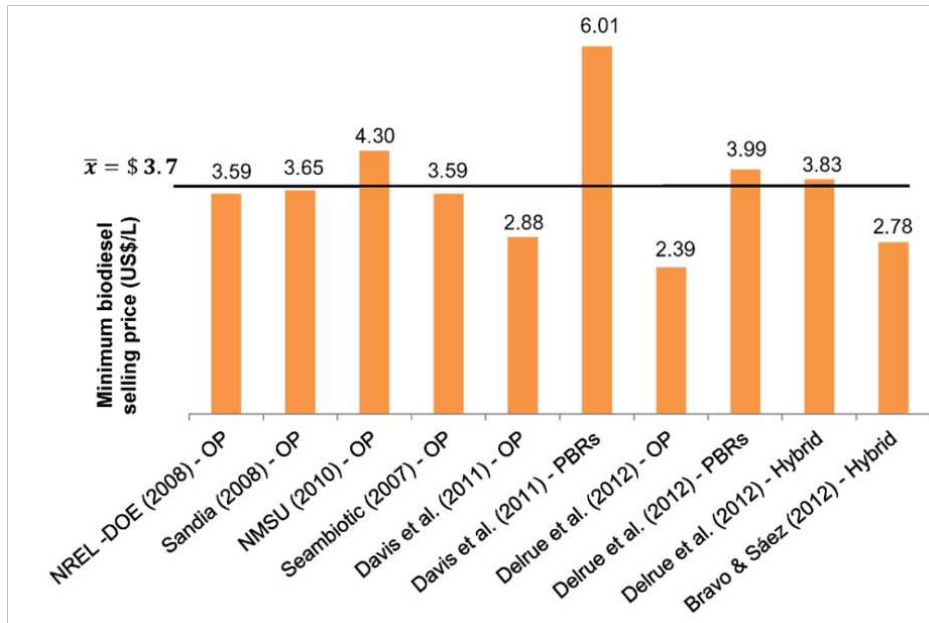


Figure 31: Estimation of the minimum biodiesel derived from microalgae selling price from [114]. OP is open ponds, PBRs refers to Photobioreactors, Hybrid is a mix of OP+PBRs.

Also, using current algae productivities, **9.25 million ha** (almost the surface area of Portugal) **would be required to supply the European market**, assuming a productivity of 40,000 liters per ha per year [44]. This surface seems unrealistic, but this is still much lower than the surface required if conventional land crops were used to supply the European market of fuel (Oil palm: 5,950 liters per ha per year, see Table 1). This productivity is based on a 3 % solar energy conversion to biomass and a biomass oil content of 50 %, under the solar conditions of Portugal.

In addition, a total of **1.8 tons of CO₂ is needed to produce 1 ton of algal biomass**, which means that 1.3 billion tons of CO₂ would be required for the production of 0.4 billion m³ biodiesel to supply the European transportation market [27]. Many studies are performed to use flue gas as a CO₂ source but the biggest difficulty is the purification of the fumes, as they should be free of growth inhibitors and toxic chemicals. Bio-mitigation of CO₂ emissions provides a complementary function that may be exploited to reduce costs and enable a sustained utilization of microalgae as a biofuel resource [115]. As the algae biomass contains 7 % nitrogen and 1 % phosphorus [44], **25 million tons of nitrogen and 4 million tons of phosphorous would be needed, which is about twice the amount of fertilizers produced in Europe**. For sustainable production of biodiesel from microalgae, it will be important to

use residual nutrient sources (about 8 million tons of nitrogen in Europe) and to recycle nutrients as much as possible. Besides Barbosa and Wijffels [116] estimate there is a need of roughly **3,000 L of water for 1 L of biofuel** (in comparison of 10,000 L for food crops). These high demands of substrate and water can be met by using algae for bioremediation, *i.e* for CO₂ sequestering [117] and wastewater treatment [118,119].

In a recent report, Takeshita [120] concluded that **the future viability of algae derived biofuel is strongly dependent on CO₂ stabilization constraints** which could probably be implemented to limit global warming according to two scenarios: Business as usual (BaU) with a limitation to 500 ppmv in the atmosphere or a limitation to 400 ppmv. The cost of algae production would increase in the same time as the CO₂ prices along with the stiffening of its stabilization constraints. Indeed, to supply biodiesel from algae at a very large scale, the feed might be pure CO₂ captured from stationary sources [121]. In the case of a stabilization to 400 ppmv by 2100, biodiesel and hydrotreated renewable jet (HRJ) fuel from microalgae would take a very small place in the global energy mix (Figure 32). With the current legislation (no CO₂ limitation), the model projects the start of large scale productions by 2050.

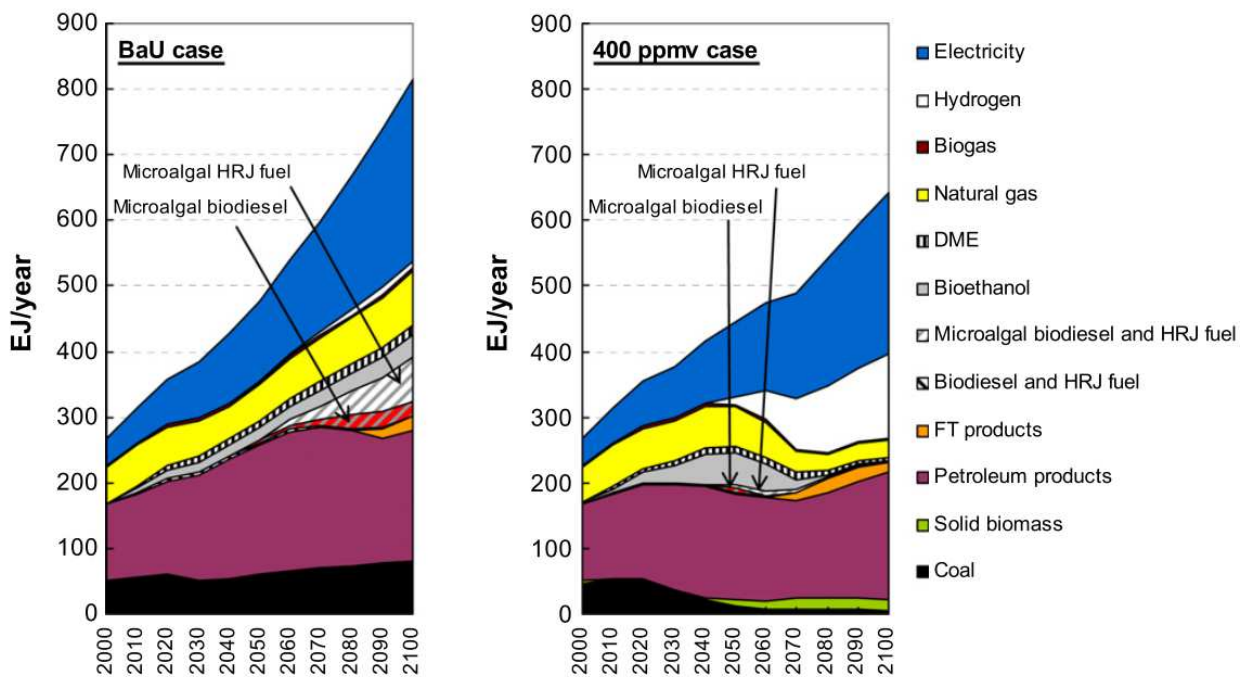


Figure 32: Part of Algae-derived microalgal biodiesel and HRJ (hydrotreated Renewable jet fuel) from algae in the case of Business as usual (BaU), or in the case of a limitation to 400 ppmv in the final energy consumption [120]. DME is a synthetic fuel: Dimethyl Ether. FT products are the Fischer-Tropsch synthetic fuels.

Nowadays, the current prices of algal technologies are too high to commercialize obulk chemicals for large markets. Worldwide microalgal manufacturing infrastructures (producing the equivalent of ~5000 tons of dry algal biomass) are limited to the production of high-value products such as carotenoids and omega 3 fatty acids used as food and feed ingredients [44][27].

v2) Biorefinery concept

The value of the biomass for biofuel production is generally evaluated by its lipid content that can be converted to biodiesel *via* trans-esterification. The valuable lipids are generally triglycerides (TAGs) and fatty acids accumulated in the cytoplasm as lipid droplets (see Chapter 2). Trans-esterification is a reaction, in which the glycerol backbone of the TAGs is replaced by methanol which esterifies fatty acids, the side chains of TAGs, into methyl esters (biodiesel). The general equation for transesterification is shown in Figure 33 [115].

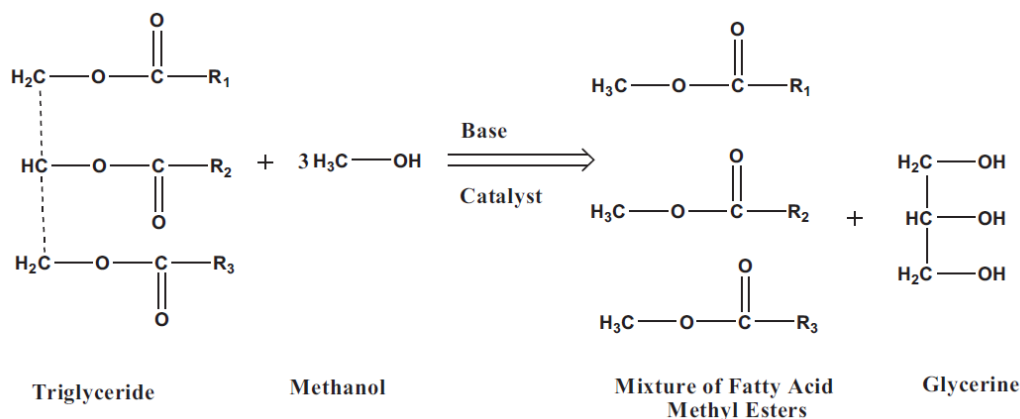


Figure 33: Base catalyzed transesterification reaction [115]

As mentioned previously, the energetic and economic value of the created biodiesel from algae may not be sufficient regarding all the costs involved during the whole cycle (see Figures 24 and 31).

A recent report evaluated that the co-production and extraction of a high value product (HVP; *e.g.*, β -carotene at 0.1 % of biomass, 600 US\$/kg) may represent the dominant revenue streams of the biomass [122]. Even if algae produce 100 times more oil than HVP on a per tonnage basis, the revenue from HVPs is about 10 times greater due to their difference in value. However, it must be noticed that HVP markets are small and easily saturable. Nevertheless, this co-production is necessary in the short term for an economic viability of algae-derived diesel. In these conditions, **a scale up of existing production plants associated with reasonable advancements in technologies, will lead to a price below 50 US\$/bbl [122], equivalent to 0.30 US\$/L, which is quite acceptable.** The list of high value products is very large: bioactive compounds such as fatty acids, carotenoids, fluorescent pigments, isotope biochemicals, drug screening molecules, *etc...* Some examples with corresponding applications and prices are listed in Table 3.

Table 3: High Value Products from microalgae [115]

High Value Products	Applications	Price (US\$)
β-Carotene	Nutritional, therapeutic, Cosmetics, Colorants, Aquaculture	300 to 3.000/kg
Astaxanthin	Colorants, Aquaculture, Nutritional, therapeutic, Cosmetics	2.500/kg
Secondary carotenoids (lutein, zeaxanthin, lycopene, bixin)	Nutritional, therapeutic, Cosmetics	
Gamma Linoleic acid (GLA)	Nutritional	

Arachidonic acid (AA)	Nutritional	
Eicosapentaenoic acid (EPA)	Nutritional	
Docosahexaenoic acid (DHA)	Nutritional	
R-phycoerythrin (PE)	Fluorescent tags, Colorants, Cosmetics, Nutritional	3.25 to 14/mg
R-phycoerythrin (PE)	Goat Anti-mouse IgC,	145/mg
Allophycocyanin (APC)	Fluorescent tags, Colorants, Cosmetics, Nutritional	6 to 17/mg
β-phycoerythrin (PE)	Fluorescent tags, Colorants, Cosmetics, Nutritional	145/mg
Sensilight PBXL1	Anti-GST	1500/mg
Mixed fatty acids	Isotopes	60/g
¹³C-mixed free fatty acids	Isotopes	200/g
¹³C-DHA (95%)	Isotopes	38,000/g
¹⁵N-alanine	Isotopes	260/g
²H₇, ¹³C, ¹⁵N₄-arginine	Isotopes	5,900/g
dATP-CN	Isotopes	26,000/g
Antioxidants		
Vitamins		

All the HVPs listed above are however produced with specific strains, in controlled conditions and using expensive extraction-purification processes. It may not be possible to extract and separate oil and HVPs with a high energy efficiency and without degrading sensitive high value products. **The process of extracting and separating a maximum of valuable compounds from microalgae is generally referred as the biorefinery.** In addition, the algae biorefinery requires a mild pre-treatment of the cells for an efficient extraction and fractionation of the chemicals. To be valuable the produced components must be functional at the end of the process cycle [116].

Residual algal biomass (algal biomass after extraction of valuable products and oil) can be further processed to obtain valuable inputs in the global life cycle, thus contributing to the economic feasibility of the process.

The various valorizations of residual biomass are listed below.

(1) Use as **fertilizer** thanks to its high N and P content (2) **Direct combustion for energy production:** biomass is burnt and releases carbon dioxide, water and heat which is stored as hot gases or converted into mechanical energy using turbines. (3) **Gasification for syngas (synthetic gas) production** [115]: the gasification step involves the reaction of biomass with air oxygen or steam to produce a gaseous mixture of CO, CO₂, H₂, CH₄ and N₂; syngas can be produced by catalytic or non-catalytic reactions. (4) **Thermochemical liquefaction for liquid biofuel production:** the high water activity of the biomass allows in sub-critical conditions to decompose biomass materials down to smaller molecules with a high energy density (liquid biofuel). (5) **Pyrolysis** (conventional, fast or flash): the thermal degradation of biomass by heat in the absence of oxygen results in the production of charcoal, bio-oil and fuel gaseous products. (6) **Anaerobic digestion** for the production of biogas (CH₄, CO₂, H₂S and others). (7) **alcoholic fermentation** for bioethanol production: it is the conversion of biomass material which contains sugar, starch and cellulose, into ethanol, using yeasts such as *Saccharomyces cerevisiae*. (8) **Direct methanolysis** (also referred as "direct transesterification" or "wet transesterification").

Alternatively with the classic lysis-extraction-transesterification steps, wet biomass is directly in contact with alcohol acting as an extraction solvent and a transesterification reagent [95].

v3) Bioengineering algae

Improving algae culture and downstream processes in order to reduce energy inputs, maximize the biomass value (by using its remediation capacities, producing high value compounds and valorizing "waste biomass") associated with a scaling up at industry scale will progressively improve the economic sustainability of algae-derived biodiesel in the near future.

A solution that must be carefully evaluated is the engineering of the biomass itself. As food crops were slowly and progressively improved from the very beginning of agricultural activities by homo-sapiens about 10,000 years ago, the improvement of algae strains has recently been investigated. The strain *Chlamydomonas reinhardtii* was the first algae with a fully sequenced genome [123]. Today, several dozens of microalgae strains including green (*Chlorophyta*), red (*Rhodophyta*) a brown (*Phaeophyta*) algae have been successively modified [124].

Improvement strategies on wild type microalgae are as numerous as the constraints and goals associated with their engineering: (1) minimize energetic losses through cell division and metabolism, (2) increase the net photosynthetic productivity [36] (3) increase nutrient assimilation capacity, (3) modify bulk energy and carbon flows, (4) enhance the algae capacity to remain dominant in contaminated cultures (*e.g.* resistance to predators, pathogens), (5) enhance the harvestability and processability of the algae biomass (for instance biology of flocculation), (6) increase the content in valuable chemicals [125], (7) develop "triggering technologies" for biotechnology (to stop and start growth, trigger programmed cell death or dissemble the cell wall upon demand) [126]. An example of optimized algae strain is illustrated in Figure 34 from [27].

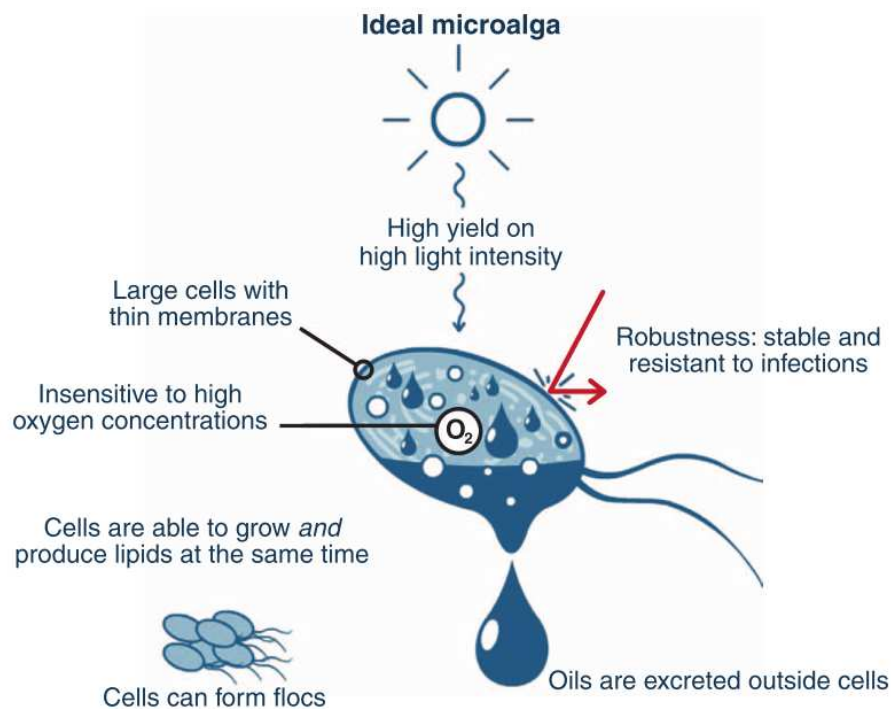


Figure 34 Ideal microalgae for oil production [27]

As an example, hyper-producing mutants generated by random insertional mutagenesis can be selected by quantitative flow cytometry and cell sorting (FCCS) [127]. The cells are analysed on the fluorescence of desired products (natural fluorescence, or molecular probes associated) and hyper-producing cells can be isolated.

Algae bio-engineering obviously raises ethical problems. Modified algae may rapidly proliferate in environment and outcompete wild type species. Is it possible to modify artificially algae in a few decades as food crops were naturally modified over 10,000 years after a long crop selection ?. Is it possible to take the risk of affecting biodiversity while trying to solve a global energy issue ? These questions must be very carefully considered.

Chapter 1 conclusion

A rapid development of biomass-derived fuels is urgently required in this 21st century due to the future depletion of crude oil sources. Although successive oil price cracks in the early years of the century have limited the development of biofuels such as bioethanol (sugar-derived fuels), biodiesel (oil-derived fuel) and biogas, these 1st and 2nd generations of biofuels have already demonstrated their economic viability to take part in the global energy production of the near future. However, the surfacic productivities of traditional crops will not be able to meet the world demand of energy. Due to their rapid growth rate, their high lipid contents in certain conditions and their ability to grow on non cultivable areas, microalgae have the potential to produce biofuel on a very large scale. However, the complex technologies of culture and downstream processes are still immature making this algae-derived biofuel not yet economical (estimated between 2.4 and 6 US\$/L) and not favorable in term of energy input/energy output ratio (hardly below 1). There is a multiplicity of culture systems; however, raceway ponds, the most simple technology, remain the reference; for them dewatering and lipid extraction represent the major energy demanding steps. It is the reason why novel technologies must be therefore developed for these steps as alternatives to current expensive and energy intensive processes such as centrifugation, drying, and cell lysis.

Globally, uncertainties of the world energy future are linked to geopolitical choices such as the decision to limit CO₂ in the atmosphere. The diversity of potential strains, culture systems, harvesting processes, lysis/extraction processes, biomass to energy processes, valorization of high value products, bioremediation and algae bioengineering offers a huge potential of improving the feasibility and sustainability of algae-derived biodiesel.

At the moment, the production of biodiesel from algae is a prospect, and only major improvements in technologies used for algae culture and lipid extraction may lead to an efficient Net Energy Ratio. Among the various processes presented in this chapter and likely to reduce the final cost of algae derived biodiesel, Pulsed Electric Fields is a very promising technology which may improve the extraction of intracellular compounds of algae as it may permeabilize cell membranes with a low energetic cost.

In this project, the use of Pulsed Electric Field (PEF) in algae downstream processing is considered in order to reduce the overall energy consumption for the extraction of lipids toward the production of biodiesel from microalgae. Algae are today mostly used to produce unsaturated fatty acids (e.g. omega 3) for nutraceutical purposes and proteins or pigments for food/feed; PEF may also be introduced in these already economic processes to reduce their production cost.

We will now focus in the chapter 2 on the metabolism of a lipid accumulating algae strain, *Chlamydomonas reinhardtii* which will be used to produce biofuel. A large part of chapter 2 is dedicated to the specific characterization methods that we developed in the framework of this PhD thesis to monitor the lipid content in algae cells.

The chapter 3 will be devoted to the use of Pulsed Electric Fields (PEF) towards the extraction of lipids from *Chlamydomonas reinhardtii*. Indeed, the main output of my PhD thesis is an energetic optimization of the PEF treatment thanks to the use of multiple fluorescent dyes. Chapter 3 also describes the first results of coupling PEF with organic solvent extraction, in order to determine if an optimized PEF treatment may improve lipid extraction.

Chapter 1 references

- [1] EIA, Global energy demand, Energy Tomorrow. (2014). <http://energytomorrow.org/energy-101/global-energy-demand>.
- [2] <http://www.connaissancedesenergies.org/>.
- [3] International Energy Agency, Key World Energy Statistics 2015, (2015) 81. doi:10.1787/9789264039537-en.
- [4] R.G. Miller, S.R. Sorrell, The future of oil supply., *Philos. Trans. A. Math. Phys. Eng. Sci.* 372 (2014) 20130179. doi:10.1098/rsta.2013.0179.
- [5] K. McCarthy, K. Rojas, M. Niemann, D. Palmowski, K. Peters, A. Stankiewicz, Basic Petroleum Geochemistry for Source Rock Evaluation, *Oilf. Rev.* 23 (2011) 32–43. http://www.slb.com/~media/Files/resources/oilfield_review/ors11/sum11/basic_petroleum.pdf.
- [6] O. After, 3 . 8 Gasoline : A Deeper Look 3 . 8 Gasoline : A Deeper Look, (n.d.) 1–4.
- [7] <http://www.cop21.gouv.fr/>.
- [8] <https://www.co2.earth/>.
- [9] M. Guo, W. Song, J. Buhain, Bioenergy and biofuels: History, status, and perspective, *Renew. Sustain. Energy Rev.* 42 (2015) 712–725. doi:10.1016/j.rser.2014.10.013.
- [10] <http://www.actu-environnement.com/ae/news/rapport-giec-2c-emissions-ges-temperatures-hausse-21395.php4>.
- [11] World oil outlook, 2015. doi:10.1190/1.1439163.
- [12] a. E. Atabani, a. S. Silitonga, I.A. Badruddin, T.M.I. Mahlia, H.H. Masjuki, S. Mekhilef, A comprehensive review on biodiesel as an alternative energy resource and its characteristics, *Renew. Sustain. Energy Rev.* 16 (2012) 2070–2093. doi:10.1016/j.rser.2012.01.003.
- [13] C. Ryan, Cultivating Clean Energy, the Promise of Algae Biofuels, *Nat. Resour. Def. Coun.* (2009) 81. http://scholar.google.co.jp/scholar?hl=en&q=cultivating+clean+energy+the+promise+of+algae+biofuels&btnG=&as_sdtp=1,5&as_sdtp=#0.
- [14] X. Ji, X. Long, A review of the ecological and socioeconomic effects of biofuel and energy policy recommendations, *Renew. Sustain. Energy Rev.* 61 (2016) 41–52. doi:10.1016/j.rser.2016.03.026.
- [15] J.M. Bergthorson, M.J. Thomson, A review of the combustion and emissions properties of advanced transportation biofuels and their impact on existing and future engines, *Renew. Sustain. Energy Rev.* 42 (2015) 1393–1417. doi:10.1016/j.rser.2014.10.034.
- [16] S.K. Hoekman, C. Robbins, Review of the effects of biodiesel on NOx emissions, *Fuel Process. Technol.* 96 (2012) 237–249. doi:10.1016/j.fuproc.2011.12.036.
- [17] A. Jagger, Biofuels for transport in 2050, *Biofuels, Bioprod. Biorefining.* 5 (2011) 481–485. doi:10.1002/bbb.330.
- [18] S.Y. No, Application of hydrotreated vegetable oil from triglyceride based biomass to CI engines - A review, *Fuel.* 115 (2014) 88–96. doi:10.1016/j.fuel.2013.07.001.
- [19] <http://www.biofuelstp.eu/index.html>.
- [20] G. Gruter, E. De Jong, Furanics : novel fuel options from carbohydrates, *Biofuels Technol.* (2009) 11–17.
- [21] <http://www.isaaa.org/kc/cropbiotechupdate/article/default.asp?ID=2991>.
- [22] P. Imhof, A.S. Dias, G.J.G. de Jong, Furanics: Versatile Molecules for Biofuels and Bulk Chemicals Applications, *Nam.Confex.Com.* 1446 (2008) 2008–2008. http://nam.confex.com/data/abstract/nam/2009/Paper_2970_abstract_1281_0.pdf.
- [23] M. Al-Qasbi, N. Raut, S. Talebi, S. Al-Rajhi, T. Al-Barwani, A Review of Effect of Light on Microalgae Growth, *Proc. World Congr. Eng. I* (2012) 8–10.
- [24] Y. Chisti, Biodiesel from microalgae., *Biotechnol. Adv.* 25 (2007) 294–306. doi:10.1016/j.biotechadv.2007.02.001.
- [25] https://en.wikipedia.org/wiki/Arable_land.
- [26] https://en.wikipedia.org/wiki/Algae_fuel#cite_note-18.
- [27] R.H. Wijffels, M.J. Barbosa, An outlook on microalgal biofuels., *Science.* 329 (2010) 796–799. doi:10.1126/science.1189003.
- [28] D.M. Karl, Solar energy capture and transformation in the sea, *Elem. Sci. Anthr.* 2 (2014) 21. doi:10.12952/journal.elementa.000021.
- [29] <http://www.algaebase.org/browse/taxonomy/>.
- [30] O. de Clerck, K.A. Bogaert, F. Leliaert, Diversity and Evolution of Algae BT - (null), 2012. [http://linkinghub.elsevier.com/retrieve/pii/B978012391499600025%5Cnfile:///Users/jbro886/Dropbox/Papers 3/Library.papers3/Files/F2/F29389F1-3B40-4E58-A753-5A676A7B4CDA.pdf%5Cnpapers3://publication/doi/10.1016/B978-0-12-391499-6.00002-5](http://linkinghub.elsevier.com/retrieve/pii/B978012391499600025%5Cnfile:///Users/jbro886/Dropbox/Papers%203/Library.papers3/Files/F2/F29389F1-3B40-4E58-A753-5A676A7B4CDA.pdf%5Cnpapers3://publication/doi/10.1016/B978-0-12-391499-6.00002-5).
- [31] http://shigen.nig.ac.jp/algae_tree/TreeE.html.
- [32] L. Pottier, J. Pruvost, J. Deremetz, J.F. Cornet, J. Legrand, C.G. Dussap, A fully predictive model for one-dimensional light attenuation by *Chlamydomonas reinhardtii* in a torus photobioreactor, *Biotechnol. Bioeng.* 91 (2005) 569–582. doi:10.1002/bit.20475.
- [33] H. Takache, J. Pruvost, J.-F. Cornet, Kinetic modeling of the photosynthetic growth of *Chlamydomonas reinhardtii* in a photobioreactor., *Biotechnol. Prog.* 28 (2012) 681–92. doi:10.1002/btpr.1545.
- [34] K.J.M. Mulders, P.P. Lamers, D.E. Martens, R.H. Wijffels, Phototrophic pigment production with microalgae: Biological constraints and opportunities, *J. Phycol.* 50 (2014) 229–242. doi:10.1111/jpy.12173.
- [35] T. De Mooij, M. Janssen, O. Cerezo-Chinarro, J.H. Mussgnug, O. Kruse, M. Ballottari, R. Bassi, S. Bujaldon, F.A. Wollman, R.H. Wijffels, Antenna size reduction as a strategy to increase biomass productivity: a great potential not yet realized, *J. Appl. Phycol.* (2014) 1063–1077. doi:10.1007/s10811-014-0427-y.
- [36] Z. Perrine, S. Negi, R.T. Sayre, Optimization of photosynthetic light energy utilization by microalgae, *Algal Res.* 1 (2012) 134–142. doi:10.1016/j.algal.2012.07.002.
- [37] G. Perin, A. Bellan, A. Segalla, A. Meneghesso, A. Alboresi, T. Morosinotto, Generation of random mutants to improve light-use efficiency of *Nannochloropsis gaditana* cultures for biofuel production., *Biotechnol. Biofuels.* 8 (2015) 161. doi:10.1186/s13068-015-0337-5.
- [38] J.U. Grobbelaar, Mass Production of Microalgae at Optimal Photosynthetic Rates, *Photosynthesis.* (2013) 357–371. doi:10.5772/55193.
- [39] J.C. Ogonna, H. Tanaka, Light requirement and photosynthetic cell cultivation – Development of processes for efficient light utilization in photobioreactors, *J. Appl. Phycol.* 12 (2000) 207–218. doi:10.1023/A:1008194627239.
- [40] http://www1.lsbu.ac.uk/water/water_vibrational_spectrum.html.

- [41] P. Varshney, P. Mikulic, A. Vonshak, J. Beardall, P.P. Wangikar, Extremophilic micro-algae and their potential contribution in biotechnology, *Bioresour. Technol.* 184 (2015) 363–372. doi:10.1016/j.biortech.2014.11.040.
- [42] <https://unfamiliarstars.wordpress.com/2013/08/25/dont-eat-the-pink-snow/>.
- [43] <http://algix.com/tag/dunaliella-salina/>.
- [44] H.M. Amaro, A.C. Guedes, F.X. Malcata, Advances and perspectives in using microalgae to produce biodiesel, *Appl. Energy*. 88 (2011) 3402–3410. doi:10.1016/j.apenergy.2010.12.014.
- [45] M.J. Barbosa, Hadiyanto, R.H. Wijffels, Overcoming Shear Stress of Microalgae Cultures in Sparged Photobioreactors, *Biotechnol. Bioeng.* 85 (2004) 78–85. doi:10.1002/bit.10862.
- [46] T.E. Murphy, B.J. Kapili, A.M. Detweiler, B.M. Bebout, L.E. Prufert-Bebout, Vertical distribution of algal productivity in open pond raceways, *Algal Res.* 11 (2015) 334–342. doi:10.1016/j.algal.2015.07.003.
- [47] http://the.honoluluadvertiser.com/dailypix/2010/Feb/12/hawaii2120351AR_b.jpg.
- [48] M.K. Lam, K.T. Lee, Biofuels from Algae, 2014. doi:10.1016/B978-0-444-59558-4.00012-7.
- [49] M. Marsullo, A. Mian, A.V. Ensinas, G. Manente, A. Lazzaretto, F. Marechal, Dynamic Modeling of the Microalgae Cultivation Phase for Energy Production in Open Raceway Ponds and Flat Panel Photobioreactors, *Front. Energy Res.* 3 (2015) 1–18. doi:10.3389/fenrg.2015.00041.
- [50] G. De Bhowmick, G. Subramanian, S. Mishra, R. Sen, Raceway pond cultivation of a marine microalga of Indian origin for biomass and lipid production: A case study, *Algal Res.* 6 (2014) 201–209. doi:10.1016/j.algal.2014.07.005.
- [51] K.C. Tran, J.L. Mendoza Martin, S. Heaven, C.J. Banks, F.G. Acien Fernandez, E. Molina Grima, Cultivation and anaerobic digestion of *Scenedesmus* spp. grown in a pilot-scale open raceway, *Algal Res.* 5 (2014) 95–102. doi:10.1016/j.algal.2014.06.001.
- [52] P.M. Slegers, M.B. Lösing, R.H. Wijffels, G. van Straten, A.J.B. van Boxtel, Scenario evaluation of open pond microalgae production, *Algal Res.* 2 (2013) 358–368. doi:10.1016/j.algal.2013.05.001.
- [53] I. Fernández, F.G. Acien, J.L. Guzmán, M. Berenguel, J.L. Mendoza, Dynamic model of an industrial raceway reactor for microalgae production, *Algal Res.* 17 (2016) 67–78. doi:10.1016/j.algal.2016.04.021.
- [54] J. Huang, X. Qu, M. Wan, J. Ying, Y. Li, F. Zhu, J. Wang, G. Shen, J. Chen, W. Li, Investigation on the performance of raceway ponds with internal structures by the means of CFD simulations and experiments, *Algal Res.* 10 (2015) 64–71. doi:10.1016/j.algal.2015.04.012.
- [55] R. Hreiz, B. Sialve, J. Morchain, R. Escudié, J.-P. Steyer, P. Guiraud, Experimental and numerical investigation of hydrodynamics in raceway reactors used for algaculture, *Chem. Eng. J.* 250 (2014) 230–239. doi:10.1016/j.cej.2014.03.027.
- [56] P.E. Gharagozloo, J.L. Drewry, A.M. Collins, T.A. Dempster, C.Y. Choi, S.C. James, Analysis and modeling of *Nannochloropsis* growth in lab, greenhouse, and raceway experiments, *J. Appl. Phycol.* (2014) 1–12. doi:10.1007/s10811-014-0257-y.
- [57] <http://www.nanovoltaics.com/content/algae-photobioreactors>.
- [58] <http://www.israel21c.org/top-12-agri-tech-companies-from-israel-2/>.
- [59] <http://www.20minutes.fr/nantes/1711883-20151018-lunettes-carburant-bitume-nantes-transforme-algues-moins-polluer>.
- [60] <http://www.wageningenur.nl/en/newsarticle/Costeffective-algae-production-within-reach.htm>.
- [61] R. Slade, A. Bauen, Micro-algae cultivation for biofuels: Cost, energy balance, environmental impacts and future prospects, *Biomass and Bioenergy*. 53 (2013) 29–38. doi:10.1016/j.biombioe.2012.12.019.
- [62] O. Jorquera, A. Kiperstok, E.A. Sales, M. Embiruçu, M.L. Ghirardi, Comparative energy life-cycle analyses of microalgal biomass production in open ponds and photobioreactors, *Bioresour. Technol.* 101 (2010) 1406–1413. doi:10.1016/j.biortech.2009.09.038.
- [63] G. Brownbridge, P. Azadi, A. Smallbone, A. Bhave, B. Taylor, M. Kraft, The future viability of algae-derived biodiesel under economic and technical uncertainties, *Bioresour. Technol.* 151 (2014) 166–173. doi:10.1016/j.biortech.2013.10.062.
- [64] J.C. Quinn, T.G. Smith, C.M. Downes, C. Quinn, Microalgae to biofuels lifecycle assessment - Multiple pathway evaluation, *Algal Res.* 4 (2014) 116–122. doi:10.1016/j.algal.2013.11.002.
- [65] O. Perez-Garcia, F.M.E. Escalante, L.E. de-Bashan, Y. Bashan, Heterotrophic cultures of microalgae: Metabolism and potential products, *Water Res.* 45 (2011) 11–36. doi:10.1016/j.watres.2010.08.037.
- [66] <http://www.ck12.org/life-science/Connecting-Cellular-Respiration-and-Photosynthesis-in-Life-Science/lesson/Connecting-Cellular-Respiration-and-Photosynthesis-MS-LS/>.
- [67] P.R. Mooij, G.R. Stouten, J. Tamis, M.C.M. van Loosdrecht, R. Kleerebezem, Survival of the fattest, *Energy Environ. Sci.* 6 (2013) 3404. doi:10.1039/c3ee42912a.
- [68] M. Gross, D. Jarboe, Z. Wen, Biofilm-based algal cultivation systems, *Appl. Microbiol. Biotechnol.* 99 (2015) 5781–5789. doi:10.1007/s00253-015-6736-5.
- [69] A. Salimbeni, W. Blanken, M. Janssen, ALGADISK -NOVEL ALGAE-BASED SOLUTION FOR CO₂ CAPTURE AND BIOMASS, (2014).
- [70] W. Blanken, A. Magalhães, P. Sebestyán, A. Rinzema, R.H. Wijffels, M. Janssen, Microalgal biofilm growth under day-night cycles, *Algal Res.* 21 (2017) 16–26. doi:10.1016/j.algal.2016.11.006.
- [71] R. Bosma, M.H. Vermuë, J. Tramper, R.H. Wijffels, Towards increased microalgal productivity in photobioreactors, *Int. Sugar J. Vol.* 112 (2010) 74–85.
- [72] A.J. Dasse, C.S. Theegala, Harvesting economics and strategies using centrifugation for cost effective separation of microalgae cells for biodiesel applications, *Bioresour. Technol.* 128 (2013) 241–245. doi:10.1016/j.biortech.2012.10.061.
- [73] Y. Liu, T. Jin, Y. Yu, C. Wu, H. Mou, Characterization of flocculating and antimicrobial activity of salmine, *Algal Res.* 16 (2016) 46–53. doi:10.1016/j.algal.2016.03.003.
- [74] T. Chatsungnoen, Y. Chisti, Harvesting microalgae by flocculation–sedimentation, *Algal Res.* 13 (2016) 271–283. doi:10.1016/j.algal.2015.12.009.
- [75] K.L. Morrissey, M.I. Keirn, Y. Inaba, A.J. Denham, G.J. Henry, B.W. Vogler, M.C. Posewitz, M.P. Stoykovich, Recyclable polyampholyte flocculants for the cost-effective dewatering of microalgae and cyanobacteria, *Algal Res.* 11 (2015) 304–312. doi:10.1016/j.algal.2015.07.009.
- [76] L. Pezzolesi, C. Samori, R. Pistocchi, Flocculation induced by homogeneous and heterogeneous acid treatments in *Desmodesmus communis*, *Algal Res.* 10 (2015) 145–151. doi:10.1016/j.algal.2015.04.024.
- [77] R. Gutiérrez, F. Passos, I. Ferrer, E. Uggetti, J. García, Harvesting microalgae from wastewater treatment systems with natural flocculants: Effect on biomass settling and biogas production, *Algal Res.* 9 (2015) 204–211. doi:10.1016/j.algal.2015.03.010.
- [78] T. Ndikubwimana, X. Zeng, Y. Liu, J.S. Chang, Y. Lu, Harvesting of microalgae *Desmodesmus* sp. F51 by bioflocculation with bacterial bioflocculant, *Algal Res.* 6 (2014) 186–193. doi:10.1016/j.algal.2014.09.004.
- [79] J.A. Gerde, L. Yao, J. Lio, Z. Wen, T. Wang, Microalgae flocculation: Impact of flocculant type, algae species and cell concentration,

- Algal Res. 3 (2014) 30–35. doi:10.1016/j.algal.2013.11.015.
- [80] W. Zhou, L. Gao, W. Cheng, L. Chen, J. Wang, H. Wang, W. Zhang, T. Liu, Electro-flotation of *Chlorella* sp. assisted with flocculation by chitosan, *Algal Res.* 18 (2016) 7–14. doi:10.1016/j.algal.2016.05.029.
- [81] M. Larronde-Larretche, X. Jin, *Microalgae* (*Scenedesmus obliquus*) dewatering using forward osmosis membrane: Influence of draw solution chemistry, *Algal Res.* 15 (2016) 1–8. doi:10.1016/j.algal.2016.01.014.
- [82] H. Chu, F. Zhao, X. Tan, L. Yang, X. Zhou, J. Zhao, Y. Zhang, The impact of temperature on membrane fouling in algae harvesting, *Algal Res.* 16 (2016) 458–464. doi:10.1016/j.algal.2016.04.012.
- [83] W. Mo, L. Soh, J.R. Werber, M. Elimelech, J.B. Zimmerman, Application of membrane dewatering for algal biofuel, *Algal Res.* 11 (2015) 1–12. doi:10.1016/j.algal.2015.05.018.
- [84] J. Pavez, F. Cabrera, L. Azócar, A. Torres, D. Jeison, Ultrafiltration of non-axenic microalgae cultures: Energetic requirements and filtration performance, *Algal Res.* 10 (2015) 121–127. doi:10.1016/j.algal.2015.04.022.
- [85] V. Discart, M.R. Bilad, R. Moorkens, H. Arafat, I.F.J. Vankelecom, Decreasing membrane fouling during *Chlorella vulgaris* broth filtration via membrane development and coagulant assisted filtration, *Algal Res.* 9 (2015) 55–64. doi:10.1016/j.algal.2015.02.029.
- [86] D.Y. Kim, T. Hwang, Y.K. Oh, J.I. Han, Harvesting *Chlorella* sp. KR-1 using cross-flow electro-filtration, *Algal Res.* 6 (2014) 170–174. doi:10.1016/j.algal.2014.10.004.
- [87] J.J. Milledge, S. Heaven, A review of the harvesting of micro-algae for biofuel production, *Rev. Environ. Sci. Biotechnol.* 12 (2013) 165–178. doi:10.1007/s11157-012-9301-z.
- [88] N. Uduman, Y. Qi, M.K. Danquah, G.M. Forde, A. Hoadley, Dewatering of microalgal cultures: A major bottleneck to algae-based fuels, *J. Renew. Sustain. Energy.* 2 (2010) 12701. doi:10.1063/1.3294480.
- [89] E. Poelman, N. De Pauw, B. Jeurissen, Potential of electrolytic flocculation for recovery of micro-algae, *Resour. Conserv. Recycl.* 19 (1997) 1–10. doi:10.1016/S0921-3449(96)01156-1.
- [90] L. Christenson, R. Sims, Production and harvesting of microalgae for wastewater treatment, biofuels, and bioproducts., *Biotechnol. Adv.* 29 (2011) 686–702. doi:10.1016/j.biotechadv.2011.05.015.
- [91] B. Serive, R. Kaas, J.-B. Bérard, V. Pasquet, L. Picot, J.-P. Cadoret, Selection and optimisation of a method for efficient metabolites extraction from microalgae., *Bioresour. Technol.* 124 (2012) 311–20. doi:10.1016/j.biortech.2012.07.105.
- [92] P.R. Postma, T.L. Miron, G. Olivieri, M.J. Barbosa, R.H. Wijffels, M.H.M. Eppink, Mild disintegration of the green microalgae *Chlorella vulgaris* using bead milling, *Bioresour. Technol.* 184 (2015) 297–304. doi:10.1016/j.biortech.2014.09.033.
- [93] J. Kim, G. Yoo, H. Lee, J. Lim, K. Kim, C.W. Kim, M.S. Park, J.-W. Yang, Methods of downstream processing for the production of biodiesel from microalgae., *Biotechnol. Adv.* 31 (2013) 862–76. doi:10.1016/j.biotechadv.2013.04.006.
- [94] . [http://web.utk.edu/~fede/high pressure homogenization.html](http://web.utk.edu/~fede/high_pressure_homogenization.html).
- [95] J. Kim, G. Yoo, H. Lee, J. Lim, K. Kim, C.W. Kim, M.S. Park, J.-W. Yang, Methods of downstream processing for the production of biodiesel from microalgae., *Biotechnol. Adv.* 31 (2013) 862–76. doi:10.1016/j.biotechadv.2013.04.006.
- [96] R. Ranjith Kumar, P. Hanumantha Rao, M. Arumugam, Lipid Extraction Methods from Microalgae: A Comprehensive Review, *Front. Energy Res.* 2 (2015) 1–9. doi:10.3389/fenrg.2014.00061.
- [97] J.A. Gerde, M. Montalbo-Lombay, L. Yao, D. Grewell, T. Wang, Evaluation of microalgae cell disruption by ultrasonic treatment, *Bioresour. Technol.* 125 (2012) 175–181. doi:10.1016/j.biortech.2012.08.110.
- [98] A.F. Ferreira, A.P.S. Dias, C.M. Silva, M. Costa, Effect of low frequency ultrasound on microalgae solvent extraction: Analysis of products, energy consumption and emissions, *Algal Res.* 14 (2016) 9–16. doi:10.1016/j.algal.2015.12.015.
- [99] M.D. Macías-Sánchez, C. Mantell, M. Rodríguez, E. Martínez de la Ossa, L.M. Lubián, O. Montero, Comparison of supercritical fluid and ultrasound-assisted extraction of carotenoids and chlorophyll a from *Dunaliella salina*., *Talanta.* 77 (2009) 948–52. doi:10.1016/j.talanta.2008.07.032.
- [100] Y.-H. Kim, S. Park, M.H. Kim, Y.-K. Choi, Y.-H. Yang, H.J. Kim, H. Kim, H.-S. Kim, K.-G. Song, S.H. Lee, Ultrasound-assisted extraction of lipids from *Chlorella vulgaris* using [Bmim][MeSO₄], *Biomass and Bioenergy.* 56 (2013) 99–103. doi:10.1016/j.biombioe.2013.04.022.
- [101] T. Kotnik, P. Kramar, G. Pucihar, D. Miklavcic, M. Tarek, Cell membrane electroporation- Part 1: The phenomenon, *IEEE Electr. Insul. Mag.* 28 (2012) 14–23. doi:10.1109/MEI.2012.6268438.
- [102] P. Bodénès, F. Lopes, D. Pareau, O. Français, B. Le Pioufle, Microdevice for studying the in situ permeabilization and characterization of *Chlamydomonas reinhardtii* in lipid accumulation phase, *Algal Res.* 16 (2016) 357–367. doi:10.1016/j.algal.2016.03.023.
- [103] B. Grant, C. Mark, F. Field, Functional Mesoporous Silica Nanoparticles for the Selective Sequestration of Fatty Acids point charges, (2012) 20.
- [104] I.T. Program, Nanoparticle Technology for Biorefinery of Non – Food Source Feedstocks, (n.d.).
- [105] G. Yoo, W.-K. Park, C.W. Kim, Y.-E. Choi, J.-W. Yang, Direct lipid extraction from wet *Chlamydomonas reinhardtii* biomass using osmotic shock., *Bioresour. Technol.* 123 (2012) 717–22. doi:10.1016/j.biortech.2012.07.102.
- [106] H.G. Gerken, B. Donohoe, E.P. Knoshaug, Enzymatic cell wall degradation of *Chlorella vulgaris* and other microalgae for biofuels production., *Planta.* 237 (2013) 239–53. doi:10.1007/s00425-012-1765-0.
- [107] M.T. Golmakani, J.A. Mendiola, K. Rezaei, E. Ib????ez, Pressurized limonene as an alternative bio-solvent for the extraction of lipids from marine microorganisms, *J. Supercrit. Fluids.* 92 (2014) 1–7. doi:10.1016/j.supflu.2014.05.001.
- [108] Feb 2015, (2015) 3194.
- [109] J. Yarnold, I.L. Ross, B. Hankamer, Photoacclimation and productivity of *Chlamydomonas reinhardtii* grown in fluctuating light regimes which simulate outdoor algal culture conditions, *Algal Res.* 13 (2015) 1–13. doi:10.1016/j.algal.2015.11.001.
- [110] M. Huesemann, B. Crowe, P. Waller, A. Chavis, S. Hobbs, S. Edmundson, M. Wigmosta, A validated model to predict microalgae growth in outdoor pond cultures subjected to fluctuating light intensities and water temperatures, *Algal Res.* 13 (2016) 195–206. doi:10.1016/j.algal.2015.11.008.
- [111] <http://algorithms.com/wp-content/uploads/2016/04/photo31.jpg>.
- [112] <http://www.wageningenur.nl/en/Expertise-Services/Facilities/AlgaePARC.htm>.
- [113] <https://asunow.asu.edu/content/asu-lead-first-ever-national-algae-testbed-awarded-15m-grant-department-energy>.
- [114] C.P. Bravo-Fritz, C.A. Sáez-Navarrete, L.A. Herrera-Zepelin, F. Varas-Concha, Multi-scenario energy-economic evaluation for a biorefinery based on microalgae biomass with application of anaerobic digestion, *Algal Res.* 16 (2016) 292–307. doi:10.1016/j.algal.2016.03.028.
- [115] T. Suganya, M. Varman, H.H. Masjuki, S. Renganathan, Macroalgae and microalgae as a potential source for commercial applications along with biofuels production: A biorefinery approach, *Renew. Sustain. Energy Rev.* 55 (2016) 909–941.

Chapter 1: The future of algae-derived biodiesel

- doi:10.1016/j.rser.2015.11.026.
- [116] M. Vanthoor-Koopmans, R.H. Wijffels, M.J. Barbosa, M.H.M. Eppink, Biorefinery of microalgae for food and fuel., *Bioresour. Technol.* 135 (2013) 142–9. doi:10.1016/j.biortech.2012.10.135.
- [117] C. Shene, Y. Chisti, M. Bustamante, M. Rubilar, Effect of CO₂ in the aeration gas on cultivation of the microalga *Nannochloropsis oculata*: Experimental study and mathematical modeling of CO₂ assimilation, *Algal Res.* 13 (2016) 16–29. doi:10.1016/j.algal.2015.11.005.
- [118] N. Neveux, M. Magnusson, L. Mata, A. Whelan, R. de Nys, N.A. Paul, The treatment of municipal wastewater by the macroalga *Oedogonium* sp. and its potential for the production of biocrude, *Algal Res.* 13 (2016) 284–292. doi:10.1016/j.algal.2015.12.010.
- [119] M. Stockenreiter, F. Haupt, J. Seppälä, T. Tamminen, K. Spilling, Nutrient uptake and lipid yield in diverse microalgal communities grown in wastewater, *Algal Res.* 15 (2016) 77–82. doi:10.1016/j.algal.2016.02.013.
- [120] T. Takeshita, Competitiveness, role, and impact of microalgal biodiesel in the global energy future, *Appl. Energy.* 88 (2011) 3481–3491. doi:10.1016/j.apenergy.2011.02.009.
- [121] V. Kovacevic, J. Wesseler, Cost-effectiveness analysis of algae energy production in the EU, *Energy Policy.* 38 (2010) 5749–5757. doi:10.1016/j.enpol.2010.05.025.
- [122] E. Stephens, I.L. Ross, Z. King, J.H. Mussgnug, O. Kruse, C. Posten, M. a Borowitzka, B. Hankamer, An economic and technical evaluation of microalgal biofuels., *Nat. Biotechnol.* 28 (2010) 126–128. doi:10.1038/nbt0210-126.
- [123] S.S. Merchant, S.E. Prochnik, O. Vallon, E.H. Harris, J. Karpowicz, G.B. Witman, A. Terry, A. Salamov, L.K. Fritz-laylin, L. Maréchal-drouard, W.F. Marshall, L. Qu, D.R. Nelson, a Sanderfoot, M.H. Spalding, V. V Kapitonov, Q. Ren, P. Cardol, H. Cerutti, G. Chanfreau, P. Ferris, H. Fukuzawa, D. González-ballester, B. Mueller-roeber, S. Rajamani, R.T. Sayre, I. Dubchak, D. Goodstein, L. Hornick, Y.W. Huang, Y. Luo, D. Martínez, W. Chi, A. Ngau, B. Otilar, A. Porter, L. Szajkowski, G. Werner, K. Zhou, V. Igor, D.S. Rokhsar, A.R. Grossman, The *Chlamydomonas* Genome Reveals the Evolution of Key Animal and Plant Functions, *Science* (80-.). 318 (2010) 245–250. doi:10.1126/science.1143609.The.
- [124] R. Radakovits, R.E. Jinkerson, A. Darzins, M.C. Posewitz, Genetic engineering of algae for enhanced biofuel production, *Eukaryot. Cell.* 9 (2010) 486–501. doi:10.1128/EC.00364-09.
- [125] V.H. Work, R. Radakovits, R.E. Jinkerson, J.E. Meuser, L.G. Elliott, D.J. Vinyard, L.M.L. Laurens, G.C. Dismukes, M.C. Posewitz, Increased Lipid Accumulation in the *Chlamydomonas reinhardtii* sta7-10 Starchless Isoamylase Mutant and Increased Carbohydrate Synthesis in Complemented Strains, *Eukaryot. Cell.* 9 (2010) 1251–1261. doi:10.1128/EC.00075-10.
- [126] E. Eroglu, S.M. Smith, C.L. Raston, Biomass and Biofuels from Microalgae, 2015. doi:10.1007/978-3-319-16640-7.
- [127] C. Cagnon, B. Mirabella, H.M. Nguyen, A. Beyly-Adriano, S. Bouvet, S. Cuiné, F. Beisson, G. Peltier, Y. Li-Beisson, Development of a forward genetic screen to isolate oil mutants in the green microalga *Chlamydomonas reinhardtii*., *Biotechnol. Biofuels.* 6 (2013) 178. doi:10.1186/1754-6834-6-178.
- [128] <https://yearbook.enerdata.net/crude-oil-production.html>.

I1. Appendix I.1: Additional information about oil production

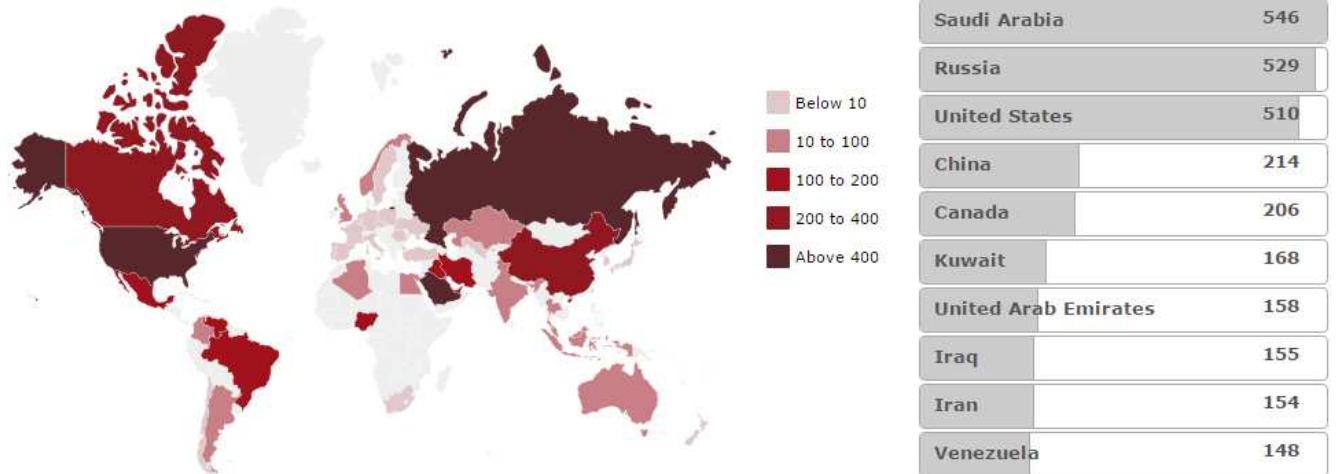


Figure 1 2014 world crude oil production, in Mt. [128]

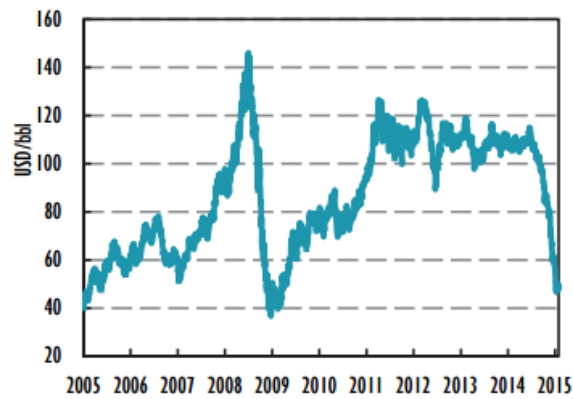


Figure 2: 2005-2015 Crude oil price variations

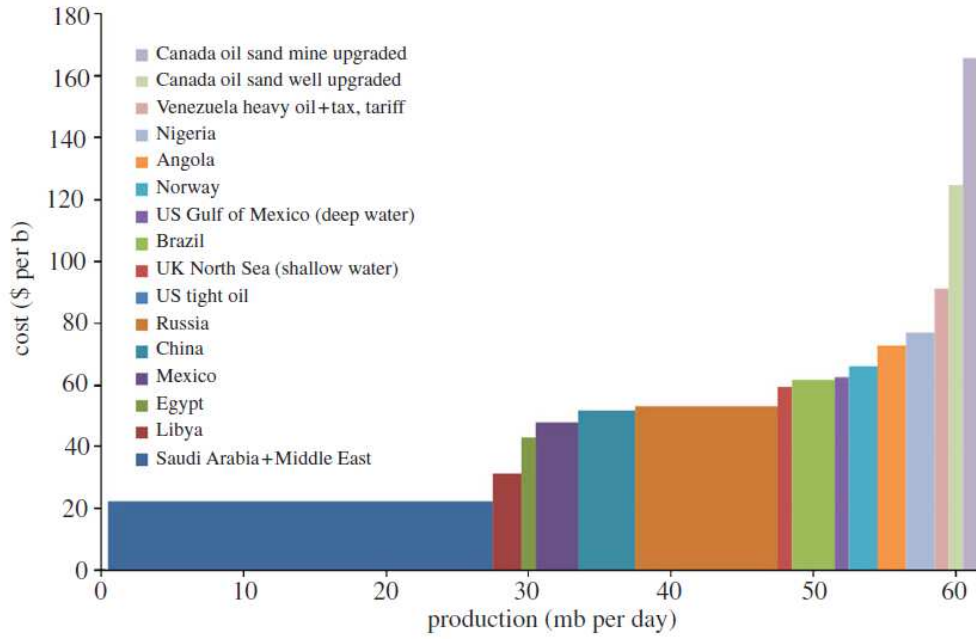


Figure 3 Estimation of the production capacities and associated costs of various oil resources [4]

Chapter 2

Inducing lipid accumulation in green microalgae and developing characterization methods

List of abbreviations:	73
Chapter 2: introduction	75
I. Morphology, composition and metabolism of green micro-algae	76
I1) Cell structure	76
I1a) Plasma membrane	76
I1b) Cell wall	77
I1c) <i>Chlamydomonas reinhardtii</i> specificities	77
I2) Respiration activity	80
I3) Photosynthetic activity	81
I3a) Chloroplasts	81
I3b) Light conversion to electrons	82
I3c) Electron transport chain	83
I3d) Dark reactions (Calvin cycle)	84
II. Lipid biosynthesis and composition	85
II1) Lipid synthesis in microalgae: From light to TAGs	85
II2) Lipid classes	87
II2a) Polar and neutral lipids	87
II2b) Fatty acids	89
II3) Culture conditions and cell composition	90
II3a) Cell composition during growth	90
II3b) Stress induction: from functional to storage lipids	91
II3c) Strategies to conciliate algae production and lipid content	93
II3d) Conditions found in literature	93
III. Review of analytical methods	95
III1) Biomass growth	95
III1a) Absorbance or Optical density (OD)	95
III1b) Cell number	95
III1c) Dry weight (DW)	98
III1d) Comparison of the different methods	99
III2) Lipid content	99
III2a) Gravimetric methods (solvent extraction)	99

III2b)	Transesterification and Gas Chromatography analyses	101
III2c)	Lipophilic dyes (Nile red and Bodipy)	101
III2d)	Colorimetric method (Sulfophosphovanillin)	105
III2e)	Conclusion about lipid quantification	107
III3)	Cell size	107
IV.	Procedure to induce lipid accumulation developed in this work	108
IV1)	1st step "growth step":	109
IV2)	2nd step "stress conditions":	109
IV3)	Discussion of the conditions chosen	110
V.	Development and validation of the methods	111
V1)	Determination of cell concentration by flow cytometry	111
V2)	Calibration curve of SPV method using Triolein	111
V3)	Development of Bodipy staining on <i>Chlamydomonas reinhardtii</i>	111
V3a)	Effect of the ratio Bodipy/cell and the presence of a washing step on <i>Chlamydomonas reinhardtii</i>	112
V3b)	Observation on <i>Chlamydomonas reinhardtii</i> cells in 7 days of stress using a Confocal Laser Scanning Microscopy (CLSM)	115
V3c)	Conclusion on Bodipy staining protocol	116
V4)	Development of a CLSM method to observe <i>Chlamydomonas reinhardtii</i> (pigments, lipids, cell wall)	116
VI.	Results	118
VI1)	Biomass growth	119
VI1a)	First step: Growth phase	119
VI1b)	Second step: Stress phase	119
VI1c)	Illustration of the two steps	120
VI2)	Chlorophyll content	121
VI2a)	First step: Growth phase	121
VI2b)	Second step: stress conditions	122
VI3)	Dry weight (stress condition)	123
VI4)	Lipid content	125
VI4a)	Identification and quantification of Fatty acids (polar + neutral FA) during stress, measured by gas chromatography (GC-FID)	125
VI4b)	Analysis of FA composition for biodiesel purpose and analytical methods	127
VI4c)	Colorimetric method: SulphoPhosphoVanillin (SPV)	128
VI4d)	Monitoring <i>Chlamydomonas reinhardtii</i> cell with CLSM imaging	130

VI4e)	Monitoring of neutral lipid content with Bodipy staining and flow cytometry	133
VI5)	Monitoring cell size	135
Chapter 2 conclusion	137
Chapter 2 references	139
II1.	Appendix II.1: Lipid production strategies in literature	143
II2.	Appendix II.2: Quantification of unsaturated fatty acids using the colorimetric Sulphophosphovanillin (SPV) method.....	145
II3.	Appendix II.3: Additional lipid estimation methods.....	148
II4.	Appendix II.4: Principle of laser granulometry.....	150
II5.	Appendix II.5: Medium preparation.....	152
II6.	Appendix II.6: Correlation cyto/malassez in growth and stress phase	156
II7.	Appendix II.7: Confocal microcopy vs fluorescence microscopy	157
II8.	Appendix II.8: CLSM optical configuration to monitor Chlamydomonas reinhardtii cells stained with Bodipy and Concanavalin TRITC (track 1: Bodipy, track 2: Chlorophyll, and track 3: concanavalin, track 4: merged channels).....	158

List of abbreviations:

- ATP Adenosine Triphosphate
- NADPH Nicotinamide adenine dinucleotide phosphate
- PEF Pulsed Electric Fields
- TAGs Triacylglycerides
- CLSM Confocal Laser Scanning Microscopy
- TRITC Tetramethylrhodamine
- Bodipy BODIPY® 505/515
(4,4-Difluoro-1,3,5,7-Tetramethyl-4-Bora-3a,4a-Diaza-s-Indacene)
- FA Fatty Acids
- SPV Sulfo-Phospho-Vanillin
- GC-FID Gas Chromatography coupled with a Flame Ionization Detector
- DW Dry weight
- TO Triolein
- CFPP Cold Filter Plugging Point
- PerCP-cy5.5 Peridinin-Chlorophyll-Protein coupled with cyanin 5.5, a far-red emitting dye
- TAP Tris-Acetate-Phosphate, medium for *Chlamydomonas reinhardtii*
- TAP N- TAP medium depleted in nitrogen, used for stress phase
- W Stands for a washing step performed after staining cells with a dye
- CMOS Complementary Metal Oxide Semiconductor (photodetector)
- NR Nile red (lipophilic dye)
- DMSO Dimethylsulphoxid
- EDTA Ethylenediaminetetraacetic acid
- FAMES Fatty Acids Methyl Esters
- SPE Solid Phase Extraction
- OD Optical Density
- PMT Photomultiplier tubes
- FSC Forward scatter signal (flow cytometry)
- SSC Side scatter signal (flow cytometry)
- a.u. Arbitrary units
- LED Light emitting diodes
- ROS Reactive Oxygen Species
- ER Endoplasmic Reticulum
- rPh Photon flow rate
- PtdIns Phosphatidylinositol
- PtdEtn Phosphatidylethanolamine
- DGTS Diacylglyceryltrimethylhomo-Ser
- SQDG Sulfoquinovosyl diacylglycerols
- PtdGro Phosphatidylglycerol
- DGDG Digalactosyldiacylglycerol
- MGDG Monogalactosyldiacylglycerol

- PUFA Poly Unsaturated Fatty Acids
- PUVLCFA Poly Unsaturated Very Long Chain Fatty Acids
- EPA Eicosapentaenoic acid
- DHA Docosahexaenoic acid
- PG Phosphatidylglycerol
- PC Phosphatidylcholine
- PE Phosphatidylethanolamine
- PS Phosphatidylserine
- PI Phosphatidylinositol
- PA Phosphatidic acid
- DGTA Diacylglycerol-O-(hydroxymethyl)-(N,N,N-trimethyl)- β -alanine
- DGCC Diacylglycerol-O-carboxyl-(hydroxymethyl)choline
- G3P Glycerol 3-phosphate
- Lyso-PA Lysophosphatidic Acid
- PA Phosphatidic acid
- DAG Diacylglycerol
- NADH Nicotinamide adenine dinucleotide
- RuBP Ribulose-1,5-bisphosphate
- CBB Calvin-Benson-Bassham cycle
- PSI (P700) Photosystem I, finale molecule: P700
- PSI (P680) Photosystem II, finale molecule: P680
- ETS Electron Transport Chain
- PAR Photo Active Radiation
- DNA Deoxyribonucleic acid
- acetyl-CoA Acetyl coenzyme A
- TCA Tricarboxylic acid cycle
- TEM Transmission electron microscopy
- Cw15 *Chlamydomonas reinhardtii* mutant (cell wall deficient derived from wild type)
- CRwt *Chlamydomonas reinhardtii* wild type.

Chapter 2: introduction

Microalgae, with their high division frequency leading to a high growth rate, outcompete conventional crops for the production of biomass feedstocks for biofuels (ethanol, biodiesel or biogas) [1–3]. The accumulation of intracellular carbohydrates for ethanol production or of triacylglycerols (TAGs) for biodiesel production requires culture conditions that generally differ from those of optimal growth [4–6].

This chapter presents (1) the main differences between growth and lipid accumulation metabolism in oleaginous microalgae, (2) the strategies to trigger lipid accumulation metabolism and (3) how to conciliate significant biomass growth and lipid accumulation in the cells.

A two-step strategy used to cultivate *Chlamydomonas reinhardtii* wild type and trigger lipid accumulation in them is thereafter presented. In this context, optimization of the culture conditions to induce growth and lipid accumulation is required. Among the parameters that affect both growth and lipid storage, duration of the growth and accumulation stages, biomass content at the different stages, light supplied to the culture, pH of the medium, temperature etc can be cited. First, these parameters were carefully chosen taking into account results from the literature.

Finally, the different methods to monitor the biomass properties during lipid accumulation are presented. Lipid contents of microalgae were detected and estimated by three different analytical methods (flow cytometry associated with the use of lipophilic dye, colorimetry, microscopy) and the results are compared. The cell size during the lipid accumulation phase was also estimated by granulometry and microscopy.

I. Morphology, composition and metabolism of green micro-algae

11) Cell structure

Chlorophyceae are one of the classes of green unicellular microalgae, including most of the strains studied in this work: *Chlamydomonas reinhardtii*, *Chlorella vulgaris*, *Parachlorella kessleri*, *Scenedesmus obliquus*. These strains may differ in size and shape but they possess similar organelles with specific functions in the cellular metabolism and enclosed in the polar lipid membrane. A plasma membrane separates the interior of the cell from the external environment. Like terrestrial plants, most of algae also possess a cell wall which provides a good mechanical resistance to the cell. A typical cell structure is presented in Figure 1.

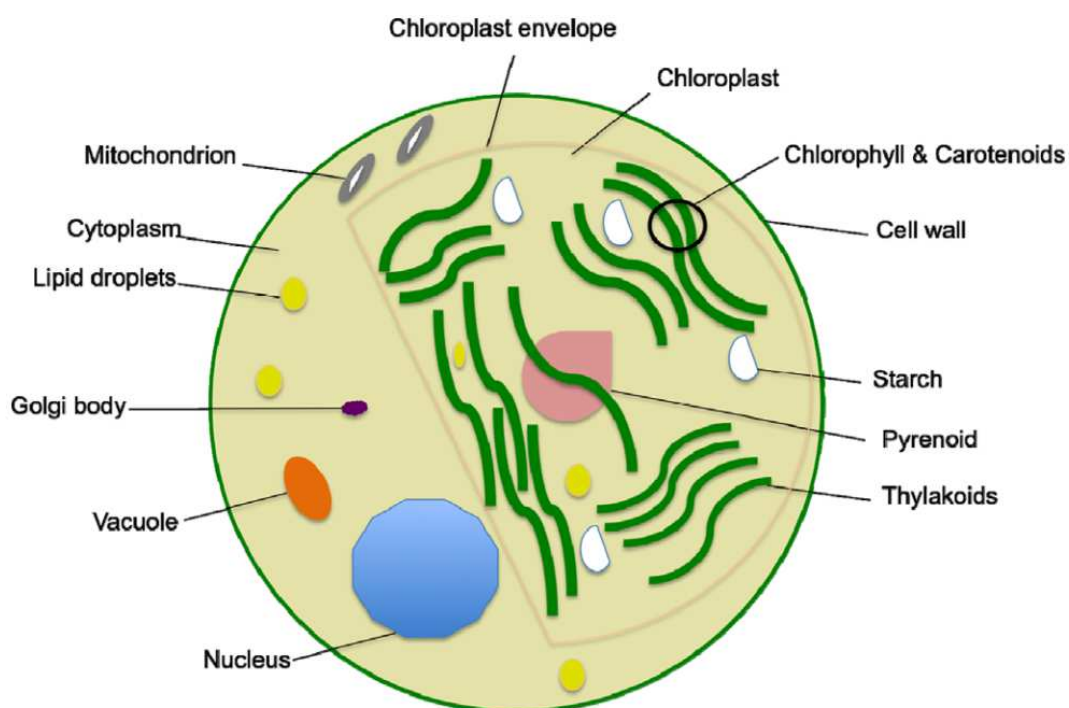


Figure 1: Green microalgae cell structure [7]. **The nucleus** is a membrane-enclosed organelle found in eukaryotic cells which contains most of the cell genetic material organized as chromosomes. **The cytoplasm** comprises the cytosol and organelles, the internal sub-structures. Cytosol represents up about 70% of the cell volume and is a complex mixture of cytoskeleton filaments (e.g. actin filaments and microtubules), dissolved molecules, and water. **Vacuoles** allow the cell to control turgor pressure [8], associated with the gradient of osmotic pressure between the interior and exterior of the cell. **The Golgi body** (also referred as Golgi apparatus) has a major role in protein glycosylation and sorting, but is also a major biosynthetic organelle that synthesizes large quantities of cell wall polysaccharides [9]. **The lipid droplets** are made up of neutral lipids (mainly triacylglycerols, TAGs) stored in the cytoplasm as energy sinks for future use.

11a) Plasma membrane

The plasma membrane (also known as cell membrane or cytoplasmic membrane) is common to all eukaryotic cells and separates the cytoplasm containing organites from the extracellular fluid (Figure 2). It consists in a phospholipid bilayer with embedded proteins. The cell membrane is selectively

permeable and able to regulate the entering and exiting of molar fluxes across itself, by transfer thanks to gradients of e.g ions, dissolved CO₂ and O₂ and other compounds.

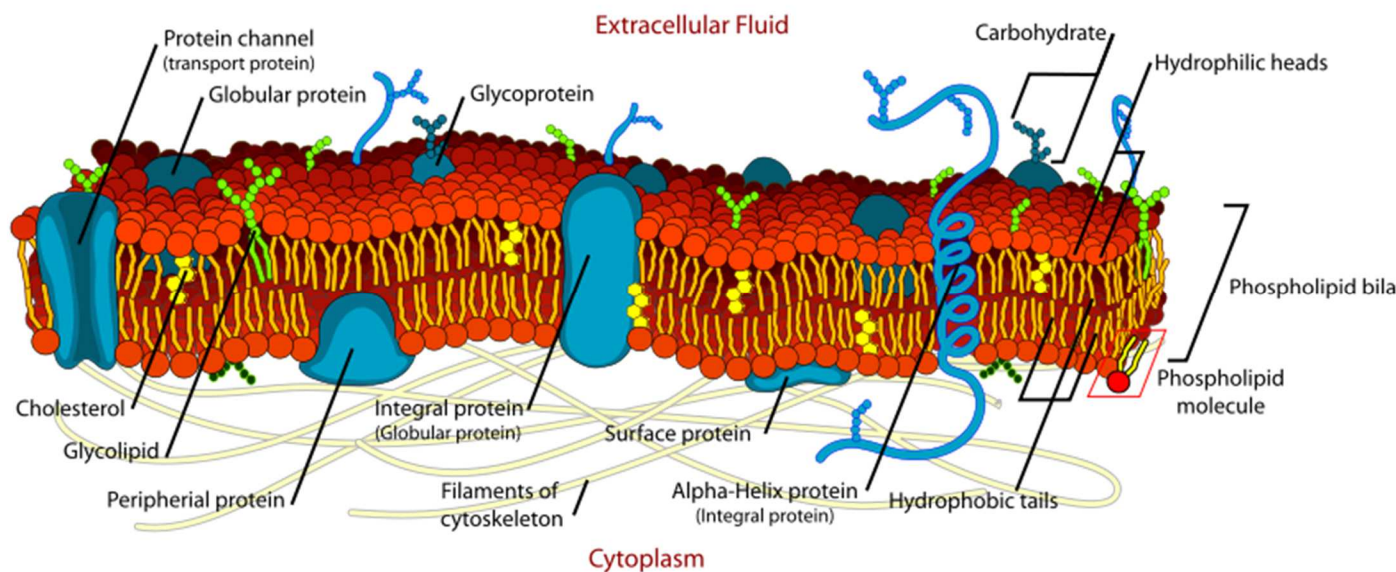


Figure 2: Diagram of the cell membrane

In addition, the transmembrane proteins enable the transport of nutrients such as sugars and amino acids into the cell and the excretion of metabolites by active pumping. The cytoskeleton underlying the cell membrane is a complex network of filaments and tubules that extends through the cytoplasm to the nucleus. It provides an internal mechanical resistance to the cell and helps to maintain its shape. The cell membrane also contains various proteins (around 50% of membrane volume) and carbohydrates.

11b) Cell wall

The cell wall is a particularity of plants, algae, fungi and prokaryotic cells and it is not present in mammalian cells. The composition and structure of algae cell walls greatly vary with strains. In most cells, the cell wall is flexible but has a considerable tensile strength. Many Chlorophyceae possess microfibrillar cellulose, homogalacturonans and rhamnogalacturonan-I, extensin and arabinogalactan constituents [10].

11c) *Chlamydomonas reinhardtii* specificities

In *Chlamydomonas*, the cell wall does not contain cellulose but is made of crystalline glycoproteins, specifically based upon aggregates of hydroxyproline-rich glycoproteins (HFGPs) and glycine-rich glycoproteins. The *Chlamydomonas reinhardtii*'s cell wall is structured in 7 layers (Figure 3). The inner layer, W1 is made of anastomosing fibers in a non-dense trabecular network of 30 to 200 nm width. Layers W2 and W6 are made of glycoproteins surrounding a granular layer W4. Layers W3 and W5 are electron-transparent regions that are probably non-dense spaces rather than true wall components. The W7 layer (outer layer) contains non-structural glycoproteins in a transitional stage prior to their release into the culture medium [11]. *Chlamydomonas reinhardtii* has been muted in several strains

with altered cell walls. The Cw15 mutant fails to assemble the central triplet W2-W6 layers and only has fibers resembling the outer layer of the wild-type wall.

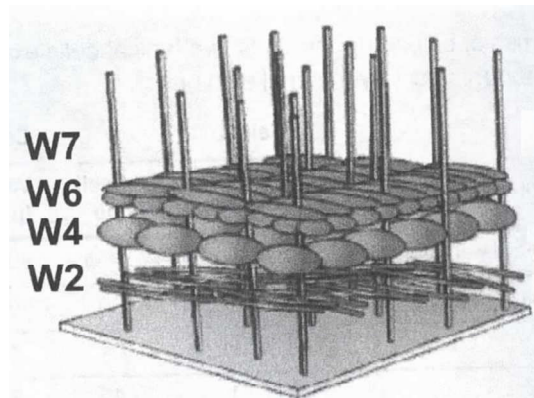


Figure 3: Diagram of the cell wall of *C. reinhardtii* [11]. W1, W3 and W7 are non-dense layers.

Chlamydomonas reinhardtii has a structure similar to the general one of a green microalga presented in Figure 1. The only specificities are (1) a U-shaped chloroplast, (2) a pair of flagella of 12 μm length and less than 0.5 μm width [12] and (3) an eyespot (Figure 4). The eyespot consists of two layers of regularly arranged electron dense granules of 80-130 nm diameter; it reflects incident light back to a rhodopsin photoreceptor situated in the plasma membrane which enables the cell to orient its movement towards light. The flagella enable the cell to swim in the direction of light, detected by the eyespot; the average forward swimming speed is about 100 - 200 $\mu\text{m}/\text{sec}$.

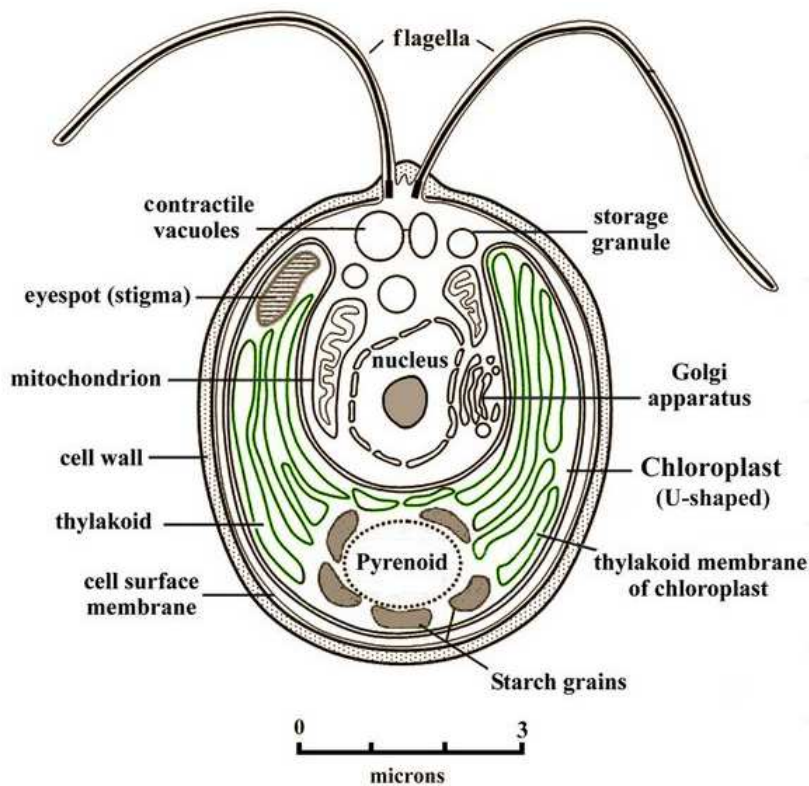


Figure 4: *Chlamydomonas reinhardtii* structure [13]

Images of *Chlamydomonas reinhardtii* recorded with Transmission Electronic Microscopy (TEM) are presented in Figure 5. The cell structure and relative composition evolve with the culture conditions; here a nitrogen depletion in the medium increases starch (grey granules) and neutral lipid content (dark spots) on the cell [14].

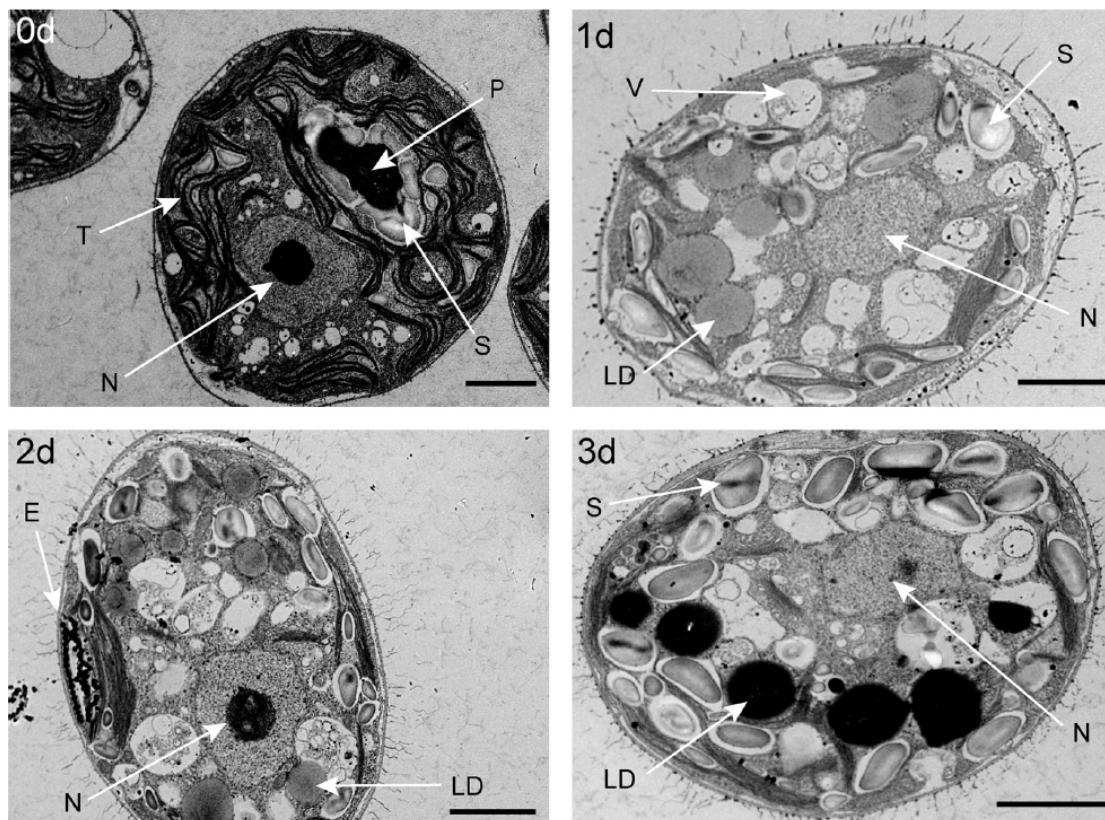


Figure 5: Ultrastructure of *Chlamydomonas reinhardtii* during N limitation [14] after 0; 1; 2; and 3 days of stress. Scale bars represents 2 μm . E, Eyespot; LD, lipid droplets; N, nucleus; P, pyrenoids; S, starch granules; T, thylakoid membranes; V, vacuoles.

Under optimal growth conditions, the cell undergoes two or three rounds of mitosis before the daughter cells are released from the old cell wall into the medium. Thus, a single growth step may result in 2 to 16 daughter cells per mother cell. In bright light at 25°C, the exponential phase cells typically divide three times to produce eight daughters, but at lower temperatures or lower light (below $100 \mu\text{mol}\cdot\text{m}^{-2}\cdot\text{s}^{-1}$) intensities, two divisions are more usual. The number of division is generally proportional to the growth rate [15]. The use of light and dark cycles synchronizes the circadian cycles and division behavior in the cell population. Cell division can be separated into two phases: interdivision and division phases (Figure 6, [16]). The mother cell increases in size during a step referred to as commitment size (G step). During this step, organelles (chloroplast, pyrenoid, golgi apparatus) and nucleus increase in size and separate in the future daughter cells. The ratio of the cell volume at the beginning of the division phase to the initial cell volume determines the number of daughter cells. S/M cycle is referred to as synthesis of DNA and mitosis steps that generate daughter cells of uniform size enclosed within a single mother cell wall. During the S/M step, the cells lose their flagella and recover it after being released individually in the medium.

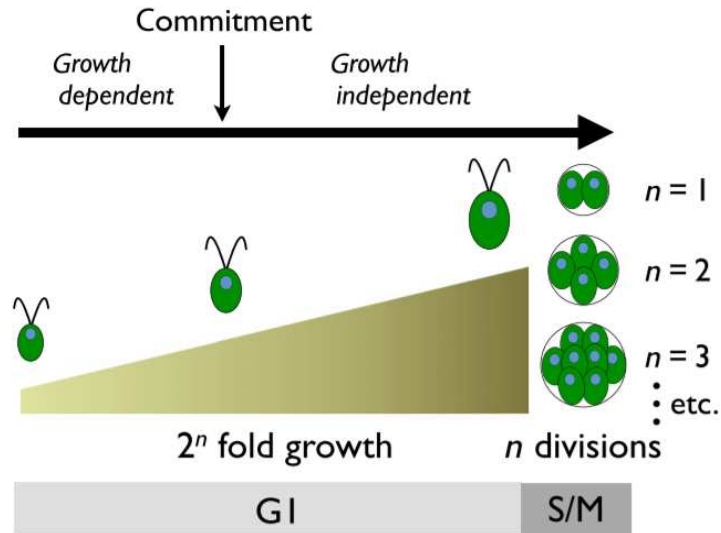


Figure 6: Commitment size (G) and synthesis/mitosis (S/M) cycles [16]. The number of division n may vary from 1 to 5 leading from 2 to 32 daughter cells.

12) Respiration activity

A **mitochondrion** is a double membrane organelle found in all eukaryotic algae cells, which produces energy as Adenosine Tri-Phosphate (ATP) through respiration (Figure 7). A mitochondrion contains outer and inner membranes composed of phospholipid bilayers and proteins. The central set of reactions of mitochondrion producing ATP is the Krebs cycle, also known as tricarboxylic acid (TCA) cycle.

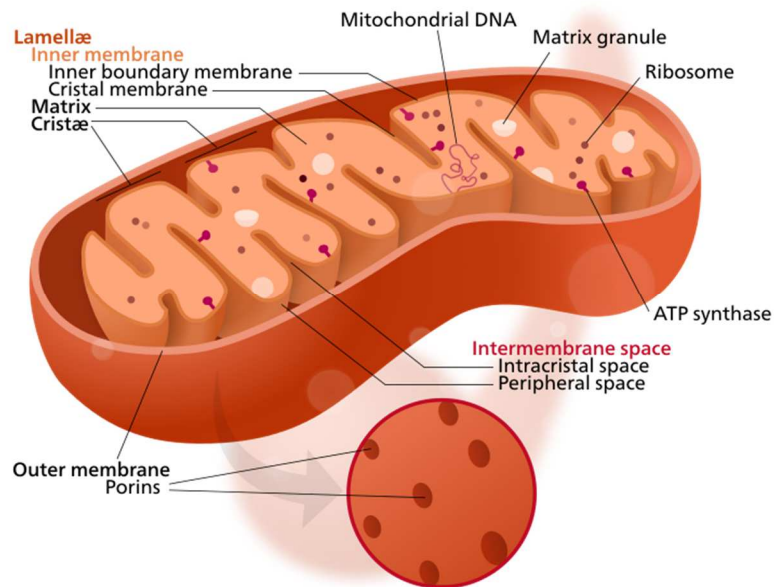


Figure 7: Mitochondrion structure [17]

The TCA cycle generates energy through the oxidation of acetyl-CoA derived from carbohydrates, fats and proteins, into CO_2 and ATP. The involved reactions are carried out by 8 enzymes with complete oxidation of acetate, in the form of acetyl-CoA, into two molecules of CO_2 and water.

13) Photosynthetic activity

13a) Chloroplasts

The chloroplast is the organelle responsible for photosynthesis. Briefly, it contains the photosynthetic pigments which capture light and are involved in a set of light reactions that produce the energy required to fix CO₂ and convert it into organic carbon (during Calvin cycle). The ellipsoid-shaped chloroplast is enclosed in a double membrane, composed of two layers separated by the intermembrane space (Figure 8). The outer layer is a semi-porous membrane which features a number of embedded membrane transport proteins. The inner chloroplast membrane borders the stroma and regulates passage of materials in both directions. Also, fatty acids, lipids and carotenoids are synthesized in the inner membrane. Enclosed by the chloroplast membrane is the **stroma**, a protein-rich, alkaline, semi-gel-like material that contains dissolved enzymes and in which the thylakoid system floats. The Calvin cycle, which fixes CO₂ into organic carbon takes place in the stroma.

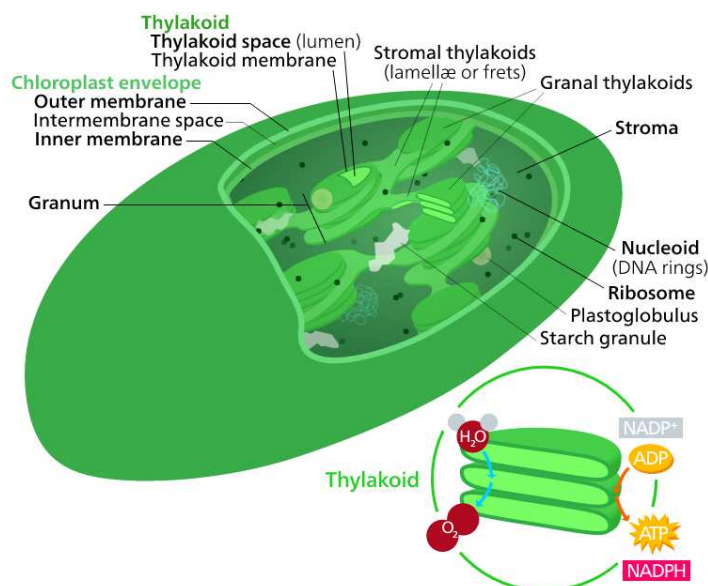
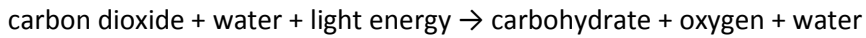


Figure 8: Cell chloroplast structure [18]

Like mitochondria, chloroplasts possess their own genomes (DNA) and **ribosomes**, they are used to synthesize chloroplast proteins, *e.g.* Rubisco (Ribulose-1,5-biphosphate-carboxylase-oxygenase), the enzyme that fixes CO₂ into sugar molecules. Rubisco self-assembles into **pyrenoids**, which is the center of carbon concentration mechanisms in microalgae. **Starch** granules are synthesized from fixed CO₂ or dissolved inorganic carbon (DIC) and are accumulated around pyrenoids.

Thylakoids are small interconnected sacks which contain the membranes where the light reaction of photosynthesis takes place. There are two types of thylakoids: granal thylakoids and stromal thylakoids. The flat tops and bottoms of granal thylakoids contain the photosystem II protein complex (detailed below). Photosystem I and ATP synthase are large protein complexes found in the stromal thylakoid membrane. The number of thylakoids and the total thylakoid area of a chloroplast are influenced by light exposure. A low amount of light leads to increased surface area in order to improve light capture. Photosystems I and II contain light-harvesting complexes with chlorophyll and carotenoids that absorb light energy and use it to energize electrons.

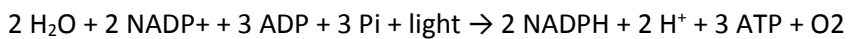
Photosynthesis provides the energy to drive the process of carbon fixation and the reducing power (NADPH) to convert carbon dioxide into a carbohydrate via a reduction reaction. The general equation of photosynthesis is written below:



Photosynthesis occurs in two separated steps (1) light-dependent reactions and (2) light independent reactions.

During light-dependent reactions, the energy of light is captured and converted to energy storage molecules ATP and NADPH.

The overall equation for the light-dependent series of reactions is:



where Pi stands for inorganic phosphate.

13b) Light conversion to electrons

Light is generally referred as the visible region of the electromagnetic radiation spectrum (in the range 400 - 740 nm) as illustrated in Figure 9.

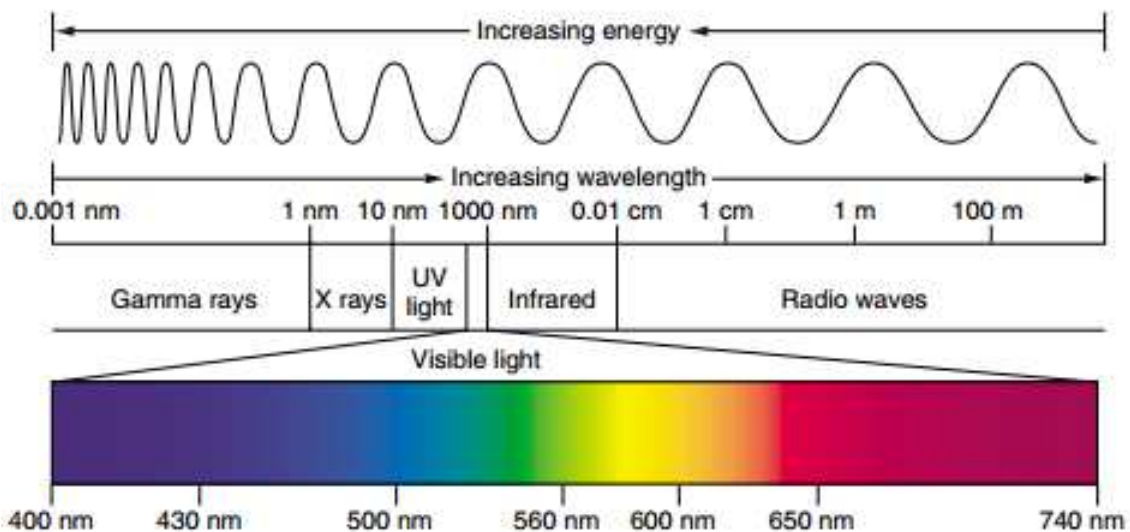


Figure 9: The electromagnetic spectrum. Light is a form of electromagnetic energy conveniently represented as a wave. The shorter the wavelength of light, the greater its energy. Visible light represents only a small part of the electromagnetic spectrum between 400 and 740 nm [19].

Light is a charge-less bundle of energy (quanta or photons) diffused as a wave or particles depending on the conditions, and thus can be described as a quantic particle like electrons. At the molecular scale of the light reaction complex, a quantum of visible light collides with photosynthetic pigments that are able to react with photons at a certain level of energy, *i.e.* at a certain wavelength.

Antenna complexes containing several pigments able to absorb photons in the range of 400 to 680 nm (known as Photosynthetic Active Radiations, PAR, and illustrated in Figure 10.a) are situated in thylakoid membranes ,

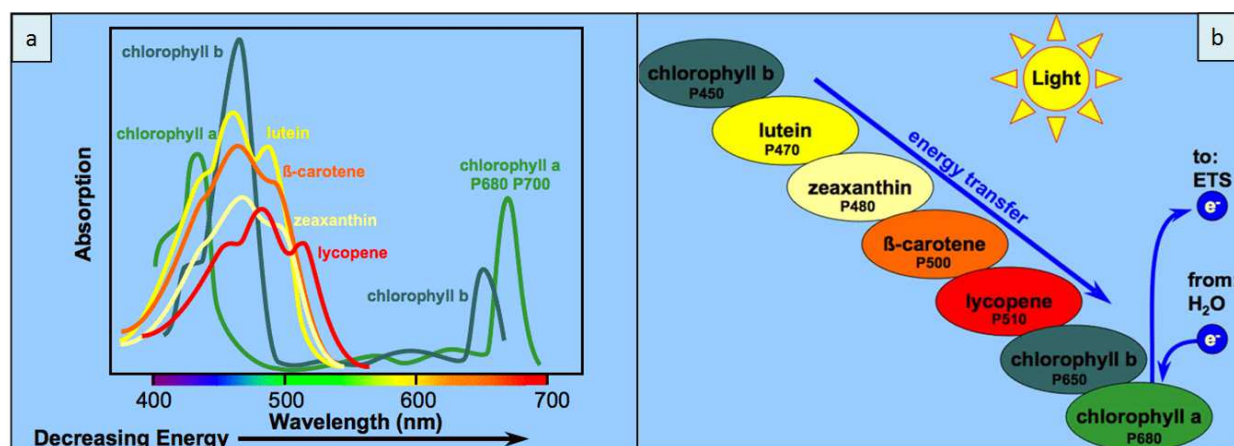


Figure 10: a) Photosynthetic pigments and corresponding capture wavelengths. b) Transmission of energy in photosystems. The Pigments composition varies with algae species and light conditions. ETS stands for Electron transport chain, detailed below.

The reaction centers of photosynthetic systems are organized as a cluster of various pigments which can absorb the visible light and transmit the energy to the reaction center constituted by a pair of Chlorophyll a molecules capturing light at the optimal wavelength of 680 (P680, Figure 10.b). In green microalgae (Chlorophyta), these pigments are chlorophyll a, b and carotenoids such as lutein, zeaxanthin, β -carotene, α -carotene, antheraxanthin, violaxanthin, astaxanthin, cantaxanthin and neoxanthin [20].

Many side pigments may also act as photoprotective pigments by converting an excess of energy into heat or act as an antioxidant to avoid the formation of triplet excited chlorophyll a. The dissipation of energy in the photosystem leads to a reduction of the photosynthetic yield.

The photosynthetic yield expressed as the fraction of light energy converted into chemical energy varies within the range of 5 – 7 % while the theoretical maximal yield is approximately 15 – 20 % of the visible light [21] (theoretical yield of 7.5 - 8.5 % when UV and Infrared are considered). The conversion yield depends on factors such as the light flow density and the pigments composition of the photosystems. The presence of characteristic pigments (carotenoids, phycobiliproteins) depends on algae species. The relative pigment composition in a cell culture may also greatly vary during time, depending on the light supplied, shading effects, nutrient depletion *etc.* to maximize the photosynthetic yield with limited heat and oxidative damages. In other words, in reduced light conditions, the algae will deploy a large antenna, while during a light inhibition the antenna is reduced. In the case of photo-inhibition, the algae may synthesize more pigments around the antenna to act as chemical quenchers that will protect chlorophyll [22].

The absorption of energy by P680 frees an electron by a process called photoinduced charge separation illustrated on the right in Figure 10.b. That free electron is transferred to the primary electron-acceptor molecule, Pheophytin a (Pheophytin a is a chlorophyll a molecule with the magnesium atom replaced by two protons).

13c) Electron transport chain

Briefly, electrons are continuously lost from photosystem II to photosystem I through a non-cyclic electron transport chain (generally referred as Z-scheme, illustrated in Figure 11), and recovered in PSII by water-splitting. Then, the electrons are excited a second time in photosystem I to a second electron transport chain to finally reduce NADP into NADPH. The first electron transport chain from PSII to PSI leads to an accumulation of protons in the stroma. This electro-chemical potential serves to generate ATP thanks to ATP synthase.

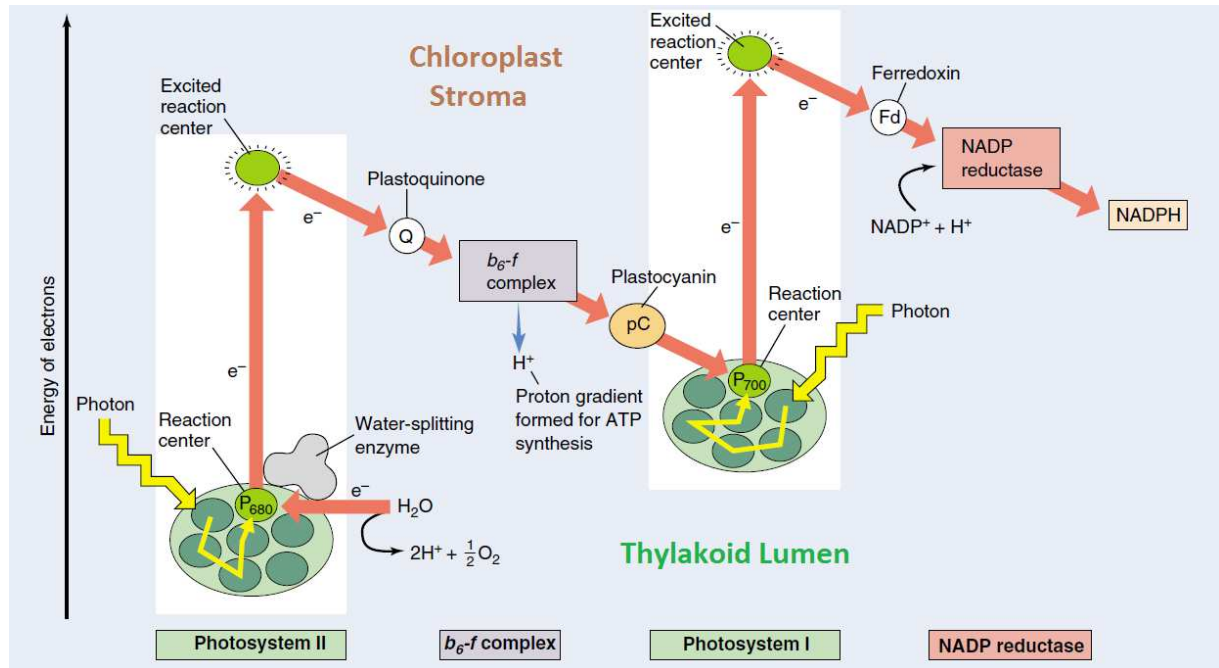
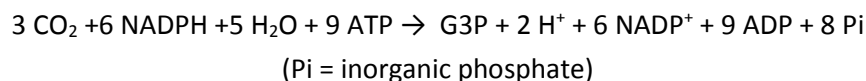


Figure 11: Light reactions of photosynthesis, modified from [19]. The electrons provided by PSII are transmitted to PSI, a photosystem with a pair of central Chlorophyll a that absorb light at 700 nm (P700). There, it is further excited by the light absorbed by P700 after a transmission of the photon through the pigments antenna. The electron is then passed along a chain of electron acceptors to which it transfers some of its energy. The energy delivered to the final electron acceptors, ferredoxin, is used to move hydrogen ions across the thylakoid membrane from the stroma to the lumen in the b₆-f complex. The protons accumulated in the stroma must pass through the channels provided by ATP synthase. As protons pass through ATP synthase, ADP is phosphorylated to ATP and released into the stroma. Since the excited electron does not return to PSII, this mechanism for making ATP is called noncyclic photophosphorylation. The electron is eventually used to reduce the co-enzyme NADP with a H⁺ to NADPH (which has functions in the light-independent reaction); at that point, the path of that electron ends. Because PSII is the electron donor of the electron transport chain, a source of electron must reduce the oxidized chlorophyll a molecule of PSII. This source of electron is water which is split into diatomic oxygen and protons thanks to a dedicated enzyme. The electrons yielded are transferred to a redox-active tyrosine residue that then reduces the oxidized chlorophyll a center P680. Oxygen is the waste product of light reactions.

13d) Dark reactions (Calvin cycle)

The **Calvin cycle**, Calvin-Benson-Bassham (CBB) cycle, also known as the dark reactions, is a series of biochemical redox reactions that take place in the stroma. This cycle fixes CO₂ into 3-phosphoglyceraldehyde (also referred as Glyceraldehyde 3-phosphate G3P) molecules and uses the energy and electrons delivered from ATP and NADPH produced in the light reactions.

The cycle can be described by the following global reaction:



The Calvin cycle can be divided into 3 simple stages as illustrated in Figure 12:

- (1) The cycle starts with the enzyme Rubisco which fixes CO₂ into a five-carbon Ribulose biphosphate (RuBP) molecule. This results in an unstable molecule with 6 carbon atoms.
- (2) The molecule created rapidly breaks down into molecules containing 3 carbon atoms and called 3-phosphoglyceric acid (3-PGA). ATP and NADPH provided by the light reactions are used to convert 3-PGA into G3P, glyceraldehyde-3-phosphate.
- (3) The next stage in the Calvin cycle is the regeneration of RuBP (Rubisco bi phosphate). Five G3P molecules produce three RuBP molecules, using three molecules of ATP.

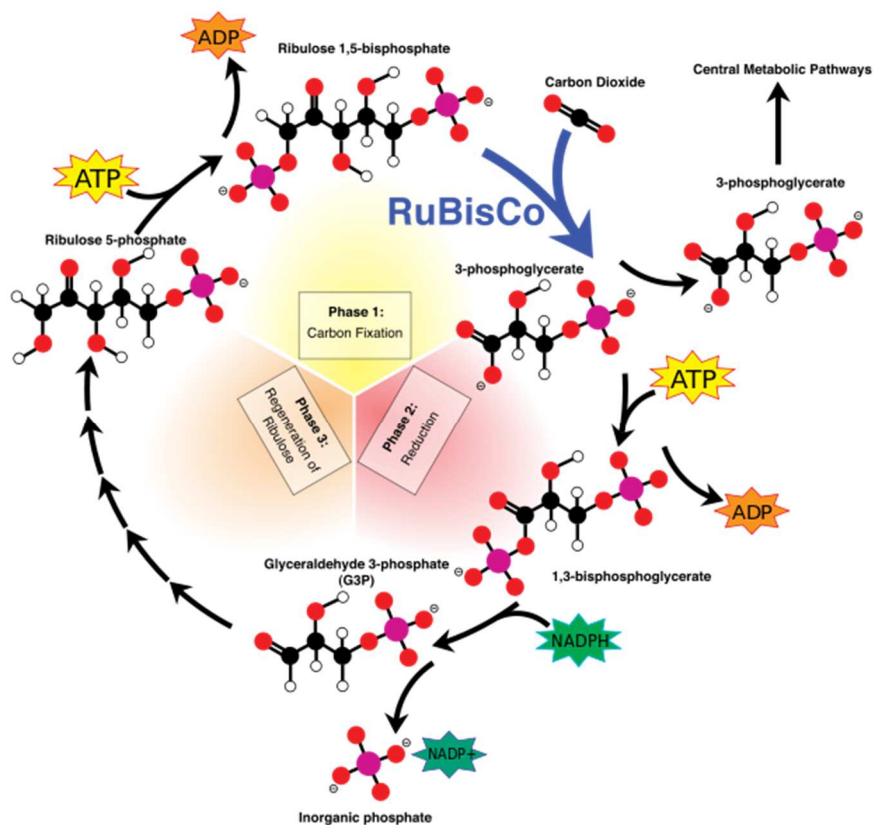


Figure 12: Dark reactions of photosynthesis

II. Lipid biosynthesis and composition

II.1) Lipid synthesis in microalgae: From light to TAGs

Lipids are essential constituents of living organisms and are defined as compounds readily soluble in non-polar organic solvents, but insoluble in water [23].

Fatty acids are the building blocks of these lipids. In algae and plants, the *de novo* synthesis of fatty acids uses as substrates the photosynthetically fixed carbon molecules of the Calvin cycle (*e.g.*, G3P) (Figure 13).

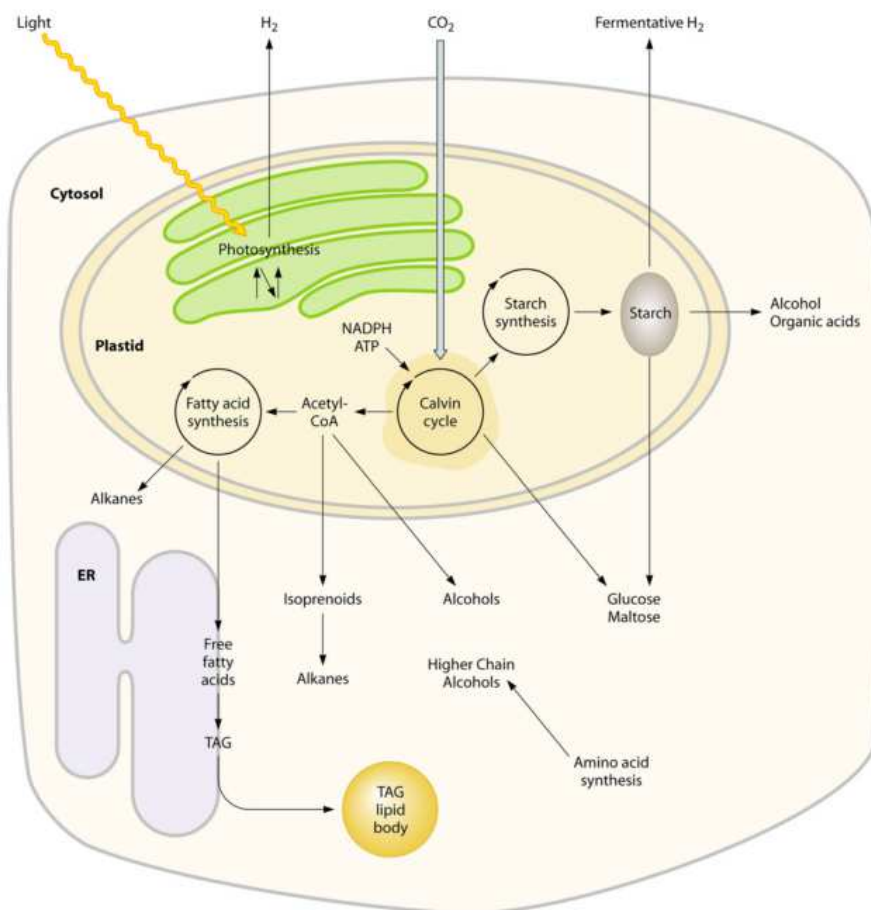


Figure 13: Microalgal metabolic pathways. ER: Endoplasmic Reticulum [24].

The fixed sugars are further processed to produce acetyl-coA (coenzyme A), a precursor for fatty acid synthesis in the chloroplast. This synthesis requires stoichiometric amounts of ATP, acetyl CoA and NADPH for each two carbon atoms added to the growing acyl chain (acyl groups are derived from hydrolyzed fatty acids). Photosynthetic reactions are thus essential in providing a carbon source and generating reducing power (NADH and NADPH) and energy (ATP) for fatty acid synthesis [25].

The first step in fatty acid synthesis is the conversion of acetyl-CoA to malonyl Coa, catalyzed by acetyl-Coa carboxylase (ACCase) [23]. Subsequently, malonyl Coa is converted to a long chain fatty acids through a complex pathway which requires successive enzymatic reactions (*e.g.* conversion of CoA to ACP catalyzed by malonyl Coa:ACP transferase).

Afterwards, the FAs synthesized in the chloroplast are transferred to the endoplasmic reticulum (ER) membranes for synthesis of membrane polar lipids and cytosolic storage neutral lipids (mainly triacylglycerols). Triacylglycerols (TAGs) are formed by the sequential acylation of glycerol-3-phosphate backbone (G3P) with three acyl-CoAs catalyzed by a group of enzymes named acyltransferases (Figure 14).

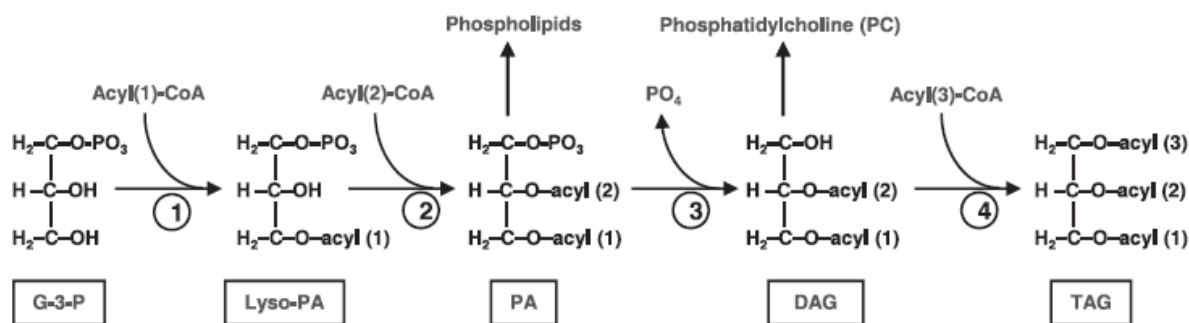


Figure 14: TAGs pathway in ER [26]. (1) Cytosolic glycerol-3-phosphate acyl transferase, (2) lyso-phosphatidic acid acyl transferase, (3) phosphatidic acid phosphatase, and (4) diacylglycerol acyl transferase.

At first, TAGs are sequestered and accumulated, due to their hydrophobicity, between the two layers of the ER membrane (Figure 15) [27]. During ongoing synthesis of TAGs, an oil droplet is formed. After reaching a certain size, this droplet is released into the cytosol as an independent oil body.

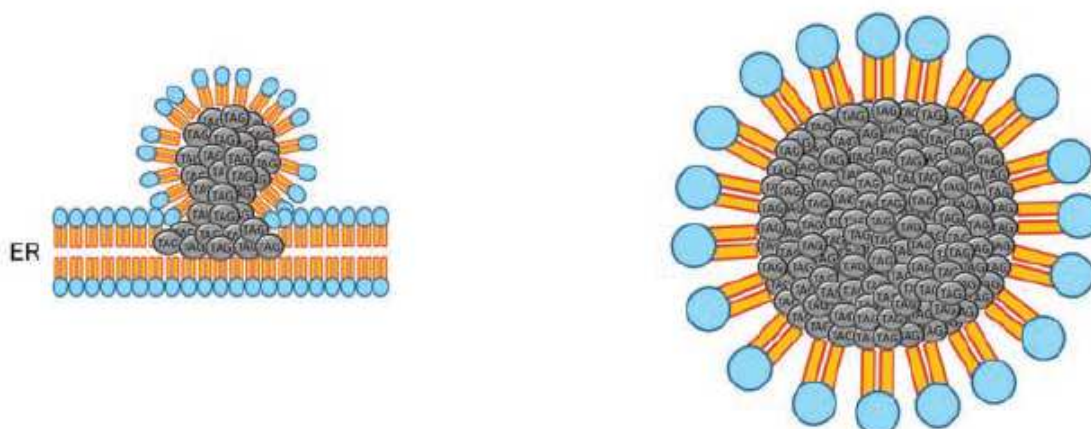


Figure 15: Oil body biosynthesis in the ER. Accumulation of TAGs between the two layers of ER (left part) and release of an independent oil body into the cytoplasm (right part).

In parallel with lipid synthesis, algae can also synthesize and store carbohydrates as starch. Many algae use starch as the primary storage of organic compounds in priority to neutral lipids. The regulation of starch and lipid syntheses and the possible interaction between both pathways is still poorly understood; but some studies are performed to inactivate the starch synthesis pathway and then increase lipid accumulation [23,28].

11.2) Lipid classes

Lipids are hydrophobic molecules containing hydrocarbons. There are four types of lipids in microalgae: **phospholipids**, **glycolipids**, **betaine lipids** and triacylglycerols (**TAGs**).

11.2a) Polar and neutral lipids

Because of their polar heads, the majority of the lipids presented here are classified as **polar lipids**. Only TAGs, consisting in three fatty acids bound to a glycerol backbone, are classified as **neutral lipids**.

TAGs as well as polar lipids contain acyl groups (represented by R in Figure 16) [27]. A minor part of the neutral lipids can also be in the form of diacylglycerol, monoacylglycerols or even free FAs.

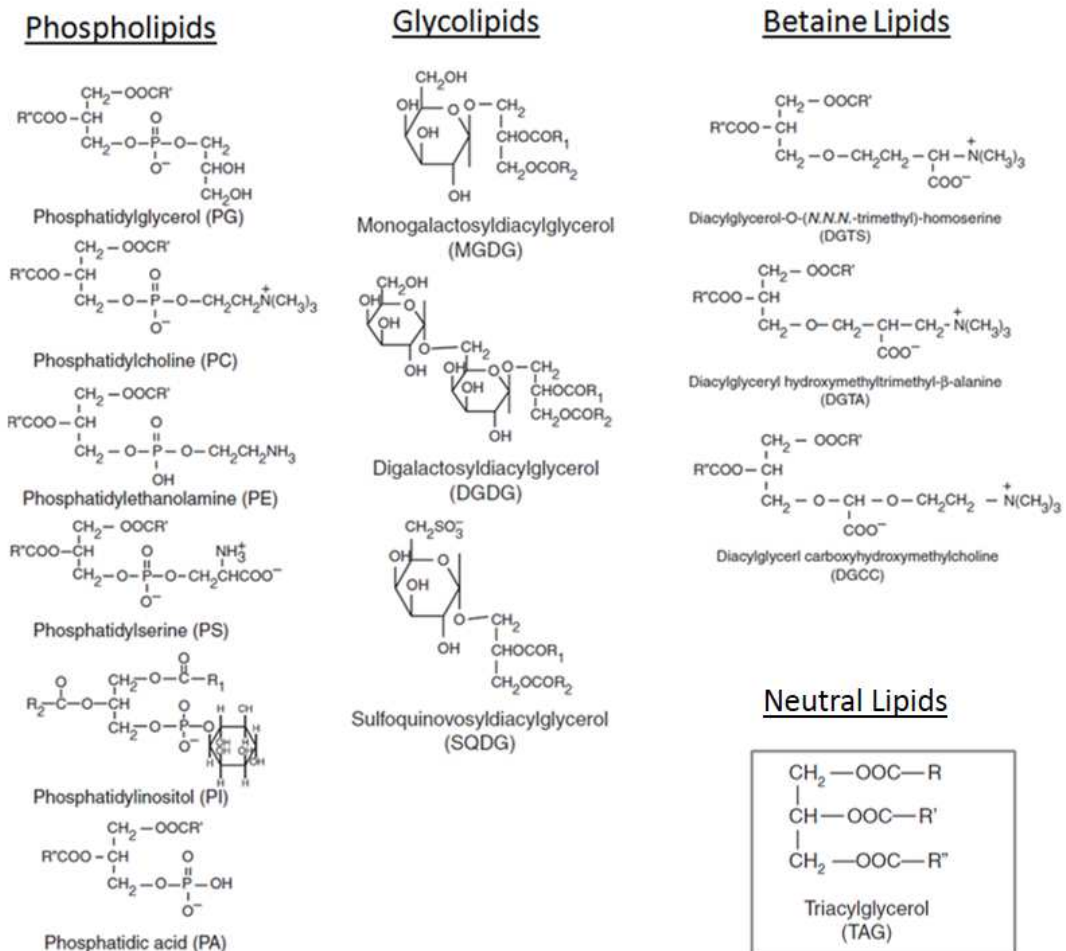


Figure 16: Lipid molecules generally found in algae modified from [29]

Polar glycolipids are predominantly located in photosynthetic membranes with MGDG (Monogalactosyldiacylglycerol, see Figure 16) and SQDG strictly restricted to the thylakoid membranes of the chloroplast while DGDG is also found in the extraplastidial membranes [29]. PG is the only phospholipid present in thylakoid membranes of the chloroplasts [25]. DGTS is a betaine glycerolipid that can also be found in the organelles of many lower plants and algae [30]. The plasma membrane of algae is mostly composed of phospholipids: PE, PC and/or PI. The composition in phospholipids varies with the photosynthetic species. For example, PC is the major phospholipid in land plants but is not present in *Chlamydomonas reinhardtii*.

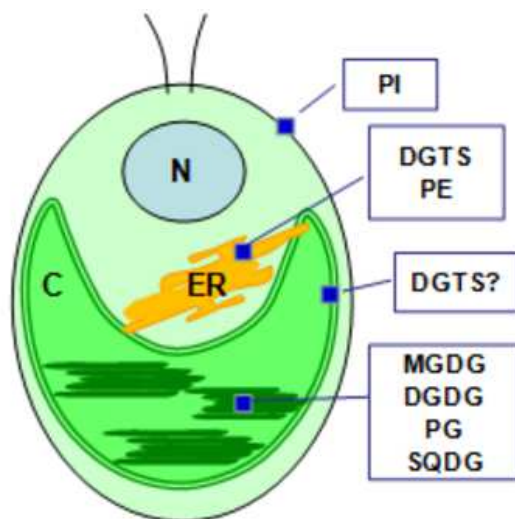


Figure 17: Major polar lipid classes in *Chlamydomonas reinhardtii* [25]

112b) Fatty acids

Fatty acids in *Chlamydomonas* usually have similar acyl chain lengths to those present in most land species [31]: 16 and 18 carbon atoms (C16-C18). The fatty acids are saturated (with no double bond C-C) (noted C16:0 and C18:0), mono-unsaturated with one double bond (C16:1 and C18:1) or poly-unsaturated with at least two double bonds (PUFA); the last class is not generally present in *Chlamydomonas*.

In other algae strains, the chain length can vary from 14 up to 22 carbon atoms with up to 6 double bounds [6]. Poly unsaturated very long-chain fatty acids (PUVLCFAs) are elongated fatty acids synthesized in specific algae groups such as euglenophytes, diatoms and haptophytes which possess desaturases/elongases enzymes able to produce PUVLCFAs from C18 and derivatives [27]; examples of PUVLCFAs are Arachidonic acid 20:4(ω -6), Eicosapentaenoic (EPA) C20:5 (ω -3) and Docosahexaenoic acid DHA C22:6 (ω -3). ω 3 EPA and DHA are high value compounds for nutrition and medicine. Complementary omega 3 fatty acids are used to increase the ω 3/ ω 6 balance to 1/1, the optimal balance for health [32] because it has a direct influence on blood fluidity. Additionally, ω 3 DHA is very important for fetus development, pregnancy outcomes, cognitive development and maintenance, learning and memory, visual function, immune system, and more.

In a prospect of producing biodiesel by transesterification of TAGs to fatty acid methyl esters (FAME), the nature and proportion of fatty acids are critical for biodiesel quality. Critical parameters like cetane number (combustion speed and compression needed for ignition), iodine value (oxidation stability) and cold filter plugging point (CFPP, fluidity and density) are correlated with the methyl ester composition. An optimal diesel production requires a high amount of mono-unsaturated fatty acids with low levels of saturated and poly-unsaturated FAs [33] as illustrated in Figure 18 (maximum of 20 % of saturated FA, between 50 to 100 % of mono-unsaturated FA and a maximum of 30 % of PUFA).

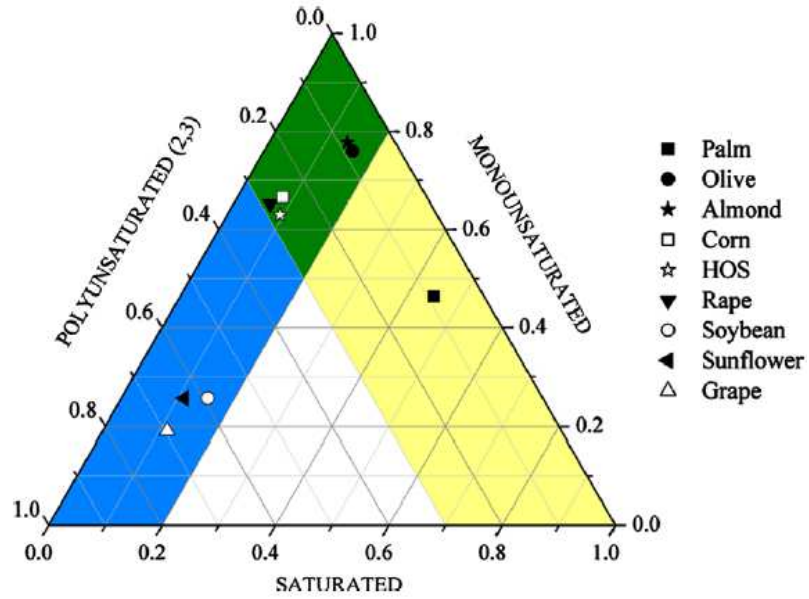


Figure 18: Finetti diagram of the biodiesel qualities according to their monounsaturated, polyunsaturated and saturated methyl esters mass fractions. Yellow: good cetane number and iodine value, blue: good CFPP, green: biodiesel that satisfies the European Standard UNE-EN 14214 [33]. The analysis of the fatty acid composition of TAGs is required to situate the oil quality produced by the algae.

113) Culture conditions and cell composition

113a) Cell composition during growth

The cell content in neutral lipids (TAGs) is low in growth conditions in the majority of microalgae. For *Chlamydomonas reinhardtii* in growth phase, the total lipid content (polar+neutral) is less than 20% of the dry weight and the TAG proportion in these lipids is only 1 % (Figure 19).

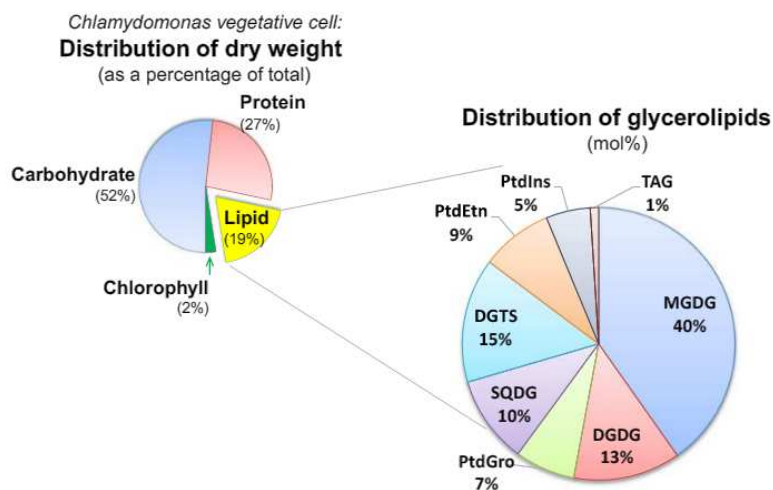


Figure 19: Cell composition in terms of carbohydrate, protein, chlorophyll and glycerolipids in *Chlamydomonas reinhardtii* (growth condition). PtdGro (PG), TtdEnt (PE), and PtdIns (PI) [34].

113b) **Stress induction: from functional to storage lipids**

Fatty acids produced in plastids of the chloroplast and modified in the ER are retained as structural components of cellular membranes [27] and serve as functional biomass together with synthesized proteins as illustrated previously.

Under certain culture conditions, carbohydrates (starch) and neutral lipids may be accumulated to store the energy supplied from the chloroplast. These storage compounds may be easily catabolized [35] and serve as a source of organic compounds in the Krebs cycle when there is no energy available from photosynthetic activity, for example when the cell is in the dark zone of a photobioreactor or during the night period.

The composition of algal biomass is strongly dependent on culture conditions [36]. A lack of nutrient in the culture medium, changes in CO₂ level, light or pH conditions may lead to a radical change in cell metabolism. In the so called "adverse growth conditions", also referred as "stress conditions", the energy available from the light reactions is not used to produce functional biomass in priority (Figure 20), many algae alter their lipid biosynthetic pathways toward the synthesis and accumulation of neutral lipids as cytoplasmic lipid bodies. In contrast, in favorable growth conditions, they synthesize fatty acids as substrates for esterification into glycerol based polar lipids [4].

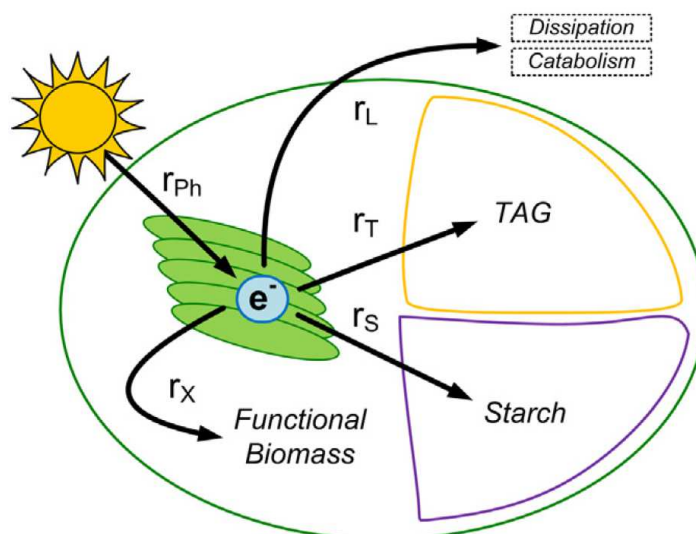


Figure 20: Schematic representation of the chemical energy distributed from the photosystem. Photons (r_{ph}) are absorbed and used to drive electrons from water, ending up in functional biomass (r_x), TAG (r_T) and starch (r_S). r_L represents the light energy dissipated in the thylakoids on one hand and used in catabolism on the other hand [36].

When the flow of photons is increased and the ability of the cell to produce functional biomass is decreased (nutrient depletion), the cell needs to trigger the energy storage pathways in order to reduce the excess of energy released in dissipation (heat) /catabolism (formation of harmful reactive oxygen species ROS). When ROS accumulate and cause irreversible damages, algae experience photoinhibition and oxidative stress [37]. In these conditions, the cell increases the pathways of starch and TAG metabolism and modify the photosynthetic apparatus as described previously.

The carbon distribution between starch and neutral lipid as energy storage compounds is highly dependent on the algal strain and on the stress duration [38]. Most green algae (Chlorophyta), as *Chlamydomonas reinhardtii* [36], produce and accumulate carbohydrates (starch) as a primary energy and carbon reserve, whereas TAGs serve as a secondary storage under growth conditions [7]. Starch storage is the immediate available energy that can be used by algae for important metabolic processes.

Some algae accumulate only starch during a stress period, some others both starch and TAGs; several strains transiently accumulate starch before forming lipids. As illustrated in figure 20, a reduced amount of nutrient (medium diluted 10 fold) leads to an accumulation of starch in the first days of stress followed by an accumulation of storage lipids for *Parachlorella kessleri* [4]. After placing cells in a nutrient rich medium (medium 1), a sharp decline in the levels of lipid and starch is observed.

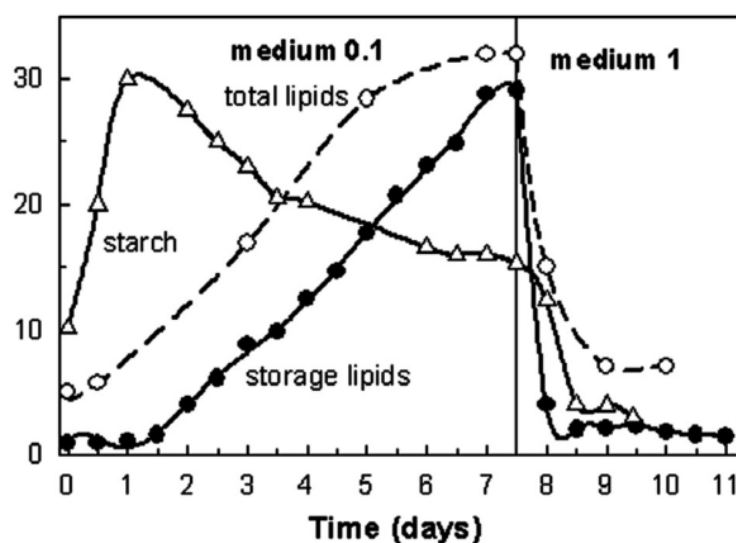


Figure 21: Change in relative starch, total lipid and storage (neutral) lipid content (% DW) in cultures of *Parachlorella kessleri*. Cultures were firstly grown in a 10 fold diluted medium to induce a stress (medium 0.1) and then transferred into a complete mineral medium (medium 1) [39].

Nutrients limitations invariably cause a steadily declining cell division rate and modify carbon partition from functional biomass to storage compounds (neutral lipids/starch) [35]. Nitrogen is the most critical nutrient affecting lipid metabolism in algae. Under nitrogen limitation the capacity for protein synthesis is reduced [40]. Sulfur and phosphorous deprivation also affect lipid biosynthesis [35].

In *Chlorella vulgaris*, nitrogen deprivation allows a good lipid productivity of $53.96 \pm 0.63 \text{ mg.L}^{-1}.\text{d}^{-1}$ while all other stresses (deprivation of potassium-phosphate, of iron and of nitrogen- potassium-phosphate and iron) resulted in lower lipid productivities [41].

Most of the time nitrogen depletion is associated with high light intensity to trigger the accumulation of neutral lipid and/or starch. In these conditions, a strong reduction of the growth rate is observed. Storage lipids can thus be considered as secondary metabolites, *i.e.* metabolites not associated with biomass growth. However, when taking into account the neutral lipids productivity, biomass growth rate and lipid content must also be considered. Thus, a lipid production strategy must conciliate the

opposite conditions of growth (complete medium, optimal light supplied) and lipid accumulation (nitrogen depletion, excess of light).

II3c) **Strategies to conciliate algae production and lipid content**

The strategies to cultivate the cells in order to obtain a high lipid content are:

(1) Two step batch method:

The cells are cultivated in a nutrient complete medium to maximize their production, they are afterwards re-suspended in a nutrient depleted medium to stop biomass production and increase the lipid storage [4,6,38,41–43]. This method is easy to set at laboratory scale with centrifugation of the cells between both steps, but technically more difficult at large scale.

(2) One step batch method

The cells are grown in a diluted medium where nitrogen and/or other nutrients are in insufficient quantities. The cells firstly grow and completely consume the nutrients; they afterwards start to accumulate lipids and/or starch [44–46]. This method is more suitable for large scale cultures.

(3) Turbidostat continuous culture:

The biomass content is maintained constant in a continuous bioreactor working at steady state ; the nutrients are adjusted to a low value [36,44]. This method aims to continuously produce new biomass while increasing its TAG content, but is rather complex. It is necessary to find a compromise between biomass growth and lipid accumulation as TGAs are secondary metabolites.

II3d) **Conditions found in literature**

Together with the nutrients supplied, both light irradiance and CO₂ are important growth parameters. In most studies, the light is supplied artificially with fluorescent tubes or light emitting diodes (LED) panels. The emission spectrum of the light supplied generally differs from a raw white light as algae pigments do not absorb the green light (~ 500 to 600 nm) [47]. Thus, artificial lights generally supply a mix of blue and red lights in order to avoid a loss of energy (and heat). LED systems are generally more expensive than fluorescent tubes but consume less energy and produce less heat.

Several culture conditions described in the literature are presented hereafter:

- Breuer *et. al* [6] used a two-step batch system to cultivate several algae strains in 250 mL Erlenmeyer filled with 100 mL liquid, supplied by an average light intensity of $150 \mu\text{mol}\cdot\text{m}^{-2}\cdot\text{s}^{-1}$ with fluorescent tubes and by air enriched with 5% CO₂, both during growth and accumulation steps. Lipid accumulation is started after centrifugation/re-suspension with an initial biomass concentration of 1 - 1.5 g/L with a medium depleted in nitrogen (KNO₃ replaced by equimolar KCl) during 14 days. The average and maximum biomass and fatty acid productivities of several strains in complete medium (N+) and nitrogen depleted medium (N-) are presented in Table 5 Appendix 1. The average TAG productivity is also presented. Nitrogen depletion (N-) decreases biomass productivities of the nine strains tested compared with the

complete medium (N+) but increases TAG productivity. The best TAG productivity was 323 mg·L⁻¹·d⁻¹ for *Scenedesmus obliquus*. For this strain, the volumetric biomass productivity was high both in nitrogen depleted (average of 719 mg·L⁻¹·d⁻¹) and nitrogen sufficient conditions (average of 767 mg·L⁻¹·d⁻¹). In most of the other strains tested, the biomass production is highly reduced in nitrogen depletion conditions. The following conditions: 1.0 mM KNO₃, 1.0 % CO₂ and 60 μmol photons·m⁻²·s⁻¹ at 25°C yielded the highest TAG productivity of 40 mg·L⁻¹·d⁻¹ [48].

- Takeshita *et al.* [49] have also used a two-step batch system to induce lipid and starch accumulation in several *Chlorella* strains, but with a sulfur stress. The pre-culture was performed in a complete medium under a 12:12 h LD cycle (light/dark cycles) at 50 μmol photons·m⁻²·s⁻¹. After reaching a certain biomass content, the cells were re-suspended in a sulfur deprived medium at a concentration of 1·10⁶ cells/mL in 93 mL test tubes containing 80 mL media, supplied with 600 μmol photons·m⁻²·s⁻¹ and air enriched with 2-3% CO₂. The biomass, lipid and starch productivities are detailed Table 6 Appendix 1.
- Praveenkumar *et al.* [41] used a white light at 300 μE·m⁻²·s⁻¹ 12:12-h LD cycle for *Chlorella sp.* BUM11008 during 16 days in complete medium and re-suspended the strains in nitrogen free medium, potassium-phosphate free medium, iron free medium or nitrogen, potassium-phosphate and nitrogen free medium.
- Mutjaba *et al.* [43] have cultivated the strain *Chlorella vulgaris* in 250 mL flasks containing 100 mL medium and supplied 80 - 100 μmol·m⁻²·s⁻¹ of continuous fluorescence illumination. Cells were then transferred into a bubble-column photobioreactor to be inoculated at less than 0.1 g·L⁻¹ of dry weight in a complete medium (stage 1). Enriched 4% CO₂ air is supplied at a rate of 0.15 vvm and white fluorescent light at 200 μmol·m⁻²·s⁻¹. When the culture reached a cell density of 1.5 - 2 g·L⁻¹, the cells were centrifuged and resuspended in a nitrogen deficient medium to accumulate lipids (stage 2). The maximum lipid content was reached after 12 - 24h of stage 2 (stress). The results of biomass and lipid productivities obtained are presented in Table 7 Appendix 1.
- Ördög *et al.* [44] inoculated *Chlorella minutissima* at a very low biomass concentration (Dry weight 10 mg·L⁻¹) in media at different concentrations of nitrogen, supplied with 130 μE·m⁻²·s⁻¹ with 14:10 h L/D cycle. Cultures were aerated with air enriched with 1.5% CO₂.
- Griffiths *et al.* [45] used white fluorescent tubes of 18W to supply light to *Chlorella vulgaris* grown in airlift photobioreactors aerated with air enriched with 0.29% CO₂. The bioreactors were inoculated with 50 mg·L⁻¹ at starting nitrate concentrations ranging from 0 to 2 g·L⁻¹. The results obtained are presented in Table 8 appendix 1.

The culture conditions for cell growth and lipid accumulation chosen in this project were selected from this literature review. They are presented in the section IV of the chapter.

A review of the microalgae characterization methods was also performed to develop fast and reliable techniques to monitor various features of the biomass. They are described hereafter.

III. Review of analytical methods

III1) Biomass growth

During a cell culture, biomass growth is usually monitored according to three measures: (1) absorbance or optical density, (2) cell number, and (3) dry weight. The principles and means to measure these parameters are detailed below.

III1a) Absorbance or Optical density (OD)

Measuring the absorbance of a culture at a given wavelength is a simple mean to obtain the biomass concentration. The absorbance is generally measured in the range of 650 – 700 nm, corresponding to the maximal absorption of chlorophyll pigments at 680nm. This method is then indirect, as it measures the biomass chlorophyll content and not the biomass concentration itself. To be reliable, it might be used only on algae with a constant pigment content; this is the case for cells maintained in optimal growth conditions. But this measurement is not appropriate in lipid accumulation phase as the chlorophyll content would constantly change. This method was thus not used in this work.

III1b) Cell number

One reliable and easy way to estimate cell number is using a **hemocytometer**. The main hemocytometers are Mallassez cells and Thoma cells. The principle of a hemocytometer is a glass slide with an incorporated "counting chamber" which possess a specific geometry. This chamber possesses a calibrated grid composed of squares of different surface areas (Figure 22 and Figure 23).

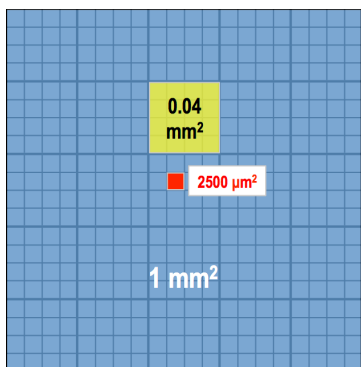


Figure 22: Square surfaces of a Malassez/Thoma hemocytometer [50]

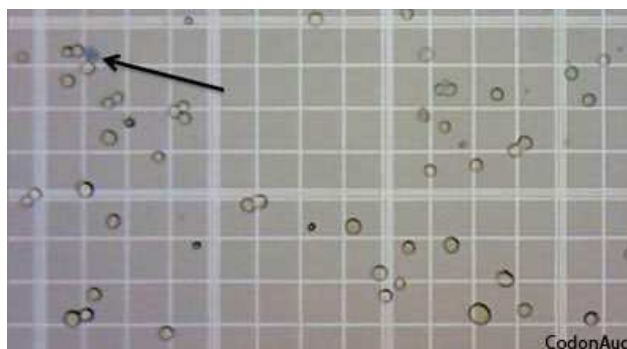


Figure 23: Cells on the grid of a hemocytometer[51]

The counting chamber is filled with a cell solution (10 - 20 μL). The solution can be diluted with the culture medium in order to avoid an excess of cells on the grid. Cell concentration is then calculated by counting with the help of a microscope a certain number of cells (100 - 250 cells) on the grid (square surfaces multiplied by the depth: 0.2 mm for Malassez cells and 0.1 mm for Thoma cells).

The cell concentration can also be estimated by automatic devices able to count the cells selectively towards cell debris and dust particles present in the culture. The two main methods to discard the cells from the other objects are impedance detection (coulter counter) and optical detection (flow cytometer).

In this project, additionally with hemocytometers, a flow cytometer Merck Guava “easycyte 5 single sample flow” (Millipore Corporation 25801 Industrial Blvd Hayward, CA 94545) was used. The instrument features are presented in Figure 24.

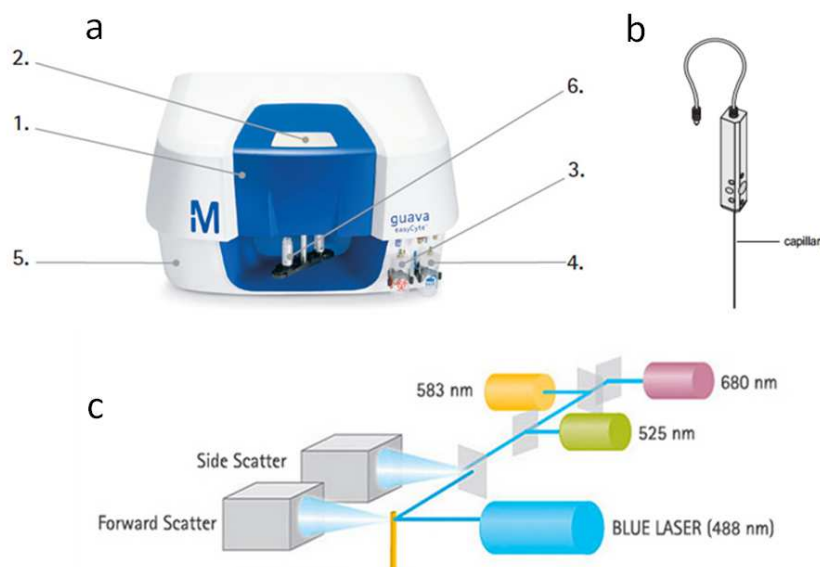


Figure 24: Flow cytometer and features. a) Guava easyCyte Single Sample Flow cytometer; 1. Up to 12 simultaneous detection parameters; 2. Microcapillary flow cell; 3. Wash vial; 4. Waste vial; 6. Single sample loader. b) scheme of the microcapillary. c) optical configuration. 50 mW blue laser (488 nm), 3 fluorescence detector channels (525 nm, 583 nm and 680 nm). The yellow line represents the micro capillary where the cells are flowed in front of the laser.

A laser beam excites the particles flowing through a micro-capillary and the intensity of light scattered is measured by two photo-multipliers (PMT): Forward scatter (FSC) and Side Scatter (SSC) (Figure 25), enabling to distinguish large algae cells from other "dust particles" which emit a lower SSC and FSC signal. The forward-scattered light is proportional to the cell-surface area or size [52]; it is a measurement of mostly diffracted light detected on the axis of the incident laser beam [53]. SSC is proportional to particle granularity, internal complexity and a minor part is proportional to cell area.

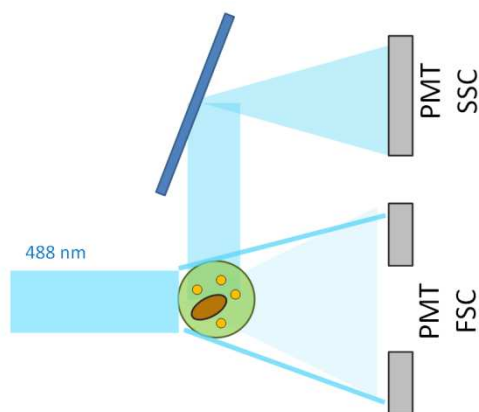


Figure 25: Light scattered by a particle to the photo-multipliers (PMT). Side (SSC) and Forward (FSC) light Scattered.

During analysis, "events" are counted, corresponding to the particles detected by the PMT FSC for which the signal is higher than a threshold; all particles giving a lower signal are considered as background noise.

In this method, the minimal FSC signal required is $1 \cdot 10^2$ a.u. displayed on the right of the vertical dashed red line in the plot of Figure 26.a. All particles detected with a FSC inferior to $1 \cdot 10^2$ a.u. are considered as a background noise and their data are not treated. Each particle detected is plotted on the graph as a dot according to its FSC/SSC coordinates. All the algae cells having similar sizes will display similar FSC/SSC values and are thus plotted as a dense cloud of points on the top right corner of the plot as they are the largest particles detected. A gate is created (red line) to select the population of algae and discard the other particles (e.g. cell debris, dust).

The analysis method used in the project was developed on the software Incyte with the following parameters:

- total count: 1000 - 2000 Events
- flow rate: 0.59 $\mu\text{L/s}$
- Gains: FSC 8.00, SSC 8.00, 5 decade acquisitions
- threshold fixed at FSC 200 a.u.
- algae gate fixed at FSC between $1 \cdot 10^3$ and $1 \cdot 10^5$ a.u. and SSC between $2 \cdot 10^2$ and $1 \cdot 10^5$ a.u.

The algae concentration is calculated by dividing the number of particles counted inside the gate by the volume of the sample. The concentration measured is displayed on the top left corner of the plot along with the percentage of events detected inside the gate.

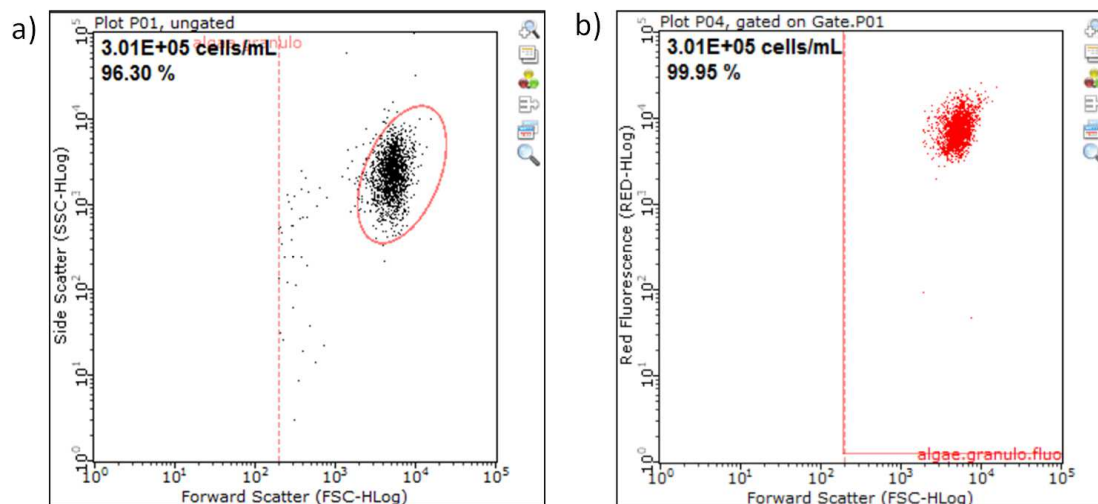


Figure 26: Measurement of cell concentration with the software Incyte. a) adjustment of FSC threshold (vertical red line) and algae gate. Cell concentration displayed on the top left corner. b) verification of algae fluorescence, minimal fluorescence threshold set at 0.5 a.u.. (horizontal red line).

The optimal algae concentration range of this method is $2 \cdot 10^5$ - $3 \cdot 10^5$ cells/mL. Each measure takes between 15 and 40 seconds.

Emission detected in the red spectrum (PMT 680 nm) is associated with chlorophyll a and b autofluorescence. A verification step was used in the project and was performed on the algae gate to ensure that algae detected by the granularity signals (FSC and SSC) emit in the red channel and indeed possess even a low amount of chlorophyll (Figure 26.b). A second threshold is set on the red fluorescence at a value of 0.1 au. Most of the time, this threshold discards less than 1% of the particles detected as algae in the FSC/SSC gate as most of the cells possess a red fluorescence within the range of $1 \cdot 10^3$ to $2 \cdot 10^4$.

The methods developed for *Chlorella vulgaris* and *Chlamydomonas reinhardtii* were validated with the help of an hemocytometer (section V1)). Indeed, concentrations given by cytometry were compared with those obtained by microscopy.

III1c) Dry weight (DW)

The dry weight is a paramount value for precise quantitative estimation of the biomass produced. It corresponds to the biomass weight contained in a known volume of culture after filtration and drying. It is generally expressed in g/L or mg/mL.

In the protocol used, the amount of biomass DW in the sample must be in the range 3 to 5 mg.. The first step is the biomass filtration through a glass fiber filter GF/C 47 mm 1.2 μ m. The glass fiber has been previously pre-filtered with distilled water, pre-dried at 105°C and weighted after being cooled in a desiccator. After sample filtration, the set of filters are dried in an oven at 105°C during 24h, cooled in a desiccator and weighed.

The dry weight is calculated by the following equation:

$$DW = \frac{\text{Filter with biomass (mg)} - \text{filter empty (mg)}}{\text{Volume of culture (mL)}} \quad (2.1)$$

Because the dry weight evaluation requires a high biomass quantity (3 to 5 mg), this method is not suitable for daily analyses in this project.

III1d) Comparison of the different methods

The different methods to evaluate biomass concentration are summarized in Table 1:

Table 1: Methods to quantify biomass

Method	Unit	Volume required per sample	Biomass required per analyze
Optical density	Absorbance (a.u.)	< 1 000 µL	OD ₆₈₀ > 0.05 a.u.
Hemocytometry	Cells/mL	< 100 µL	100 cells on the grid
Flow cytometry	Cells/mL	50 - 1000 µL	1 000 cells
Dry weight	g/L	Minimum 3 000 µL (for DW > 1 g/L)	3 mg

In this work, for daily analyses, the cell concentration was systematically evaluated by flow cytometry as this method is fast and reproducible. Dry weight measurements were performed only when needed, generally at the end of the experiments. The optical density method was not used.

III2) Lipid content

Because the cell lipid content greatly evolves with the culture conditions, it is necessary to be able to evaluate it at any time; and the same for the lipid contents before and after extraction, as one of the main purposes of this PhD thesis is to evaluate the extraction efficiency of different methods. Several methods for this type of analysis will be described below.

III2a) Gravimetric methods (solvent extraction)

Gravimetric methods consist in the extraction of total lipids (neutral + polar) with a harsh solvent mixture (the constraints are different in lipid extraction for commercial valorization where hazardous solvent are avoided). The gravimetric methods are generally adapted from the well-known Blight and Dyer [54] or Folch methods [55]; the total lipids are extracted into an organic solvent which is afterwards evaporated; weighing is then performed on the residue. These methods were proposed more than 50 years ago and are not adapted to the extraction of lipids from microalgae, due to the high amount of biomass needed for analysis.

These two techniques use a mixture of a polar solvent (methanol) and a non-polar one (chloroform) to extract lipids out of the cell. The mechanism for lipid extraction is explained in Figure 27.

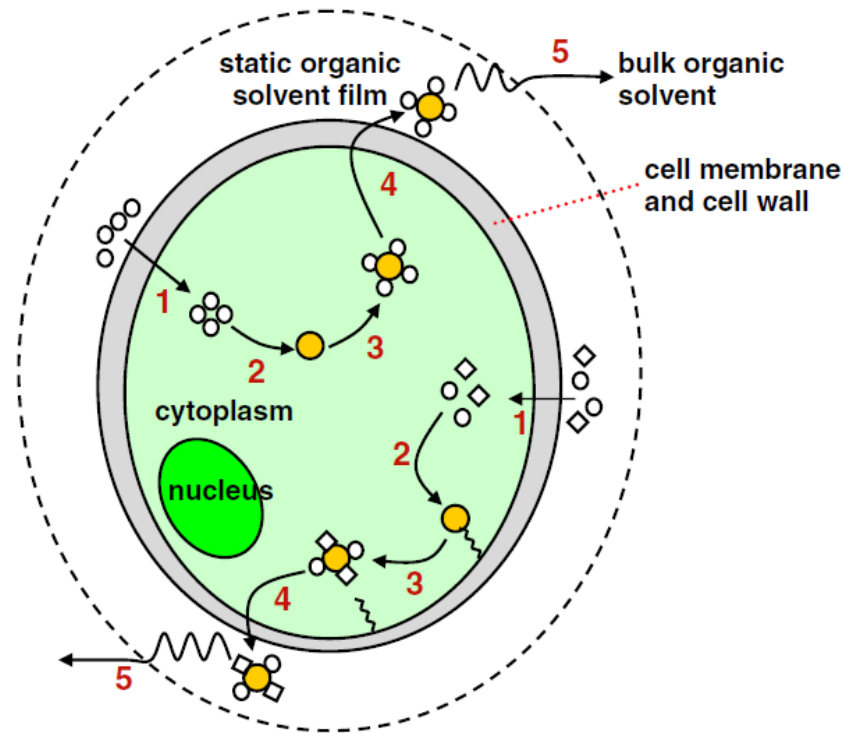


Figure 27: Schematic diagram of the proposed organic solvent extraction mechanisms. yellow circle: lipids, white circle: non-polar organic solvent, white diamonds: polar organic solvent. [56].

The non-polar organic solvents, such as hexane or chloroform, are able to cross the cell membrane, enter the cytoplasm and interact with neutral lipids using van der Waals forces to form organic solvent-lipid complexes; these complexes are then transferred across the cell membrane. It should be highlighted that a part of the fatty acids is forming polar lipid complexes with some of the organelles. Only non-polar:polar solvent mixtures (represented by white circles and white diamonds) are able to extract these membrane-based lipid-proteins associations. The polar solvents form hydrogen bonds with the polar part of the lipids [57]. The created hydrogen bonds are strong enough to displace the lipid-protein associations binding the lipid complex to the cell membrane. Addition of polar solvents facilitate therefore the extraction of membrane-associated neutral lipid complexes, and inevitably leads to the co-extraction of polar lipids.

Folch method and Blight & Dyer methods were proposed more than 50 years ago and are not specific to the extraction of lipids from microalgae. The method Folch was originally made to extract lipid from animal tissues, the method Blight and Dyer was optimized for the extraction of lipids from fish muscle [58].

Some recent methods were adapted to the constraints of algae cultures. Unlike animal tissues, algae cells possess a high interstitial water content (even after centrifugation) and a cell wall which may alter solvent penetration. The use of drying and cell wall breaking steps is then often necessary to estimate the lipid content accurately.

Axelsson and Gentili [59] proposed a single step method which requires less steps than the two classic methods proposed above and allows at least five times higher sample throughput (less solvent used): 30 mg of DW biomass could be extracted with 10 mL solvent mixture. The procedure was proposed to reduce time and biomass sample use in comparison with the classic methods though allowing fast qualitative-quantitative analyses of total fatty acids.

The solvent mixture must be adapted to the polarities of the lipids extracted. Several pure solvents or mixtures are possible: chloroform:methanol 1:1, chloroform:methanol 2:1, dichloromethane:ethanol 1:1, hexane-isopropanol 3:2, acetone, diethyl ether, methyl-tert-butyl ether-methanol 10:3. Because of the large variety of lipids present in microalgae, highly varying in polarity, the extracted lipid quantity and composition vary with the solvents used [60].

Ryckebosch et al. [58] showed that chloroform:methanol 1:1 is the best solvent mixture for extraction of total lipids from microalgae. The use of mechanical (*e.g.* bead milling, pressing, autoclaving, lyophilization, microwaving, high pressure homogenization, ultrasonication) or chemical (acid, enzyme, osmotic shock) processes together with solvent extraction may drastically improve the total lipid extraction yield in comparison with a simple mixing of intact biomass with solvents [56,61–64].

In the case of lipid analysis, the use of one or several disruptive pre-treatments is very common, despite the high energy consumption. The non-fatty acid containing lipids, like pigments and steroids, are however also estimated [60], giving interferences. But the main drawback is the high amount of biomass needed for analysis.

III2b) **Transesterification and Gas Chromatography analyses**

Another method, able to determine lipids is FA transesterification into fatty acid methyl esters (FAMES) followed by their quantification and identification using **gas chromatography** with a flame ionization detector (GC-FID). This method enables to greatly reduce the amount of biomass required (5 mg of DW instead of several g) and provides the composition of fatty acids present in microalgal biomass. Lipids in TAGs and membranes can be detected. A separation step can be added using solid phase extraction (SPE) columns [60].

III2c) **Lipophilic dyes (Nile red and Bodipy)**

Lipophilic dyes (also referred as fluorescent probes or fluorophores), able to bond to intracellular neutral lipids, can be used to estimate TAGs contents in microalgae.

Nile Red (NR, 9-diethylamino-5Hbenzo[α]phenoxazine-5-one) was discovered in the early 20th century [65], but its interest in measuring neutral lipids in microalgae has rapidly increased since 2000. A more recent dye, BODIPY 505/515 (4,4-difluoro-1,3,5,7-tetramethyl-4-bora-3a,4-diaza-s-indacene) appears to be also convenient.

The principle of fluorescence can be explained as follows: when a photon is absorbed by an electron of a fluorescent particle, this particle is raised to an excited state (Figure 28). A part of this energy is dissipated as a photon to relax to the ground state [66]; but another part of the energy is lost, the emitted photon then carries less energy and thus has a higher wavelength. This shift in wavelength is called the Stokes shift and illustrated in Figure 29. Excitation/emission is cyclical until the fluorescent molecule is irreversibly damaged (photobleached).

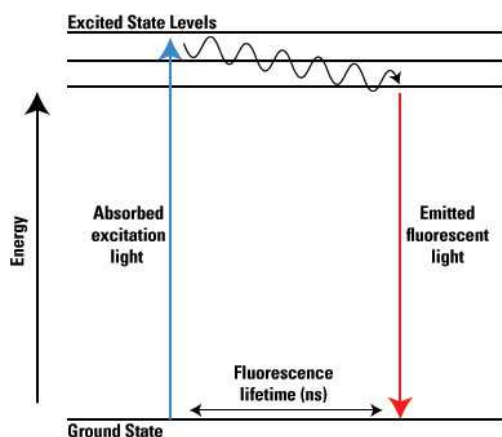


Figure 28: Jablonski energy diagram of fluorescence [66]

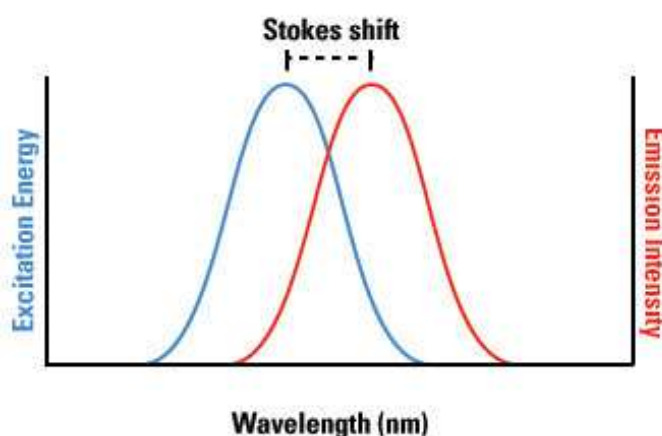
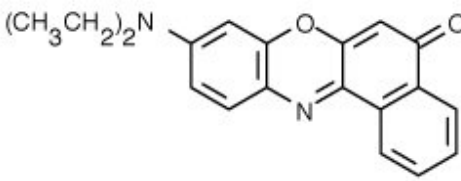
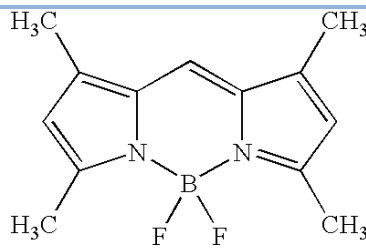
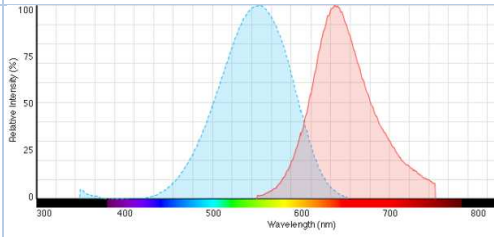
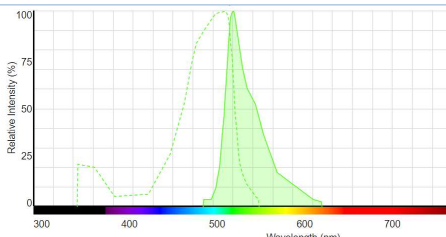


Figure 29: The Stokes shift of the excitation and emission spectra of a fluorophore

Nile red (NR) and Bodipy have different excitation/emission spectra, as illustrated in Table 2 (*n.b.* NR spectra also vary with environmental conditions [67]).

Table 2: Characteristics of the lipophilic fluorochromes Nile Red and Bodipy 505/515 and advised staining protocols

Molecule	Nile red	Bodipy 505/515
Structure	 <p>[65]</p>	 <p>[68]</p>
Formula	C ₂₀ H ₁₈ N ₂ O ₂ [69]	C ₁₃ H ₁₅ BF ₂ N ₂ [69]
Molecular weight (g/mol)	248.08 [69]	318.37 [69]
Target	TAGs [69]	Lipid droplets[69]
Spectra	 <p>[70]</p>	 <p>*spectrum of Bodipy ex 500/ em 510</p>
Stain carrier	DMSO (5% v/v - 25% v/v)	DMSO [69]

	Glycerol (0.1-0.125 mg/mL) EDTA (3.0-3.8 mg/mL) [65]	Glycerol
Dye and cell Concentrations	0.25-2.0 µg/mL [65] 5·10 ⁴ to 1·10 ⁶ cells/mL [69]	0.04-2.6 µg/mL 5·10 ⁴ to 1·10 ⁶ cells/mL [69]
Incubation time	5-40 min [65] 5-15 min [69]	5-15 min [69]
Temperature	30-40 °C [65]	

DMSO: Dimethyl sulfoxide; EDTA: Ethylenediaminetetraacetic.

According to the solvent used, the light absorption of NR varies in wavelength and intensity, a property known as solvatochromism [65] and illustrated in Figure 30. Its absorption and emission bands vary in spectral position, shape and intensity with the nature of the solvent [67].

The magnitude of fluorescence is proportional to the amount of dye in the cell and the size of the neutral-lipid droplet. Because of the solvatochromism property of NR, excitation/emission wavelengths of the dye vary with the lipid bound. Thus, different excitation/emission wavelengths have been reported for various microalgae species or even for the same strain in different conditions. In addition the metachromatic properties of NR induced by the environment polarity can be exploited to estimate the polarity distribution of the lipids [71,72]; a low wavelength (575 nm) corresponds to neutral lipids while a higher wavelength (625 nm) indicates polar lipids. The use of NR is then very complex, however most of the studies are performed with this dye as it is well known.

BODIPY may show a better cell penetration [73], a more stable fluorescence [74], and an easier differentiation from pigments auto-fluorescence [69,75]. But it gives a very strong green auto-fluorescence in the medium when using a too high concentration [73] (Figure 31); in this example 0.067 µg/mL Bodipy was used for 1·10⁶ cells/mL instead of 0.05 µg/mL, the optimal concentration found for *C. vulgaris*.



Figure 30: Nile red under visible and ultraviolet (366 nm) light un different solvents. From left to right: 1. water, 2. methanol, 3. ethanol, 4. acetonitrile, 5. dimethylformamide, 6. acetone, 7. ethyl acetate, 8. dichloromethane, 9. n-hexane, 10. methyl-tert-butylether, 11. cyclohexane, 12. toluene.

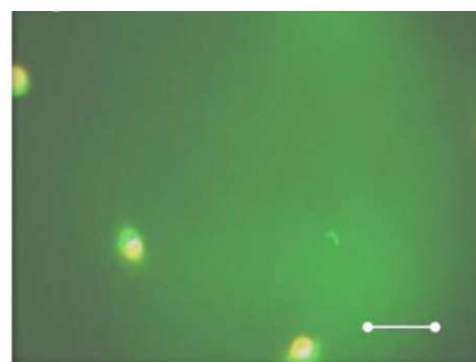


Figure 31: Bodipy auto-fluorescence in the medium, resulting from an excess of dye (0.067 µg/mL of Bodipy for 1·10⁶ cells/mL of *C. vulgaris*)

In some works, these methods are successfully correlated with quantitative methods such as gravimetry [69]. The review of Rumin et al. [69] reported 20 works that showed a good correlation between dye fluorescence and gravimetric determination. But in all these works a specific staining protocol was developed for each microalgal species.

The cell penetration of NR can be difficult because of the dense cell wall of some algae strains. A cell pre-treatment can be used in order to facilitate permeation; it can be chemical (*e.g.* use of DMSO to permeate the cell and carry the dye toward the cytoplasm) or physical (staining assisted by microwaves, electric field, lyophilization) [76].

The methods used to estimate lipid quantities with the fluorescent dyes NR and Bodipy are the following: (1) fluorimetry (also called Fluorescence spectroscopy), (2) flow cytometry and (3) Confocal Laser Scanning Microscopy (CLSM).

Some studies are still performed by fluorimetry (principle explained in Appendix 2), but nowadays, intracellular fluorescence is mostly estimated using flow cytometry. Flow cytometry only estimates the fluorescence of detected particles; it is an important advantage over fluorimetry which gives the total fluorescence of the volume (cells + medium).

To estimate the lipid quantity in cells by using algae staining and fluorescence measurements, controls must be carefully considered, especially in the case of NR [76].

(1) The chlorophyll/pigments auto-fluorescence needs to be withdrawn from the measure. This first control or blank is made with non-stained cells.

(2) As reported before, the dye auto-fluorescence can also be significant. The second blank is made on the stained culture medium, without cells [77], but only in the case of fluorimetry.

Whether fluorescence intensity is estimated by fluorimetry or flow cytometry, an optimal staining protocol is paramount to ensure that the fluorescence intensity is correlated to the lipid content. An excess/lack of dye, a poor control of the staining conditions (incubation time, temperature, mixing) will alter the validity of the measured fluorescence intensity.

In conclusion, measuring the fluorescence of lipids is an interesting approach when intending to locate the lipid droplets within the intracellular compartment. Nevertheless, it can barely be used for precise quantification, due to the fluorescence background of the cell and/or the medium and its high sensitivity to operating conditions.

The last method is Confocal Laser Scanning microscopy (CLSM). This technique is based on the analysis of microscopy images and can estimate the volume of the stained objects, instead of measuring fluorescence intensities. But the CLSM method requires the development of a much more complex protocol. Fixing cells on a surface (*e.g.* poly-L-lysine coating [78], agarose-gel [79]) is often necessary to obtain good quality images. As an example Wong and Franz [78] used 0.25 μm /slice increments to estimate on 800 x 800 pixels (0.132 μm /pixel), the number and volume of lipid bodies per cell of *Phaeodactylum triornutum* and *Tetraselmis suecica* using Bodipy 505/515 (Figure 32). The volumes of the droplets were estimated by Z-projections in ImageJ with 5 μm green fluorescent polymer microspheres as reference. Liang et al. [79] used chlorophyll auto-fluorescence and Bodipy fluorescence to estimate oil bodies and chloroplast volumes (Figure 33).

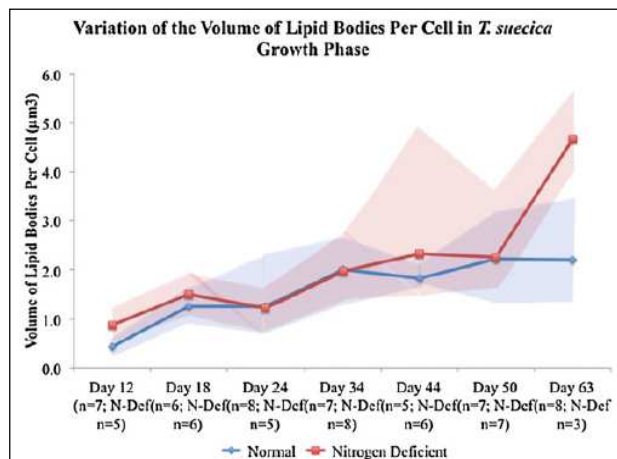


Figure 32: Volume of lipid bodies per cell in *T. suecica* (Normal and Nitrogen deficient conditions) [78]

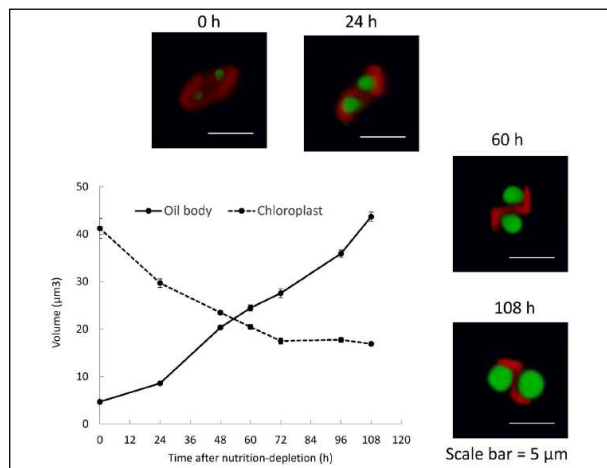


Figure 33: Volumetric changes of oil bodies and chloroplasts in *F. solaris* in response to nutrient limitation [79].

A similar method was used for *Tetraselmis subcordiformis* by Xu et. al [80].

III2d) Colorimetric method (Sulfophosphovanillin)

Finally, colorimetric methods are alternatives to measure lipid content of the cells. The most widely used is the Sulfophosphovanillin (SPV) method, especially in medical applications, such as lipid analysis in human serum [81,82] and in algal production [83,84].

The method is illustrated below in Figure 34. The complete protocol is detailed in Appendix 3.

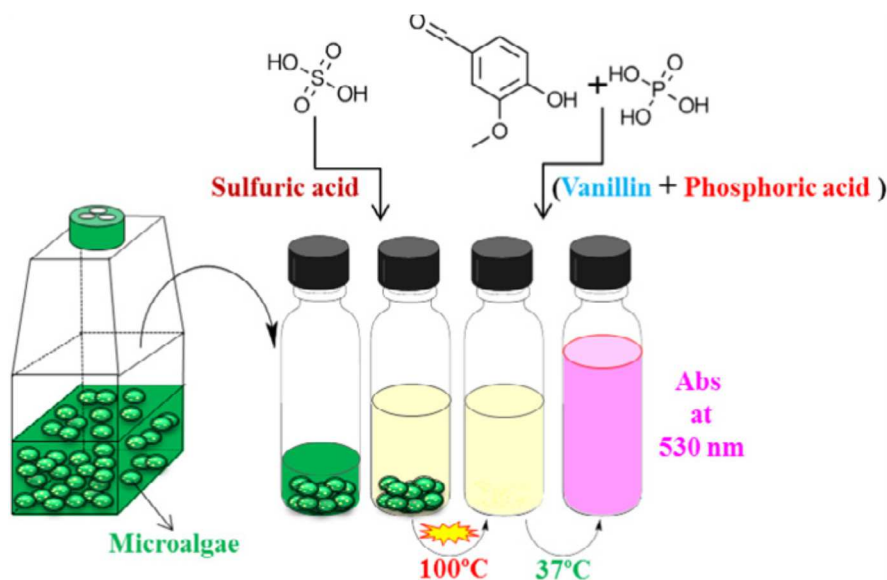


Figure 34: Illustration of the SPV method [84].

The SPV reaction is performed in three steps (Figure 35) [82]. First the chromogen formation is based on the electrophilic addition of sulfuric acid to an alkene by acid-aldehyde reactions (a). In the second step, a vanillin phosphate ester is formed which then reacts with chromogen (b). Finally, after an incubation period, a purple-red chromophore, detected by its absorbance at 530 nm, is formed (c).

The absorbance is proportional to the amount of unsaturated fatty acids contained in the sample, in a given range of concentrations.

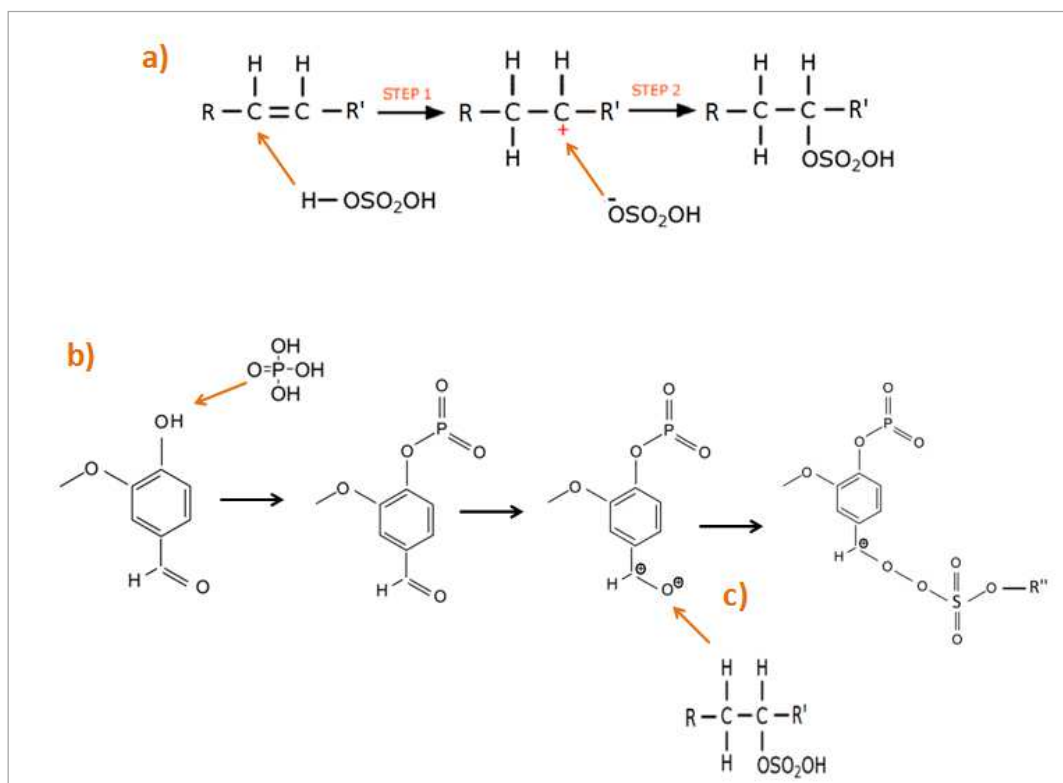


Figure 35: Proposed reactions for the SPV method, modified from Knight et al. [85]. a) Chromogen formation, sulfuric acid reacts with unsaturated carbon atoms of fatty acids. b) Vanillin reacts with phosphoric acid to form a phosphovanillin complex. c) the phosphovanillin complex binds with sulfur which the chromogen to form sulfophosphovanillin chromophores.

The advantage of this technique, in comparison with gravimetric methods, is the **limited amount of biomass required**. According to Mishra *et al.* [84], the absorbance must be higher than 0.05, several hundred of microliters of alga suspension are generally sufficient.

Furthermore, SPV detects unsaturated FA only, but both polar (FA in the membrane) and neutral FA (FA as TAGs). But the result also depends on the structure of the molecule: oleic acid (C18:1) gives a higher response than linoleic acid (C18:2) and linolenic acid (C18:3) [85], with a difference of about 5-10 % as illustrated in Figure 36.

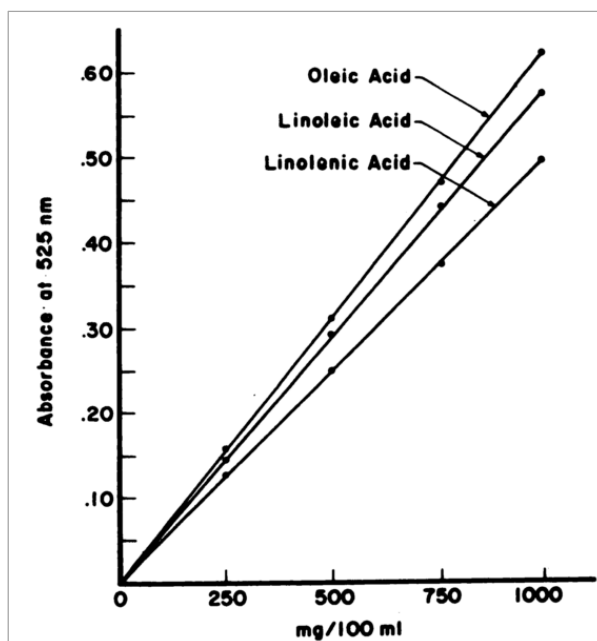


Figure 36: SPV response for oleic acid (C18:1), linoleic acid (C18:2) and linolenic acid (C18:3) [85]

The major difficulty when using SPV on algae, is the necessity to have a **suitable reference lipid** and its choice is generally complicated. Indeed, the reference must have a FA composition (especially the ratio of saturated/unsaturated FA) as close as possible to the composition of the algae analyzed. This problematic requires to know *a priori* the FA composition of the algae (*e.g.* using gas chromatography) and to find a reference oil with the same composition.

Finally, the interference of other carbon-carbon double bonds presents in algae (pigments, vitamins) is quite unstudied in literature. To conclude, SPV method is a simple, straightforward method to estimate lipid content but is certainly not as precise as a chromatography method.

III2e) Conclusion about lipid quantification

To conclude about lipid quantification, several techniques were investigated during this project, our principal constraint was the possibility of using low amounts of biomass, due to the specificity of our experiments (microsystems, electroporation cuvettes). Bodipy-associated methods were coupled with flow cytometry for qualitative images and semi-quantitative measurements (fluorescence associated values). In addition we used the SPV method using the protocol proposed by Mishra *et al.* [84]. Finally, gas chromatography was performed with the help of an external laboratory to obtain the exact composition of FA in *Chlamydomonas reinhardtii* at different stages of lipid accumulation.

Additional lipid estimation techniques, not studied in this project, are presented in Appendix 4.

III3) Cell size

On one hand cell size measurements were required in order to estimate their behavior during lipid accumulation. A precise estimation of the size is also necessary when selecting electroporation parameters as the applied electric potential must be proportional to the cell diameter (see Chapter 3).

Two methods were studied: **laser granulometry** and **microscopic measurements**.

The laser granulometer used in this work was a Malvern Mastersizer 3000. The principles of the method are described in appendix 5.

In addition with laser granulometry, microscopic measurements were performed using an inverted microscope Nikon Eclipse Ti-S equipped with x40 magnification objective LWD 40x/0.55 Ph1 ADL and a CMOS colored camera Nikon DS-Ri2 (captor size 4908 x 3264 pixels) with an additional magnification lens. The diameter estimation was performed by measuring the longer membrane to membrane length on a minimum of 200 cells with the software NIS Elements D as illustrated in Figure 37.

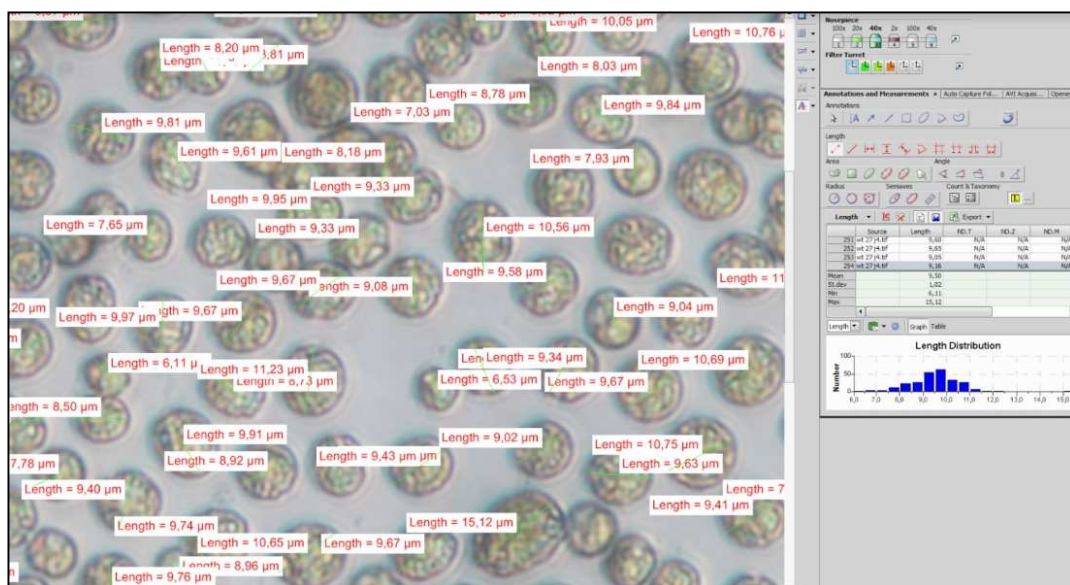


Figure 37: Estimation of diameter distribution of a cell population with the software NIS Elements D. Image recorded with *Chlamydomonas reinhardtii* after 4 days of stress.

IV. Procedure to induce lipid accumulation developed in this work

In the early stage of the project, several algae strains were cultivated in order to test their ability to produce high intracellular lipid contents.

Afterwards, the culture was restricted to the most suitable strain, to study PEF: *Chlamydomonas reinhardtii* which is large (~ 7 to 10 µm diameter), can accumulate high amount of lipids, and is a freshwater strain. Cell size and medium conductivity are indeed paramount features in a PEF treatment (see chapter 3).

Algae strains were obtained from the Culture Collection of Algae at the University of Goettingen (EPSAG, Nikolausberger Goettingen, Germany). *Chlamydomonas reinhardtii* SAG 34.89 (wild type), and *Chlamydomonas reinhardtii* SAG 83.81 (Cell wall deficient muted strain from the wild type 34.98, also known as cw15) were cultivated in TAP Medium [86]. Other strains, *Acutodesmus Obliquus* SAG 13.80

(also known as *Scenedesmus Obliquus*) and *Parachlorella kessleri* SAG 13.80 were cultivated in B3N medium. The media are detailed in Appendix 6.

All the cultures were axenic and prepared with media and vessels autoclaved at 121°C. The lipid accumulation was performed in two steps as described previously: cell growth in optimal conditions and re-suspension in a nitrogen depleted medium.

IV1) 1st step "growth step":

Algae strains were maintained in optimal growth conditions in an incubator Minitron Infors HT (Figure 38).

The conditions are:

- Inoculation at a low cell concentration (inferior to $5 \cdot 10^4$ cells·mL⁻¹)
- Re-inoculation at low concentration as soon as the mother culture reaches a limit concentration ($1 \cdot 10^7$ cells·mL⁻¹) in order to avoid light limitation
- Continuous light supply: $20 - 40 \mu\text{mol} \cdot \text{m}^{-2} \cdot \text{s}^{-1}$
- Low volume to surface ratio because of the low light supply. Maximum 50 mL of medium in 250 Erlenmeyer flasks (Fischerbrand) as shown in Figure 39.
- Ambient air enriched at 1.5 % CO₂. Erlenmeyer flasks equipped with air-permeable silicone plugs (S-type).
- Temperature maintained at $24 \pm 1^\circ\text{C}$.
- Mixing at 100 rpm.



Figure 38: Minitron HT incubator used to grow algae



Figure 39: Maximum 50 mL of medium in 250 mL Erlenmeyer flasks. Culture at $24 \pm 1^\circ\text{C}$, $20-40 \mu\text{mol} \cdot \text{m}^{-2} \cdot \text{s}^{-1}$, 1.5 % CO₂.

After reaching a certain quantity of biomass, the cells are centrifuged at 6000 g during 5 minutes and re-suspended in a depleted medium, as explained below.

IV2) 2nd step "stress conditions":

Lipid accumulation is performed using nitrogen deprivation associated with high light conditions. The centrifuged cells were re-suspended in 40-60 mL of a nitrogen depleted medium in 250 mL Erlenmeyer

flasks (Fisherbrand) with a silicon plug S-type and placed in a home-made lipid accumulation system (Figure 40), where the supplied light intensity supplied is higher than in the growth conditions. The preparation of the depleted medium is detailed in Appendix 6.

The conditions are:

- Nitrogen depleted medium: TAP N- in the case of *Chlamydomonas reinhardtii*, Bristol N- in the case of other strains.
- Inoculation with centrifuged cells at a concentration of $3 \cdot 10^6$ cells·mL⁻¹.
- Continuous light supply with blue/red lamps (Arcadia FMH24T5, 24W) to provide an average light intensity of 100 -150 $\mu\text{mol} \cdot \text{m}^{-2} \cdot \text{s}^{-1}$.
- Mixing at 100 rpm.
- Temperature maintained at $24 \pm 1^\circ\text{C}$ (system in a temperature controlled room + ventilators).
- Ambient air (0.04 % CO₂).

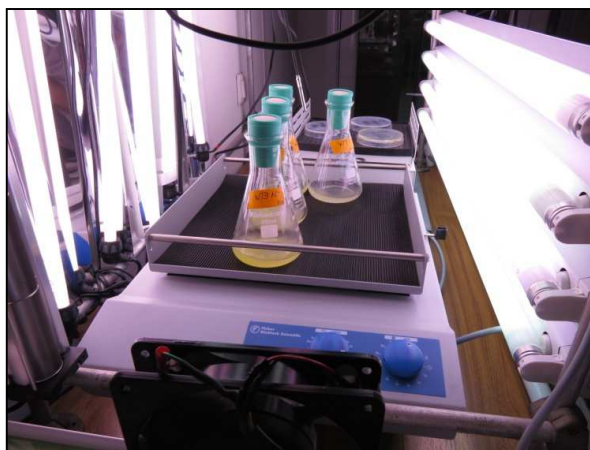


Figure 40: Lipid accumulation system. 40-60 mL of medium in 250 mL Erlenmeyer flasks. Culture at $24 \pm 1^\circ\text{C}$, 100-150 $\mu\text{mol} \cdot \text{m}^{-2} \cdot \text{s}^{-1}$, 1.5% CO₂. Media depleted in nitrogen.

IV3) Discussion of the conditions chosen

The conditions of culture were optimized to obtain, as possible, reproducible algae suspensions for the following electroporation and extraction experiments.

The conditions presented above in “**growth conditions**”, that lead to a **high growth rate** (μ), without light stress or limitation, are applied. During experiments, the cell concentration was monitored over time to verify that cultures were in the exponential growth phase and to ensure reproducibility. Attention was paid on avoiding light limitation due to an excess of biomass in the culture. This is the reason why algae cells were generally re-inoculated after 3-4 days of growth in a new fresh medium at a reduced concentration. Particular attention was paid on the pigment content (autofluorescence per cell) during growth, to verify that it remained rather constant. In our conditions, light was constantly provided, with no light/dark cycles. Without light/dark cycles which mimic a natural sun cycle, interdivision and division phases are not synchronized in the culture. The very low light intensity

supplied to the culture during growth constraints the cell to develop their antenna size in order to maximize light absorption. This sur-development of antenna size during growth leads to a maximum light stress when the cells are incubated in lipid accumulation conditions with no nitrogen and high light supplied as an excess of photon will reach the center of photosystem II [87,88].

During the second phase aiming at **accumulating neutral lipids**, a sufficient quantity of biomass was necessary for the further experiments and analyzes, but it was also required to use a reduced cell concentration to trigger a high light stress. In the case of *Chlamydomonas reinhardtii*, the concentration used at the beginning of stress conditions was generally $3 \cdot 10^6$ cells/mL in 40 - 60 mL. In some experiments, multiple parallel cultures were prepared under stress conditions to satisfy the demand of particular measurements (e.g. lipids measured by GC-FID and biomass quantity characterized by dry weight). The lipid accumulation system was specifically set-up for this project. Improvements of the set-up would be possible such as an increase in the carbon dioxide concentration and a higher light irradiance but after setting up the protocol, changes in culture conditions were avoided.

The limited volume of cultures, of several dozens of milliliters, were chosen in order to avoid light limitation.

V. Development and validation of the methods

v1) Determination of cell concentration by flow cytometry

The cell concentration of *Chlamydomonas reinhardtii* wild type was monitored by flow cytometry. A method was developed for cells in stress and exponential growth phase conditions. As previously reported, data obtained using flow cytometry were compared with those obtained by microscopy (Malassez method) in order to validate the former method; a very good correlation was obtained for *Chlamydomonas reinhardtii* wild type both in growth phase (Figure 73) and after 14 days of stress (Figure 74). The average difference between flow cytometry and Malassez cells was 11 % and 18 % for respectively growth phase and stress conditions. In addition, when using flow cytometry at concentrations about $3 \cdot 10^5$ cells/mL, the difference between flow cytometry and hemocytometry is only 8 % and 9 % in growth and stress phases, respectively.

v2) Calibration curve of SPV method using Triolein

The SPV method was calibrated with triolein dissolved in chloroform (2 mg/mL) and evaporated in different quantities (from 12.5 to 125 μ L) as described in Appendix II2. Triolein is composed of three molecules of oleic acid 18:1 and a molecule of glycerol. As discussed in the results, triolein is the main unsaturated FA present in our algae. When estimating lipid quantities on algae solutions, the absorbance response can be converted into a triolein equivalent (TO_{eq} in μ g). The correlations obtained are presented in the appendix 3 of the chapter 3.

v3) Development of Bodipy staining on *Chlamydomonas reinhardtii*

The main difficulty of Bodipy staining is to optimize the amount of dye, which depends on (1) the number of lipid containing cells and (2) the neutral lipid content per cell. The latter varies with the microalgae strain, the culture conditions and in our case, with the stress duration. Questions such as: Should the amount of dye vary with the stress duration? What would happen if there is an excess or a lack of dye? are raised.

To optimize the dye dosage, experiments using different quantities of it, with or without a washing step (centrifugation + resuspension in an unstained medium), were conducted. We thought to use an excess of dye to entirely stain the lipid droplets and wash the cells to remove the excess of dye not bound to neutral lipids. According to Govender et. al, [73], Bodipy specifically bonds to lipid droplets. No dye is thus expected to stay unbound in the cytoplasm of the cell. In addition, if conditions are conveniently optimized, no excess of the dye should be observed in microscopy. In order to confirm these facts, tests were carried out using confocal scanning imaging and flow cytometry; a washing step was first added to the staining protocol (see hereafter) in order to eliminate dye excess.

Two methods were used in our work to optimize lipid staining: (i) microscopic observations (epi-fluorescence or confocal microscopy), and (ii) quantitative measurements using e.g. flow cytometry; this consists of measuring the mean green fluorescence per cell (at 530 nm).

These two options have major drawbacks: (i) the observations may greatly vary with the acquisition parameters: lamp intensity, attenuation filters, objective, exposure duration and gain. Moreover, Bodipy bleaching (fluorescence degradation due to lamp exposure) occurs. (ii) quantitative results can be obtained through flow cytometry but the interpretation of data can be difficult. This point will be further discussed.

In the following sections, the detailed procedure to optimize Bodipy staining is described and discussed.

V3a) **Effect of the ratio Bodipy/cell and the presence of a washing step on *Chlamydomonas reinhardtii***

Conditions from Govender et al. [73] were first considered to establish our staining protocol. To verify the effect of a washing step on Bodipy fluorescence, the quantity of Bodipy was higher than the one suggested by Govender et al. [73] which recommend 0.067 μg of Bodipy for 1 million of *Chlorella vulgaris* cells. The amount of Bodipy used was adjusted according to the bio-volume of *Chlamydomonas reinhardtii* cells in comparison with *Chlorella vulgaris* ones: the ratio of cell radius equal to 3.5 (*Chlamydomonas reinhardtii* and *Chlorella vulgaris* radii estimated to respectively 3.5 and 1 μm) leads to a ratio of biovolume of 43. Thus, a Bodipy quantity ranging from 0.5 to 2 μg for 1 million of *Chlamydomonas reinhardtii* cells in lipid accumulation phase (13 days of stress) was tested. The mean green fluorescence (530 nm) per cell was measured for a Bodipy ratio of 0.5, 1, 1.5 and 2 μg for $1 \cdot 10^6$ cells, with and without an additional washing step (noted W). Results are presented in Figure 41. Cells were incubated with Bodipy during 7 minutes and then diluted to be measured by flow cytometry (concentration of $2.5 \cdot 10^5$ cells/mL, 2 000 cells measured). In the case of the washing step, cells were centrifuged at 6 000 g during 5 minutes and resuspended in fresh medium (TAP N-).

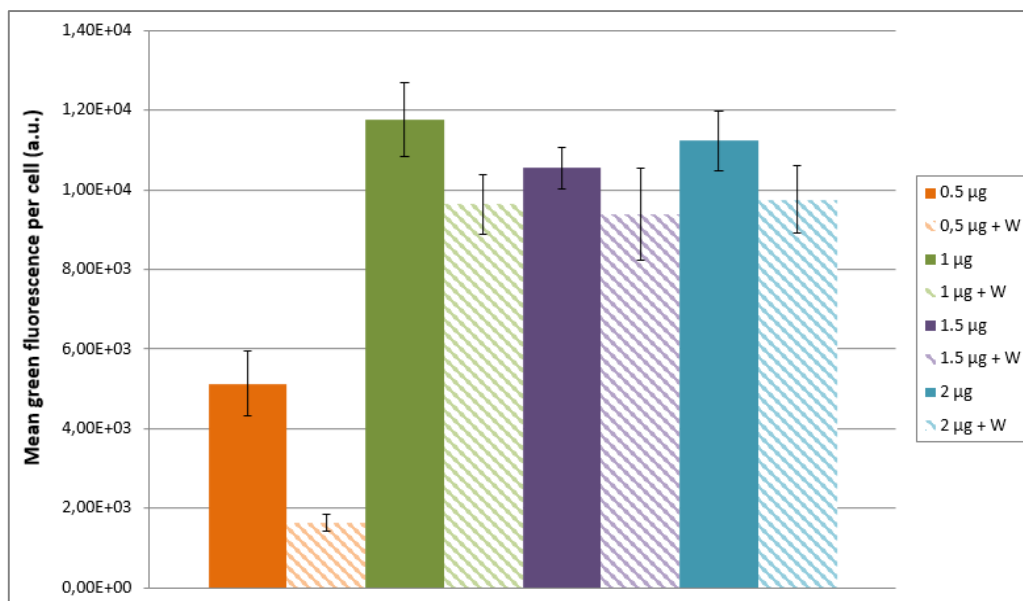


Figure 41: Bodipy fluorescence measured by flow cytometry for *Chlamydomonas reinhardtii* in lipid accumulation phase (13 days of stress) for various Bodipy and cell ratios (quantity in micrograms of Bodipy for 1 million of cells) with and without a washing step (centrifugation + resuspension in fresh medium after staining).

From Figure 41, it is clear that the ratio of 0.5 µg of Bodipy for $1 \cdot 10^6$ cells is not enough to stain neutral lipids accumulated in *Chlamydomonas reinhardtii* after 13 days of stress. Indeed, increasing the ratio to 1 µg, resulted in a great increase in fluorescence. But for higher ratios (1.5 µg and 2 µg) there is no further increase. This shows that the ratio 1 µg for $1 \cdot 10^6$ cells seems to be optimal for *Chlamydomonas reinhardtii* at 13 days of lipid accumulation stress.

The effect of the washing step on fluorescence intensity is difficult to understand. As flow cytometry does not take into account the medium fluorescence washing slightly reduces the amount of intracellular Bodipy (for ratio of 1 and more) even if this is not very significant. However, for the lowest Bodipy concentration (0.5 µg for 10^6 cell) for which neutral lipids are only partially stained, the decrease related to washing is very high.

This observation raises the question about the lability of Bodipy bound to neutral lipids, which is a strong drawback for this method. Another question must be answered: does Bodipy keep in the cytoplasm and stain molecules other than lipid droplets?

Chlamydomonas reinhardtii cells at 6 days of stress stained with Bodipy (1 µg + washing step, 1 µg and 1.5 µg for 1 million of cells) are shown in Figure 42. The fluorescence seems to be well related to lipid droplets but it is hard to distinguish direct fluorescence from fluorescence coming from nearby objects: *i.e.* a small fluorescence is observed in the cytoplasm between droplets, but this could be due to the fluorescence diffracted from surrounding droplets. More precision could be obtained with confocal microscopy, as the field observed is illuminated and recorded pixel by pixel to avoid the light emitted out of the focus.

In conclusion, from the images, no clear difference could be observed between cells stained with 1 µg of Bodipy for 1 million cells with or without a washing step. No fluorescence seems to be observed out of the cells, in the background of the image, suggesting that **Bodipy is not in excess**. This was previously observed by Govender et al. [73].

Finally, the cells stained with 1.5 μg of Bodipy for 1 million of cells show a very slight fluorescence in the background of the image. We can therefore hypothesize that the optimal Bodipy to stain 1 million of *Chlamydomonas reinhardtii* cells at 6 days of stress would be comprised between 1 and 1.5 μg .

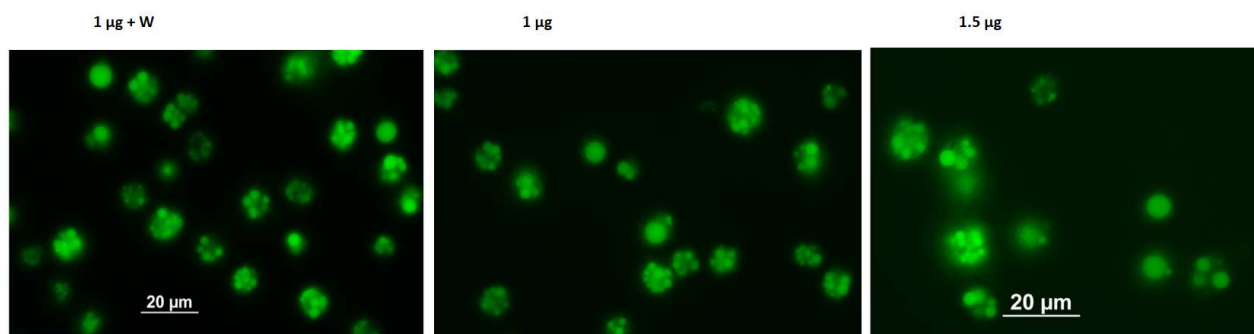


Figure 42: Bodipy staining step. *Chlamydomonas reinhardtii* cells at 6 days of stress observed with an epi-fluorescence microscope (1 μg + washing step, 1 μg and 1.5 μg for 1 million of cells)

Furthermore, *Chlamydomonas reinhardtii* cells in growth phase were stained under the same conditions, i.e. 1 μg of Bodipy for $1 \cdot 10^6$ cells and observed by epifluorescence microscopy (Figure 45).

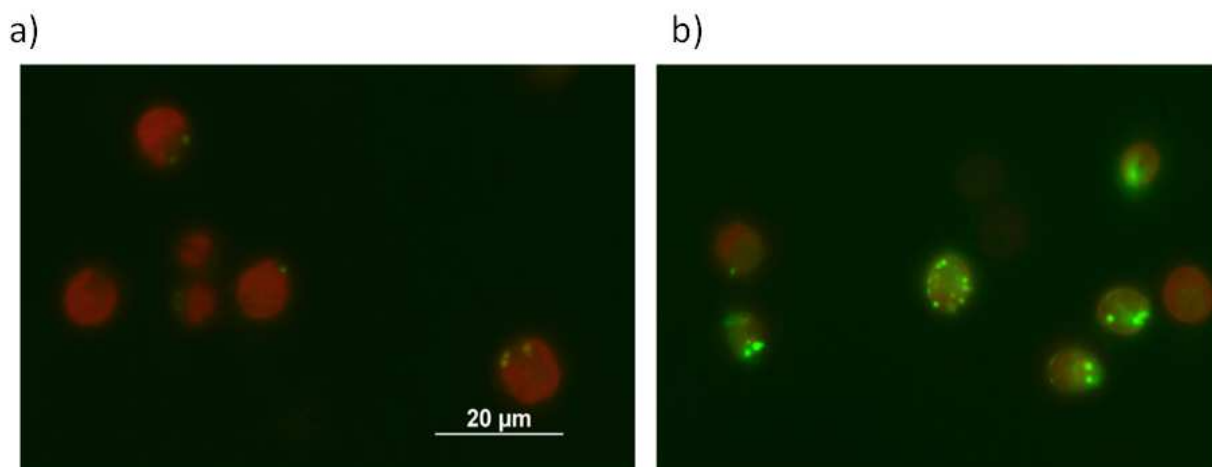


Figure 43: Bodipy staining (1 μg for $1 \cdot 10^6$ cells) on *Chlamydomonas reinhardtii* in growth conditions observed with an epi-fluorescence microscope. a) Washing step, b) no washing step. Chlorophyll autofluorescence (red) and Bodipy fluorescence (green).

In Figure 43, we observe a clear difference with (a) and without (b) a washing step suggesting that there was a clear excess of dye (1 μg for $1 \cdot 10^6$ cells) in contrast to the Figure 42 where no effect was observed with or without washing. This may indicate that the amount of dye used should vary with stress duration as the amount of lipid droplets increases during stress. In the case of an excess of dye used (Figure 43.b), Bodipy fluorescence is observed (1) in lipid droplets, (2) on plasma membranes, (3) in the cytoplasm, and (4) in the medium out of the cells.

The washing step seems therefore to affect Bodipy fluorescence in the medium and also in the cells: cytoplasm and membranes when using an excess of dye. In Figure 42, for stress conditions, no clear difference could be observed on cells with or without a washing step: the fluorescence is indeed so strong due to a high lipid content that it is very hard to identify its origin. In conclusion, fluorescence

microscopy seems to be not suitable for optimizing the staining protocol and select if a washing step is necessary or not.

V3b) **Observation on *Chlamydomonas reinhardtii* cells in 7 days of stress using a Confocal Laser Scanning Microscopy (CLSM).**

The confocal laser scanning microscopy (CLSM) allows a more efficient observation of the fluorescence emitted by Bodipy stained cells. In comparison with epi-fluorescence microscopy, **CLSM increases optical resolution by adding a spatial pinhole which eliminates out-of-focus light** [89]. With the help of laser (instead of lamps in the case of epi-fluorescence microscopy), the sample is scanned point by point to avoid the excitation of the surrounding sample. This technique gains in resolution in space, but loses in rate of acquisition compared with the epi-fluorescence microscope equipped with a color camera presented previously. To better understand the difference with wide field fluorescence, see Appendix 7.

Because of the low rate of image acquisition (several seconds per image), the algae sample must keep stable during image acquisition in confocal microscopy. When the algae cells are immobilized, it is possible to acquire a high resolution image of *Chlamydomonas reinhardtii* stained with Bodipy (1 μg for $1 \cdot 10^6$ cells at 7 days of stress) as presented in Figure 44. In this image, acquisition is performed on X/Y and also in Z plans. This figure presents the acquisition on 15 Z plans, each distanced by 0.35 μm .

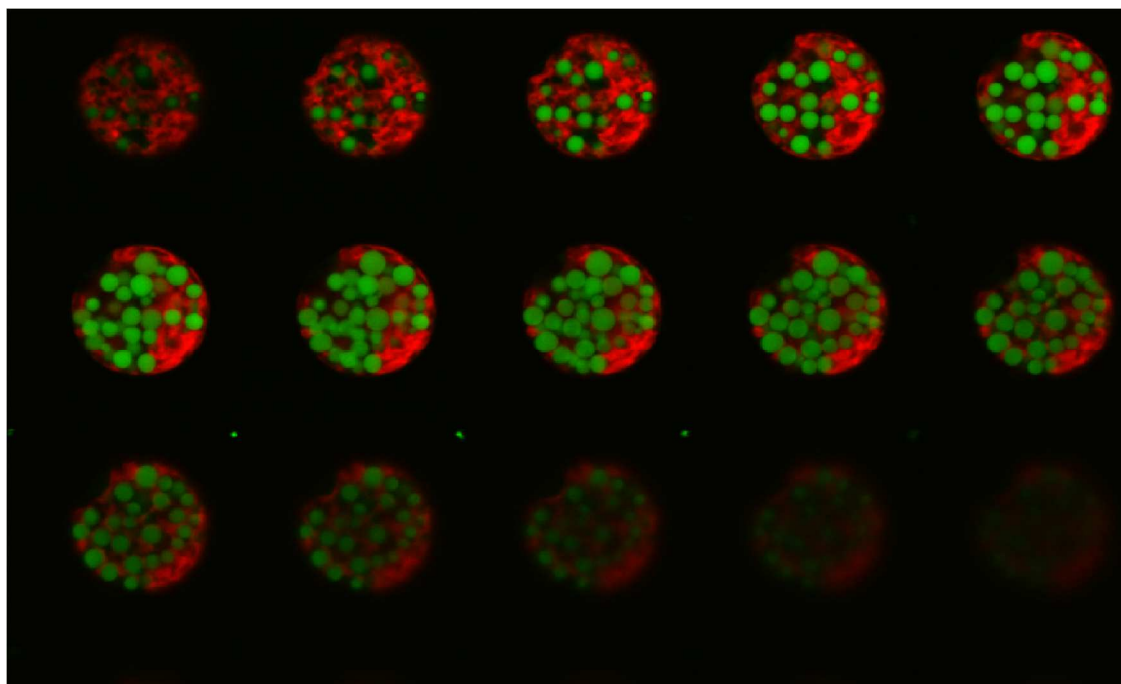


Figure 44: 15 Z stacks of a *Chlamydomonas reinhardtii* cell stained with Bodipy (1 μg for $1 \cdot 10^6$ cells at 7 days of stress, no washing step), 0.35 μm between each Z slice. Bodipy is detected in the green channel, Chlorophyll autofluorescence is detected in the red channel. Diameter of the cell: 11 μm . Recording is performed from the bottom to the top.

The use of CLSM enables to visualize precisely the numerous lipid droplets which are inside the cytoplasm. On the example of Figure 44, about 30 to 40 lipid droplets of a diameter ranging from 0.1 to 1 μm were counted in the cytoplasm. The first slices (top left on the figure 46) seem well illuminated by the laser, but the 5 last slices (bottom right of Figure 44) are shadowed, probably because the laser

could not penetrate the whole cell. **Despite the absence of washing step, Bodipy seems to stain only lipid droplets, and not the lipids associated with the membranes.** The use of a washing step is therefore not justified, provided the observation is made with CSLM.

V3c) **Conclusion on Bodipy staining protocol**

When studying *Chlamydomonas reinhardtii* cells with a high lipid content (after 13 days of stress), **we found that 0.5 µg Bodipy/million cell is not a sufficient ratio to stain correctly the lipids, whereas 1 µg/million cell is enough; higher ratios do not result in different staining.** As for the growth conditions (where the cells contain few lipids), **1 µg Bodipy/million cell seems to be excessive, as a green fluorescence is observed in the medium out of the cells and in other parts of the cells** (Figure 43.b). As expected, we confirm that the **optimal quantity of Bodipy strongly depends on the lipid content of the cells.**

When using an excess of Bodipy for staining, the medium fluorescence can be eliminated by a **washing step** (removal of the medium after staining and resuspension in fresh medium). But unfortunately the **washing step also removes a part of the intra-fluorescence**; flow-cytometry indeed confirmed a decrease in the mean fluorescence per cell after washing due to a **loss of Bodipy of the cells.**

Finally, **CLSM imaging on cells in stress conditions (7 days) performed without a washing step and with an adequate ratio of Bodipy, showed an efficient staining of the lipid droplets**; no Bodipy is observed in the cytoplasm or in the membrane.

Bodipy agglomeration in membranes or in the cytoplasm then seems to be related to an excess of Bodipy

v4) **Development of a CLSM method to observe Chlamydomonas reinhardtii (pigments, lipids, cell wall).**

The use of multiple fluorescence probes to specifically detect algae compounds, as presented in the previous section, must take into account the excitation/emission of the dyes (see Figure 28 and Figure 29 for further information on excitation/emission) to **avoid overlapping of each dye with chlorophyll auto-fluorescence** and with the other ones.

An additional dye was also used to **stain the cell wall of Chlamydomonas reinhardtii** in order to help characterizing the global shape of the alga.

This section aims to explain how the cell wall dye was used taking into account the fluorescence properties of Chlorophyll and Bodipy, and then, how the optical configuration was chosen to record CLSM images (excitation/emission used in the different channels). These issues were also considered for all fluorescent molecules used in this work, including viability/permeability probes presented in Chapter 3.

A fluorescence configuration can be analyzed with a tool called “**spectra viewer, or spectra analyzer**”, which illustrates the excitation/emission spectrum for all the fluorescent molecules considered. The tool can be found on internet.

Chlorophyll a autofluorescence can be mimicked in the tool by selecting the fluorophore **PerCP-cy5.5** which refers to the Peridinin chlorophyll protein (PerCP). As it can be observed in Figure 45.a, Chlorophyll a excitation has a large band from 350 to 720 nm with two maximum peaks at 490 and 670

nm. The maximum emission peak is at 680 nm but the whole emission band is in the range of 670 to 860 nm. When considering that emission below 650 nm is negligible, the possible dyes must have an emission below 650 nm.

As shown in Figure 45.b, **Bodipy (dye for lipids) matches with Chlorophyll a as its maximum emission is in the range of 510-520 nm.** The Bodipy maximum excitation spectrum (in green dashed line) is between 450 and 500 nm, a region where Chlorophyll is also excited. This is not a problem as the emission peaks do not overlap. In Figure 45.b, blue rectangles indicate the possible emission regions for another dye staining for example the cell wall: a first region in the UV-blue (400-450 nm), and a second narrow region in the orange (600 nm).

Few cell wall dyes could be found in literature: Hernandez and Palmer used the dye **Hoechst 33258** (352/461), a dye generally use to stain the DNA and chromatin, to stain the cellulosic cell wall of a primary plant [90]. In algae biotechnology, **calcofluor white** (350/440) was commonly used to stain the cellulosic cell wall of *C. vulgaris*, *A. platensis*, *P. cruentum*, *H. pluvialis*, *N. oculata*, *N. salina*, *S. acuminatus*, and *Haematococcus* [91,92]. It was also shown to stain the chitin of the cell wall of the sponge *Spongilla lacustris* [93] and the cell wall of yeasts [94,95]. These two dyes were tested in this project and showed to efficiently stain the cell wall of various algae. However, an excitation of these **molecules in the UV region (350 nm) is required and constitutes a drawback.** Many microscopes are indeed not equipped with laser or lamps able to excite molecules in the UV region, which prevents the use of these dyes. Alternatives were thus tested. To the best of our knowledge **concanavalin a** is poorly scarcely used in algae biotechnology. Concanavalin a is a lectin used in to bind α -mannopyranosyl and α -glucopyranosy contained in the cell wall of bacteria [96], yeasts [97], and recently algae [98]. When associated **with various fluorescent molecules, it can be used as a cell wall probe** [99].

In this project, we use concanavalin a bounded with tetramethylrhodamine (TRITC), a molecule which excitation/emission spectrum is shown in Figure 45.c (excitation in yellow dashed line, emission in straight line): the **emission spectrum of concanavalin a TRITC** (yellow straight line) **interferes with the emission spectrum of Bodipy** (green straight line). This is not a problem, as TRITC can be excited at 550 nm without exciting BODIPY. It is then possible to visualize concanavalin a TRITC without interference with BODIPY when using different lasers (550 nm for concanavalin a TRITC and 480 nm for Bodipy).

To conclude, **Chlorophyll a and Bodipy can be excited with the same laser (blue) and observed in different fluorescence channels (green for Bodipy and red for Chlorophyll a, Figure 45.b).** The cell wall can be observed at 580 nm with **concanavalin a TRITC using a different laser (at 550 nm) to avoid the excitation of Bodipy.**

Contrary to Bodipy staining, it is highly recommended **in the case of cell wall staining to use a washing step to remove the dye excess in the medium because lectin can bind with many impurities or elements as for example the glass substrate used for cell observation, as noticed in our work.**

For double staining of cells with concanavalin and Bodipy, concanavalin a is used in excess (200 $\mu\text{g}/\text{mL}$); the solution containing concavalin is first mixed for 30 min – 1h and then the cells were separated and washed before Bodipy staining. According to the spectra presented in Figure 45, the optical configuration chosen for CLSM is detailed in Appendix 8.

Finally, chlorophyll was excited with a red laser (639 nm) to avoid the excitation of the other dyes.

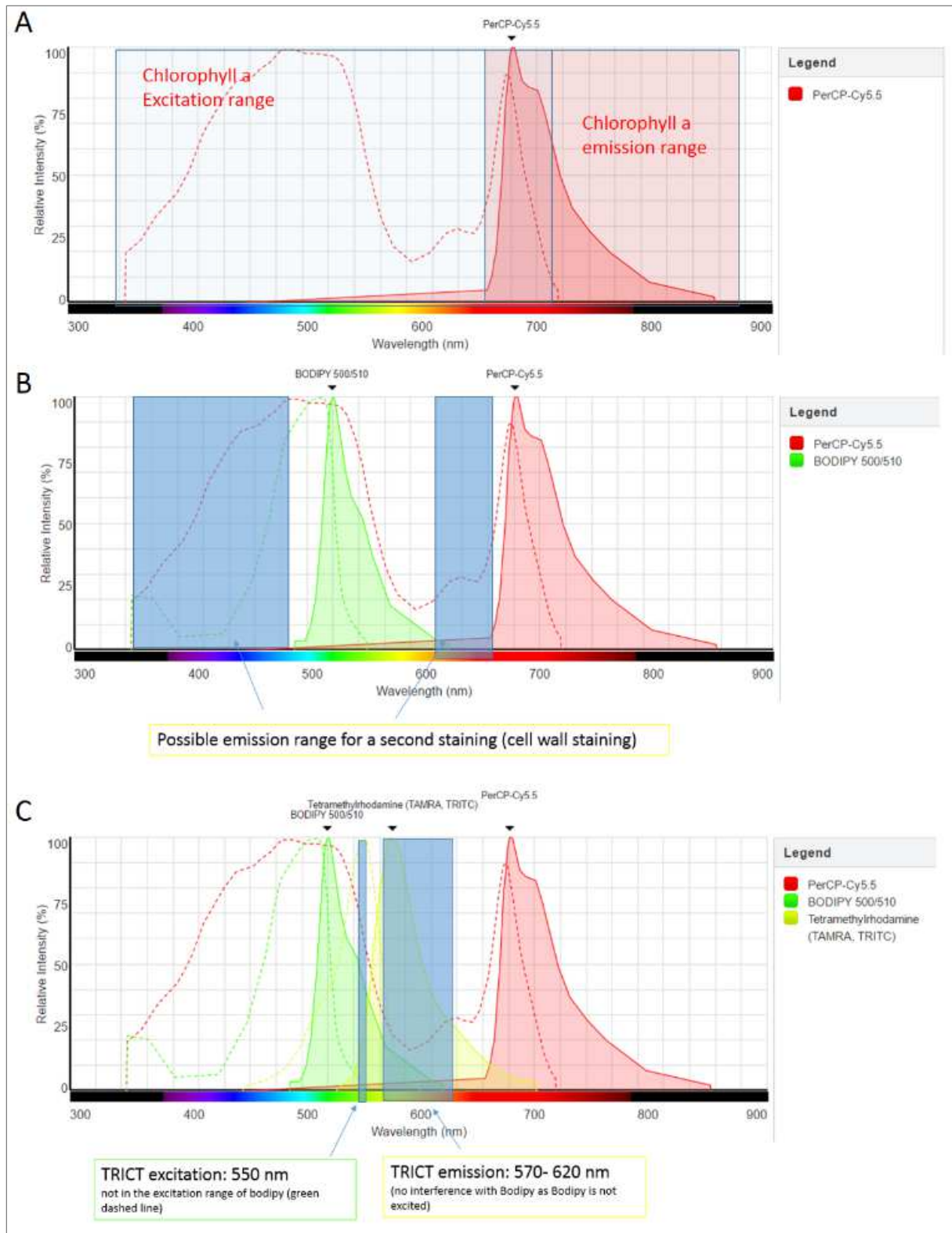


Figure 45: Spectra viewer of Chlorophyll a mimicked by Peridinin chlorophyll protein (PerCP), Bodipy, and Concanavalin Tetramethylrhodamine (TRITC). Dashed and full lines correspond to excitation and emission spectra respectively.

VI. Results

VI1) Biomass growth

The specific growth rate, μ , was estimated on the exponential growth phase according to equation 3.

$$\mu = \frac{(\ln N_f - \ln N_i)}{t_f - t_i} \quad (\text{Equation 2.2 [46]})$$

Where t_i and t_f are the initial and final culture times and N_i and N_f (cells/mL) correspond to cell concentrations at t_i and t_f respectively

VI1a) First step: Growth phase

The growth patterns and the specific growth rates determined for cultures developed in the growth (Figure 38) are compared in Figure 46. The concentration was measured by flow cytometry as described in Figure 26.

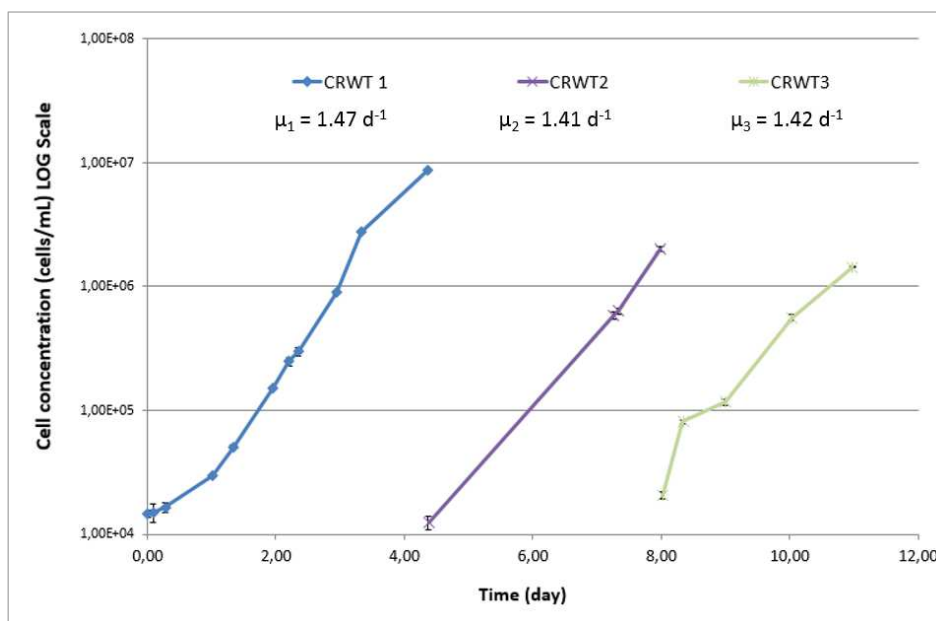


Figure 46: Cell concentration measured over time for *Chlamydomonas reinhardtii* wild type. Cells are grown in 250 mL Erlenmeyer flasks. Growth incubator: low light intensity ($20 - 40 \mu\text{mol}\cdot\text{m}^{-2}\cdot\text{s}^{-1}$) and enriched CO_2 atmosphere (1.5). All cultures were inoculated in TAP N+.

The growth rate was quite similar in the three cultures performed in the growth incubator, the mean growth rate measured was $1.43 \pm 0.03 \text{ d}^{-1}$. The growth rate in the light incubator was a little higher $1.71 \pm 0.03 \text{ d}^{-1}$. According to this result, light seems to be more limiting than CO_2 , as an increase in light and a decrease in CO_2 leads to a slight increase in the growth rate.

VI1b) Second step: Stress phase

During the stress phase (figure 50), the cell concentration increases from $(3.26 \pm 0.36) \cdot 10^6$ cells/mL, generally during the first 4 days of stress, and stagnate after at a maximal concentration. The culture

2 exhibits a particular behavior, with no significant variation of cell concentration, which cannot be explained. After 7 days of stress, the cell concentration reached varies from $4 \cdot 10^6$ cells/mL to $1 \cdot 10^7$ cells/mL.

It must be noted that the cells growth behavior may greatly vary among cell cultures This could be related to the pre-culture conditions, e.g. cell concentration of the culture before centrifugation/re-suspension.

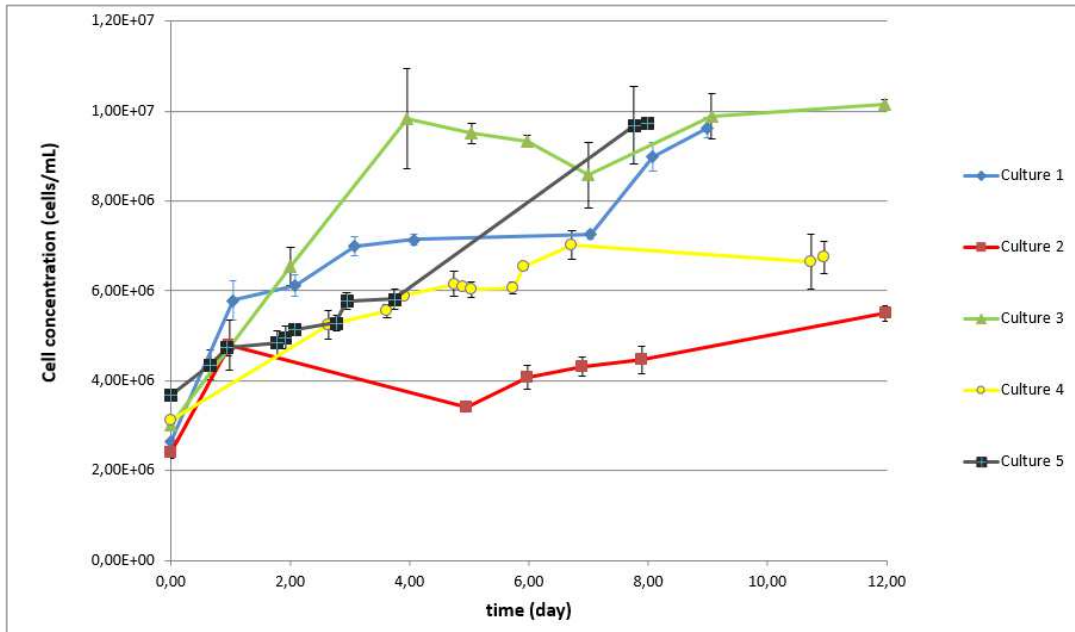


Figure 47: Cell concentration over time for 5 cultures of *Chlamydomonas reinhardtii* WT in stress conditions

VI1c) Illustration of the two steps

The evolution of cell concentration during growth step and stress is presented in Figure 48. The measurements on the two steps presented here were performed on two different cell cultures but the figure illustrates the reduction of growth rate always observed during stress in comparison with the exponential growth during the growth phase.

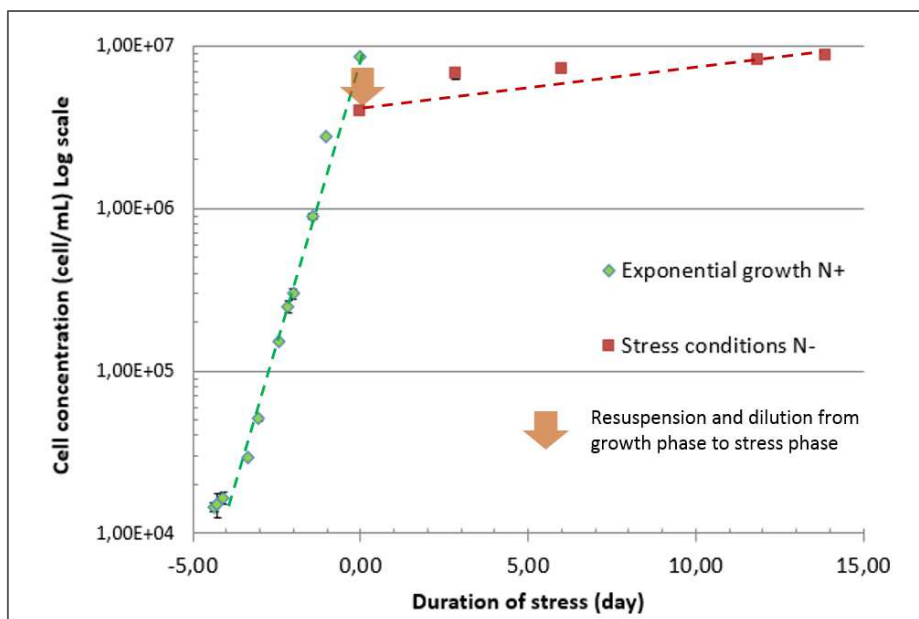


Figure 48: Illustration of the two steps: exponential growth and stress conditions, with a resuspension and dilution from growth phase to stress phase.

VI2) Chlorophyll content

Chlorophyll concentration together with cell concentration were determined by cytometry. The former was detected by measuring red autofluorescence at 680 nm (gain set for red fluorescence: 8).

VI2a) First step: Growth phase

The evolution of red fluorescence per cell over time for several cultures in growth phase is illustrated in Figure 49. The average mean red fluorescence measured for over 30 algae samples in exponential growth at different times was equal to $1.05 \cdot 10^4 \pm 0.32 \cdot 10^4$ au.

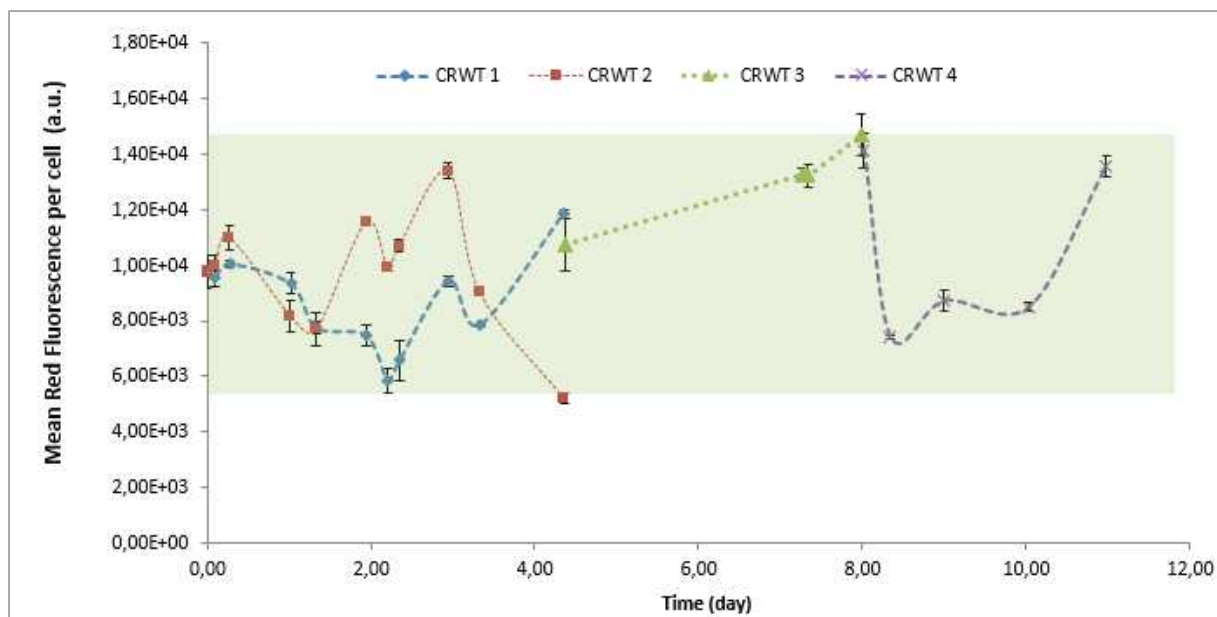


Figure 49: Mean red fluorescence (associated with chlorophyll autofluorescence) measured over time for 4 *Chlamydomonas reinhardtii* WT cultures in optimal growth conditions. Mean red fluorescence and standard deviation is shown in a green bar.

Red fluorescence varies around the mean value of approximately $1 \cdot 10^4$ au. This variation could be due to cell cycles in which the pigment content per cell would increase before division into daughter cells. In addition, the pigment content could adapt to light distribution inside the culture. But in exponential phase red autofluorescence does not exhibit any global tendency to decrease or increase with time.

VI2b) Second step: stress conditions

The evolution of mean red autofluorescence of four cultures in stress conditions (high light intensity of $100 - 150 \mu\text{mol} \cdot \text{m}^{-2} \cdot \text{s}^{-1}$, nitrogen depletion) is shown in Figure 50 (mean red fluorescence per cell in log scale).

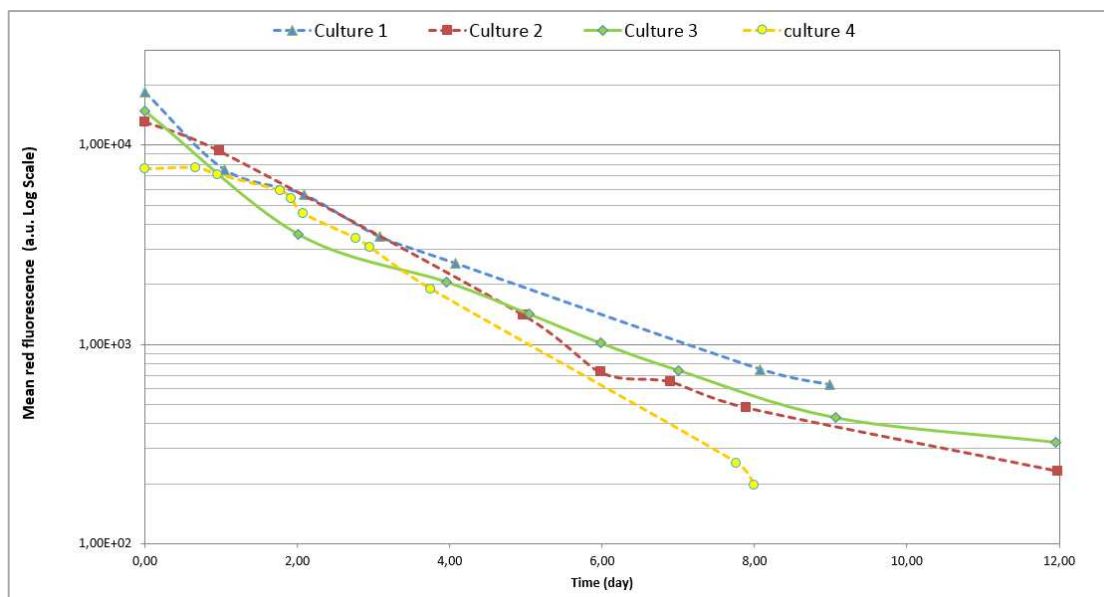


Figure 50: Mean red fluorescence per cell over time for two cultures of *Chlamydomonas reinhardtii* WT in stress conditions.

In contrast with growth conditions, red fluorescence drastically falls for both cultures from about $1 \cdot 10^4$ a.u. to less than $4 \cdot 10^2$ a.u. in 8 days. The decrease is exponential in the first 8 days of stress with an average decrease of $-0.408 \pm 0.047 \text{ d}^{-1}$ when plotting the logarithm of the mean red. The decrease of pigment content can be easily explained by the absence of nitrogen in the medium which prevents cell division (see Figure 49 and Figure 50). The inability of the cell to divide and an increase of light supplied to the culture results in an high excess of energy at the outlet of the photosystem (see Figure 20). The first strategy of the cell to reduce this harmful energy is to decrease the quantity of photons absorbed by degrading a part of the pigments. The nitrogen contained in chlorophyll molecules could also be used a source of nitrogen source.

It would be interesting to correlate the red fluorescence per cell measured with flow cytometry with the determination of chlorophyll content per cell with a quantitative method (*e.g.* chromatography analysis).

v13) Dry weight (stress condition)

The evolution of dry weight of 3 cultures during stress (cultures 1, 2 and 3, Figure 47) is presented in Figure 51. The dry weight protocol requires a high quantity of culture volume and was thus only perform on 3 cultures. Interestingly, while the 3 cultures showed different cell concentration pattern (Figure 47, the highest cell concentration was determined for culture 3 after 7 days of stress and the lowest one was measured for culture 2), the total dry weight of biomass per unit of volume increased similarly in the 3 cultures from $0.3 - 0.4 \text{ g} \cdot \text{L}^{-1}$ to approximately $1 \text{ g} \cdot \text{L}^{-1}$ after 8 days of stress (Figure 51).

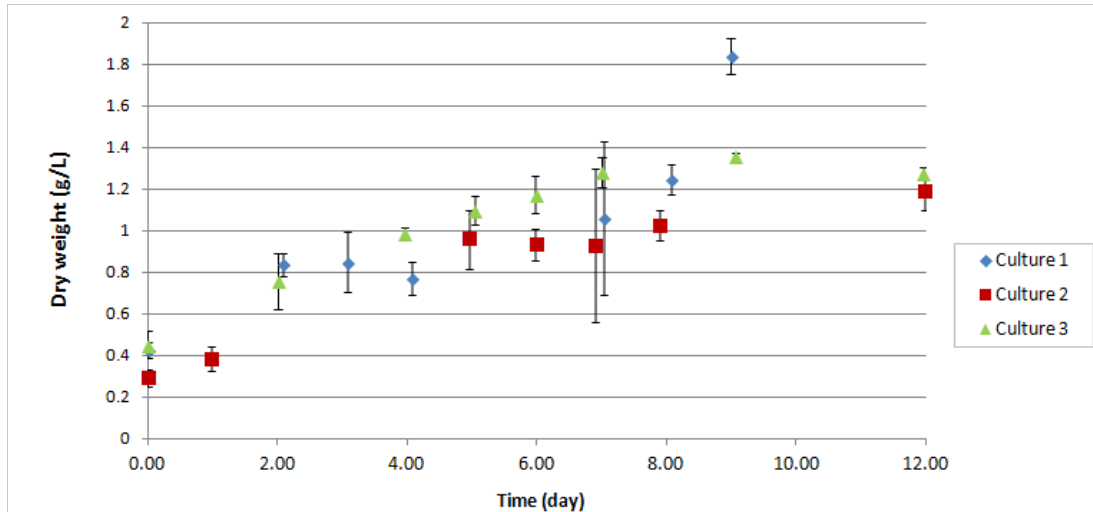


Figure 51: Dry weight over time for three cultures of *Chlamydomonas reinhardtii* WT in stress conditions.

The mean dry mass per cell is illustrated in Figure 52.

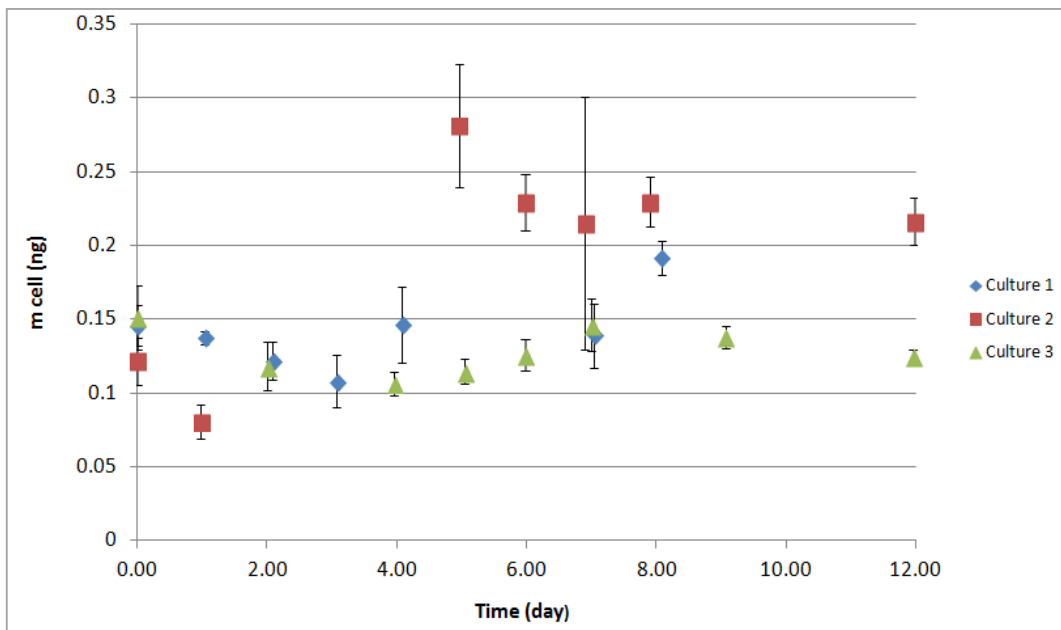


Figure 52: Evolution of the dry mass per cell over time for *Chlamydomonas reinhardtii* WT in stress conditions.

The dry weight per cell in growth phase (*i.e.* at $t=0$ in the graph) is equal to 0.140 ± 0.016 ng/cell. From the data, a reduction of this mass is observed in the first days of stress, down to about 0.1 ng/cell. This decrease can be associated, among other possibilities, with the rapid decrease in photosynthetic pigments showed previously. In the following days of stress, a slight increase of dry weight per cell is observed, however this increase greatly varies for the three cultures. Culture 2 increased from 0.080 ± 0.012 ng/cell at day 1 to 0.281 ± 0.041 ng/cell at day 5. For the other two cultures, the dry weight per cell increases back to the initial value but there is no significant global weight increase. We could hypothesize that the specific cell weight (Figure 52) compensate the cell concentration (Figure 47) to reach a similar volumetric dry weight in the culture (Figure 51); a volumetric dry weight governed by the quantity of light supplied. For a given quantity of light supplied, less cells receive more light and

thus can accumulate more secondary metabolites (such as starch and TAGs in the case of *Chlamydomonas reinhardtii*). But overall, if considering that the photosynthetic yield (conversion of light into algae mass) is similar in the different cultures, the volumetric mass is similar (g/L). It is possible that the cultures who divided more has spent more resources in the production of biomass than the production of secondary metabolites.

Mulders and colleagues [100] described this phenomenon of increased specific cell production in reduced cell concentration in Figure 53.

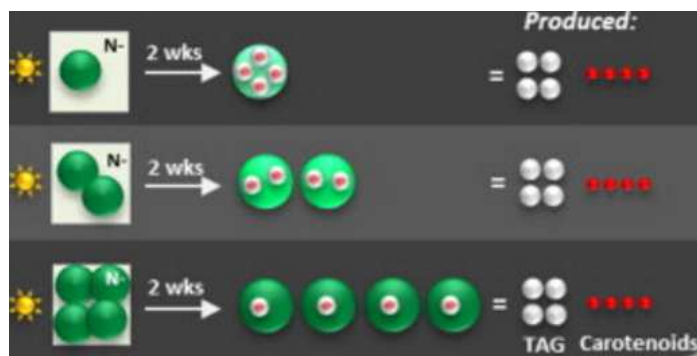


Figure 53: Illustration of the effect of biomass concentration on cellular productivity and volumetric productivity [100]

VI4) Lipid content

VI4a) Identification and quantification of Fatty acids (polar + neutral FA) during stress, measured by gas chromatography (GC-FID).

The FA analyzes for *Chlamydomonas reinhardtii* wild type were performed one single time by an external laboratory (Bioprocess Engineering group, Wageningen University and Research Center, Netherlands). The analytical method [60] was described in the section “Gas Chromatography analyses” of this chapter.

Total lipids are completely extracted and then separated by Solid Phase Extraction (SPE) into a polar FA (Fatty Acids) pool (membrane associated FA) and a neutral FA pool (FA accumulated as TAGs in the cytoplasm).

The results in terms of total FA composition are presented in Figure 54: 8 samples from culture 3 (in Figure 47, Figure 51 and Figure 52), corresponding to different stress durations were analyzed in triplicate. FA compositions in the polar pool (A) and in the neutral pool (B) are presented in Figure 55.

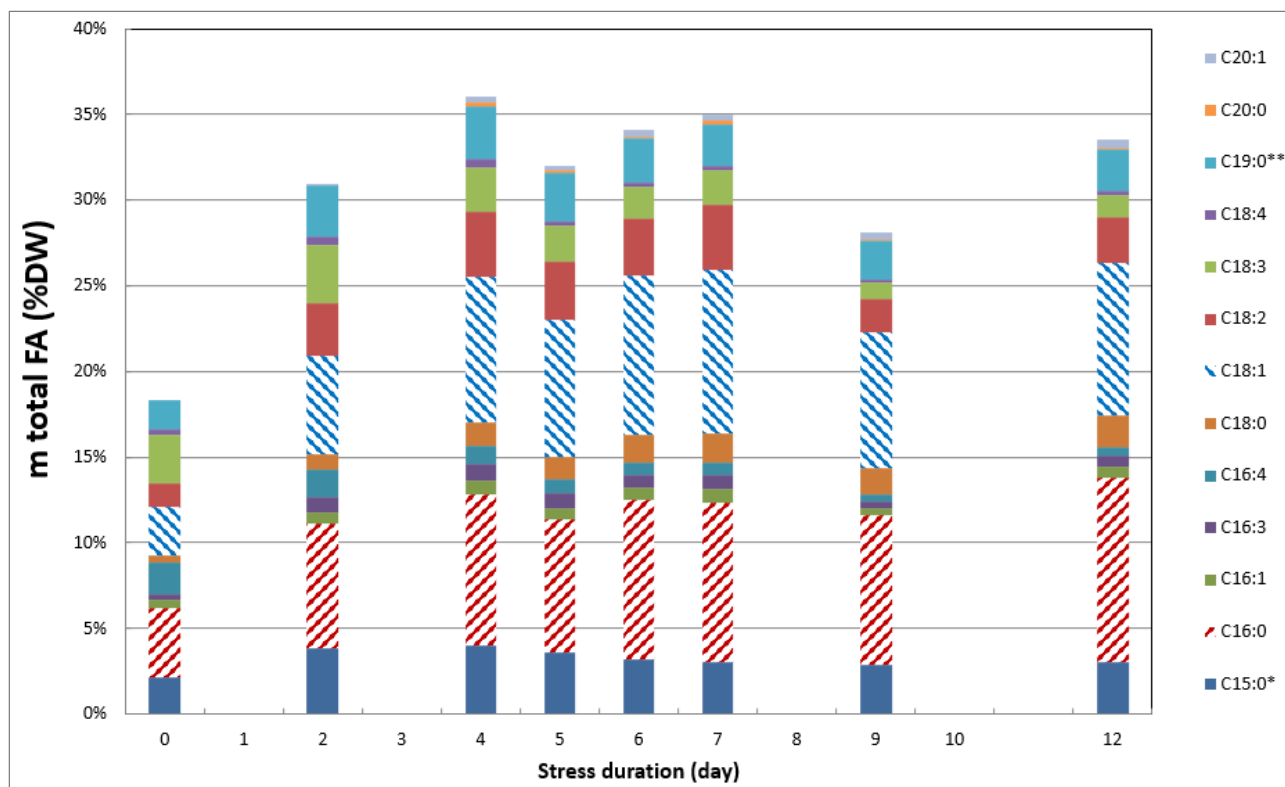


Figure 54: Evolution of total fatty acids and their composition (neutral FA + polar FA) in *Chlamydomonas reinhardtii* over time (12 days of stress). *FA only detected in the polar FA pool, ** FA only detected in the neutral FA pool.

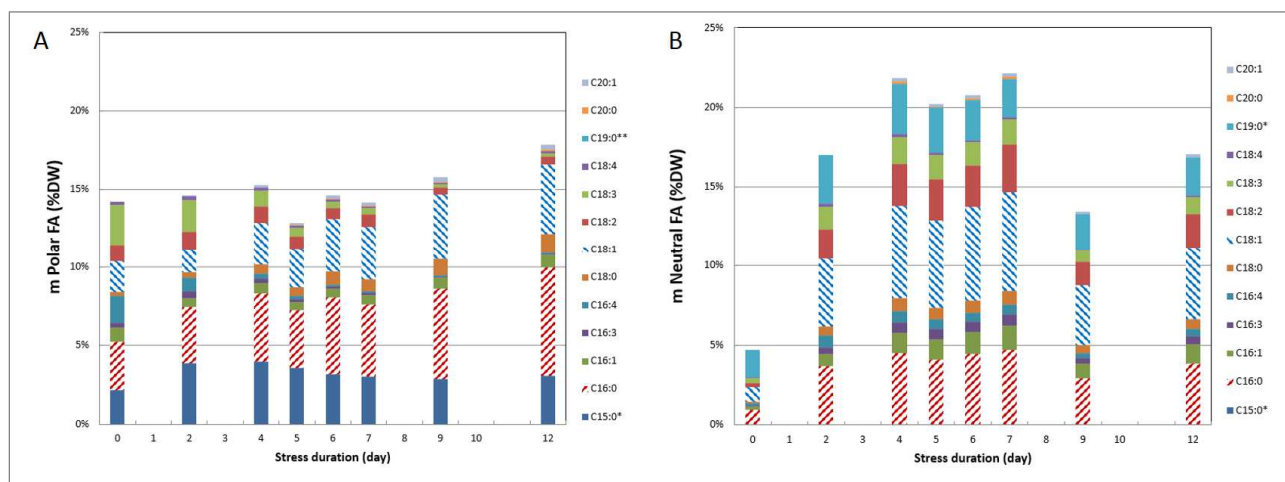


Figure 55: Evolution of total fatty acids and their composition *Chlamydomonas reinhardtii* over time (12 days of stress) A polar FA, B neutral FA. *FA only detected in the polar FA pool, ** FA only detected in the neutral FA pool.

The **mass fraction of polar FAs** (dry mass of polar FAs per dry mass of cells) is **roughly constant** during the whole stress period till 7 days, at approximately 14.55 ± 2.40 % (Figure 55.A). A slight increase in this mass fraction, up to 18.25 ± 2.75 %, is observed afterwards. But their composition greatly varies: the proportion in C16:0 and C18:1 increases to the detriment of C16:4 and C18:3 FA. This corresponds to a hydrogenation of some unsaturated FA which reduce their degree of saturation (from C16:4 to C16:0 and from C18:3 to C18:1).

On the contrary, the **mass fraction of neutral FAs increases during stress** from 4.86 ± 0.21 % DW at the beginning of experiment to 17.79 ± 2.75 % DW after 2 days of stress and 23.11 ± 2.06 % DW after 7 days of stress (Figure 55.B). At the beginning of stress, the main FA in neutral FA pool is C19:0 (1.69 ± 0.09 % of total DW). The two other main FA are C16:0 and C18:1 which represent respectively 0.95 ± 0.03 and 0.91 ± 0.05 % of DW). After 7 days of stress, the 6 main FA are: C18:1, C16:0, C18:2, C19:0, C18:3 and C16:1 respectively at 6.22 ± 0.17 , 4.68 ± 0.15 , 3.02 ± 0.23 , 2.39 ± 0.02 , 1.59 ± 0.20 and 1.52 ± 0.10 %. Long chained FA are more present in the neutral FA pool than in the polar FA pool. C19:0 is not found in membrane associated FA (*i.e.* polar FA). On the contrary C15:0 is found in the polar pool but not in the neutral pool.

Finally, when neutral and polar FA are considered together as a total FA present in the biomass, the **lipid content increases from 19 % up to 36 – 37 %** (Figure 54). After 7 days of stress, C18:1 represents 9.58 % DW and C16:0 9.28 % of DW. After these two main FA, the most represented FA are C18:2 (3.82 %), C15:0 (3.03 %), C19:0 (2.39 %), and C18:3 (2.00 %). Work *et al.* [101] also measured C18:1 and C16:0 as the two main FA accumulated by *Chlamydomonas reinhardtii* wt during stress but the others main FA found were C16:1, C16:2, C16:3 and C18:0. In the work of Breuer *et al.* [60] where 9 the FA composition of 9 oleaginous strains was analyzed, C18:1 and C16:0 were also found to be the main FA with C18:1 mostly found in the neutral FA pool. Whether in Work *et al.* [101] or Breuer *et al.* [60], the FA 19:0 is not found. In another study, Breuer *et al.* [42] has showed that the FA composition in a culture varies with temperature and pH.

VI4b) Analysis of FA composition for biodiesel purpose and analytical methods

In addition, with polar and neutral pool relative compositions, it is interesting to **distinguish saturated FA (Cn:0) from mono-unsaturated FA (Cn:1) and poly-unsaturated FA (Cn:2,3,4,)**. This consideration is important for biofuel production (see section II2), Figure 18) and for SPV method (see section III2), Figure 35).

When considering **FA identified in the non-polar pool (TAGs)** analyzed (Figure 58B) **which could be transesterified to biodiesel**, about 1/3 are saturated and 2/3 are unsaturated (about 45% mono-unsaturated and 20% poly-unsaturated). When comparing with data from Figure 18, FA from our samples can be transesterified to biodiesel (neutral FA); the representative point on figure 17 would be in the yellow region with **good cetane number and iodine value, but the cold filter plugging point (CFPP)** is not sufficient as it requires a minimum of 80% of mono-unsaturated FA.

Our results are also important when considering the SPV (SulfoPhosphoVanillin) method that will be used to quantify total lipids as previously reported (section III2d), Appendix II2 and hereafter). It should be reminded that only **unsaturated FA, both polar and non-polar FA** (membranes associated FA and TAGs, respectively) **are detected with this method**. To correlate chromatography analysis with SPV method (see hereafter), **saturated FA (C15:0, C16:0, C18:0, C20:0)** are **discarded from data presented in Figure 54**.

The evolution of the mass of unsaturated FA per cell of *Chlamydomonas reinhardtii* during stress conditions is therefore presented in Figure 56 (**the relative composition of FA** in % of total dry weight

can be converted to a relative composition of FA in nano-grams per cell (10^{-9} grams) by using the cell concentration and cell dry weight of the culture (data from culture 3, Figure 47 and Figure 52).

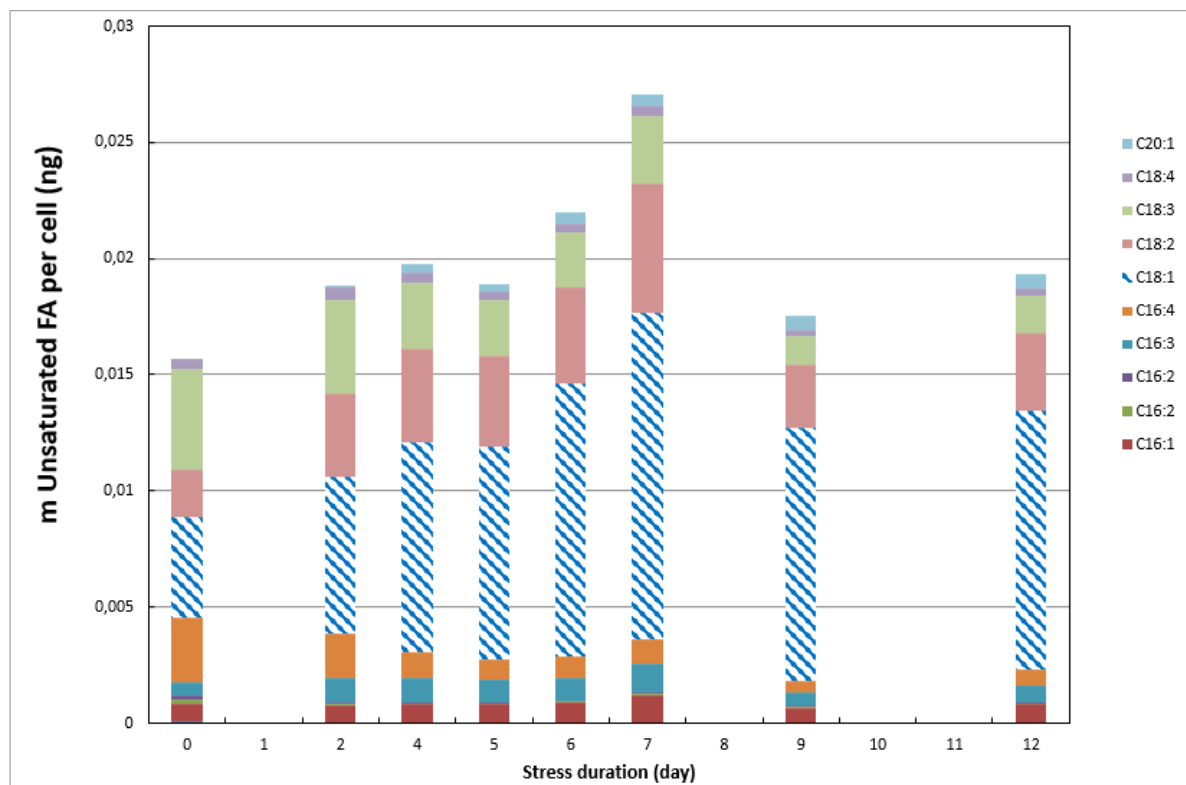


Figure 56: Mass of unsaturated FA per cell over time measured for *Chlamydomonas reinhardtii* in stress conditions.

In Figure 56, it can be observed that the mass of unsaturated FA increased during stress from approximately 0.015 ng per cell to 0.027 ng. This increase is mostly due to the increase content of oleic acid C18:1 and linoleic acid C18:2. Between day 7 and day 9 of stress, the mass of unsaturated FA per cell decreases back to the less than 0.020 ng. During stress, after a period of neutral lipid accumulation due to an energetic imbalance at the outlet of photosystems of cells Figure 20, the cells may degrade their carbon stored in the cytoplasm to use it as a source of organic energy.

When comparing the evolution of biomass (Figure 47) and lipid accumulation presented above, it is interesting to observe that until day 4 the cell concentration (in cell number per volume) increases in the same time as the neutral FA content (from 5 to 23% of DW). After day 4, the cell concentration and the FA content (in % DW) tend to stabilize. However, an increase in dry weight per cell is observed in the culture 3 from day 4 to day 7 (Figure 52), indicating that the **FA fraction may evolve between day 0 and day 4 of stress** (Figure 54) and **then the cell continues to accumulate FA** until day 7 (Figure 56) and other energy storage compounds (*e.g.* starch) without modifying the relative FA content per cell. When comparing the other cultures, it would have been interesting to analyze culture 2 which has a higher cell weight to verify if this culture has accumulated very high amount of neutral FA compared to the culture 1.

VI4c) **Colorimetric method: SulphoPhosphoVanillin (SPV).**

The SPV method described by Mishra and colleagues [84] was used to rapidly estimate the lipid quantity in algae cultures (see section III.2), Figure 34, Figure 35). Algae in stress conditions (7 days of stress) at different concentrations were used to verify the linearity of the response with cell number. Thus algae were concentrated at different factors from 0.5 (dilution) to 8, corresponding to a cell concentration ranging from $5 \cdot 10^6$ to $4 \cdot 10^7$ cells/mL and thus $5 \cdot 10^6$ to $4 \cdot 10^7$ cells (100 μ L of aqueous phase added). Algae in growth phase were also tested with the SPV reaction. The results are gathered in table 3.

First absorbances were plotted towards concentration factors; a good straight line ($r^2= 0.994$) is obtained confirming the feasibility of the method for analyzing algae.

Its equation is $Abs = 0.117 \cdot (\text{Concentration Factor})$. The triolein equivalent mass (TO_{eq}) was calculated by converting the absorbance into TO_{eq} (μ g) by using the correlation found in appendix III.3 ($Abs = 0.003 \cdot TO_{eq}$). C18:1 in the main unsaturated FA found in our algae (Figure 56).

Table 3: Estimation of the Triolein equivalent per cell: *Chlamydomonas reinhardtii* in stress (7 days) and in growth phase

	7 days of stress					Growth phase
Concentration factor	0	0.5	1	2	4	4
Cell number (cells)	0	4.97E5	9.94E5	1.99E6	3.98E6	4.56E6
Mean abs 530 nm	0	0.055 ± 0.014	0.130 ± 0.016	0.250 ± 0.016	0.455 ± 0.015	0.323 ± 0.064
TO_{eq} (μ g)	0	17.74	41.94	80.65	146.77	104.19
TO_{eq} per cell (ng)	0	0.036 ± 0.009	0.042 ± 0.005	0.041 ± 0.001	0.037 ± 0.001	0.023 ± 0.004

Color development for the various concentrations tested is illustrated in Figure 57.



Figure 57: SPV colorations obtained for algae in 7 days of stress concentrated by a factor from 0.5 to 8 (from the left to the right).

The triolein content per cell estimated with the SPV method is 0.039 ± 0.003 ng for the algae at 7 days of stress and 0.023 μ g for the algae in growth phase.

These results can be compared with the masses of unsaturated FA per cell presented in Figure 56. The contents in equivalent triolein estimated with SPV method for cells in exponential phase and at 7 days of stress are compared with the masses of unsaturated FA estimated with GC-FID (Table 4).

Table 4: Comparison SPV/GC-FID method for cells in growth phase and in 7 days of stress

	Growth	7 days stress
TO eq SPV (ng)	0.023	0.039
Mass unsaturated FA GC-FID (ng)	0.016	0.027

As it can be observed, the quantities of FA per cell obtained with the SPV method and with GC-FID are in the **same order of magnitude: from 0.015 to 0.040 ng per cell. The response found with the SPV method in triolein equivalent is higher in comparison with the chromatography analysis giving the exact mass of lipids; but there is the same factor of 1.44 between them**, both in growth and stress phases. As expected the FA mass per cell is 1.69 times higher after 7 days of stress in comparison with the one corresponding to growth conditions, with both SPV and GC methods.

Additional assays are required to understand the correlation between SPV method and GC method in the same culture. Pure mono-unsaturated and poly-unsaturated FA that compose algae (C16:1, C16:2, C18:2, C18:3) must be reacted with SPV method to be able to correlate the absorbance measured to the unsaturated fatty acid equivalent that compose our algae (Figure 56) : indeed the SPV response may vary with the FA composition (Figure 36). In our experiments, we calculate a triolein equivalent as if the only unsaturated FA present in our algae was C18:1.

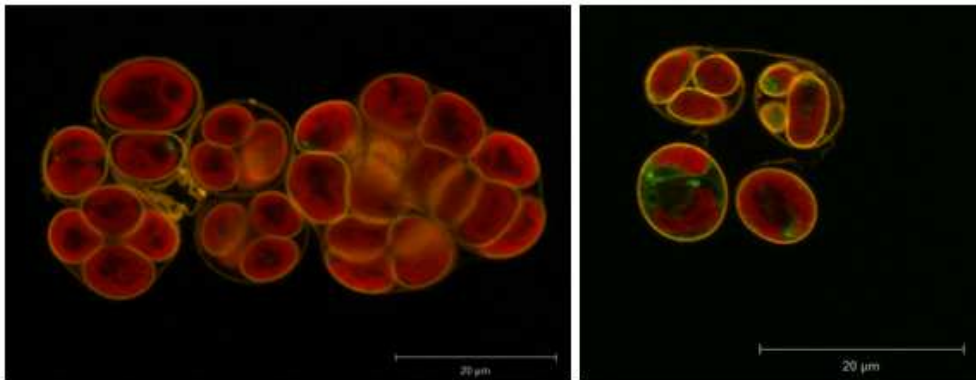
To ensure that only lipids are quantified by the SPV method, their extraction from microalgae with chloroform/methanol could be performed and tested instead of using the entire biomass (see method, appendix II2). Also, the eventual interference of pigments on the SPV method response should be verified. Assays using pure commercial pigments should therefore be carried out. Although more experiments are required to fully validate the SPV method, data obtained for cells in exponential and stress conditions are of the same order of magnitude which encourages us to apply it in this work.

VI4d) **Monitoring *Chlamydomonas reinhardtii* cell with CLSM imaging**

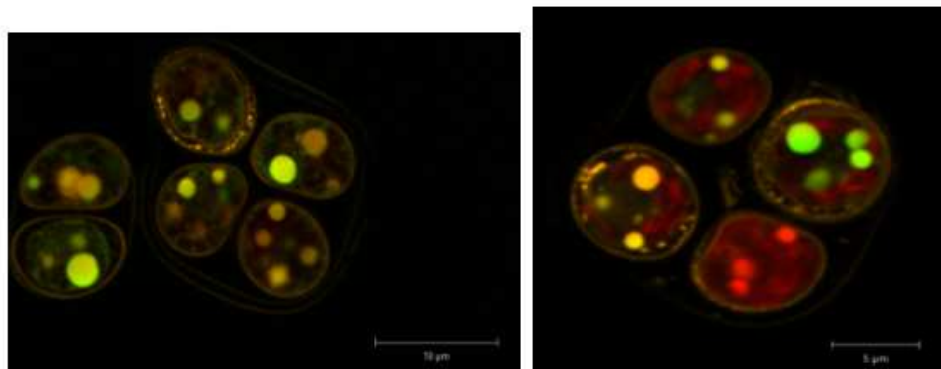
As described in the sections V3) and V4), the lipophilic dye **Bodipy 505/515** was used to stain neutral fatty acids accumulated as **lipid droplets** in the cytoplasm of *Chlamydomonas reinhardtii*. CLSM was found to be the best method to characterize qualitatively the cellular lipid content, in comparison with fluorescence microscopy (see Appendix II.7: Confocal microscopy vs fluorescence microscopy)

Observations of lipid droplets, cell wall and chlorophyll in several *Chlamydomonas reinhardtii* cells in growth phase, at 3.5 and 7 days of stress by CLSM are presented in Figure 58.

A. *Chlamydomonas reinhardtii* in growth phase



B. *Chlamydomonas reinhardtii* (3.5 days of stress)



C. *Chlamydomonas reinhardtii* (7 days of stress)

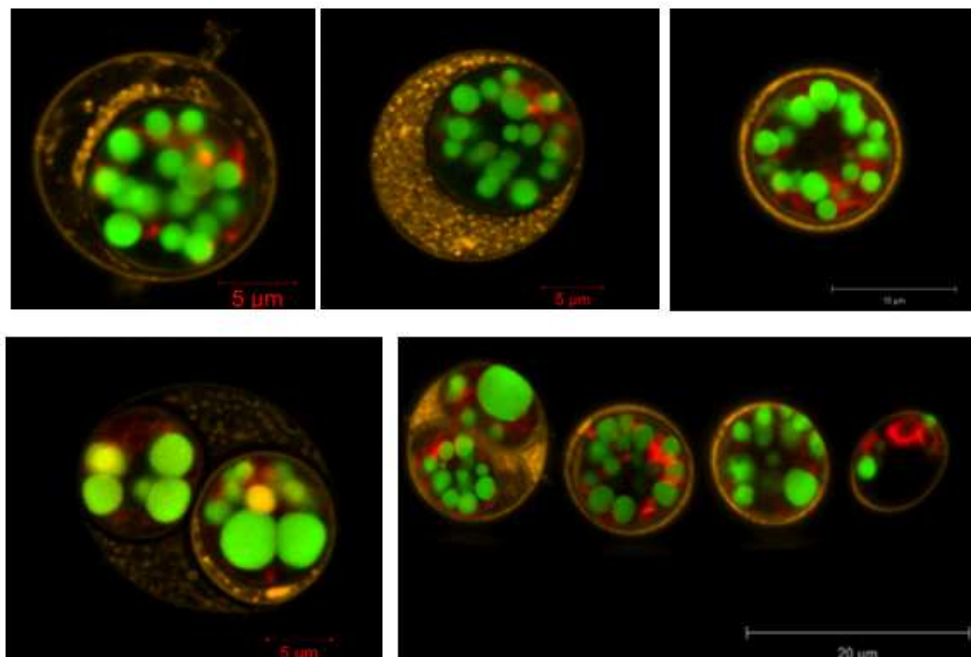


Figure 58: CLSM imaging of *Chlamydomonas reinhardtii* cells at different phases of stress (A: growth phase, B: 3.5 days of stress and C: 7 days of stress). Lipid droplets stained by Bodipy 505/515 in green, cell wall stained by concanavalin TRITC in yellow, chlorophyll autofluorescence in red.

Concerning auto-fluorescent pigments (mainly chlorophyll a and b), the observations are in accordance with the results in Figure 50, which showed a decrease in the chlorophyll fluorescence per cell. Indeed, the chlorophyll content decreased by a factor 9 in the first 4 days of stress and then by a factor 4 between day 4 and day 7. The observation of chlorophyll in the cells in growth phase are in accordance with the structure represented in Figure 4, where the thylakoid membranes cover approximately 70 to 80 % of the cytoplasmic surface. Interestingly, though a large space is occupied (Figure 61), chlorophyll represents a lower percentage of the dry weight of vegetative cells, 2% according to Figure 19. It should however be highlighted that the chlorophyll content is strongly affected by the culture conditions, such as light and nutrients concentrations. In our conditions, a chlorophyll content higher than 2 % is certainly expected.

Concerning lipids, a very high increase of lipid droplet volume per cell is observed between day 0 (growth phase) and 7 days of stress. Interestingly, the increase in volume appears more important between day 3.5 and 7 than at the beginning of the stress phase. In addition, the size of the lipid droplets varies between 0.1 μm to several μm , from a few droplets to several dozens per cell. These observations can be compared with the neutral FA content per cell presented in Figure 59.

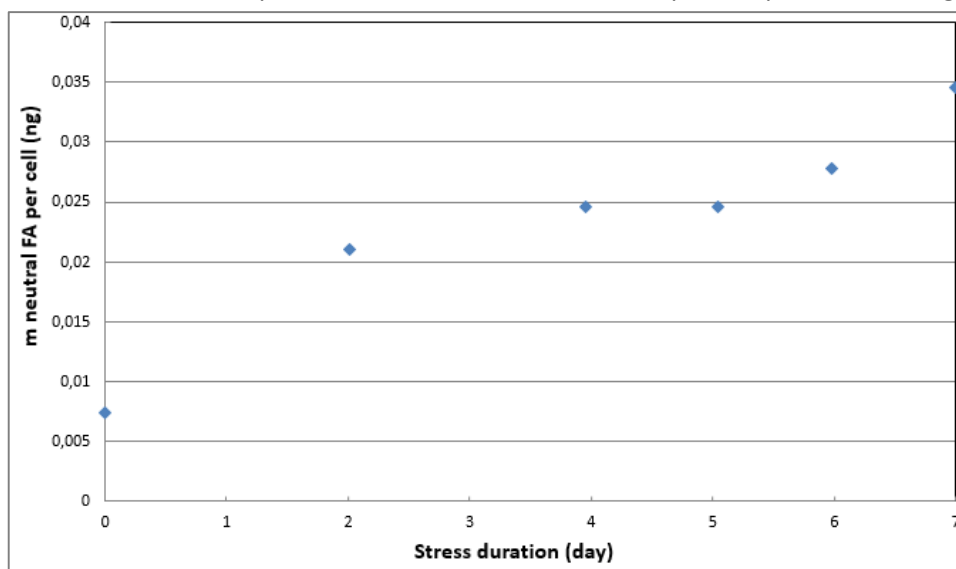


Figure 59: Mass of neutral FA (TAGs) per cell during stress, estimated from GC measurements Data of the culture 3: cell concentration and cell dry weight (Figure 47 and Figure 52) and the neutral FA lipids (Figure 55.b)

The mass of neutral FA per cell increases from 0.007 ng to 0.035 ng per cell (increase by a factor 5). This increase calculated from GC measures seems lower than the one suggested by CLSM observations where the increase in lipid droplet volume per cell seems much more important as almost no lipid droplet is observed in Figure 58.A (exponential growth) and a very high bio-volume of lipid droplets is observed in Figure 58.C (7 days of stress). The difference could be explained by 2 main hypotheses: (1) the variability between the cultures. The neutral lipid content per cell measured in culture 3 (Figure 59) could be lower than that of many other cultures. This could be related to the high cell concentrations of this culture compared to other cultures (Figure 47), which strongly affects light penetration and therefore lipid accumulation. As illustrated in Figure 53, it is possible that the accumulation of energy per cell is minimized by an increased cell concentration and (2), it is possible

that some neutral FA were measured by GC-FID but not stained by Bodipy, e.g., neutral FA associated to the endoplasmic reticulum membrane (see Figure 15).

Concerning the cell wall observations, *Chlamydomonas reinhardtii* cells in growth phase are packaged as 1,2 or 4 cells during their division in small cell wall orbs and contained in a larger cell wall which encompasses the daughter cells (see Figure 58 **Erreur ! Source du renvoi introuvable.**). The cell wall is about a hundred nanometer thick. During stress, the cell wall enlarges into multiple layers of various thicknesses and densities as previously illustrated (Figure 3), up to a total thickness of several micrometers (Figure 60).

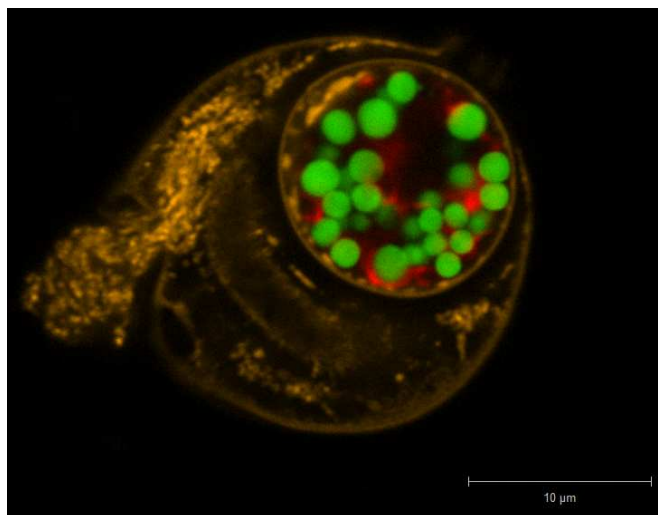


Figure 60: CLSM image of *Chlamydomonas reinhardtii* wild type cell which possesses a thick cell wall (stained by concanavalin a TRITC in yellow).

VI4e) **Monitoring of neutral lipid content with Bodipy staining and flow cytometry**

Bodipy fluorescence per cell was monitored by flow cytometry after an optimization of the staining protocol (section V3)). The mean fluorescence per cell, measured on over 2,000 cells in triplicate for 4 cultures of *Chlamydomonas reinhardtii* in different days of stress is presented in Figure 61. The following conditions were applied: 1.5 μg or 1 μg of Bodipy was used to stain $1 \cdot 10^6$ cells for cultures 1, 2 and 3 (1.5 μg) and culture 4 (1 μg) respectively, with 10 minutes of incubation, No washing step (removal of the excess of Bodipy from the medium) was performed.

At the beginning of the assay, (day 0), the Bodipy mean fluorescence varies from 120 a.u. per cell (culture 4) to 314 a.u. (cultures 1 and 2). After 7 days of stress, the mean Bodipy fluorescence per cell varies from 751 a.u. (culture 3) up to 6,718 a.u. (order of magnitude between the two cultures: 9). The ratio of mean Bodipy fluorescences at day 7 over day 0 varies from 4.75 to 25 in the 4 cultures (Figure 61).

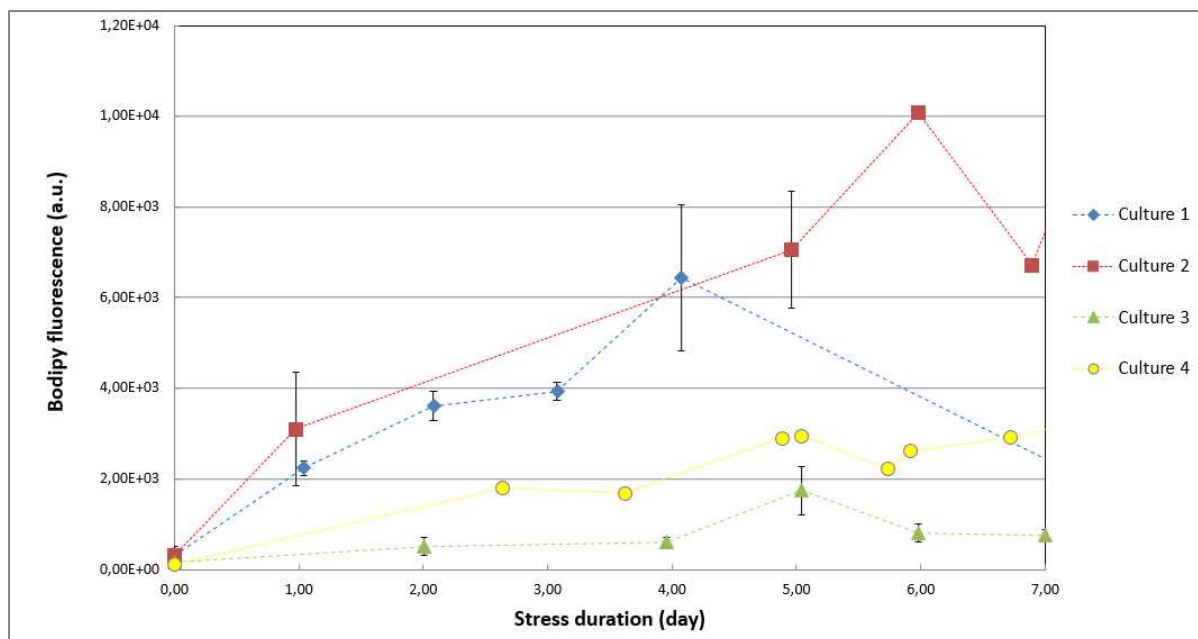


Figure 61: Mean green fluorescence per cell (associated with Bodipy fluorescence) measured by flow cytometry measured on 4 cultures of *Chlamydomonas reinhardtii* in stress conditions. Bodipy added: 1.5 μg of Bodipy for $1 \cdot 10^6$ cells/mL, no washing step, 10 min of staining (for culture 4, the quantity added is 1.5 μg of Bodipy for $1 \cdot 10^6$ cells/mL).

These results confirm the accumulation of lipid droplets in the cells as the mean fluorescence increases during time. However, the mean fluorescence value measured in the 4 cultures at day 7 of stress is much higher than the other cultures. Questions are therefore raised: is this variation due to a difference of cell behavior for the four cultures? We hypothesized that less lipid content had been accumulated per cell in culture 3 because of the higher biomass concentration of this culture (Figure 47). This could explain the lower fluorescence values of culture 3 in comparison with the other cultures *e.g.* culture 1. But the differences of fluorescence could also be due to a variation of the Bodipy penetration in the cells. Many side experiments have been carried and results showed that Bodipy fluorescence per cell varies greatly with conditions such as those related to cell permeability [76] and lipid droplets structure. For instance, the presence of several small lipid droplets or few large affects strongly the mean fluorescence measured though similar lipid contents in the cell.

To validate or invalidate the Bodipy staining protocol, additional assays must be performed where correlations between Bodipy fluorescence and neutral lipid content per cell measured by gas chromatography analysis would be determined [76]. In the view of the results obtained in this project, the correlation could not be validated yet although, the mean Bodipy fluorescence increased by a ratio of 4.75 (Figure 61) and the mass of neutral FA per cell increased by a ratio of 4.66 for the culture 3 (culture both measured on chromatography and Bodipy) (Figure 59).

An additional correlation between SPV and Bodipy fluorescence responses could be also performed. However, these two methods do not measure the same parameter: one is supposed to measure neutral lipids (Bodipy staining associated to flow cytometry) and the other one to quantify total unsaturated fatty acids in algae solutions (neutral plus polar lipids). These two methods are really fast and easy to perform, but are much less precise and reliable than the costly and time consuming GC analysis. They were however the main methods used to evaluate lipid extraction from microalgae in

this work as they are the most adapted taking into account the biomass volume used during PEF (Pulse Electric Field) experiments in microsystems and electroporation cuvettes (see Chapter 3).

v15) Monitoring cell size

The mean cell diameter of *Chlamydomonas reinhardtii* wild type was in the range of 6 to 10.5 μm depending on stress durations.

Two methods were used, (1) laser granulometry and (2) manual optical measurements (see section III3)) More precisely, mean cell diameters of 6.54 ± 0.03 , 6.61 ± 0.04 and 7.38 ± 0.03 for 0, 7 and 14 days of stress, respectively, were determined by Laser granulometry (Figure 62) whereas 6.79 ± 0.08 , 9.95 ± 0.14 , and 10.02 ± 0.04 were measured for 0, 7 and 15 days of stress, respectively, by microscopy (Figure 63).

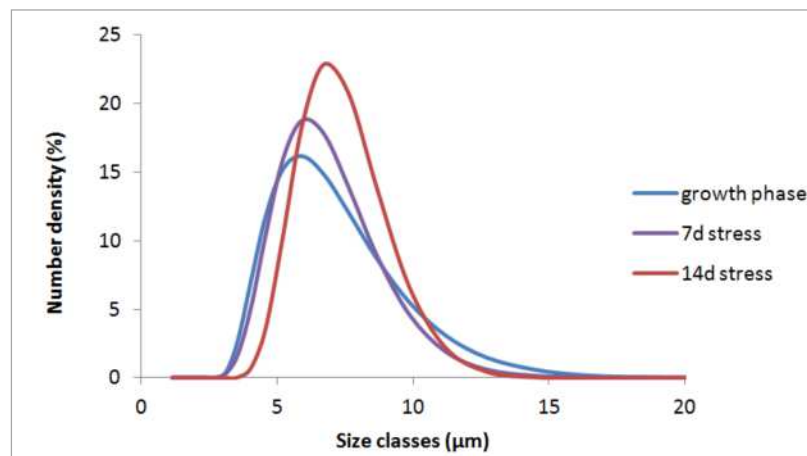


Figure 62: Distribution of number density (%) per size classes estimated from *Chlamydomonas reinhardtii* wt at different lipid accumulation stages by laser granulometry

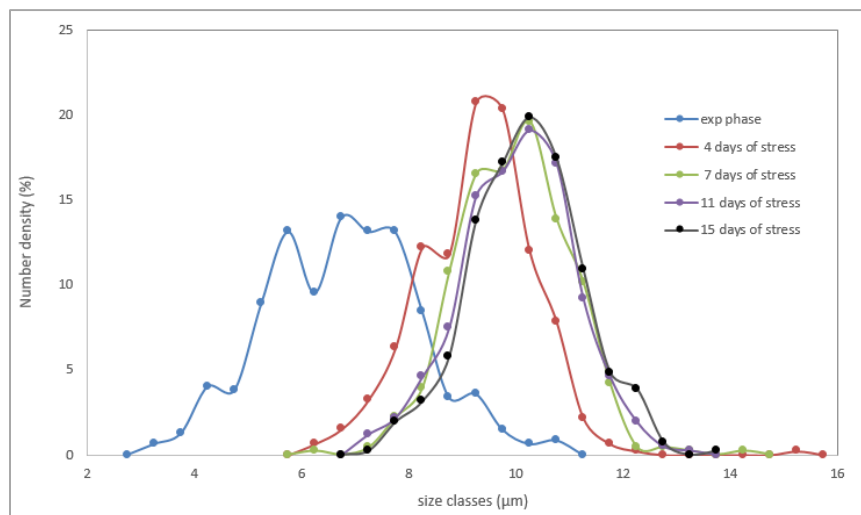


Figure 63: Distribution of number density (%) per size classes estimated from *Chlamydomonas reinhardtii* wt at different lipid accumulation stages by laser granulometry

The evolution over time of the mean diameter estimated with the two methods is shown in Figure 64.

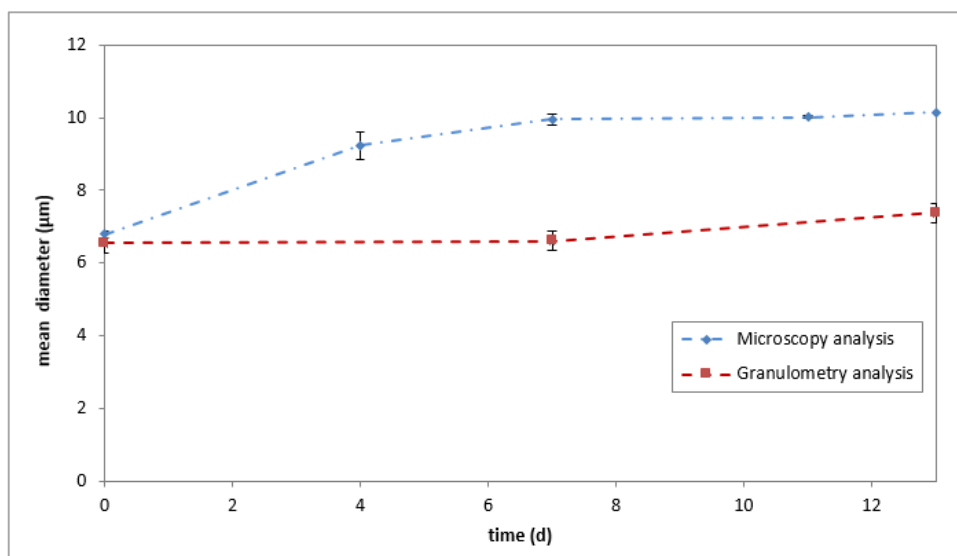


Figure 64: Evolution of the mean diameter over time for *Chlamydomonas reinhardtii* wt in stress conditions (estimation carried out with laser granulometry and manual optical measurements). The culture shown is another culture than the ones presented for lipid analysis.

The mean diameter of *Chlamydomonas reinhardtii* wild type in exponential phase is similar for both methods approximatively 6.5 - 6.8 µm. However, the mean cell diameter determined by microscopy significantly increases during stress, up to 10 µm after 7 days of stress while granulometry measurements only showed a very slight increase (from 6.5 to 7.4 µm).

Work et. al [101] reported an increase of the mean diameter from 5.9 ± 1 to 7.5 ± 1.1 for *Chlamydomonas reinhardtii* wild type after 4 days of stress (nitrogen depletion, $50 \mu\text{mol}\cdot\text{m}^{-2}\cdot\text{s}^{-1}$) which is in agreement with the results of manual measurements (Figure 64) although their values are slightly lower than the values presented in our study. The rise in cell diameter can be correlated with the increase of lipid content and the variation of the specific cell weight (Figure 52). From the data of cell weight during stress (Figure 51), we think that the lipid accumulation per cell can vary between the cultures depending on cell concentration. In addition, data on the cell diameter are of great importance when considering Pulsed Electric Fields that will be applied to *Chlamydomonas* cells in the next step of this work (see chapter 3).

Chapter 2 conclusion

In the first section of this chapter, the mechanisms of accumulation of neutral lipids in algae cells are presented. The conversion of inorganic carbon into organic compounds through photosynthesis is regulated by culture conditions. In the so called “optimal growth conditions”, *i.e.* optimal light irradiance and nutrient concentration, algae will mainly synthesize molecules to produce functional biomass and will divide at high rate.

A depletion of nitrogen in the medium combined with an increase of the photon flow rate will lead to a rapid decrease in the photosynthetic activity and cell division and a rapid increase in neutral lipid and/or starch contents in the majority of green microalgae strains. These carbon chains stored in the cytoplasm consist of an energy sink to be converted back into functional biomass as soon as the optimal conditions are reestablished.

In this context, a two steps strategy to induce neutral lipids accumulation in *Chlamydomonas reinhardtii* was used and seems to be efficient to obtain biomass rich in lipids.

A reduction of microalgae specific growth rate from 1.4 d^{-1} in growth conditions to a complete stop of cell division after approximately 4 days of stress.

Moreover, cell chlorophyll content, given by the auto-fluorescence intensity (flow cytometry), decreased by a factor of 50 to 100 during stress conditions compared with growth phase. The cell concentration rapidly reaches a maximum value within the range of $5 \cdot 10^6$ - $1 \cdot 10^7$ cells/mL after approximately 7 days of stress from a starting concentration of $3 \cdot 10^6$ cells/mL at the beginning of stress. Furthermore, an increase in cell diameter, estimated at $6\ \mu\text{m}$ at the beginning of stress conditions up to $10\ \mu\text{m}$ after 7 days was observed.

The volumetric dry weight increases from 0.3 to 1 g/L after 6-7 days of stress. The evolution of dry weight per cell followed a pattern inverse from the one of cell concentration. This result tends to indicate that a high photon rate per cell (a reduced cell concentration for a similar light irradiance of $100 - 150\ \mu\text{mol} \cdot \text{m}^{-2} \cdot \text{s}^{-1}$ results in a higher specific photon flow rate) increases cellular weight rise during stress because of an increased energy received per cell. In other ways, a reduced cell concentration may result in a higher neutral lipid content (and/or starch content) per cell. Anyway this behavior would have few impact on volumetric lipid productivity.

The evolution of the FA composition measured by GC-FID analysis as shown that the lipid content increases from 18 % to 35 % of the dry weight after 4 days of stress. The mass of polar lipids (membrane associated FA) tends to be stable at 14 % DW. However, the relative mass of neutral fatty acids (TAGs) increased from 5 to above 20 % DW after 4 days of stress, and then stabilizes. For polar FA, the relative abundance of poly-unsaturated FA (*e.g.* C16:4 and C18:3) decreases during stress for an increase abundance of C16:0 and C18:1 in the membranes. In neutral TAGs, the main FA found after 4 days of stress are C18:1, C16:0, C18:2 and C19:0.

From the results presented in this chapter, *Chlamydomonas reinhardtii* wt cells at maximum stress duration of 7 days should be used for lipid extraction as no increase in neutral lipid content is observed after this time.

In this chapter, the development and optimization of methods to quantify cell lipid content were also described. The choice of using fluorescent dyes detected by flow cytometry and a colorimetric method was justified by the fact of dealing with very low biomass volumes when performing electroporation assays in micro-systems or in electroporation cuvettes (few micro-liters to a maximum of one milliliter of algae solution) (see Chapter 3).

First, cell lipid contents in triolein equivalent determined by the SPV method (colorimetry) are in the same order of magnitude as those measured by the classical and commonly used GC-FID chromatography. Moreover, results confirm that lipid droplets accumulation in the cell can be detected by measuring the mean Bodipy fluorescence by flow cytometry. SPV and Bodipy staining methods are indeed fast and adapted to reduced biomass amounts and daily monitoring but more work is required to further correlate their data to those of GC-FID chromatography.

Bodipy can also be used for microscopic observations, performed here to detect lipid droplets in micro-systems. On the other hand, SVP method is correlated with unsaturated total FA content (neutral FA accumulated as TAGs + polar membrane associated FA) and thus is less adapted for total neutral lipid quantification. Still, results obtained with the SPV method seemed more reproducible than a method based on Bodipy fluorescence which can be influenced with many parameters.

Chapter 2 references

- [1] M.K. Lam, K.T. Lee, *Biofuels from Algae*, 2014. doi:10.1016/B978-0-444-59558-4.00012-7.
- [2] A. Darzins, P. Pienkos, L. Edye, Current status and potential for algal biofuels production., *Natl. Renew. Energy Lab. NREL A Rep. to Bioenergy Task 39. Report T39* (2010) 146. http://www.globalbioenergy.org/uploads/media/1008_IEA_Bioenergy_-_Current_status_and_potential_for_algal_biofuels_production.pdf.
- [3] a. E. Atabani, a. S. Silitonga, I.A. Badruddin, T.M.I. Mahlia, H.H. Masjuki, S. Mekhilef, A comprehensive review on biodiesel as an alternative energy resource and its characteristics, *Renew. Sustain. Energy Rev.* 16 (2012) 2070–2093. doi:10.1016/j.rser.2012.01.003.
- [4] X. Li, P. Přibyl, K. Bišová, S. Kawano, V. Cepák, V. Zachleder, M. Čížková, I. Brányíková, M. Vítová, The microalga *Parachlorella kessleri*—a novel highly efficient lipid producer., *Biotechnol. Bioeng.* 110 (2013) 97–107. doi:10.1002/bit.24595.
- [5] A. Klok, Optimization of lipid production in microalgae, n.d.
- [6] G. Breuer, P.P. Lamers, D.E. Martens, R.B. Draaisma, R.H. Wijffels, The impact of nitrogen starvation on the dynamics of triacylglycerol accumulation in nine microalgae strains., *Bioresour. Technol.* 124 (2012) 217–26. doi:10.1016/j.biortech.2012.08.003.
- [7] C. Safi, B. Zebib, O. Merah, P.-Y. Pontalier, C. Vaca-Garcia, Morphology, composition, production, processing and applications of *Chlorella vulgaris*: A review, *Renew. Sustain. Energy Rev.* 35 (2014) 265–278. doi:10.1016/j.rser.2014.04.007.
- [8] B. Becker, Function and Evolution of the Vacuolar Compartment in Green Algae and Land Plants (Viridiplantae), *Int. Rev. Cytol.* 264 (2007) 1–24. doi:10.1016/S0074-7696(07)64001-7.
- [9] P. Dupree, D.J. Sherrier, The plant Golgi apparatus, *Biochim. Biophys. Acta - Mol. Cell Res.* 1404 (1998) 259–270. doi:10.1016/S0167-4889(98)00061-5.
- [10] D.S. Domozych, M. Ciancia, J.U. Fangel, M.D. Mikkelsen, P. Ulvskov, W.G.T. Willats, The Cell Walls of Green Algae: A Journey through Evolution and Diversity., *Front. Plant Sci.* 3 (2012) 82. doi:10.3389/fpls.2012.00082.
- [11] E.H. Harris, *The Chlamydomonas Sourcebook. Volume 1, second edition.*, 2009.
- [12] C.D. Sifflow, P. a Lefebvre, Assembly and motility of eukaryotic cilia and flagella. Lessons from *Chlamydomonas reinhardtii*., *Plant Physiol.* 127 (2001) 1500–1507. doi:10.1104/pp.010807.
- [13] <http://www.athenapub.com/17Records-06.htm>.
- [14] E.R. Moellering, C. Benning, RNA interference silencing of a major lipid droplet protein affects lipid droplet size in *Chlamydomonas reinhardtii*, *Eukaryot. Cell.* 9 (2010) 97–106. doi:10.1128/EC.00203-09.
- [15] M. Vítová, K. Bišová, M. Hlavová, S. Kawano, V. Zachleder, M. Čížková, *Chlamydomonas reinhardtii*: duration of its cell cycle and phases at growth rates affected by temperature., *Planta.* 234 (2011) 599–608. doi:10.1007/s00425-011-1427-7.
- [16] F.R. Cross, J.G. Umen, The *Chlamydomonas* cell cycle, *Plant J.* 82 (2015) 370–392. doi:10.1111/tpj.12795.
- [17] <https://en.wikipedia.org/wiki/Mitochondrion>.
- [18] <https://en.wikipedia.org/wiki/Chloroplast>.
- [19] Raven, *Photosynthesis*, *Biol. Plants.* (2013) 183–204.
- [20] K.J.M. Mulders, P.P. Lamers, D.E. Martens, R.H. Wijffels, Phototrophic pigment production with microalgae: Biological constraints and opportunities, *J. Phycol.* 50 (2014) 229–242. doi:10.1111/jpy.12173.
- [21] J.F. Cornet, Calculation of optimal design and ideal productivities of volumetrically lightened photobioreactors using the constructal approach, *Chem. Eng. Sci.* 65 (2010) 985–998. doi:10.1016/j.ces.2009.09.052.
- [22] F. Ramel, S. Birtic, S. Cuiné, C. Triantaphylidès, J.-L. Ravanat, M. Havaux, Chemical quenching of singlet oxygen by carotenoids in plants., *Plant Physiol.* 158 (2012) 1267–78. doi:10.1104/pp.111.182394.
- [23] Y. Li, D. Han, G. Hu, M. Sommerfeld, Q. Hu, Inhibition of starch synthesis results in overproduction of lipids in *Chlamydomonas reinhardtii*, *Biotechnol. Bioeng.* 107 (2010) 258–268. doi:10.1002/bit.22807.
- [24] R. Radakovits, R.E. Jinkerson, A. Darzins, M.C. Posewitz, Genetic engineering of algae for enhanced biofuel production, *Eukaryot. Cell.* 9 (2010) 486–501. doi:10.1128/EC.00364-09.
- [25] <http://lipidlibrary.aocs.org/Biochemistry/content.cfm?ItemNumber=40313>.
- [26] Q. Hu, M. Sommerfeld, E. Jarvis, M. Ghirardi, M. Posewitz, M. Seibert, A. Darzins, Microalgal triacylglycerols as feedstocks for biofuel production: perspectives and advances., *Plant J.* 54 (2008) 621–39. doi:10.1111/j.1365-313X.2008.03492.x.
- [27] A. Cagliari, R. Margis, F. dos S. Maraschin, A.C. Turchetto-Zolet, G. Loss, M. Margis-Pinheiro, Biosynthesis of Triacylglycerols (TAGs) in plants and algae, *Int. J. Plant Biol.* 2 (2011) e10. doi:10.4081/pb.2011.e10.
- [28] V.H. Work, R. Radakovits, R.E. Jinkerson, J.E. Meuser, L.G. Elliott, D.J. Vinyard, L.M.L. Laurens, G.C. Dismukes, M.C. Posewitz, Increased lipid accumulation in the *Chlamydomonas reinhardtii* sta7-10 starchless isoamylase mutant and increased carbohydrate synthesis in complemented strains., *Eukaryot. Cell.* 9 (2010) 1251–61. doi:10.1128/EC.00075-10.
- [29] M. Kumar, C.R.K. Reddy, C. Salt, M. Che, <Functional ingredients from algae for foods and nutraceuticals-Woodhead Publishing-Book 2013.pdf>, 2013. doi:10.1533/9780857098689.
- [30] V.M. Dembitsky, O. a Rozentsvet, Distribution of polar lipids in some marine, brackish and freshwater green macrophytes, *Phytochemistry.* 41 (1996) 483–488. doi:10.1016/0031-9422(95)00570-6.
- [31] M. Siaut, S. Cuiné, C. Cagnon, B. Fessler, M. Nguyen, P. Carrier, A. Beyly, F. Beisson, C. Triantaphylidès, Y. Li-Beisson, G. Peltier, Oil accumulation in the model green alga *Chlamydomonas reinhardtii*: characterization, variability between common laboratory strains and relationship with starch reserves., *BMC Biotechnol.* 11 (2011) 7. doi:10.1186/1472-6750-11-7.
- [32] S.D. Doughman, S. Krupanidhi, C.B. Sanjeevi, Omega-3 fatty acids for nutrition and medicine: considering microalgae oil as a vegetarian source of EPA and DHA., *Curr. Diabetes Rev.* 3 (2007) 198–203. doi:10.2174/157339907781368968.
- [33] M.J. Ramos, C.M. Fern??ndez, A. Casas, L. Rodr??guez, ??ngel P??rez, Influence of fatty acid composition of raw materials on biodiesel properties, *Bioresour. Technol.* 100 (2009) 261–268. doi:10.1016/j.biortech.2008.06.039.
- [34] Y. Li-Beisson, F. Beisson, W. Riekhof, Metabolism of acyl-lipids in *Chlamydomonas reinhardtii*, *Plant J.* 82 (2015) 504–522. doi:10.1111/tpj.12787.
- [35] K.K. Sharma, H. Schuhmann, P.M. Schenk, High Lipid Induction in Microalgae for Biodiesel Production, *Energies.* 5 (2012) 1532–1553. doi:10.3390/en5051532.

- [36] A.J. Klok, J. a Verbaanderd, P.P. Lamers, D.E. Martens, A. Rinzema, R.H. Wijffels, A model for customising biomass composition in continuous microalgae production., *Bioresour. Technol.* 146 (2013) 89–100. doi:10.1016/j.biortech.2013.07.039.
- [37] A. Packer, Y. Li, T. Andersen, Q. Hu, Y. Kuang, M. Sommerfeld, Growth and neutral lipid synthesis in green microalgae: A mathematical model, *Bioresour. Technol.* 102 (2011) 111–117. doi:10.1016/j.biortech.2010.06.029.
- [38] T. Takeshita, S. Ota, T. Yamazaki, A. Hirata, V. Zachleder, S. Kawano, Starch and lipid accumulation in eight strains of six *Chlorella* species under comparatively high light intensity and aeration culture conditions, *Bioresour. Technol.* 158 (2014) 127–134. doi:10.1016/j.biortech.2014.01.135.
- [39] B. Fernandes, J. Teixeira, G. Dragone, A. a Vicente, S. Kawano, K. Bišová, P. Příbyl, V. Zachleder, M. Vítová, Relationship between starch and lipid accumulation induced by nutrient depletion and replenishment in the microalga *Parachlorella kessleri*., *Bioresour. Technol.* 144 (2013) 268–74. doi:10.1016/j.biortech.2013.06.096.
- [40] Z. Kolber, J. Zehr, P. Falkowski, Effects of Growth Irradiance and Nitrogen Limitation on Photosynthetic Energy Conversion in Photosystem II., *Plant Physiol.* 88 (1988) 923–929. doi:10.1104/pp.88.3.923.
- [41] R. Praveenkumar, K. Shameera, G. Mahalakshmi, M.A. Akbarsha, N. Thajuddin, Influence of nutrient deprivations on lipid accumulation in a dominant indigenous microalga *Chlorella* sp., BUM11008: Evaluation for biodiesel production, *Biomass and Bioenergy.* 37 (2012) 60–66. doi:10.1016/j.biombioe.2011.12.035.
- [42] G. Breuer, P.P. Lamers, D.E. Martens, R.B. Draaisma, R.H. Wijffels, Effect of light intensity, pH, and temperature on triacylglycerol (TAG) accumulation induced by nitrogen starvation in *Scenedesmus obliquus*., *Bioresour. Technol.* 143 (2013) 1–9. doi:10.1016/j.biortech.2013.05.105.
- [43] G. Mujtaba, W. Choi, C.-G. Lee, K. Lee, Lipid production by *Chlorella vulgaris* after a shift from nutrient-rich to nitrogen starvation conditions., *Bioresour. Technol.* 123 (2012) 279–83. doi:10.1016/j.biortech.2012.07.057.
- [44] V. Ördög, W. a. Stirk, P. Bálint, J. Staden, C. Lovász, Changes in lipid, protein and pigment concentrations in nitrogen-stressed *Chlorella minutissima* cultures, *J. Appl. Phycol.* 24 (2011) 907–914. doi:10.1007/s10811-011-9711-2.
- [45] M.J. Griffiths, R.P. van Hille, S.T.L. Harrison, The effect of nitrogen limitation on lipid productivity and cell composition in *Chlorella vulgaris*., *Appl. Microbiol. Biotechnol.* 98 (2014) 2345–56. doi:10.1007/s00253-013-5442-4.
- [46] P. Zhao, X. Yu, J. Li, X. Tang, Z. Huang, Enhancing lipid productivity by co-cultivation of *Chlorella* sp. U4341 and *Monoraphidium* sp. FXY-10., *J. Biosci. Bioeng.* xx (2014) 10–15. doi:10.1016/j.jbiosc.2013.12.014.
- [47] P.S.C. Schulze, L.A. Barreira, H.G.C. Pereira, J.A. Perales, J.C.S. Varela, Light emitting diodes (LEDs) applied to microalgal production, *Trends Biotechnol.* 32 (2014) 422–430. doi:10.1016/j.tibtech.2014.06.001.
- [48] J.-M. Lv, L.-H. Cheng, X.-H. Xu, L. Zhang, H.-L. Chen, Enhanced lipid production of *Chlorella vulgaris* by adjustment of cultivation conditions., *Bioresour. Technol.* 101 (2010) 6797–804. doi:10.1016/j.biortech.2010.03.120.
- [49] T. Takeshita, Competitiveness, role, and impact of microalgal biodiesel in the global energy future, *Appl. Energy.* 88 (2011) 3481–3491. doi:10.1016/j.apenergy.2011.02.009.
- [50] <http://www.hemocytometer.org/2013/04/11/hemocytometer-square-size/>.
- [51] <http://bitesizebio.com/13687/cell-counting-with-a-hemocytometer-easy-as-1-2-3/>.
- [52] C.E. Seed, I. Larma, J.L. Tomkins, Cell size selection in *Chlamydomonas reinhardtii* gametes using fluorescence activated cell sorting, *Algal Res.* 16 (2016) 93–101. doi:10.1016/j.algal.2016.03.004.
- [53] No Title, (n.d.). <http://nikitavsurpatne.yolasite.com/optics.php>.
- [54] E.G. BLIGH, W.J. DVER, *Canadian Journal of Biochemistry and Physiology*, 37 (1959).
- [55] J. Folch, M. Lees, G. Sloane Stanley, a Simple, 55 (1987) 999–1033.
- [56] R. Halim, M.K. Danquah, P. a Webley, Extraction of oil from microalgae for biodiesel production: A review., *Biotechnol. Adv.* 30 (2012) 709–32. doi:10.1016/j.biotechadv.2012.01.001.
- [57] A.R. Medina, E.M. Grima, A.G. Gimenez, M.J.I. Gonzalez, Downstream processing of algal polyunsaturated fatty acids, *Biotechnol. Adv.* 16 (1998) 517–580. doi:10.1016/S0734-9750(97)00083-9.
- [58] E. Ryckebosch, K. Muylaert, I. Foubert, Optimization of an Analytical Procedure for Extraction of Lipids from Microalgae, *J. Am. Oil Chem. Soc.* 89 (2011) 189–198. doi:10.1007/s11746-011-1903-z.
- [59] M. Axelsson, F. Gentili, A single-step method for rapid extraction of total lipids from green microalgae., *PLoS One.* 9 (2014) e89643. doi:10.1371/journal.pone.0089643.
- [60] G. Breuer, W.A.C. Evers, J.H. de Vree, D.M.M. Kleinegris, D.E. Martens, R.H. Wijffels, P.P. Lamers, Analysis of Fatty Acid Content and Composition in Microalgae, *J. Vis. Exp.* 80 (2013) e50628. doi:10.3791/50628.
- [61] B.H.J. Yap, S. a Crawford, G.J. Dumsday, P.J. Scales, G.J.O. Martin, A mechanistic study of algal cell disruption and its effect on lipid recovery by solvent extraction, *Algal Res.* 5 (2014) 112–120. doi:10.1016/j.algal.2014.07.001.
- [62] J.Y. Lee, C. Yoo, S.Y. Jun, C.Y. Ahn, H.M. Oh, Comparison of several methods for effective lipid extraction from microalgae, *Bioresour. Technol.* 101 (2010) 575–7. doi:10.1016/j.biortech.2009.03.058.
- [63] P. Mercer, R.E. Armenta, Developments in oil extraction from microalgae, *Eur. J. Lipid Sci. Technol.* 113 (2011) 539–547. doi:10.1002/ejlt.201000455.
- [64] B. Serive, R. Kaas, J.-B. Bérard, V. Pasquet, L. Picot, J.-P. Cadoret, Selection and optimisation of a method for efficient metabolites extraction from microalgae., *Bioresour. Technol.* 124 (2012) 311–20. doi:10.1016/j.biortech.2012.07.105.
- [65] G.S. Alemán-Nava, S.P. Cuellar-Bermudez, M. Cuaresma, R. Bosma, K. Muylaert, B.E. Ritmann, R. Parra, How to us Nile Red, a selective fluorescent stain for microalgal neutral lipids, *J. Microbiol. Methods.* 128 (2016) 74–79. doi:10.1016/j.mimet.2016.07.011.
- [66] No Title, (n.d.). <https://www.thermofisher.com/fr/fr/home/life-science/protein-biology/protein-biology-learning-center/protein-biology-resource-library/pierce-protein-methods/fluorescent-probes.html>.
- [67] P. Greenspan, S.D. Fowler, Spectrofluorometric studies of the lipid probe, Nile Red., *J. Lipid Res.* 26 (1985) 781–789.
- [68] <http://www.google.com.na/patents/WO2003090604A2?cl=en>.
- [69] J. Rumin, H. Bonnefond, B. Saint-Jean, C. Rouxel, A. Sciandra, O. Bernard, J.-P. Cadoret, G. Bougaran, The use of fluorescent Nile red and BODIPY for lipid measurement in microalgae, *Biotechnol. Biofuels.* 8 (2015) 42. doi:10.1186/s13068-015-0220-4.
- [70] <https://www.thermofisher.com/order/catalog/product/N1142>.
- [71] A. De la Jara, A. Martel, C. Molina, L. Nordström, V. De la Rosa, R. Díaz, Flow cytometric determination of lipid content in a marine dinoflagellate, *J. Appl. Phycol.* (2003) 433–438.
- [72] H. Mendoza Guzmán, A. de la Jara Valido, K. Freijanes Presmanes, L. Carmona Duarte, Quick estimation of intraspecific variation of fatty acid composition in *Dunaliella salina* using flow cytometry and Nile Red, *J. Appl. Phycol.* 24 (2012) 1237–1243. doi:10.1007/s10811-011-9768-y.

- [73] T. Govender, L. Ramanna, I. Rawat, F. Bux, BODIPY staining, an alternative to the Nile Red fluorescence method for the evaluation of intracellular lipids in microalgae., *Bioresour. Technol.* 114 (2012) 507–11. doi:10.1016/j.biortech.2012.03.024.
- [74] N. Velmurugan, M. Sung, S.S. Yim, M.S. Park, J.W. Yang, K.J. Jeong, Evaluation of intracellular lipid bodies in *Chlamydomonas reinhardtii* strains by flow cytometry., *Bioresour. Technol.* 138 (2013) 30–7. doi:10.1016/j.biortech.2013.03.078.
- [75] P. Hyka, S. Lickova, P. Přibyl, K. Melzoch, K. Kovar, Flow cytometry for the development of biotechnological processes with microalgae., *Biotechnol. Adv.* 31 (2012) 2–16. doi:10.1016/j.biotechadv.2012.04.007.
- [76] J. Rumin, H. Bonnefond, B. Saint-Jean, C. Rouxel, A. Sciandra, O. Bernard, J.-P. Cadoret, G. Bougaran, The use of fluorescent Nile red and BODIPY for lipid measurement in microalgae., *Biotechnol. Biofuels.* 8 (2015) 42. doi:10.1186/s13068-015-0220-4.
- [77] G.D. Feng, F. Zhang, L.H. Cheng, X.H. Xu, L. Zhang, H.L. Chen, Evaluation of FT-IR and Nile Red methods for microalgal lipid characterization and biomass composition determination, *Bioresour. Technol.* 128 (2013) 107–112. doi:10.1016/j.biortech.2012.09.123.
- [78] D.M. Wong, A.K. Franz, A comparison of lipid storage in *Phaeodactylum tricornutum* and *Tetraselmis suecica* using laser scanning confocal microscopy., *J. Microbiol. Methods.* 95 (2013) 122–8. doi:10.1016/j.mimet.2013.07.026.
- [79] Y. Liang, K. Osada, Y. Sunaga, T. Yoshino, C. Bowler, T. Tanaka, Dynamic oil body generation in the marine oleaginous diatom *Fistulifera solaris* in response to nutrient limitation as revealed by morphological and lipidomic analysis, *Algal Res.* 12 (2015) 359–367. doi:10.1016/j.algal.2015.09.017.
- [80] D. Xu, Z. Gao, F. Li, X. Fan, X. Zhang, N. Ye, S. Mou, C. Liang, D. Li, Detection and quantitation of lipid in the microalga *Tetraselmis subcordiformis* (Wille) Butcher with BODIPY 505/515 staining., *Bioresour. Technol.* 127 (2013) 386–90. doi:10.1016/j.biortech.2012.09.068.
- [81] G.T. Vatassery, M.A. Sheridan, A.M. Krezowski, A.S. Divine, H.L. Bach, Use of the sulfo-phospho-vanillin reaction in a routine method for determining total lipids in human cerebrospinal fluid, *Clin. Biochem.* 14 (1981) 21–24. doi:10.1016/0009-9120(81)90120-X.
- [82] K.R. Johnson, G. Ellis, C. Toothill, The sulfophosphovanillin reaction for serum lipids: a reappraisal, *Clin. Chem.* 23 (1977) 1669–1678.
- [83] Y.S. Cheng, Y. Zheng, J.S. VanderGheynst, Rapid quantitative analysis of lipids using a colorimetric method in a microplate format, *Lipids.* 46 (2011) 95–103. doi:10.1007/s11745-010-3494-0.
- [84] S.K. Mishra, W.I. Suh, W. Farooq, M. Moon, A. Shrivastav, M.S. Park, J.W. Yang, Rapid quantification of microalgal lipids in aqueous medium by a simple colorimetric method, *Bioresour. Technol.* 155 (2014) 330–333. doi:10.1016/j.biortech.2013.12.077.
- [85] J.A. Knight, S. Anderson, J.M. Rawle, Chemical basis of the sulfo-phospho-vanillin reaction for estimating total serum lipids, *Clin Chem.* 18 (1972) 199–202. http://www.ncbi.nlm.nih.gov/entrez/query.fcgi?cmd=Retrieve&db=PubMed&dopt=Citation&list_uids=5020813.
- [86] TAP Medium, <http://www.chlamy.org/TAP.html>. (n.d.).
- [87] T. De Mooij, M. Janssen, O. Cerezo-Chinarro, J.H. Mussgnug, O. Kruse, M. Ballottari, R. Bassi, S. Bujaldon, F.A. Wollman, R.H. Wijffels, Antenna size reduction as a strategy to increase biomass productivity: a great potential not yet realized, *J. Appl. Phycol.* (2014) 1063–1077. doi:10.1007/s10811-014-0427-y.
- [88] Z. Perrine, S. Negi, R.T. Sayre, Optimization of photosynthetic light energy utilization by microalgae, *Algal Res.* 1 (2012) 134–142. doi:10.1016/j.algal.2012.07.002.
- [89] H.C. Ishikawa-Ankerhold, R. Ankerhold, G.P.C. Drummen, Advanced fluorescence microscopy techniques-FRAP, FLIP, FLAP, FRET and FLIM, *Molecules.* 17 (2012) 4047–4132. doi:10.3390/molecules17044047.
- [90] L.F. Hernandez and J.H. Palmer, Fluorescence staining of primary plant cell wall using Bizbenzimidazole (33258 Hoechst) Fluorochrome, (1988).
- [91] C. Safi, A.V. Ursu, C. Laroche, B. Zebib, O. Merah, P.-Y. Pontalier, C. Vaca-Garcia, Aqueous extraction of proteins from microalgae: Effect of different cell disruption methods, *Algal Res.* 3 (2014) 61–65. doi:10.1016/j.algal.2013.12.004.
- [92] I. Pouneva, EVALUATION OF ALGAL CULTURE VIABILITY AND PHYSIOLOGICAL STATE BY FLUORESCENT MICROSCOPIC METHODS, 23 (1997) 67–76.
- [93] H. Ehrlich, O. V Kaluzhnaya, E. Brunner, M. V Tsurkan, A. Ereskovsky, M. Ilan, K.R. Tabachnick, V. V Bazhenov, S. Paasch, M. Kammer, R. Born, A. Stelling, R. Galli, S. Belikov, O. V Petrova, V. V Sivkov, D. Vyalikh, S. Hunoldt, G. Wörheide, Identification and first insights into the structure and biosynthesis of chitin from the freshwater sponge *Spongilla lacustris*., *J. Struct. Biol.* 183 (2013) 474–83. doi:10.1016/j.jsb.2013.06.015.
- [94] M.N. Stagoj, R. Komel, A. Comino, Microtiter plate assay of yeast cell number using the fluorescent dye calcofluor white M2R., *Biotechniques.* 36 (2004) 380–2. <http://www.ncbi.nlm.nih.gov/pubmed/15038150>.
- [95] K. a Henderson, A.L. Hughes, D.E. Gottschling, Mother-daughter asymmetry of pH underlies aging and rejuvenation in yeast., *Elife.* (2014) e03504. doi:10.7554/eLife.03504.
- [96] R.J. Doyle, D.C. Birdsell, Interaction of concanavalin A with the cell wall of *Bacillus subtilis*., *J. Bacteriol.* 109 (1972) 652–658.
- [97] J.S. Tkacz, E.B. Cybulska, J.O. Lampen, Specific staining of wall mannan in yeast cells with fluorescein-conjugated concanavalin A., *J. Bacteriol.* 105 (1971) 1–5.
- [98] B. Fontaniella, A.M. Millanes, C. Vicente, M.E. Legaz, Concanavalin A binds to a mannose-containing ligand in the cell wall of some lichen phycobionts, *Plant Physiol. Biochem.* 42 (2004) 773–779. doi:10.1016/j.plaphy.2004.09.003.
- [99] L. Ex, Concanavalin A Conjugates | 2 Before You Begin, *Biochem. Proc Nat Acad Sci.* 32 (1993) 1–3.
- [100] K.J.M. Mulders, J.H. Janssen, D.E. Martens, R.H. Wijffels, P.P. Lamers, Effect of biomass concentration on secondary carotenoids and triacylglycerol (TAG) accumulation in nitrogen-depleted *Chlorella zofingiensis*, *Algal Res.* 6 (2014) 8–16. doi:10.1016/j.algal.2014.08.006.
- [101] V.H. Work, R. Radakovits, R.E. Jinkerson, J.E. Meuser, L.G. Elliott, D.J. Vinyard, L.M.L. Laurens, G.C. Dismukes, M.C. Posewitz, Increased lipid accumulation in the *Chlamydomonas reinhardtii* sta7-10 starchless isoamylase mutant and increased carbohydrate synthesis in complemented strains., *Eukaryot. Cell.* 9 (2010) 1251–61. doi:10.1128/EC.00075-10.
- [102] T.H. Lee, J.S. Chang, H.Y. Wang, Current developments in high-throughput analysis for microalgae cellular contents, *Biotechnol. J.* 8 (2013) 1301–1314. doi:10.1002/biot.201200391.
- [103] O. Samek, Z. Pilát, J. Ježek, M. Šerý, S. Bernatová, P. Zemánek, L. Nedbal, M. Trtílek, Raman microspectroscopy monitoring of lipids in algal cells, 8651 (2011) 8651. doi:10.1364/FIO.2011.FTuA6.
- [104] G.O. James, C.H. Hocart, W. Hillier, H. Chen, F. Kordbacheh, G.D. Price, M.A. Djordjevic, Fatty acid profiling of *Chlamydomonas reinhardtii* under nitrogen deprivation, *Bioresour. Technol.* 102 (2011) 3343–3351. doi:10.1016/j.biortech.2010.11.051.
- [105] A.P. Dean, D.C. Sigeo, B. Estrada, J.K. Pittman, Using FTIR spectroscopy for rapid determination of lipid accumulation in response

Chapter 2: *Inducing lipid accumulation in green microalgae and developing characterization methods*

- to nitrogen limitation in freshwater microalgae, *Bioresour. Technol.* 101 (2010) 4499–4507. doi:10.1016/j.biortech.2010.01.065.
- [106] B. Fuchs, R. S????, K. Teuber, M. Eibisch, J. Schiller, Lipid analysis by thin-layer chromatography-A review of the current state, *J. Chromatogr. A.* 1218 (2011) 2754–2774. doi:10.1016/j.chroma.2010.11.066.
- [107] K.J. Choi, Z. Nakhost, E. Barzana, M. Karel, Lipid content and fatty acid composition of green algae *Scenedesmus obliquus* grown in a constant cell density apparatus., *Food Biotechnol.* 1 (1987) 117–128. doi:10.1080/08905438709549660.
- [108] E. Lee, R.L. Heng, L. Pilon, Spectral optical properties of selected photosynthetic microalgae producing biofuels, *J. Quant. Spectrosc. Radiat. Transf.* 114 (2013) 122–135. doi:10.1016/j.jqsrt.2012.08.012.

III. Appendix II.1: Lipid production strategies in literature

Table 5: Average productivities and the highest observed productivities between two consecutive time points of biomass, total fatty acids, as well as the average TAG productivity for nitrogen-sufficient (N+) and deficient (N-) cultures [6].

Species	Volumetric biomass productivity (mg.l ⁻¹ .day ⁻¹)		Volumetric fatty acid productivity (mg.l ⁻¹ .day ⁻¹)		Average volumetric TAG productivity (mg.l ⁻¹ .day ⁻¹)
	Average	Max	Average	Max	
<i>C. vulgaris</i> N-	217	489	130	173	134
<i>C. vulgaris</i> N+	668	771	77	91	1
<i>C. zofingiensis</i> N-	508	674	251	301	242
<i>C. zofingiensis</i> N+	792	973	80	97	3
<i>D. tertiolecta</i> N-	341	680	38	46	22
<i>D. tertiolecta</i> N+	487	503	56	61	0
<i>I. galbana</i> N-	149	276	65	76	26
<i>I. galbana</i> N+	401	620	56	67	1
<i>N. oleabundans</i> N-	426	799	202	265	216
<i>N. oleabundans</i> N+	451	776	62	122	15
<i>Nannochloris</i> sp N+	264	340	36	40	15
<i>Nannochloris</i> sp N+	524	776	46	56	2
<i>P. cruentum</i> N-	308	679	38	58	8
<i>P. cruentum</i> N+	679	710	35	37	21
<i>P. tricomutum</i> N-	122	413	51	109	45
<i>P. tricomutum</i> N+	486	530	64	73	11
<i>S. obliquus</i> N-	719	822	360	498	323
<i>S. obliquus</i> N+	767	883	68	73	6

Table 6: Biomass, lipid and starch productivity in eight strains of six *Chlorella* species. Biomass and lipid productivity were measured after 5 days of sulfur deprivation, maximum starch productivities indicated were measured after 4 or 5 days [38].

Strain	Biomass		Lipid		Starch	
	Final g/L	g/L/day	Final g/L	g/L/day	Final g/L	g/L/day
<i>C. viscosa</i>	2.9	0.57	0.42	0.081	0.170	0.034
<i>C. vulgaris</i>	2.8	0.55	1.50	0.290	0.277	0.069
<i>C. sorokiniana</i>	2.9	0.57	0.21	0.039	0.471	0.094
<i>C. emersonii</i>	5.4	1.00	1.30	0.230	0.699	0.180
<i>P. beijerinckii</i>	4.6	0.87	1.00	0.190	0.326	0.065
<i>P. kessleri</i> CCALA 255	3.4	0.61	1.10	0.200	0.405	0.100
<i>P. kessleri</i> NIES-2159	5.6	1.00	1.20	0.210	0.662	0.170
<i>P. kessleri</i> NIES-2152	4.9	0.93	1.70	0.330	0.875	0.220

Table 7: Comparisons of biomass and lipid productivities between growth-associated lipid production and two-stage production [43]

	Growth-associated production (stage-I)		Two-stage production (stage I + stage II)	
	Without N-feeding	With N-feeding	12-h PCI	24-h PCI
Biomass concentration (g/L)	1.28	1.87	1.9	1.6
Time (d)	10	10	10.5	11
Biomass productivity (g/L/d)	0.128	0.187	0.181	0.145
Final lipid content (%)	24.6	15.5	43.0	53.0
Lipid productivity (mg/L/d)	31.5	29.0	77.8	77.1

Table 8: Time of nitrogen exhaustion in the medium, maximum specific growth rate (μ_{max}), maximum biomass productivity, and maximum instantaneous lipid productivity of *C. vulgaris* batch cultures at different starting nitrate concentrations [45]

Initial nitrate concentration (mg·L ⁻¹)	N exhaustion (days from inoculation)	μ_{max} (day ⁻¹)	Maximum biomass productivity (g·L ⁻¹ ·day ⁻¹)	Maximum lipid productivity (mg·L ⁻¹ ·day ⁻¹)
0	0	0.4	0.016	3
40	1.2	1.5	0.149	30
70	1.7	1.5	0.200	48
100	2.0	1.5	0.265	53
170	2.2	1.4	0.326	57
420	4.9	1.4	0.335	55
570	8.6	1.4	0.352	48
1,200	19.7	1.3	0.366	29
2,000	-	1.1	0.373	31

II.2. Appendix II.2: Quantification of unsaturated fatty acids using the colorimetric Sulphophosphovanillin (SPV) method

Principle

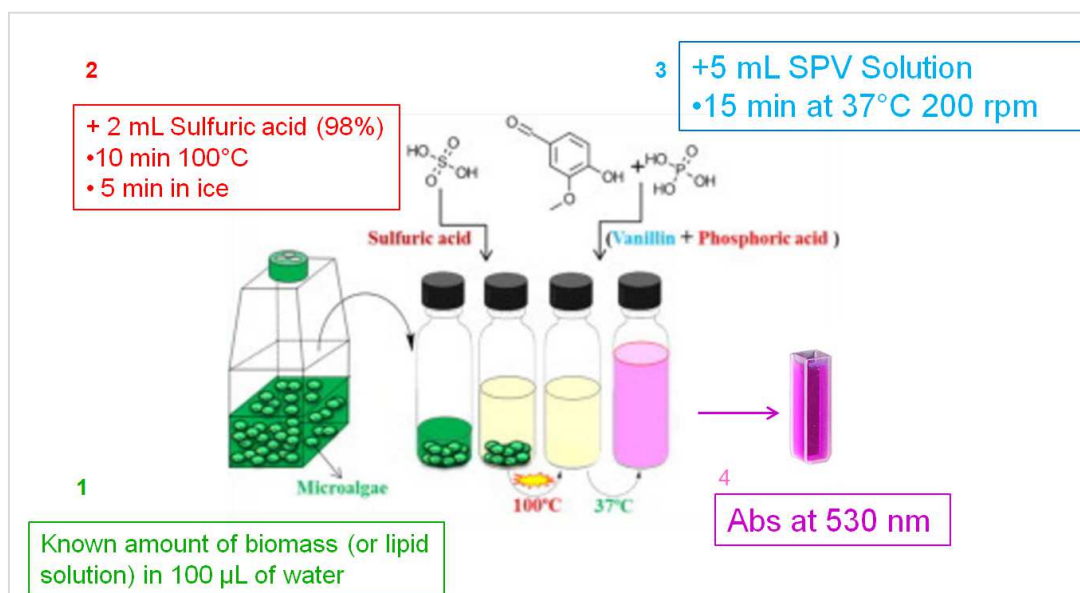


Figure 65: Principle of the method [84]

Material

Vanilin 99% (ref: 10387020)	0.6 g
Absolute ethanol	10 ml
Deionized water	(-) ml
Distilled water	(-) ml
Orthophosphoric acid 85% (ref: 10102060)	400 mL
Glycerine trioleate 99% (ref: 10190612)	20 mg
Chlorophorm	10 ml
Sulfuric Acid (98%)	2 ml (per sample)
100 °C Heater	x1
37°C, 200 Rpm incubator	x1
Glass cuvettes for spectro	x1
glass tubes + caps (15 mL min)	x9
Ice	(-)
Vanilin solution	5 ml (per sample)
-20 °C freezer	X1
37°C, 200 rpm incubator	X1

Preparation of SPV Solution

- Dissolve 0.6 g of vanilin in 10 ml absolute ethanol
- add 90 ml of deionized water
- add 400 ml of concentrated phosphoric acid
- store the 500 mL bottle in the dark before use
- **Fresh SPV solution needs to be prepare before use**

Calibration curve (Triolein in chlorophorm)

- Dissolve 20 mg of triolein in 10 mL of chloroform (2 mg/ml)
- store at -20°C before use
- Add different quantities of triolein in glass tubes:

Lip qty (µg)	0	10	20	30	40	50	60	70
Triolein sol (µl)	0	5	10	15	20	25	30	35

- Evaporate the chloroform at 60°C during 10 minutes
- In each tube, add 100 µl of distilled water
- In each tube, add 2 mL of concentrated sulfuric acid (98%)
- Heat at 100°C during 10 min
- Cool the tubes in ice during 5 min
- add 5 mL of SPV solution (**caution, solution becomes very hot after mixing**)
- incubate the tubes at 37°C, 200 rpm during 15 min
- transfer the content in glass absorbance cuvettes
- read the absorbance at 530 nm. Dilute if needed with the blank solution (0 µg lipid).



Figure 66: Tube heater (WTW CR3200) and ice cooling



Figure 67: Mixing device (ELMI Intelli-Mixer, Mode 60, 99 Rpm) in a oven at 37°.

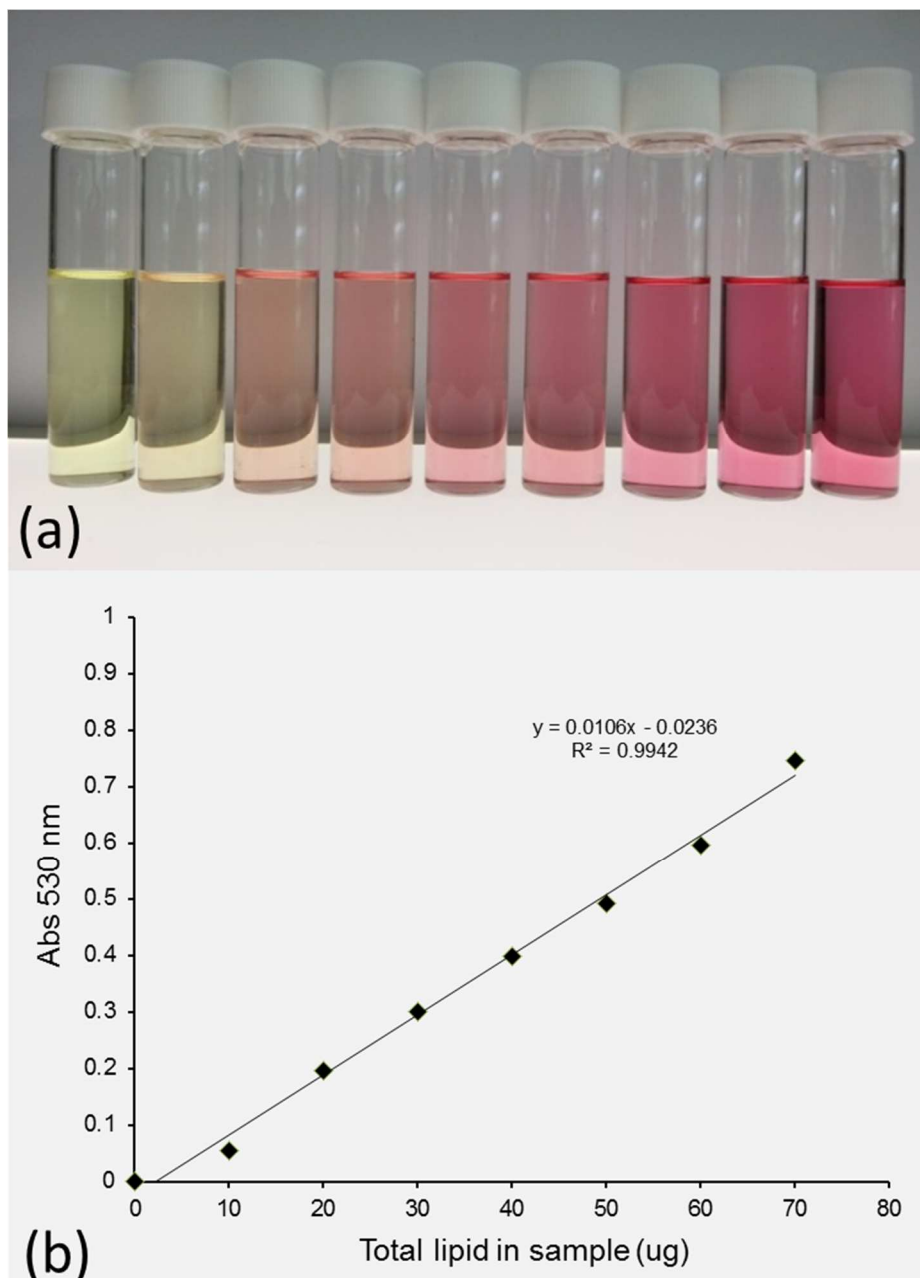


Figure 68: (a) From the left to right, the color change with the increasing concentration of lipid (Canola Oil) and (b) the corresponding linear relationship of absorption enhancement at 530 nm against lipid quantity in the sample (canola oil in the picture from [84])

II.3. Appendix II.3: Additional lipid estimation methods

Raman spectroscopy for analyzing microalgae content is a recent option in development which could have been used in this project. Raman spectroscopy is based on the Raman effect in which a photon emitted at a very specific wavelength of the visible light interacts with a molecule at a ground excited state. Light can be scattered in two ways: elastically (Rayleigh scattering) or inelastically (Raman scattering). Only one in a million of photons will be Raman scattered. A photon excites the molecule and result in a rovibronic state that is a different rotational or vibrational state than the one in which the molecule was originally. The energy of the inelastically scattered photons can either be shifted slightly higher or slightly lower than that of the incident photon. This induce a shift in the wavelength of the photon. This shift of a reduced frequency is designated as a Stokes shift (or anti Stokes shift when the energy is increased). Raman spectrometry detects the emitted lights from light excited molecules and assimilate each distinct mode of vibration with a specific molecular structure [102]. Exposition of a 785 nm laser beam to an isolated cell can enable to detect the volume of a lipid body thanks to the excitation of the β -carotene contained in lipid bodies [103].

Fourier transform infrared spectroscopy (FTIR) is an absorption spectroscopy technique where mid-infrared light is passed through the sample. The difference with Raman is there is no peaks corresponding with molecules oscillated but dips, showing the resonant absorption at various wavelengths and take into account Rayleigh scattering (change in dipole moment). FITR spectroscopy was efficiently used to estimate lipid accumulation in *Chlamydomonas reinhardtii* during nitrogen deprivation [104,105].

Thin-layer chromatography (TLC) for the quantification of lipids from algae is also possible [106]. Choi *et al.* used thin layer chromatography to analyze the lipids of *Scenedesmus obliquus* [107] on plates pre-coated with 0.25 or 0.5 mm layer of silica gel. They used a solvent system of petroleum ether-ethyl ether-acetic acid (80:20:1, v/v) for the neutral lipid fraction. Chloroform-methanol-acetic acid-water (70:30:20:7, v/v) was used for glycolipid and phospholipid fractions. Lipids were identified by comparing R_f values with literature, pure standards of by using specific spray reagents. Thin layer chromatogram of neutral lipids is presented Figure 69.

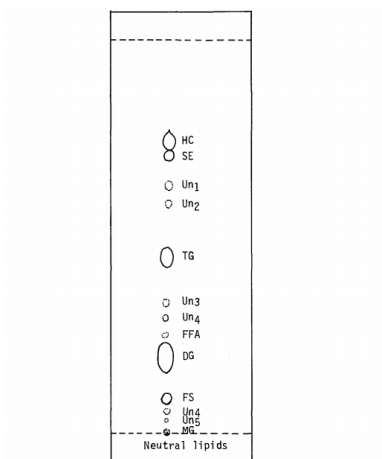


Figure 69: Thin layer chromatogram of neutral lipids of *Scenedesmus obliquus*. The spots of neutral lipid fraction were as follow: HC: Hydrocarbons, SE: Sterol esters, TG: Triglycerides, FFA: Free fatty acids, DG: Diglycerides, FS: Free sterols, MG: Monoglycerides, Un1-Un5: Unidentified components.

II.4. Appendix II.4: Principle of laser granulometry

Laser granulometry is based on dynamic light scattering where two lasers (blue: 470 nm and red: 633 nm) are used to illuminate a sample (particles flowed in the laser beam) illustrated figure 51. The two laser beams are scattered in multiple directions and multiple angles. This repartition of diffracted light is measured with several detectors situated as several angles. From the analyzes of light diffraction of the multiple detectors, size repartition of the particles can be estimated using an optical model of light diffraction. The theory mostly used with this device, in the case of algae, is the Mie theory, which supposes a particle size superior to the wavelength of the lasers ($>1 \mu\text{m}$). The other optical diffusion models, Rayleigh/Fraunhofer, Raman, Brillouin are adapted for molecular diffusion for particles smaller than wavelength.



Figure 70: Malvern Mastersizer 3000 and measurement devices. From left to right: Liquid sample (manual), Dry sample, Liquid sample (automatic)

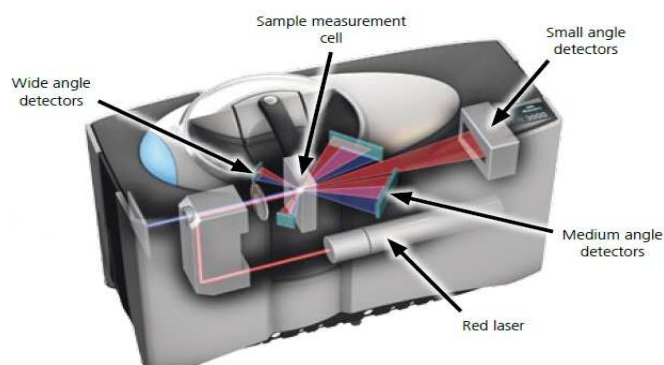


Figure 71: Optical h of the laser granulometer Malvern Mastersizer 3000

An optical model must be created choosing the optical model used, dispersant refractive index (RI), size distribution of the particles analyzed, if the particles are spherical or non spherical, and the refraction/absorption index of the particles at 470 and 633 nm. The model is validated when the fit of the model corresponds with the data obtained with the detectors. Also, residual and weighted residual must be as low as possible (lower than 1) and be similar.

Analyses were performed with the Hydro MV module using following parameters: Non-spherical particle mode; dispersant: water (RI=1.330); additional blue light measurements; 3 measurements; stirrer speed: 3000 rpm; no ultrasound; analysis model: general purpose; number distribution; result range: 1-150 μm .

The optical properties of *Chlamydomonas reinhardtii* cells were determined using the tool "Optical Properties Optimizer" of the device after entering values found in literature and illustrated on figure 52 [108]. Two optical models were created for the measurements: one is specific for growth phase conditions, the other model for lipid accumulation conditions. Optimal parameters found are detailed in table 9.

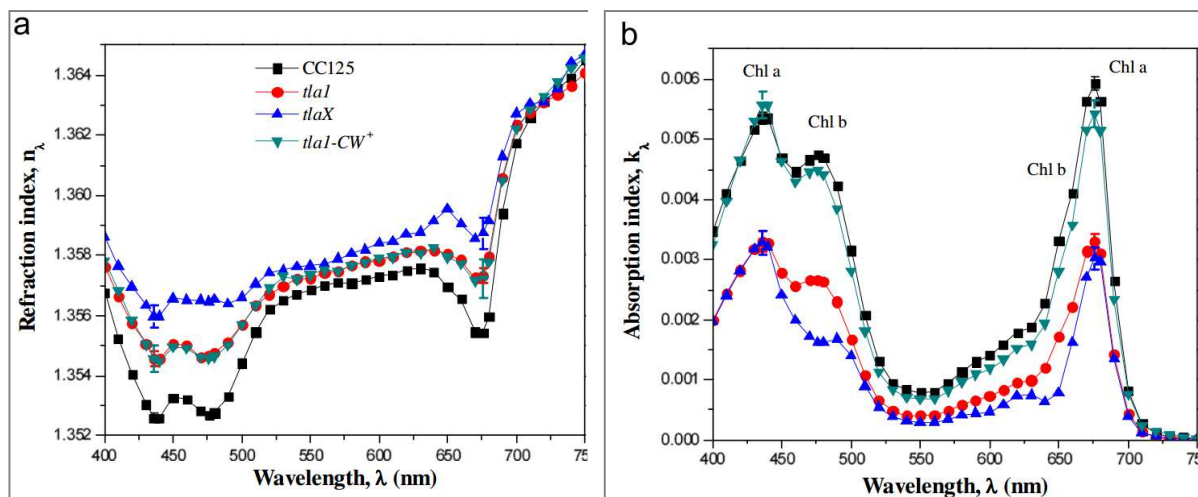


Figure 72: Refraction (a) and Absorption (b) Index measured for four *Chlamydomonas reinhardtii* strains CC125, *tla1*, *tlaX* and *tla1-CW+* measured on the visible spectrum [108].

Table 9: Refraction and absorption index found for *Chlamydomonas reinhardtii* SAG 34.89 (wild type) for blue laser (470 nm) and red laser (633 nm) with the tool "Optical properties optimizer" of the laser granulometer. Different optimal values were found for at different lipid accumulation periods: growth phase, 7 days of stress and 14 days of stress.

<i>Optical model</i>	RI _{633nm}	AI _{633nm}	RI _{470nm}	AI _{470nm}
<i>Cr growth phase</i>	1.527	0.0030	1.527	0.0030
<i>Cr lipid 7d</i>	1.560	0.0001	1.560	0.0001
<i>Cr lipid 14d</i>	1.560	0.0001	1.6800	0.00065

II5. Appendix II5: Medium preparation

Modified Bristol Medium 3N

Bristol medium results of the mix up of three stock solutions (A,B and C) prepared separately. In three flasks of 1L blends the components in each flask making up the volume with distilled water:

Table 1 – Composition of stock solution A for Bristol medium.

Components	Quantity (g)	Concentration (M)	Quantity in the solution (g)
NaNO ₃	75.0	0.0088	75.1093
CaCl ₂	1.9	1.93 x 10 ⁻⁴	1.9172
MgSO ₄ .7H ₂ O	7.5	3.045 x 10 ⁻⁴	7.5812
FeEDTA	2.0	5,75 x 10 ⁻⁵	2.0052

Table 2 – Composition of stock solution B for Bristol medium.

Components	Quantity (g)	Concentration (M)	Quantity in the solution (g)
K ₂ HPO ₄	7.5	4.3 x 10 ⁻⁴	7.5062
KH ₂ PO ₄	17.5	0,00128	17.5395
NaCl	2.0	3.41 x 10 ⁻⁴	2.0121

Table 3 – Composition of stock solution C for Bristol medium.

Components	Quantity (g)	Concentration (M)	Quantity in the solution (g)
H ₃ BO ₃	2.86	4.61 x 10 ⁻⁵	2.8714
MnCl ₂ .4H ₂ O	1.81	1.20 x 10 ⁻⁵	1.8059
ZnSO ₄ .7H ₂ O	0.220	1.149 x 10 ⁻⁶	0.2266
CuSO ₄ .5H ₂ O	0.070	4.221 x 10 ⁻⁷	0.0704
MoO ₃ , 99.0-100 %	0.036	1,5 x 10 ⁻⁷	0.0379
CoSO ₄ .7H ₂ O	0.090	4.86 x 10 ⁻⁷	0.0113

- 1) Maintain these three solutions in the refrigerator for obtaining final Bristol medium;
- 2) For each liter of the solutions prepared, add to an 1L flask 10 mL of solution A; 10 mL of solution B and 1 mL of solution C;
- 3) The pH is adjusted to 7 and goes to autoclave (T=121°C);
- 4) The medium is prepared to use (is maintain in refrigerator for a few days).

Medium for Lipid accumulation – Solution A

The introduction of microalgae culture into Stage II (Lipid Accumulation) was done by changing the composition of Bristol medium modified 3N used in Stage I.

Modifications were done specifically in Solution A by replacing NaNO_3 component to Na_2SO_4 . This changing was done with purpose of having a medium in nitrogen starvation, ie, that applies more to lipid accumulation.

In flask of 1L were blended the components by making up the volume with distilled water:

Table 1 – Composition of stock solution A for Bristol medium in nitrogen depletion.

Components	Quantity (g)	Amount used with 4x dilution (g)	Quantity in the solution (g)
Na_2SO_4	124.0	31.0	31.0041
CaCl_2	1.9	0.475	0.4844
$\text{MgSO}_4 \cdot 7\text{H}_2\text{O}$	7.5	1.875	1.8778
FeEDTA	2.0	0.5	0.5016

For one Erlenmeyer of 1L with this medium(nitrogen starvation) is pipetted 16 mL of this new Solution A, 4 mL of Solution B and 400 μL of Solution C.

PBS

For 1 L:

- 1) Add to an flask of 1L each one component described to approximately 900 mL of H_2O .

Table 4 – Composition of PBS solution.

Components	Quantity (g)	Concentration (mM)
NaNO_3	0,250	2,94
$\text{CaCl}_2 \cdot 2\text{H}_2\text{O}$	0,025	0,17
$\text{MgSO}_4 \cdot 7\text{H}_2\text{O}$	0,074	0,3
K_2HPO_4	0,075	0,43
KH_2PO_4	0,175	1,29
NaCl	0,025	0,43

- 2) Make up the volume of the solution to 1L;
- 3) Mix up all the solution (pH adjust to 7) and cover well;
- 4) Store in the autoclave ($T=121^\circ\text{C}$).

TAP medium

from Gorman, D.S., and R.P. Levine (1965) *Proc. Natl. Acad. Sci. USA* **54**, 1665-1669.

This is probably the most widely-used medium at present for experimental work.

Make the following stock solutions:

1. TAP salts

NH ₄ Cl	15.0 g
MgSO ₄ · 7H ₂ O	4.0 g
CaCl ₂ · 2H ₂ O	2.0 g
water to 1 liter	

2. phosphate solution

K ₂ HPO ₄	28.8 g
KH ₂ PO ₄	14.4 g
water to 100 ml	

3. Hutner's trace elements (follow this [link](#))

To make the final medium, mix the following:

2.42 g Tris
25 ml solution #1 (salts)
0.375 ml solution #2 (phosphate)
1.0 ml solution #3 (trace elements)
1.0 ml glacial acetic acid
water to 1 liter

For solid medium, add 15 g agar per liter

Autoclave.

For Tris-minimal medium omit the acetic acid and titrate the final solution to pH 7.0 with HCl

Hutner's trace elements

Hutner et al. (1950) *Proc. Am. Philos. Soc.* **94**, 152-170

This mixture is used both in [TAP](#) and in the [Sueoka high salt](#) medium.

For 1 liter final mix, dissolve each compound in the volume of water indicated.

The EDTA should be dissolved in boiling water, and the FeSO_4 should be prepared last to avoid oxidation.

compound	amount	water
EDTA disodium salt	50 g	250 ml
$\text{ZnSO}_4 \cdot 7 \text{H}_2\text{O}$	22 g	100 ml
H_3BO_3	11.4 g	200 ml
$\text{MnCl}_2 \cdot 4 \text{H}_2\text{O}$	5.06 g	50 ml
$\text{CoCl}_2 \cdot 6 \text{H}_2\text{O}$	1.61 g	50 ml
$\text{CuSO}_4 \cdot 5 \text{H}_2\text{O}$	1.57 g	50 ml
$(\text{NH}_4)_6\text{Mo}_7\text{O}_{24} \cdot 4 \text{H}_2\text{O}$	1.10 g	50 ml
$\text{FeSO}_4 \cdot 7 \text{H}_2\text{O}$	4.99 g	50 ml

Mix all solutions except EDTA. Bring to boil, then add EDTA solution. The mixture should turn green. When everything is dissolved, cool to 70 degrees C. Keeping temperature at 70, add 85 ml hot 20% KOH solution (20 grams / 100 ml final volume). Do NOT use NaOH to adjust the pH.

Bring the final solution to 1 liter total volume. It should be clear green initially. Stopper the flask with a cotton plug and let it stand for 1-2 weeks, shaking it once a day. The solution should eventually turn purple and leave a rust-brown precipitate, which can be removed by filtering through two layers of Whatman#1 filter paper, repeating the filtration if necessary until the solution is clear. Store refrigerated or frozen convenient aliquots. Some people shorten the time for formation of the precipitate by bubbling the solution with filtered air.

If no precipitate forms, the solution is still usable. However, you might want to check the pH in this case and adjust it to around 7.0 using either KOH or HCl as needed.

To prepare sulfur-free trace elements for hydrogen generation, the sulfate salts can be replaced with equimolar chloride salts (ZnCl_2 10.0 g; $\text{CuCl}_2 \cdot 2 \text{H}_2\text{O}$ 1.00 g; $\text{FeCl}_2 \cdot 4 \text{H}_2\text{O}$, 3.60 g)...

II.6. Appendix II.6: Correlation cyto/malassez in growth and stress phase

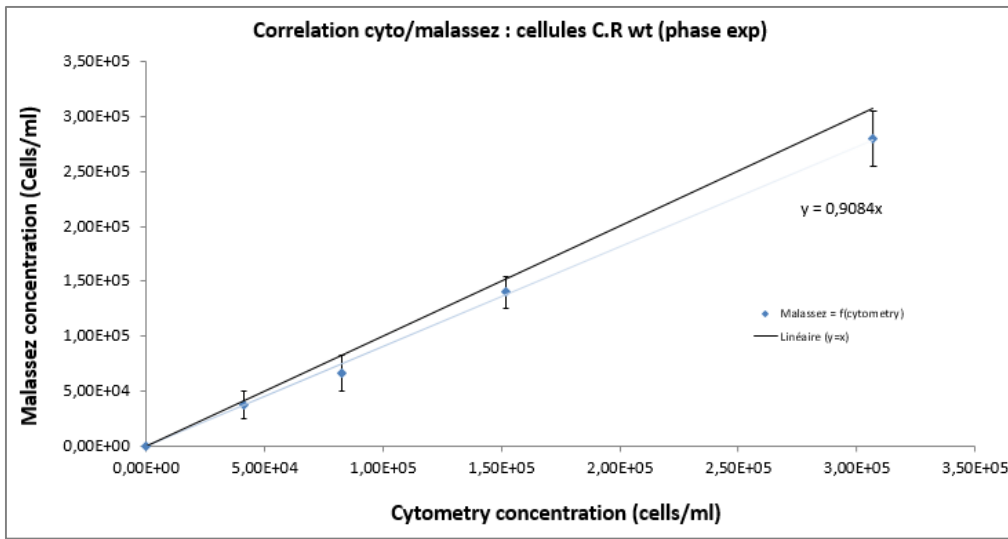


Figure 73: Correlation between cell concentration determined by cytometry and microscopy using Malassez chamber for *Chlamydomonas reinhardtii* wild type (growth phase); correlation in blue; first bisector in black. .

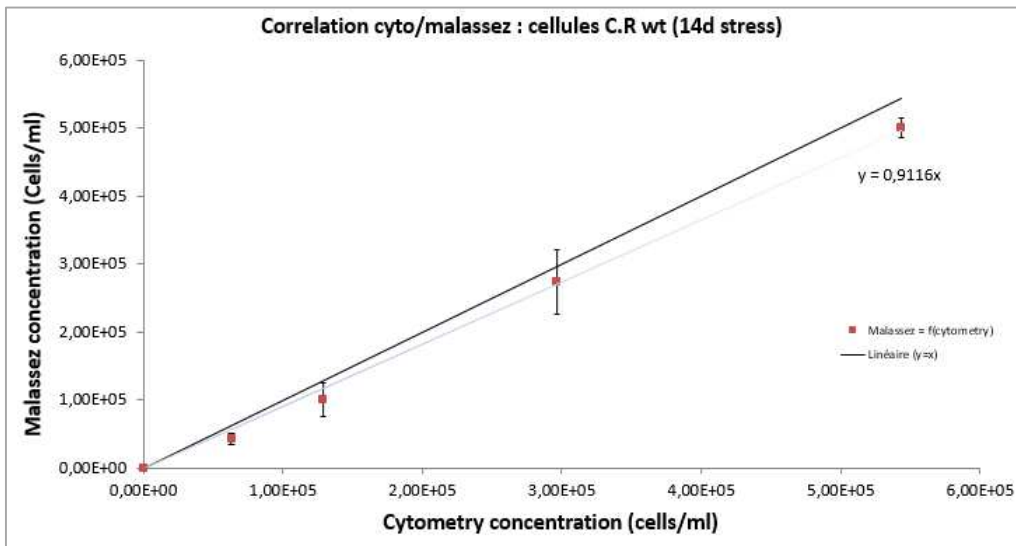


Figure 74: Correlation between cell concentration determined by cytometry and microscopy using Malassez chamber for *Chlamydomonas reinhardtii* wild type (stress phase). correlation in blue; first bisector in black

II7. Appendix II.7: Confocal microscopy vs fluorescence microscopy

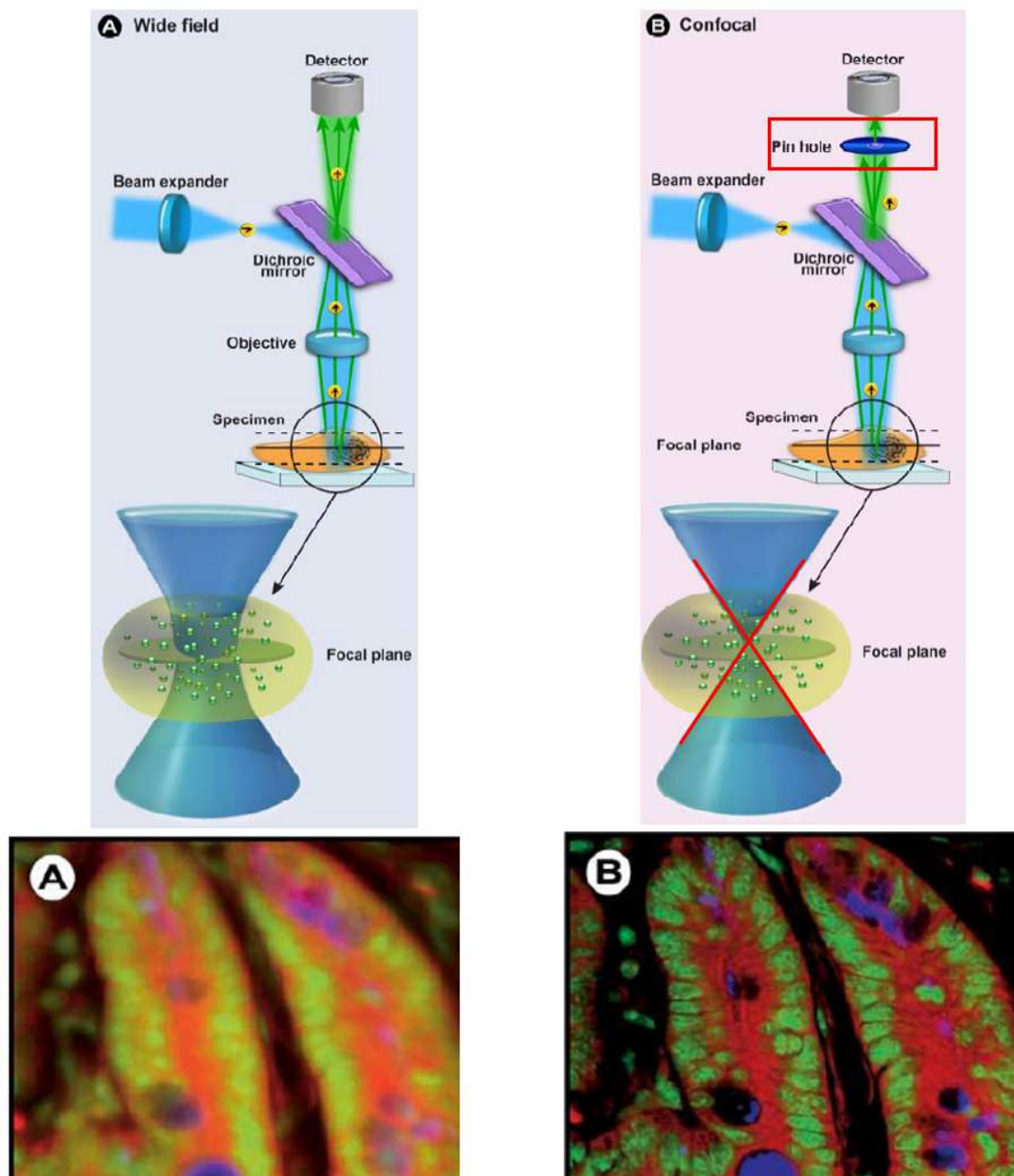


Figure 75: In confocal microscopy (B) the detection beam emitted from the illuminated sample path a pinhole aperture (red rectangle) in front of the detectors. This enable to reduce the light emitted above and below the focal plane. The reconstitution of the specimen illuminated has a higher resolution in comparison with wide field fluorescence (A) [89].

II.8. Appendix II.8: CLSM optical configuration to monitor *Chlamydomonas reinhardtii* cells stained with Bodipy and Concanavalin TRITC (track 1: Bodipy, track 2: Chlorophyll, and track 3: concanavalin, track 4: merged channels)

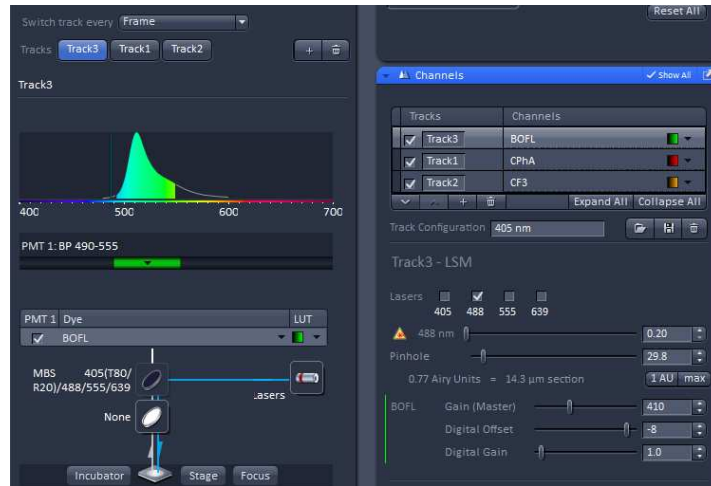


Figure 76: LCSM Track 1 configuration (Bodipy)

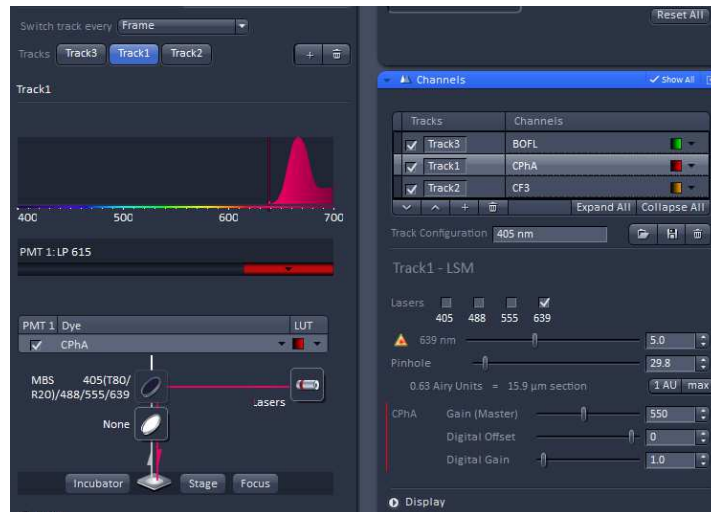


Figure 77: LCSM Track 2 configuration (Chlorophyll)



Figure 78: LSM Track 3 configuration (Concanavalin)

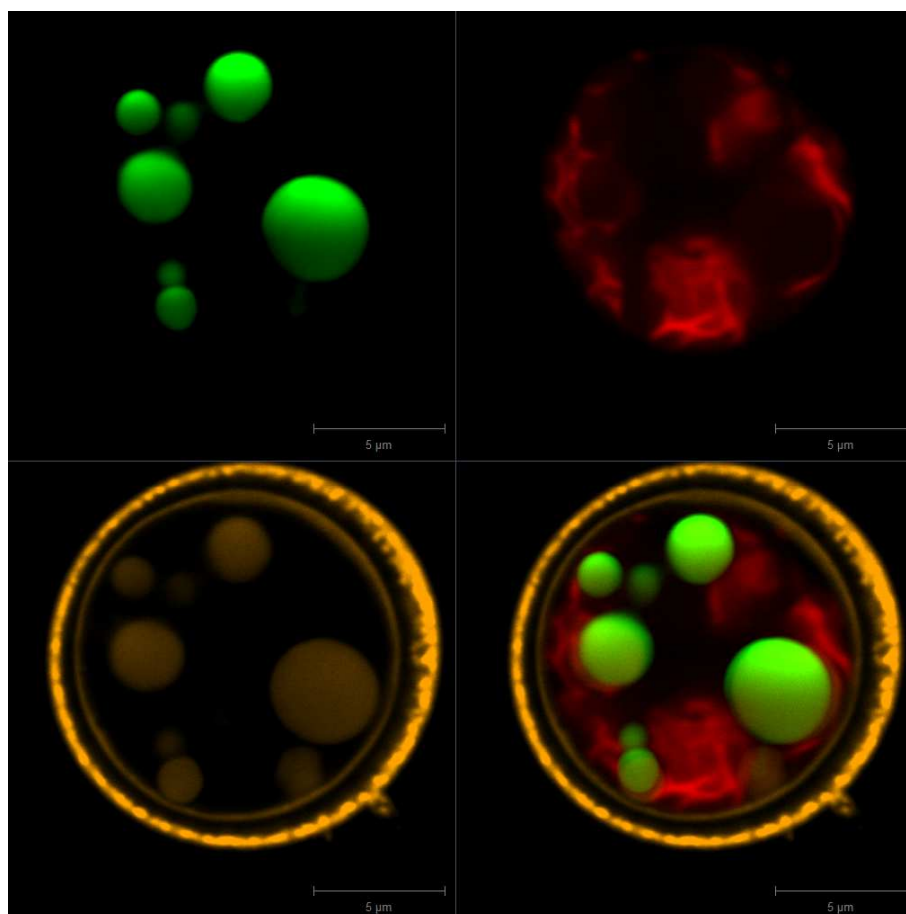


Figure 79: CLSM imaging of *Chlamydomonas reinhardtii* in stress phase. Track 1, lipid droplets stained with Bodipy, Track 2: chlorophyll autofluorescence, Track 3: concanavalin fluorescence, Track 4: merged channels.

Chapter 3

The use of Pulsed Electric Fields for the extraction of lipids from *Chlamydomonas reinhardtii*: study in microdevice and electroporation cuvettes

Summary

List of abbreviations:	164
Chapter 3: introduction.....	165
I. State of the art	166
I1) Principle and interests of Pulsed Electric Field (PEF)	166
I1a) Principle.....	166
I1b) Theory.....	168
I1c) Side effects	170
I1d) Treatment parameters	172
I1e) Applications.....	174
I2) Use of PEF in algae biotechnology	175
I3) Use of bio-micro-devices to monitor algae cells <i>in situ</i>	178
I3a) Cell culture monitoring on a chip	178
I3b) Investigation of dielectric properties	178
I3c) Investigation cell lysis <i>in situ</i> via DEP forces.....	180
II. Material and methods	181
II1) Micro-device for studying the in situ permeabilization and characterization of <i>Chlamydomonas reinhardtii</i>	181
II2) Electroporation in cuvettes	183
II3) Viability/permeability measurements	184
II3a) Choice of the dyes	185
II3b) Determination of the optimal staining conditions.....	187
II3c) Validation of the PI and FDA optimal conditions	189
II3d) Development and validation of the staining methods by flow cytometry	191
II3e) Measure of the permeabilization level in the micro-device	193
II3f) Measure of permeability (irreversible permeabilization (IP) and reversible permeabilization (RP)) and viability in the electroporation cuvettes	195
II4) Measurement of lipid extraction with/without PEF	196
II4a) Characteristics of the solvent.....	196
II4b) Mixing protocol	198
II4c) SPV analysis after extraction	199
III. Results	200
III1) Electroporation in the micro-device	200
III1a) Calculation of the theoretical critical electrical field and charging time.....	201

III1b)	Determination of the critical electric field for <i>Chlamydomonas reinhardtii</i> (membrane fully charged).....	201
III1c)	Experiments.....	202
III1d)	Relation between energy consumption and permeabilization.....	205
III1e)	Sensitivity of <i>Chlamydomonas reinhardtii</i> to PEF at various stages of lipid accumulation 206	
III1f)	Qualitative observations by optical and epifluorescence microscopy.....	207
III2)	Electroporation in cuvettes	209
III2a)	Measurement of viability and irreversible permeability after PEF treatment.....	209
III2b)	Reversible and irreversible permeabilization for different pulse durations	210
III2c)	Reversible/irreversible permeabilization parameters, energy and temperature increase 212	
III2d)	Life cycle of reversible pores	214
III2e)	Transport of various molecules through the pores.....	215
III2f)	Observations of the cell structure and lipid droplets by CLSM	215
III3)	Association of PEF to solvent for lipid extraction	216
III3a)	Cell lysis	216
III3b)	CLSM imaging of cells after solvent extraction	218
III3c)	Lipid extraction.....	220
III3d)	Conclusion on lipid extraction	223
Chapter 3 conclusion	224
Chapter 3 references	226
III1.	Appendix III.1: Lipid production strategies in literature. List of viability related dyes, from [62]. Dyes can be classified according to their application: (1) permeability dyes, (2) membrane potential dyes, and (3) cellular enzyme activity dyes [62].	229
III2.	Appendix III.2: Temperature profiles in the microdevice simulated in COMSOL	230
III3.	Appendix III.3: Calibration curves of triolein dissolved in hexane	232

List of abbreviations:

- PEF Pulsed Electric Field
- $\Delta\psi_i$ Induced membrane potential (V)
- E Electric field (kV/cm)
- V_m Membrane resting potential (V)
- $\Delta\Psi_{crit}$ Critical membrane potential (V)
- Δt_{pu} Pulse duration (s)
- τ_m Membrane charging time (s): time duration to reach 63% of the full charge
- r_s Rising time (s): time duration to reach the full charge
- r_d Resting duration between two pulses (V=0)
- ΔT_{pu} Joule heating due to one pulse ($^{\circ}K$ or $^{\circ}C$)
- Δt_{treat} Total pulse duration (s)
- ΔT_{treat} Total joule heating of the treatment ($^{\circ}K$ or $^{\circ}C$)
- W_{pu} Energy delivered from one pulse (W)
- W_{treat} Energy delivered from the treatment (W)
- F Pulse frequency (Hz)
- f_{CM}^* Clausius-Mossotti factor
- ϵ_p^* Complex permittivity (F/m)
- PDMS Polydimethylsiloxane
- S1805 Positive photoresist
- SU8 Negative photoresist
- CMOS Complementary Metal Oxide Semiconductor
- SG Sytox Green (permeability dye)
- PI Propidium Iodide (permeability dye)
- FDA Fluorescein Diacetate (viability dye)
- FITC Fluorescein isothiocyanate
- PerCP-Cy5.5 Peridinin-Chlorophyll-Protein coupled with cyanin 5.5, a far-red emitting dye
- PMT Photomultiplier
- TAP Tris-Acetate-Phosphate, medium for *Chlamydomonas reinhardtii*
- LogP partition-coefficient which corresponds the logarithmic ratio of concentration between octanol and water
- FA Fatty acids
- SPV Sulpho-phospho-Vanillin
- E_{crit} Critical electric field of permeabilization (kV/cm)
- Dye staining Percentage of dye in cell population measured (%)
- Dye uptake Percentage of dye in cell population offset by the value before treatment (%)
- NP Naturally permeabilized cells (before PEF treatment)
- RP Reversibly permeabilized cells
- IP Irreversibly permeabilized cells
- SA Cells stained by a dye 1 h after PEF treatment (only stains NP+IP)
- SB Cells in contact with the dye before PEF treatment (NP+RP+IP)

Chapter 3: introduction

As discussed in the Chapter 1, downstream processes in microalgae production are strongly dependent on the strains and culture conditions used, and most of all on the target compound and market aimed. For massive markets with a final low cost product, such as biodiesel, the energy involved in the downstream processes has a high impact on the cost of the product [1]. For biodiesel production from microalgae, the average final cost is estimated at 3.7 US\$/L [2], which must be reduced to 1 US\$/L in order to be competitive with the expected price of fossil fuels by 2030 - 2050. One or several technological breakthroughs must be accomplished in order to make algae derived biofuels competitive in the future.

The standard downstream processes used in feed and food industries are hardly used in microalgae production. This is first related to the immaturity of microalgae biotechnology and second to the difficulty to treat with common downstream processes the suspensions containing small cells, some of those with thick cell walls.

Thus, despite the huge and wide potential of microalgae, their cultures are mainly carried out to produce high value compounds because of the high energy costs associated to culture, harvesting and extraction steps. In this context, the development of innovative processes for molecules extraction from microalgae is of primary importance. Pulsed Electric Field (PEF), a technology discovered about fifty years ago, which starts to demonstrate plenty of applications in various fields, may be a candidate to facilitate the extraction of intracellular compounds at a low energetic cost.

The aim of the work presented in this Chapter is to study the impact of PEF on *Chlamydomonas reinhardtii* membrane permeability and on lipid extraction.

After setting-up of the culture system and optimization of characterization methods (Chapter 2), **a dedicated micro-device**, miniaturized to the scale of algae cells, **is built to study *in situ* the effect of PEF on cells** The goal is to develop a microscopic method to **evaluate cell permeabilization *in situ*** for several treatment conditions. The purpose is to determine the set of parameters that permeabilize algae cells while limiting the energy spent. Besides, the effects of PEF on lipids and cell wall are visualized using microscopic tools (optic/fluorescence and confocal laser scanning microscopes).

Afterwards, additional experiments are performed at an upper scale **to characterize the reversibility/irreversibility of the pores** created. Finally, **PEF pre-treatment is associated with solvent extraction to assess the interest of electroporating algae cells to improve lipid extraction.**

I. State of the art

1) Principle and interests of Pulsed Electric Field (PEF)

1.1a) Principle

The principle of Pulsed Electric Field (PEF) consists of applying on cells or tissues repeated short pulses of an electric field E (expressed in V/cm) created between two electrodes. The application of repeated electric fields leads to **cell membrane poration** [3]. This phenomenon is explained by a **phospholipid bilayer destabilization** when the induced trans-membrane voltage ($\Delta\psi_i$) reaches a critical value ($\Delta\psi_c$) [4] as illustrated in Figure 1. This destabilization often results in the apparition of pores, initiated by the penetration of polar molecules (represented by red and grey spheres in the Figure 1) between the polar heads of the bilayer (represented with green spheres). Pore creation proceeds with the migration of the phospholipid head groups in the inner part of the membrane which then stabilizes into a pore. Pore annihilation begins at the end of the electric field application. At this step, the pore size starts to decrease, the polar head groups migrate back to their initial position and reseal the membrane. Finally, the remaining polar molecules, such as water, trapped in the membrane, are moved out to restore the initial membrane structure.

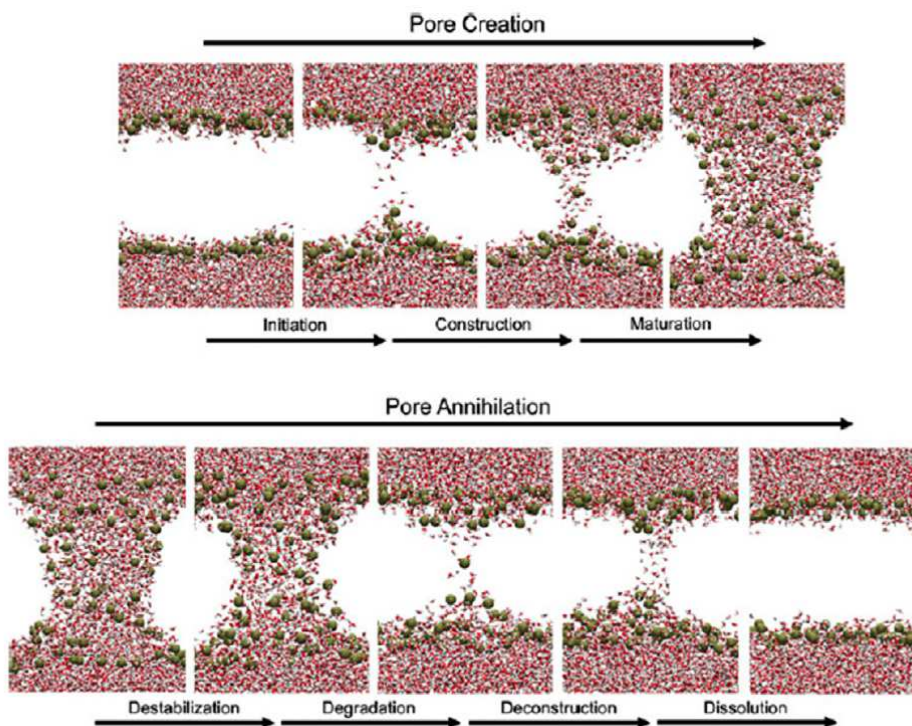


Figure 1: Molecular dynamic simulation of an electropore in a lipid bilayer [5]. Water is represented by red and grey spheres while phosphorus atoms of the polar fatty acids are seen as large green spheres (apolar tails of phospholipids not represented). “Pore creation in an electric field begins with the introduction water defect into the bilayer, followed by the reorganization of the phospholipid head groups in each leaflet around the defect (pore construction). Migration of additional water and head groups into the pore continues until an arbitrarily defined mature pore structure is formed (pore maturation). Pore annihilation begins with the removal of the porating electric field. The pore structure is quasi-stable at this time (pore destabilization), but soon there is a decrease in pore size as head groups and water begin to migrate out of the membrane interior (pore degradation). The head groups separate again into two groups (pore deconstruction). Water quickly follows (pore dissolution) and the intact structure of the bilayer is restored.”

It must be clear that Figure 1 illustrates a **simulation of the behavior of a single phospholipid bilayer** during the application of a pulse. **The phenomenon is much more complex in a plasma membrane** as the structure contains proteins, cytoskeleton filaments, transport channels or glycolipids [6] (see Chapter 2). **It should be stressed that PEF may also lead to long term effects despite the resealing of the created pores.** Indeed, a so called **memory effect** [4] may exist after the treatment as the membrane structure may be affected by the presence of molecules, mainly water, or by the destructure of the cytoskeleton [7].

The **size and localization** of the pores **depend on the treatment intensity**. Also the **dynamics of pore creation and deconstruction is highly dependent on temperature** [8]. When the **conditions are steep** (high electric field, long pulse durations), **the pores created are very large and/or very numerous and the membranes are unable to reseal**. This phenomenon is referred as **irreversible electroporation** and often leads to cell death.

The electric field E induced by the application of a potential leads to a **charge displacement inside the cell** (cytoplasm medium) and **outside the cell** (external medium). This induced ionic gradient on the cellular poles leads to a **new induced potential on the membranes facing the electrodes** [3] as illustrated in Figure 2 (from a to c). When the induced potential reaches a critical value, a pore is created. **A charge displacement at the interface of the pore created modifies the charge gradient inside the cell** which leads to **additional pores** as illustrated in Figure 2.d.

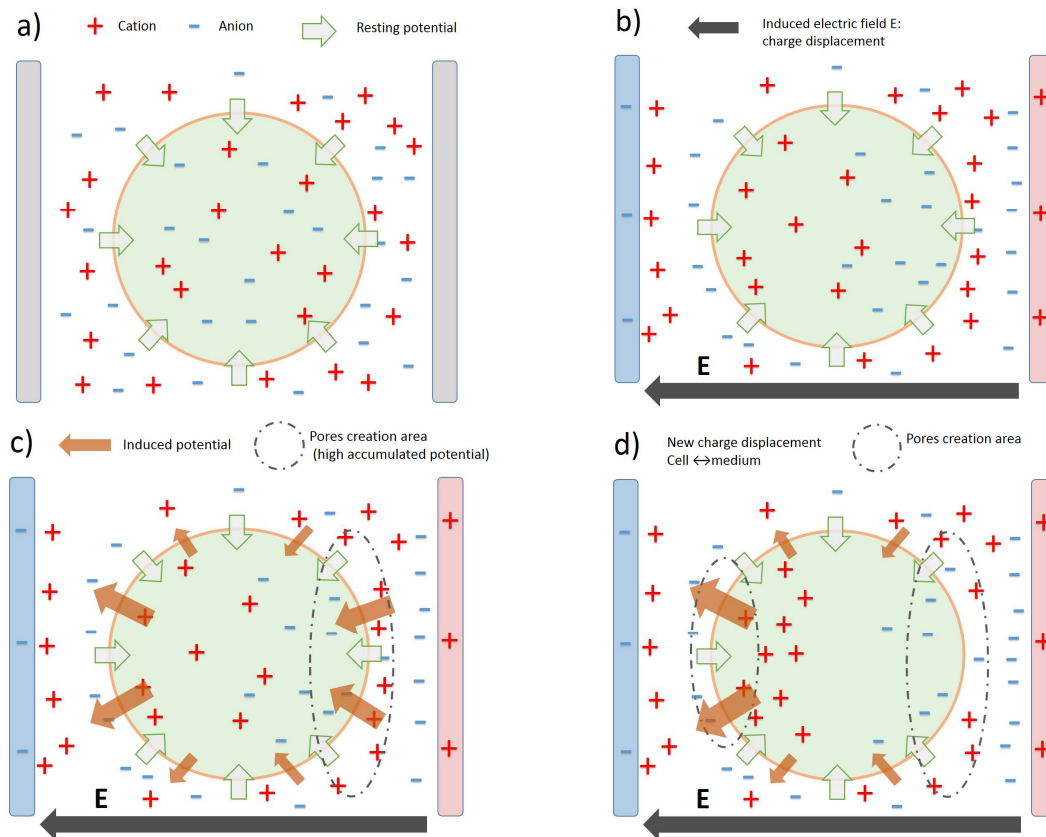


Figure 2: Charge displacement during the application of a pulse in a cell and surrounding medium. a) resting potential illustrated with grey arrows, b) charge displacement due to the application of an electric field E , c) illustration of the induced potential $\Delta\Psi_i$ with brown arrows: high accumulated potential (resting potential + induced potential) leads pores

creation on the membrane area facing the cathode, d) pores creation leads to a new charge displacement and a redistribution of transmembrane potential: new pores may appear on the membrane facing the anode.

11b) Theory

The **resting potential** V_m , illustrated in Figure 2 with a grey arrow, can be determined from the Goldman equation [9]:

$$V_m = \frac{RT}{F} \ln \left(\frac{\sum_i^N P_{M_i^+} [M_i^+]_{out} + \sum_j^M P_{A_j^-} [A_j^-]_{in}}{\sum_i^N P_{M_i^+} [M_i^+]_{in} + \sum_j^M P_{A_j^-} [A_j^-]_{out}} \right) \quad (3.1)$$

P_{ion} is the permeability for the considered ion ($m \cdot s^{-1}$), $[ion]_{in}/[ion]_{out}$ the ratio of the concentrations of each ion in the cytoplasm and external medium. R the ideal gas constant equal to $8.314 \text{ JK}^{-1} \cdot \text{mol}^{-1}$, T the temperature (K), F the Faraday constant equal to $96.485 \text{ C} \cdot \text{mol}^{-1}$.

The resting potential is most of the time negative, in the range of -50 mV to -100 mV for mammalian cells and measured at -100 mV for *Nitella Expensa*, a superior plant [10].

The **critical potential** $\Delta\psi_{crit}$ required to trigger membrane permeabilization is known to be **in the range of 0.2 - 1.5 V for mammalian cells** [11].

The **induced trans-membrane potential** $\Delta\psi_i$ on a spherical cell at time t is given by the Schwan equation (equation 3.2) [12].

$$\Delta\psi_i(t) = -\frac{3}{2} \cdot r \cdot E \cdot \cos(\theta) \cdot \left[1 - e^{-\frac{t}{\tau_m}} \right] \quad (3.2)$$

with $\Delta\psi_i$ (V) the induced potential applied on the membrane, r(m) the cell radius, E (V/m) the electric field applied, θ (rad) the angle between $\Delta\psi_i$ and the applied electric field, τ_m (s) the membrane charging time constant.

It should be noted that the strength and direction of $\Delta\psi_i$ vary with the position **on the cell surface**, as they depend **on the angle θ of $\Delta\psi_i$** with the applied field direction. This may **restrain the effect of PEF on a small region of the membrane** [13]. As illustrated in Figure 2, the induced field is added to the resting potential.

Schwan equation (equation 3.2, [12,14]) underlines the **importance of cell size**. **A cell with a large diameter will undergo a stronger induced potential**. Besides the induced electric field is always proportional to the electric field applied E (potential V applied divided by the distance between the electrodes, expressed in V/m).

Conventional electroporation uses pulses which duration t_{pu} is longer than plasma membrane charging time (τ_m). This parameter is calculated according to equations 3.3 and 3.4 depending on the model used: in the double shell model the cell wall is taken into account in contrast with the single shell model [15]. Single shell model is the common model for mammalian cells. However, **for vegetal cells, which possess a cell wall, the double shell model is more relevant** [16].

Membrane lipid bilayer can be considered as a capacitor C_m , as the membrane charging requires the displacement of positive and negative charges in the cytoplasm and in the surrounding medium, (Figure 2.b). Charging duration is inversely proportional to cytoplasm and medium conductivities σ .

$$\tau_m = r \cdot C_m \left(\frac{1}{\sigma_{cyt}} + \frac{1}{2 \sigma_{med}} \right) \text{ single shell model [15]} \quad (3.3)$$

$$\tau_m = r \cdot C_m \left(\frac{1}{\sigma_{cyt}} + \frac{\sigma_{med} + \sigma_{cw}}{2 \sigma_{med} \sigma_{cw}} \right) \text{ double shell model [16]} \quad (3.4)$$

with C_m the membrane capacitance, estimated at $0.01 \text{ F} \cdot \text{m}^{-2}$ [17]; σ_{cyt} , σ_{med} , and σ_{cw} cytoplasm, medium and cell wall conductivities, respectively ($\text{S} \cdot \text{m}^{-1}$). The charging time is in the range 0.4 to $1 \mu\text{s}$ for mammalian cells [18].

It should be noted that the determination of the membrane charging time constant τ_m (time duration to charge 63% of the maximal voltage) illustrated Figure 3, is important especially when using short pulses to **compensate the inability to reach the full charge with a higher electric field applied** (see equation 3.2 the relation between t and τ_m): the application of an electric field of 1 kV/cm during a pulse of $1 \mu\text{s}$ would result in an electric field of 0.63 kV/cm (63 % of the full charge of the membrane) illustrated in Figure 3. To counterbalance the charging effect, an application of an electric field of 1.59 kV/cm would result in an electric field of 1 kV/cm on the membrane after $1 \mu\text{s}$.

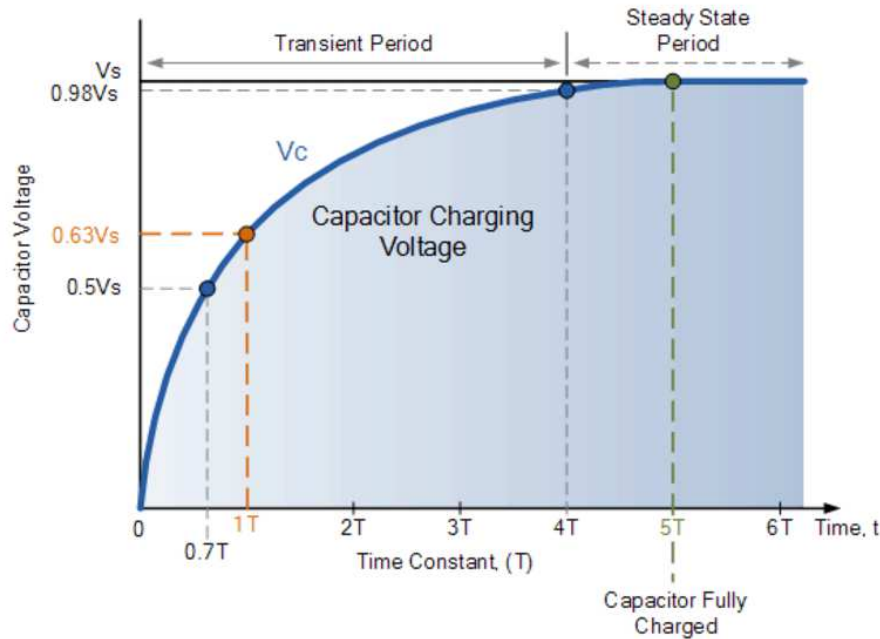


Figure 3 : Illustration of the membrane charging dynamic, modeled by a RC charging circuit curve [19]

The full charge of the membrane, corresponding to a pulse duration higher or equal to the charging time of the membrane, **requires a duration of the electric field application longer than several times the charging time τ_m** ($\Delta t_{pu} > 5 \tau_m$ to reach 95% of the final charge, when considering equation 3.2).

11c) Side effects

Undesirable side effects may come up when applying an electric field to a liquid medium: **joule heating** and **water electrolysis**. **Joule effect** is a **volume effect** due to the propagation of the electric field in the medium. **Water electrolysis** is a **surface effect** on the interface electrode (electronic conduction) / medium (ionic conduction).

Considering there is no external heat exchange (diffusion, convection), the temperature increase due to Joule effect ΔT_{pu} for one single pulse can be estimated with equation 3.5 [11]. **The temperature increase** (in °K or °C) **directly depends on field strength E** ($V \cdot m^{-1}$), **pulse duration Δt_{pu}** (s), medium **conductivity σ_{med}** ($S \cdot m^{-1}$), medium heat capacity C_p ($J \cdot K^{-1}$) and medium volumetric mass density ρ (kg/m^3).

$$\Delta T_{pu} = \frac{W}{C_p \cdot \rho} \quad (3.5)$$

Where **W** is the spent energy

$$W = |E|^2 \cdot \Delta t_{pu} \cdot \sigma_{med} \quad (3.6)$$

Consequently, the total temperature increase due to the treatment $\Delta T_{treat\ max}$ (considering no cooling) can be upper bounded thanks to equation 3.7:

$$\Delta T_{treat\ max} < \Delta T_{pu} \cdot N_{pu} \quad (3.7)$$

with N_{pu} , the number of pulses used during the treatment.

While the heat capacity C_p can be considered as constant in the aqueous medium, **medium conductivity can increase** because of the release of ionic substances [20] (*e.g* calcium from the endoplasmic reticulum [21]). **To prevent heating, some PEF treatments on microalgae are performed in a low conductivity buffer [22,23], or heat is eliminated using a cooling system [24,25]**. Without any of these precautions, temperature may increase by several dozens of degrees depending on treatment parameters, thus affecting cells viability and metabolites stability.

Increasing temperature by several dozens of degrees may result in a phase transition (melting) of the membrane [26] (Figure 4) from a gel (solid ordered phase) to a fluid (disorganized phase). Heating from 20 °C to 35-40 °C destabilizes the membrane to give a ripple phase (intermediate phase) and above 40°C a fluid phase. A transition phase corresponds to an increase of per volume lipid ($\text{Å}^3/\text{lipid}$) in the membrane as showed in the Y axis of the Figure 4. This increased volume in fluid phase is due to an increased head-head distance in the bilayer as the membrane thickness is reduced in this state.

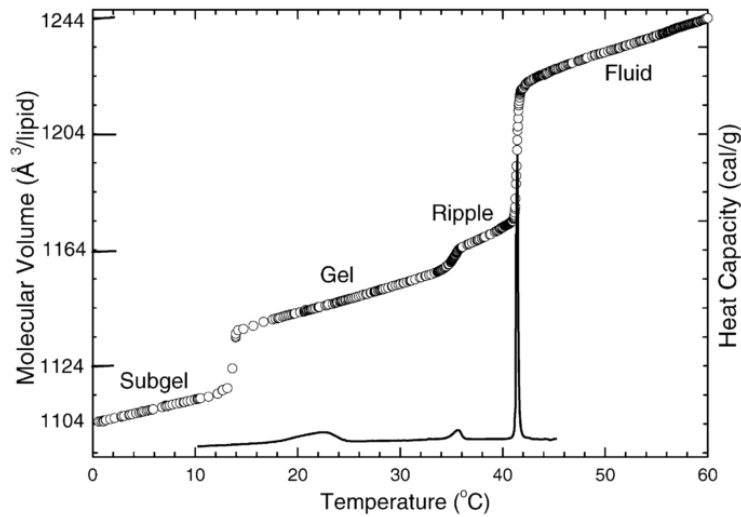


Figure 4: Phase transition in a membrane bilayer depending on temperature [26].

Cell membrane permeabilization can be associated with the phase transition, electroporation is associated to the induced electric field.

Water electrolysis may also occur on both electrodes. This phenomenon leads to the formation of gas bubbles at the cathode (hydrogen) and the anode (oxygen). The electrolysis potential with current in function for various electrode materials is showed in Figure 5. As shown, gold and platinum are the best material to avoid water electrolysis.

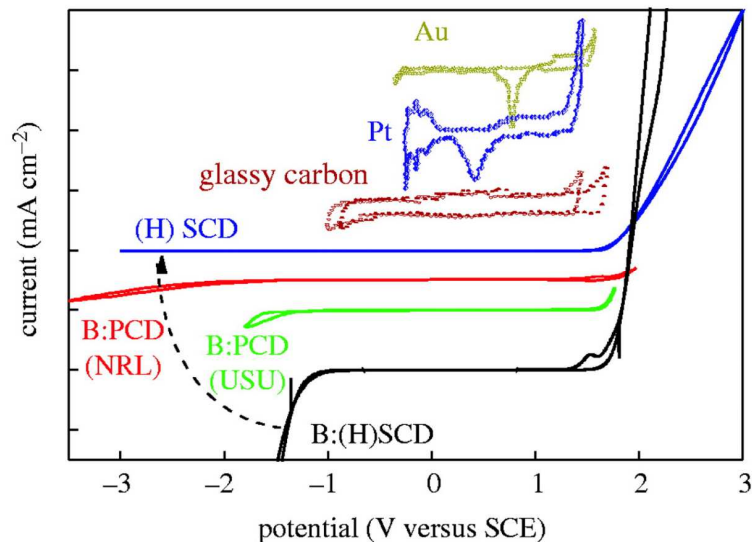


Figure 5 : Electrolysis potential with current in aqueous medium for various electrode materials. The graphs are shifted vertically for comparison. Au, gold; Pt, platinum; B:PCD are two polycrystalline films boron-doped diamond; B:SCD is a single crystalline boron-doped diamond; and SCD is a single-crystal-line undoped diamond [27].

Both mechanisms (temperature increase and water electrolysis) may have many consequences during PEF application: interferences on electric field distribution, generation of reactive oxygen species and mechanical stresses on cells due to bubbles. Moreover, both temperature [28] and reactive oxygen

species [29] can affect the permeabilization threshold (critical potential to induce permeabilization $\Delta\psi_c$).

11d) Treatment parameters

PEF treatment can be characterized by many parameters. As mentioned previously the pulse **duration Δt_{pu} and the electric field applied E have a paramount importance on cell permeabilization**. Also, pulses can be defined by their **shapes and frequencies**.

Frequency (Hz) is equal to the number of cycles per second:

$$F (Hz) = \frac{1}{P (s)} \quad (3.8)$$

with P the duration between two positive pulses (Figure 6).

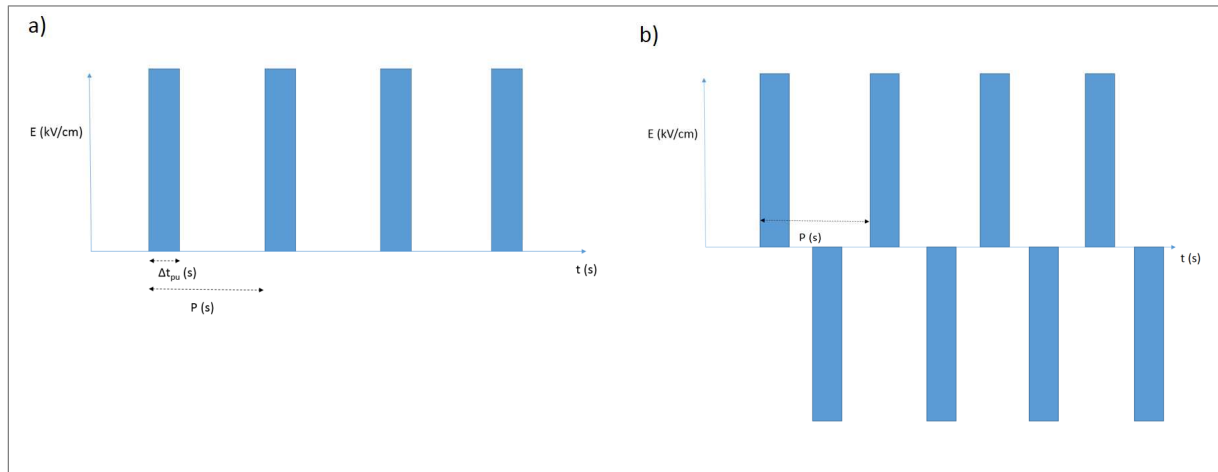


Figure 6 : Square shaped pulses: (a) monopolar pulses, and (b) bipolar pulses.

PEF can also be performed with so called “**bipolar pulses**” where the two electrodes alternate between the cathode state and the anode state. In such case, the **charges will move in different directions with each polarity change**.

The evolution with time of the applied potential between electrodes (*i.e* electric field) may also have a **sinusoidal shape**, corresponding to a cyclic bipolar signal where the potential applied is always rising or decreasing. Figure 6 illustrates **square shaped pulses**. Pulses may also have a trapezoidal, exponential or bell shape.

The rising time, r_s , is generally used to indicate the **duration required to reach the maximum pulse potential**, starting from 0. In the case of a square shaped pulse, the rising time is neglected in comparison with the pulse duration.

The resting duration, r_d , is the **duration where the electric field is equal to 0**, leading to a redistribution of charges within the medium and cytoplasm.

In the majority of PEF treatments, the resting duration is very long in comparison to the pulse duration. Indeed, **the application of a sufficient electric field in a very short duration leads to membrane breakdown with negligible energy spending and associated side effects.**

A large range of PEF (pulse duration/electric field strength) conditions are found in the literature. The **pulse duration may range from 1 ns to 1 s and the strength of the applied field from 0.1 kV/cm to 100 kV/cm** for several kinds of cells [11].

It is well established that the treatment effect is highly correlated to the couple pulse duration/electric field strength [30], *i.e.* **shorter pulses require higher fields** to obtain the same effect on the cell membrane. Figure 7 represents the close relation between pulse duration and electric field strength and their associated effects on mammalian cells. These latter are the common models used to study PEF effects on living organisms.

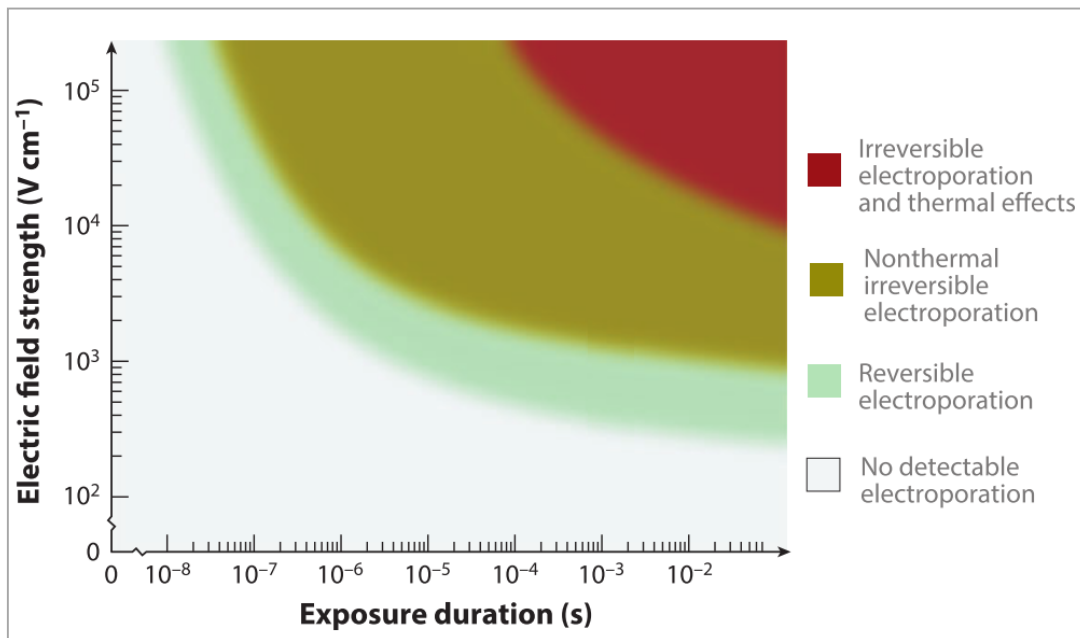


Figure 7: Electroporation and thermal effects caused by exposure of mammalian cells to electric fields. Reversible electroporation, irreversible electroporation and thermal damage as functions of electric field strength and duration [30]. Exposure duration stands for one single pulse duration.

Very short pulses ($\Delta t_{pu} < 1 \mu s$), referred as nanopulses, may lead to **cell apoptosis** by affecting internal organelles, **while the membrane charge does not reach the permeabilization level** [31]. As shown in Figure 7, the electric fields associated with nanopulses are much higher than those generally used in conventional electroporation (several tens of kV/cm). On the opposite, **long pulse durations** (long pulses, low electric field) **can lead to increased pore radius and resealing time** [32,33] (time needed for the membrane to recover, if the permeabilization is reversible). Moreover, applying an **electric field during a long duration** ($\Delta t_{pu} > 1 ms$) also leads to **electrophoresis**. Electrophoresis is the transport of charged species toward the opposite charged electrode. **This effect contributes to the diffusion of small charged species across the membrane** [34]. In some medical applications, pulses of different durations (nano-micro and millisecond) are combined, first short pulses of high intensity to permeabilize the membrane and then long pulses with low intensity to enhance gene or drug transport

[35]. In addition to electrophoretic effects, **millisecond pulses can be applied in order to weaken cell mechanical resistances** such as cytoskeleton [7] or cell wall [23]. **The knowledge about the impact of PEF on mechanical resistances is still limited** whether in theoretical or experimental approaches.

11e) Applications

Membrane permeabilization by PEF is used in several domains and applications. Historically, **PEF was used to introduce foreign substances such as DNA into cells** [36]. This process has been extended **towards electro-chemotherapy for drug delivery into tissue cells** [30,37]. PEF is also applied in food processes: for the **treatment of fruit juice** [38,39] in **substitution of heat pasteurization** [40,41], to **extract sugar from beets** [36,42] or **pigments from potatoes** [43]. Various applications of reversible and irreversible permeabilization are illustrated in Figure 8. Some concrete examples of PEF applications for food industry, biomedical engineering and environment are presented in Figure 9.

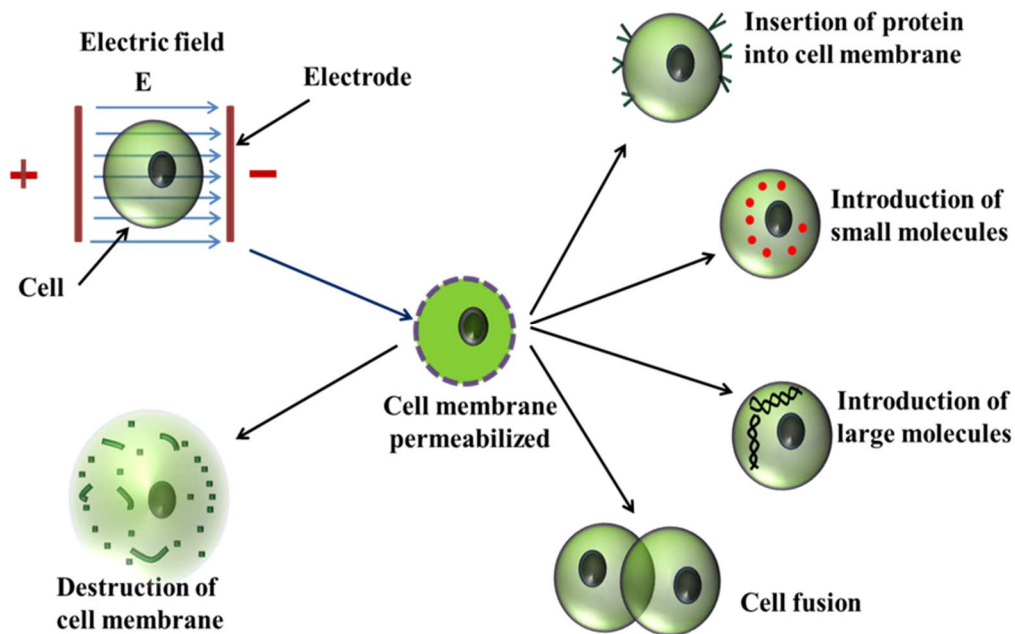


Figure 8: Different applications of single cell electroporation. When applied electric field reaches the threshold value of the cell membrane $\Delta\psi_{crit}$, then cell membrane can permeabilized to deliver protein, small and large molecules inside the cell. If two single cells are close to each other, then cell fusion can occur. To apply an intense electric field, which exceeds certain critical value, irreversible electroporation can occur resulting cell membrane rupture and finally cell death from [37].

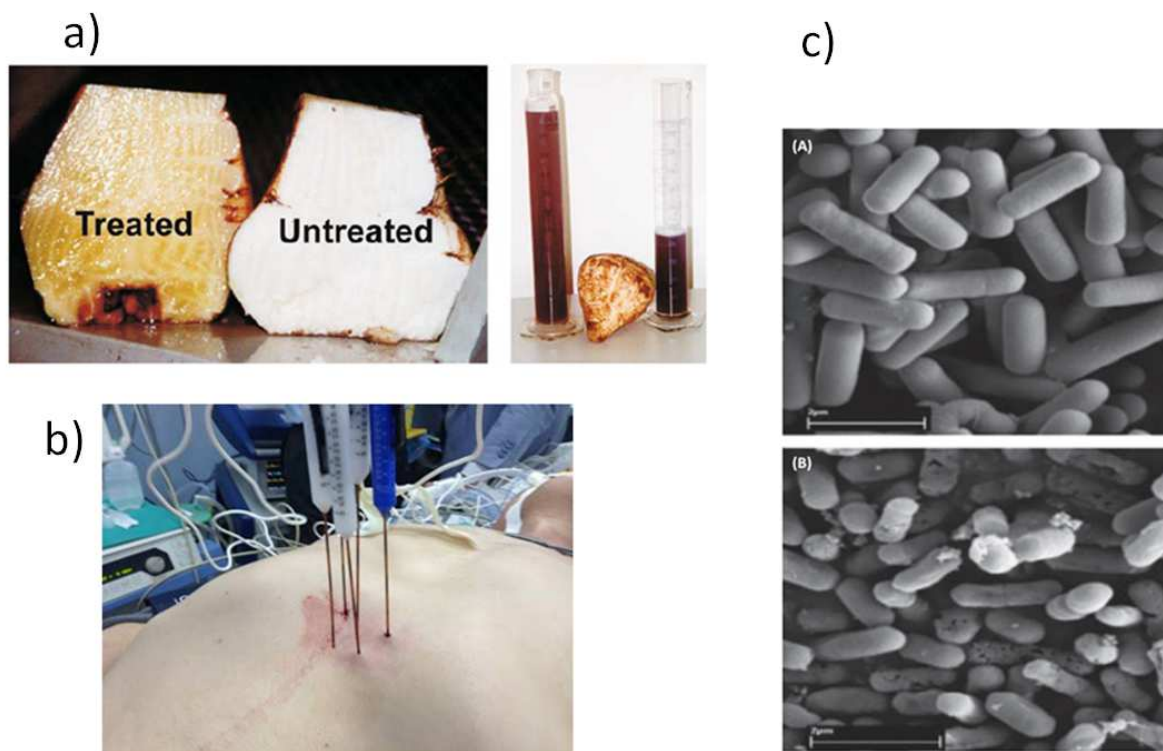


Figure 9: a) PEF treated/untreated sugar beets and corresponding yield of juice obtained by cold pressing with 32 bar pressure for 15 minutes [44]. b) Nanoknife technology: treatment of cancer tissues by irreversible electroporation [45]. c) Bacteria before and after PEF treatment observed by scanning electron micrographs (7.5 kV/cm, 4 ms pulses, scale bar: 2 μ m) [46].

12) Use of PEF in algae biotechnology

Despite the high potential of microalgae applications, **several technological and economical bottlenecks must be overcome before large-scale production of biodiesel from microalgae** takes place. It is now clearly recognized that the downstream processes (harvesting/dewatering and lipids extraction steps) have a high environmental footprint and impact negatively the cost efficiency of the whole process. The development of innovative and environmentally friendly downstream processes is thus of utmost importance (see Chapter 1).

As for superior plants, **PEF may be a breakthrough technology which can change dramatically the downstream processes used for the fractionation of valuable compounds from microalgae**. There are indeed three main challenges in the current used downstream technologies: (1) **reducing the energy** associated with algae dewatering and extraction of the target compounds, (2) **reducing the environmental impact** of the whole process and (3) **avoiding the degradation of the valuable compounds and recovering them separately**.

The use of PEF for algae fractionation in various valuable compounds has a high potential and is illustrated in Figure 10 [46].

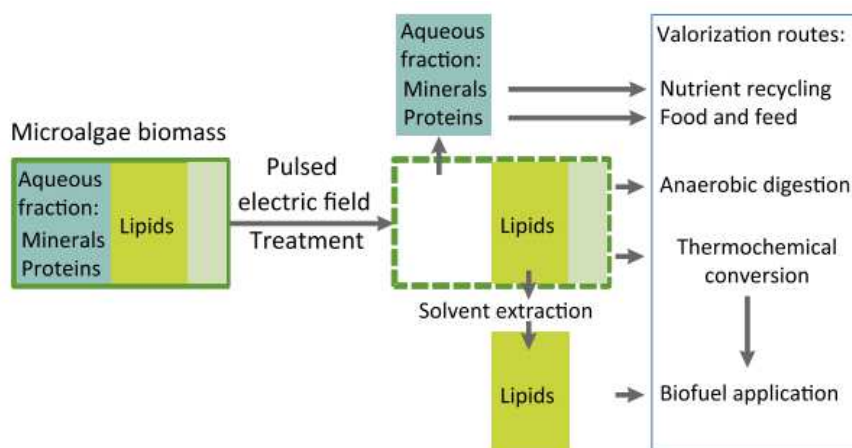


Figure 10: PEF treatment of microalgae biomass [46]. After treatment, the aqueous fraction is released into the extracellular medium, whereas lipids may require further solvent extraction. The biomass residues may then be used in thermochemical conversion and for methane production. New processing route combinations for complete microalgae biomass valorization are then possible.

Various studies have recently emerged to evaluate the use of PEF to improve the extraction of valuable compounds from microalgae, mostly hydro-soluble proteins and lipids. The treatment conditions may greatly vary depending on the target compound and strain. **The impact of treatment parameters such as pulse duration and amplitude, pulse number and shape, frequency on extraction remains unclear as PEF is a very young process in plant/microalgae technology** [44]. Some studies are performed on diluted culture media (wet extraction) and in low conductivity buffers; others deal with algae pastes obtained after pre-concentration or water extraction. Several studies describing the application of PEF on eukaryotic algae cells to recover target compounds are briefly presented hereafter and summarized in table 1.

Table 1: PEF conditions for the extraction of valuable compounds

Study	Pulse duration (μs)	Electric Field ($\text{kV}\cdot\text{cm}^{-1}$)	Pulse shape	Pulse number	Strain	Cell diameter (μm)	Target compound
1 [25]	0.36	45	Exponential decay	7 200	<i>Ankistrodesmus falcatus</i>	2.5 large 36-65 long	Lipid
2 [20]	1	23 - 43	Square	20 - 110	<i>Auxenochlorella protothecoides</i>	5 - 8	Proteins Carbohydrates
3 [22]	6 - 150	10 -25	Square	50	<i>Chlorella vulgaris</i>	2 - 4	Carotenoids
4 [47]	10	20	Exponential decay	1 - 600	<i>Nannochloropsis</i>	2 - 3	Proteins
5 [48]	100	2.7	Square	21	<i>Chlorella vulgaris</i>	2 - 4	Lipid
6 [23]	2 000	3-6	Square bipolar	30	<i>Chlorella vulgaris</i> <i>Nannochloropsis</i>	2 - 4 2 - 3	Proteins

- **Zbinden et. al** [25] (study 1) obtained a significant **enhancement in the rate of lipid recovery** with ethyl acetate when using PEF compared with the control (without PEF and in the presence of the solvent). This result was certainly linked to the high cell lysis (90%) observed. The total energy input was estimated at 42 J/mL (11 kWh/m³) for 1.9 g/L of algae.
- **Goettel et. al** [20] (study 2) observed an increase **in conductivity of the treated suspension** (from 0.6 mS/cm to 3 mS/cm 2 hours after PEF treatment), revealing the **release of ionic**

substances from the cells. In addition, carbohydrates and proteins were drained out of the cell. The temperature increase was of 15.5°C for an energy input of 100 kJ/kg_{sus} (36-167 g dry weight per kg suspension). **Lipids were not excreted** at all despite their high amount in the cells.

- **Luengo et. al** [22] (study 3) **studied PEF coupled to ethanol extraction to recover pigments from *C. vulgaris*** [49]. The best extraction yields of carotenoids, chlorophyll a and chlorophyll b were obtained 1h after PEF (20 kV·cm⁻¹, 75 μs pulses). The extraction of carotenoids, chlorophyll a and chlorophyll b increased by a factor of 1.2, 1.6 and 2.1, respectively, compared to the control, as a result of an **irreversible electroporation**. Reversible permeabilization was obtained when using less drastic conditions: 50 pulses of 3 μs with an electric field of 10 kV·cm⁻¹.
- **Parniakov et. al** [47] (study 4) observed that a **PEF pre-treatment could be efficient to extract ionic components and water soluble proteins**. PEF was however less efficient than sonication for pigment extraction, but with a lower energy consumption.
- **Flisar et. al** [48] (study 5) **compared PEF with solvent extraction (chloroform/methanol) for lipids recovery** (0.43 g lipid/g dry biomass). The cells treated by PEF in a flow chamber were left in a refrigerator for 1 week; **oil was then recovered at the surface of the medium**. The application of 10, 20 or 40 pulses (corresponding to 7.2, 14.4 and 28.8 kJ/L) gave a yield of respectively 23, 31 and 32 %, compared with solvent extraction alone (100 % extraction).
- **Coustets et. al** [23] (study 6) **demonstrated that protein extraction from species of *Nannochloropsis* and *Chlorella* was more efficient with PEF compared with the control, by a factor 5 -10**. The tests were performed in pure water to reduce heating effects (100 μS/cm for *Nannochloropsis*, 200 μS/cm for *Chlorella*) and the electric field strength was adapted to each strain (6 kV/cm for *Nannochloropsis*, and 3 kV/cm for *Chlorella*). The use of a high-ionic strength buffer was shown to improve protein extraction from *Chlorella vulgaris* compared to pure water. Moreover, according to the authors, improvements in extraction were obtained when re-suspending *Chlorella* samples in glycerol and dithiothreitol in order to increase wall porosity.

The previous data clearly demonstrate that **conditions to permeabilize algae cells using PEF are highly dependent on microalgae strains properties** (species, size, ...) and medium conditions (cell concentration, medium properties, ...). Besides, **PEF showed positive effects in extracting various compounds from microalgae, such as lipids, proteins, pigments and carbohydrates**. Improvements in extraction yields were obtained when using media containing compounds that strongly increase cell wall porosity.

In the specific case of **lipids**, they seem to be **highly restrained by the cell wall**. An enhancement in lipid extraction was observed when using an **organic solvent coupled to PEF** [25] or PEF alone [48] as hydrophobic lipids coagulate and float on the surface after cell lysis.

Additionally, **the temperature increase during the PEF treatment may have a major role both on solvent transport and cell wall structure**. In some works, the cells are re-suspended in **low**

conductivity media in order to reduce the thermal effects [23,47] but this requires an additional step in the process which is not recommended in higher scale systems.

13) Use of bio-micro-devices to monitor algae cells *in situ*

The use of **micro-devices** for algal biotechnology was greatly increased in the recent years **to help understanding complex phenomena at the cell scale**. Some research works describing the application of such tools for the study of microalgae are presented hereafter.

13a) Cell culture monitoring on a chip

Matsumura et. al [50] monitored **cell division of *Chlamydomonas reinhardtii* over time using a single-cell cultivation** system with several micro-cultivation chambers . Nutrients were continuously supplied in order to mimic an optimal growth environment.

Min et. al [51] used a **PDMS microfluidic device to apply a compressive stress on *Chlamydomonas reinhardtii* cells** in 2 - 2.5 μm high micro-channels (Figure 14.a). This mechanical stress induced a physiological response, increasing the lipid content of the cells and modifying cell growth patterns.

In another study, **Kwak et. al** [52] designed a complex microfluidic system made of multiple layers of PDMS where the culture medium was supplied by a central inlet, to **cultivate various strains of oleaginous algae in growth or stress conditions and to perform lipid extraction *in situ*** (Figure 14.b).

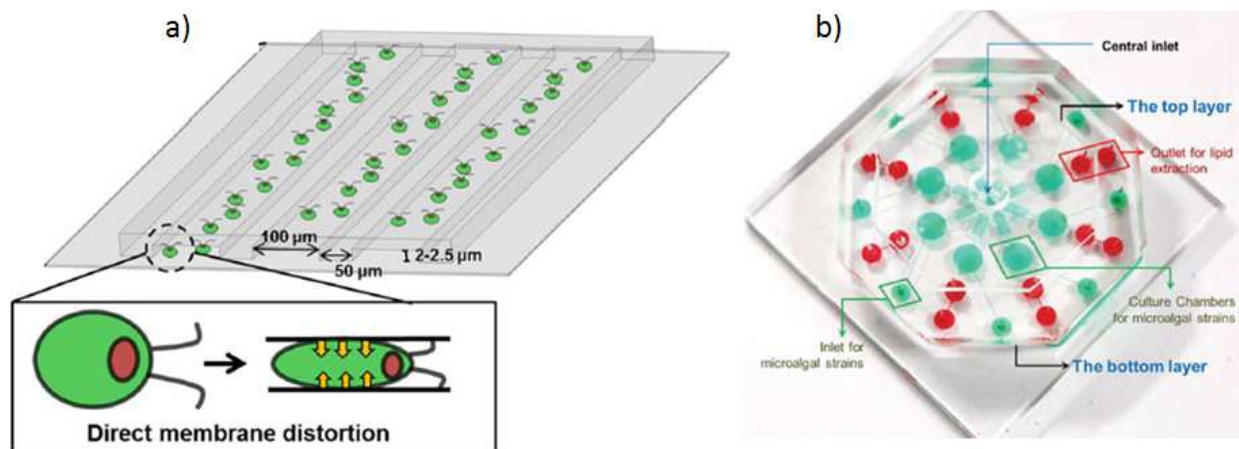


Figure 11 Examples of microfluidic systems to study *Chlamydomonas reinhardtii*. a) Study of the impact of membrane distortion on the physiology of *Chlamydomonas reinhardtii* [51] and b) [52] a multiplex microfluidic for the screening of oleaginous strains - with integrated harvesting and purification (solvent injection) steps.

13b) Investigation of dielectric properties

The **dielectric characteristics** of cells can be determined using **bio-impedance measurements** [53] *in situ*. In this context, the micro-devices are used to trap cells near electrodes.

The characterization is performed by measuring the **electromechanical behavior of the cells subjected to alternative electric fields** as the cell will undergo **dielectrophoresis forces (DEP)**. DEP are dependent on a key parameter, named Clausius Mossotti factor f_{CM}^* .

$$f_{CM}^* = \frac{\varepsilon_p^* - \varepsilon_m^*}{\varepsilon_p^* + 2\varepsilon_m^*} \quad (3.9)$$

The **Claussius Mossotti** complex factor depends on the **complex permittivities** difference between the medium ε_m^* and the particle ε_p^* . The latter can be expressed as follows:

$$\varepsilon_p^* = \varepsilon_{memb}^* \frac{\left(\frac{r}{r-d}\right)^3 + 2\left(\frac{\varepsilon_{cyt}^* - \varepsilon_{memb}^*}{\varepsilon_{cyt}^* - 2\varepsilon_{memb}^*}\right)}{\left(\frac{r}{r-d}\right)^3 - \left(\frac{\varepsilon_{cyt}^* - \varepsilon_{memb}^*}{\varepsilon_{cyt}^* - 2\varepsilon_{memb}^*}\right)} \quad (3.10)$$

with r cell radius, d membrane thickness, ε_{cyt}^* the complex permittivity of the cytoplasm and ε_{memb}^* the complex permittivity of the membrane.

Monitoring algae cells submitted to different electric field frequencies in media of various conductivities enables to **evaluate the cytoplasm conductivity**. Indeed, when the real part of the **Claussius Mossoti** factor is **positive**, the cells are **attracted by high electric fields**, *i.e.* near the electrodes. When the real part of the Clausius Mossoti factor is negative, cells are rejected to low electric fields, *i.e.* far from the electrodes. Data from one experiment performed at the lab demonstrates this statement (Figure 12).



Figure 12 : *Chlorella vulgaris* cells in negative DEP at 50 kHz (a) and positive DEP at 100 kHz (b). Distance between the electrodes: 25 μm . (c) device used for the experiments. Electrodes in platinum, square chip in silicon (size: 2.5 x 2.5 μm)

The study of DEP forces can be an innovative tool to **detect cells with high lipid content or even to separate** [54] them from the other cells as the **cytoplasm conductivity is reduced when the cell accumulates neutral lipids** [15,55].

Another innovative single cell spectroscopic method, named **electro-rotation**, based on the effect of the **dielectrophoretic torque generated by rotating electric fields** (Figure 13), links the **rotational behavior** (rotation speed, sense of rotation) with the **dielectric properties** of the cell.

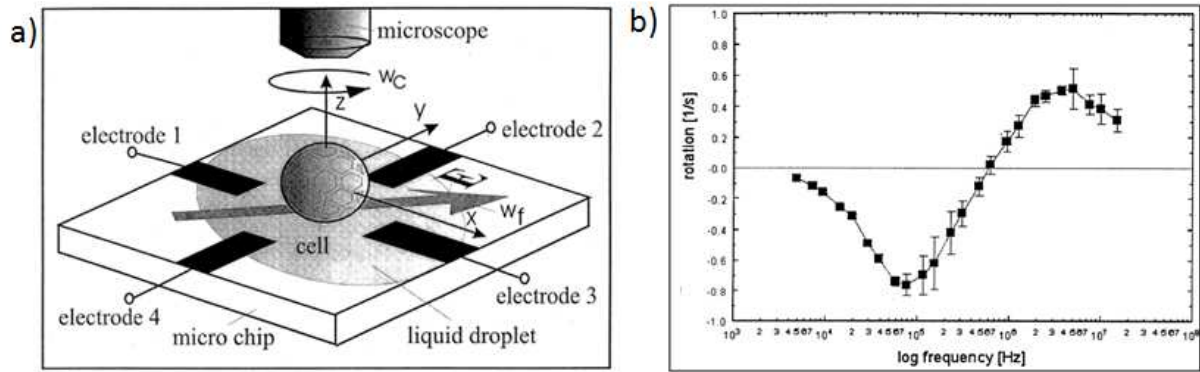


Figure 13: a) Scheme describing the electrorotation technique [56]. Four electrodes, processed by photo-lithography, are radially arranged and driven with four 90°-phase-shifted signals producing a rotating field. Angular velocity of the cell is measured via a microscope. b) Rotation spectra of algae at field strength of 20 kV/m on zygotes of *Chlamydomonas nivalis* measured at 4°C.

Measuring the rotational spectra of a single algae cell and its protoplast (wall-free cell), in dedicated microdevices, enables one to **determine conductivity, permittivity and thickness of cell wall, membrane and cytoplasm** [56]. Such measurements can also be used to characterize the **cell properties before/after permeabilization** [57].

13c) Investigation cell lysis *in situ* via DEP forces

Other devices are used to study cell permeabilization coupled to DEP inducing conditions. In the study of Bahi *et. al*, a microdevice was used to **visualize *in-situ* permeabilization** of the toxic marine microalgae *Karenia brevis* [58]. **Permeabilization was performed with an alternative electric field of 30 kV/cm at a frequency of 600 kHz** which also attract the cells to the electrodes with a DEP force.

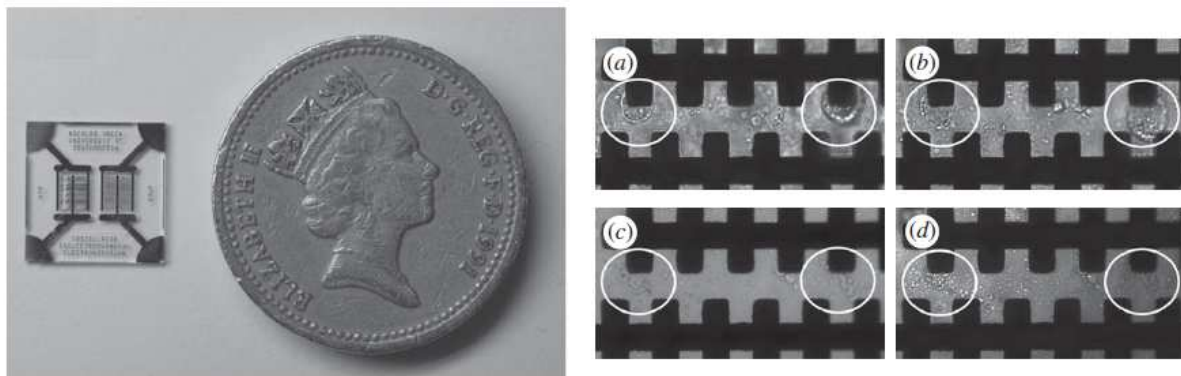


Figure 14: Left: Image of the microchip next to a UK pound coin for size reference. Right a) *Karenia brevis* cells trapped on the electrodes (white circle) with positive DEP with 1 V field at 200 kHz for 20 s. Electroporation of 60 V (30 kV/cm) field at 600 kHz for 5 s (b), 10 s (c) and 15 s (d) [58]. Electrodes are made with a 200 nm platinum layer on a glass substrate. Electrode distance: 20 μm .

Figure 14 shows the deconstruction of the cell membrane and cytoplasm leakage in a wall deficient strain.

II. Material and methods

II.1) Micro-device for studying the in situ permeabilization and characterization of *Chlamydomonas reinhardtii*

To better understand the **impact of PEF on *Chlamydomonas reinhardtii***, a dedicated micro-device was built. Effects on a single cell or **on a small population of algae cells were monitored**.

The bio-device was designed to **trap microalgae in visualization chambers**. The cells were monitored by microscopy, **in bright or fluorescence fields**, before, during and after application of PEF.

The **chambers** were made of a thick photoresist as detailed hereafter and were **placed above a parallel electrode network**.

The biochip, illustrated in Figure 15, consisted of two layers: an **electric layer to deliver pulsed electric fields and a fluidic layer to trap the cells**. It was fabricated using a conventional micro-fabrication process in a **clean room** [59].

For the electrodes, a **20 nm chromium adhesion layer**, covered by a **150 nm gold layer**, was sputtered on a quartz substrate. A first **photolithography** step was employed **to pattern** the electric layer. This process includes the deposition of **S1805 Shipley photoresist** by spin coating ($t = 30$ s, $v = 1000$ rpm), followed by a prebaking (115 °C, 1 min) and UV exposure (365 nm, intensity = 120 mJ·cm⁻²) (Figure 15.a). A developing step was then performed (developer 351, 1min) (Figure 15.b), followed by **gold etching** with KI (4 g KI, 1 g I₂, 40 mL H₂O, 7 s) and **chromium etching** (ChromeEtch18 micro resist technology, 45 s) (Figure 15.c). Photoresist removal was done using acetone and isopropanol (IPA).

The **microfluidic level** was patterned with a second photolithography step: the **25 μm high microfluidic chamber** was defined by negative thick photoresist (SU8 2025, Microchem©) spin coated in two steps: 5 s at 500 rpm and 30 s at 2700 rpm. A soft-baking (3 min at 65 °C and 15 min at 95 °C), followed by UV exposure (365 nm, intensity = 240 mJ·cm⁻²) (Figure 15.d) gave the pattern for the micro-device design (Figure 15.e). A post exposure baking was then performed (3 min at 65 °C and 15 min at 95 °C) before development (MicroChem © SU8 developer, 6 min) associated to a hard-baking step (175 °C, 30 min, slope 5 °C·min⁻¹) to fix the thick resist level (3h).

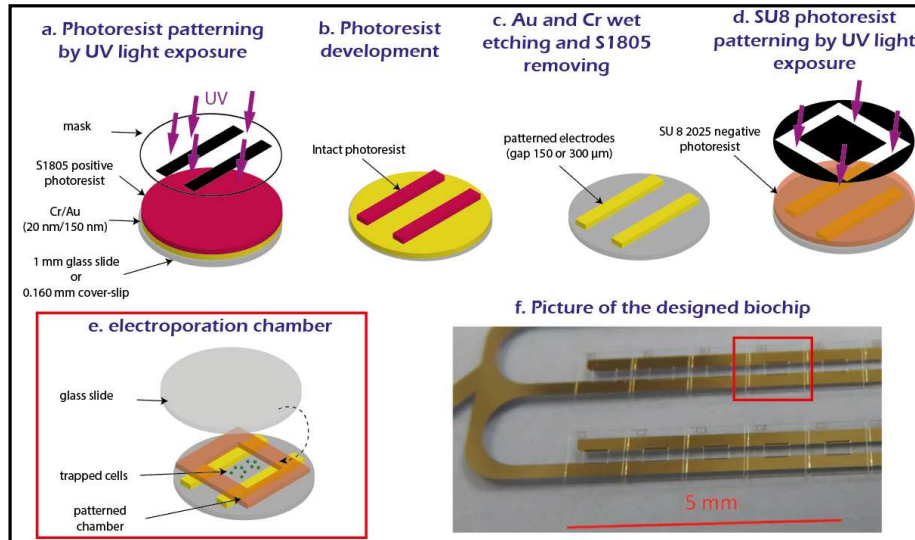


Figure 15: Microfabrication process of the biodevice. The electrode layer is patterned on a glass substrate in 3 steps: photoresist patterning by UV light exposure (a), photoresist development (b), and Au/Cr wet etching and photoresist removing (c). A fluidic layer is patterned above the electrode layer by a second UV light exposure (d) to obtain several multiple electroporation chambers shown on the scheme (e) and picture (f).

The electrode gap was small enough to achieve high electric fields [60], up to $30 \text{ kV}\cdot\text{cm}^{-1}$ and $60 \text{ kV}\cdot\text{cm}^{-1}$, with gaps of respectively $300 \mu\text{m}$ and $150 \mu\text{m}$ using an accessible voltage generator (up to 1 kV). Large chambers have an internal dimension of $720 \mu\text{m} \times 480 \mu\text{m}$, designed to be observed with a **20 x objective**. Small chambers possess an internal dimension of $360 \mu\text{m} \times 150 \mu\text{m}$ designed for observation with a **40 x objective** (Figure 16). The device was designed to be observed with a CMOS (Complementary Metal Oxide Semi-conductor) camera sensor $36.0 \times 23.9 \text{ mm}$ with a resolution 4908×3264 pixels (16.25 megapixel) equipped with a mount F type with 2.5 x magnification T2-T2 SLR.

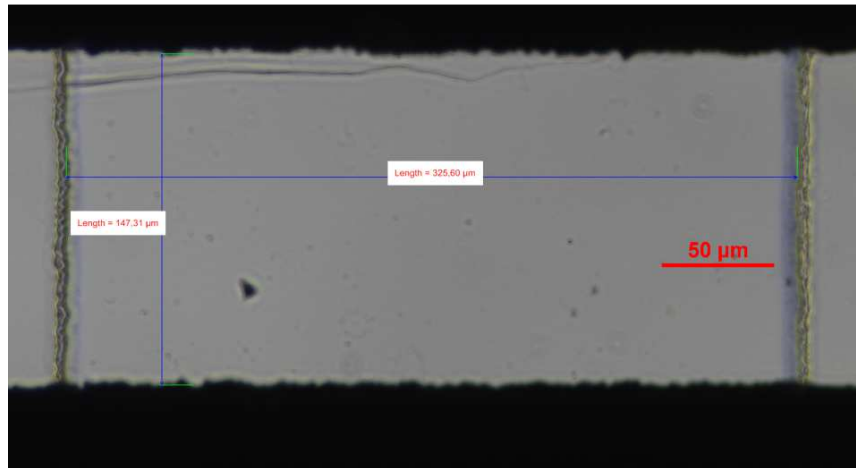


Figure 16 : Small chamber (x length: $325 \mu\text{m}$, z length: $147 \mu\text{m}$) observed with the 20 x objective.

The generator used was a **Betatech Electrocell B10 HVLV**. The generator characteristics are the following: $U = -1000$ to $+1000 \text{ V}$ (bipolar pulses), $\Delta t_{pu} = 5 - 50,000 \mu\text{s}$ (pulse duration), $T_i = 5-50,000 \mu\text{s}$ (duration between positive and negative pulses), P (period of one pulse cycle) ranging $80 \mu\text{s}$ to 10 sec , burst of pulses: $1 - 10,000$ pulses.

The **microfluidic layer** (white layer in Figure 17.a) was designed as a set of **6 lines of 15 chambers for a total of 90 numerated closed chambers**. There were 3 lines of 45 large chambers (gap of 300 μm) or 3 lines of 45 smaller chambers (gap of 150 μm) as illustrated in the figure. The electric layer (orange layer in Figure 17.a) connects the various chambers with parallel electrodes. The electroporation micro-device was connected to the pulse generator by a homemade supporting base fastened above the microscope objectives and designed to support up to 2 kV DC voltage (Figure 17.b).

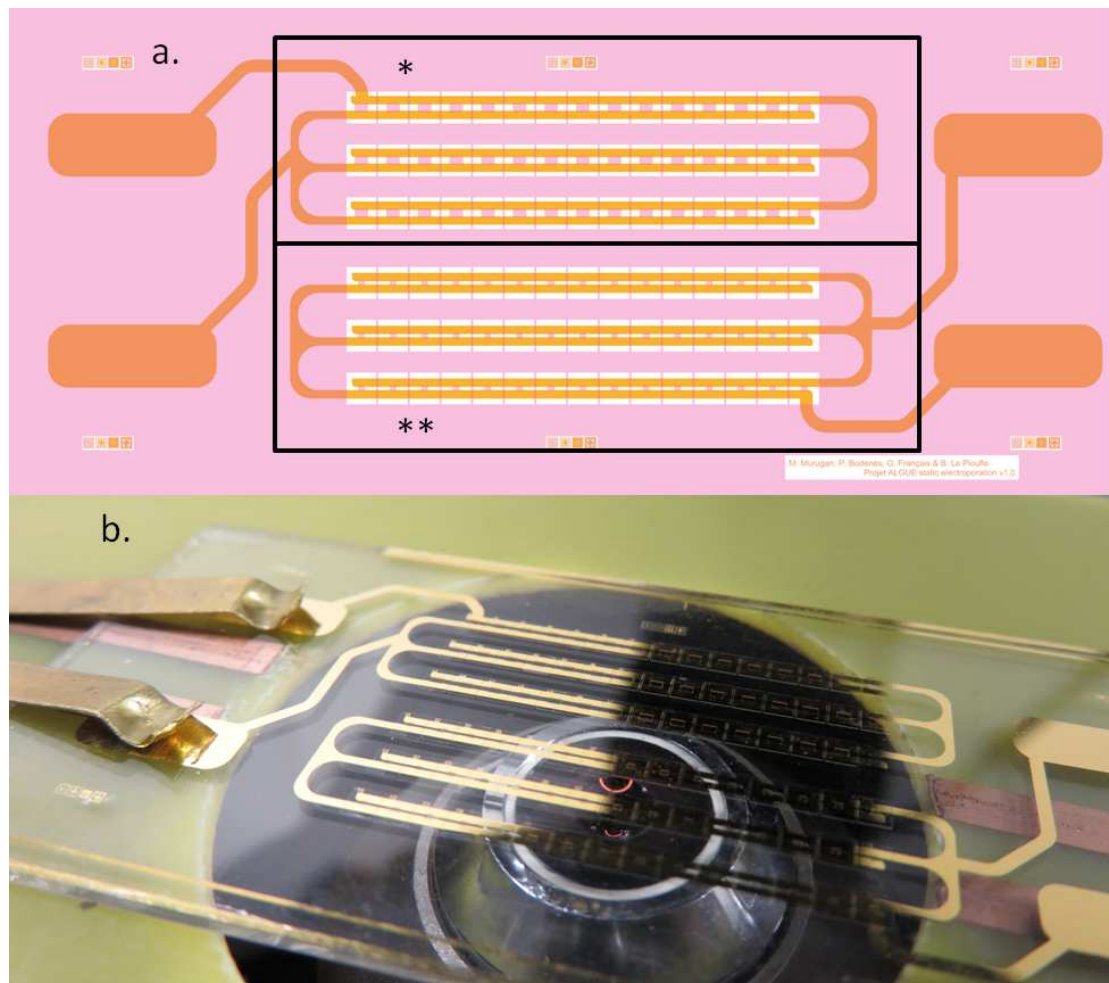


Figure 17 a. Scheme of the overall design of the electroporation micro-device. Orange: electric level, white: fluidic level. (*) 45 large chambers (internal dimensions: 720 μm x 480 μm , electrode gap: 300 μm) designed to be observed with a 20 x objective, (**) 45 small chambers (internal dimensions: 360 μm x 150 μm , electrode gap: 150 μm) designed to be observed with a 40 x objective. b. Picture of the chip connected to the generator, placed above a microscope objective.

112) Electroporation in cuvettes

The use of dedicated micro-devices coupled with direct cell observation by microscopy gives a first **insight into the electroporation phenomena**. However, in order to further quantify **PEF effects** on cells (e.g. viability) and molecules extraction, **additional analyses** must be performed on cells recovered after electroporation. **Another electroporation device was then used.**

Electroporation cuvettes are plastic squared cuvettes made in transparent plastic which possess aluminum electrodes with a gap of 4, 2 or 1 mm (Figure 18). With this higher electrode distance compared with micro-devices (several millimeters instead of hundreds micrometers), the electric field which could be applied in such systems is **limited to 5 kV/cm (2 mm) and 10 kV/cm (1 mm)** (for the micro-device: 30 kV/cm with an electrode gap of 300 μm). **In the 2 mm and 1 mm cuvettes, 500 and 120 μL of cell suspension can be treated, respectively**

Electroporation cuvettes were used to perform **multiple complementary experiments to those carried out with the micro-device.**

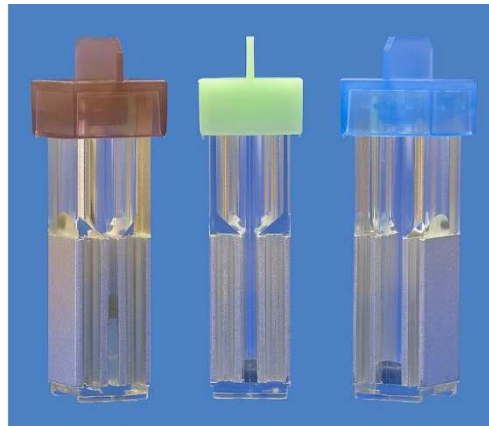


Figure 18 : Electroporation cuvettes.
Electrode distance: 1 mm, 120 μL (brown cap); 2 mm, 500 μL (green cap); 4 mm, 2 000 μL (blue cap).

113) Viability/permeability measurements

Cell viability and membrane permeability are among the parameters that were measured to assess the **impact of PEF** on microalgae cells.

In this context, chlorophyll autofluorescence is usually correlated with photosynthetic activity. According to the study of **Sato *et. al*** [61], the **fluorescence intensity** can be therefore **used to sort viable from non-viable cells** as non-viable cells greatly lose their fluorescence intensity as shown in Figure 19. Accordingly, viable cells are seen in red, from chlorophyll autofluorescence, and non-viable are detected in green from staining with a so called "viability dye": Sytox green (SG).

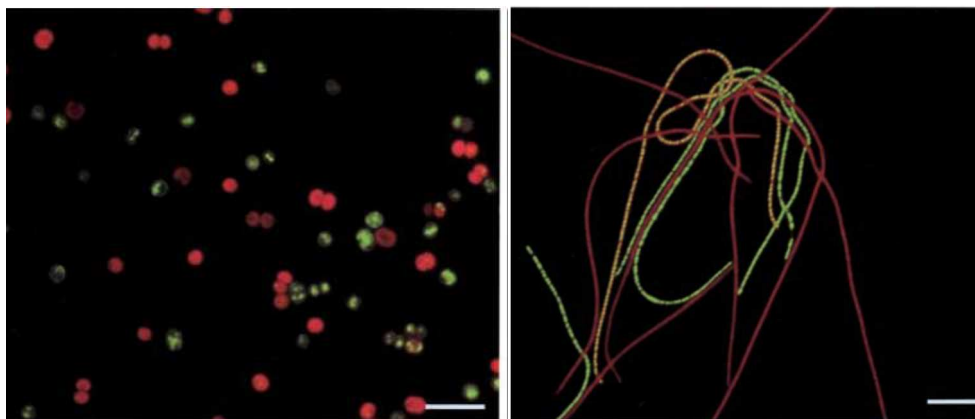


Figure 19: Images of cells showing SG fluorescence (non-viable, green) and pigments autofluorescence (viable, red) [61]. Sample contains 50% viable cells. Left: *Synechocystis* sp. (scale bar: 10 μm), right: *Oscillatoria agardhii* (scale bar 50 μm).

The use of **chlorophyll auto-fluorescence** to detect viability is **not suitable when the cells are in lipid inducing stress conditions** which greatly affect cell chlorophyll content. Several dyes can be used to sort viable and non-viable cells.

II3a) Choice of the dyes

Several fluorescent dyes can be used to monitor cell viability and membrane permeability. Hyka *et al.* [62] published a review of the dyes used in algae biotechnology with different targets: **permeability** (staining of nucleic acid in permeabilized cells), **membrane potential** (potentiometric probes) and **cellular enzyme activity**; **all these methods can be associated with cell viability**. The list of dyes is presented in appendix II.1 (Chapter 2).

Four probes were tested in this project using microscopy and flow cytometry methods: two permeability dyes, Propidium iodide (PI) and Sytox green (SG), and two enzyme activity dyes, Calcein-AM and Fluorescein Diacetate (FDA) were used.

Propidium Iodide and **Sytox Green** are molecular probes that **bind to DNA in the cells**. However, because of their high molecular weight (PI, 668; SG, 600 Da [63]), **they cannot pass through intact membranes to stain the cell DNA**. They are then mostly used **to sort non permeable cells**, generally associated with viable cells, **and permeable or non-viable cells**. In the case of electroporation, **cells can however be permeabilized for a very short time without affecting viability**.

The use of PI (ex. 536 nm/em. 636 nm) to evaluate cell permeability through flow cytometry was not appropriate in our work. In fact, **the optimal excitation wavelength for PI is 536 nm** and the **blue laser of the flow cytometer** used for this study **emits light at 488 nm**. Moreover, **PI fluorescence may overlay with chlorophyll auto fluorescence** excited at 488 nm [62]. This problem may be overcome when using **adapted laser or filters to excite PI in the orange spectrum which increases the selectivity of PI over chlorophyll**.

The non-fluorescent dyes **FDA** and **Calcein AM** passively diffuse into the cells and are **hydrolyzed by cellular enzymes to form polar fluorescent** molecules; these molecules remain in the cells if their **cytoplasmic membrane is intact** [62]. Therefore, these dyes indicate at the same time **enzymatic activity and membrane permeability**.

On the other hand, **when using flow cytometry to evaluate permeabilization in cuvettes, SG was preferred as previously discussed** (excitation at 488 nm). **FDA** was used to evaluate **enzymatic activity**.

When choosing dyes, it is important to verify their compatibility with the equipment (laser, lamps, photomultiplier). If a multiple staining is planned, the **compatibility of the dyes between themselves and with pigments auto-fluorescence must be evaluated** to avoid an overlapping of the fluorescence spectra in the detection channels.

It is highly recommended to use a **spectra viewer tool** to verify that the dyes are correctly excited, as close as possible to their maximum excitation peak and to use a detector band in the optimal emission spectrum, as previously reported (Chapter 2).

The **optical configuration** of our Merck flow cytometer is illustrated in Figure 20 with the **blue laser** at 488 nm and the **green, orange and red detectors**. It can be clearly seen that a green dye, such as **FDA**, **is adapted to our device**. Indeed, the **laser matches with the green dashed excitation spectrum**, and the **green detector perfectly corresponds to the emission spectrum**. **PI is excited with the blue laser** but **not at its optimal excitation wavelength** (shown in orange dashed line). This will result in a low emission (orange line) which is poorly adapted to our detectors. Emission in the red region will overlap with chlorophyll autofluorescence at 680 nm and the emission at yellow fluorescence is very low. Thus, this kind of orange dye such as **PI** (or Nile red in the case of lipid detection), **is not adapted** for a flow cytometer which possesses this optical configuration.

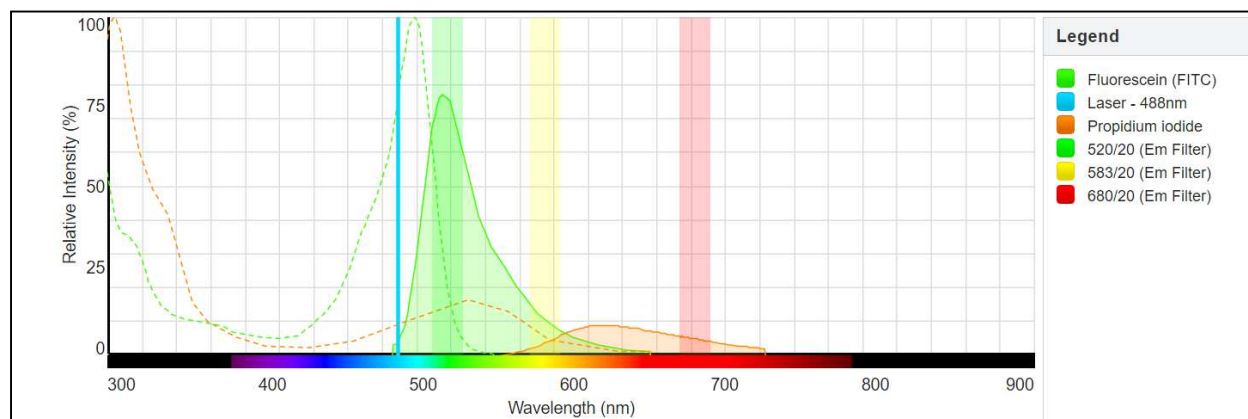


Figure 20: Excitation (dashed lines)/Emission (straight lines) spectra for two dyes: FDA (green) and PI (orange) for the optical configuration of the flow cytometer Easycyte 5. Optical configuration: 50 mW blue laser (488 nm), 3 fluorescence detector channels (525 nm, 583 nm and 680 nm).

Chlorophyll autofluorescence can be mimicked with the **Peridinin-Chlorophyll-Protein (PerCP-Cy5.5)** with the spectra viewer as shown in the Chapter 2. When comparing Figure 20 and chlorophyll emission peaks, **PI must clearly be detected before 650 nm**, when the emission of the chlorophyll is low. Light harvesting complex of *Chlamydomonas reinhardtii* also contains chlorophyll b [64] which may however be more problematic than chlorophyll a (chlorophyll a/b ratio of approximately 2.3 in

Chlamydomonas reinhardtii [65]). Carotenoids fluorescence may also interfere (chlorophyll/carotenoids ratio ranging from 4 in low light to 2 in high light conditions [65]).

Although flow cytometry is unsuitable to PI measurements, cell permeabilization by PEF in the **micro-device** coupled to microscopy was evaluated by **PI fluorescence**. The choice was based on the fact that PI is the most widely used dye to assess permeability. Moreover, in our study, special attention was paid to avoid the overlap of fluorescence of cell pigments and PI, *i.e.* by using an **adapted fluorescence filter**.

The **orange dye (PI)** can be detected with the optical configuration of the epi-fluorescence microscope: the light source is a Xenon lamp and the **fluorescence filters are FITC (485/530), CY3 (545/610), CY5 (620/700), and B2A (470/490+)** (in Figure 21). The xenon lamp gives a light on the whole visible spectrum from 350 to 870 nm.

Fluorescence filters enable to select a particular excitation band, discard the others and also detect the emitted fluorescence in a narrow band. The **excitation spectrum of the CY3 filter (530 - 560 nm)** very well matches with the excitation peak of PI; the resulting fluorescence is then high and adapted with the **emission range of the CY3 filter (573 - 648)**. If a double staining FDA (fluorescein)/PI is performed, FDA (FITC fluorescence) and PI fluorescence overlap at 600 nm because FDA is also excited with the CY3 filter, though not at its optimal wavelength.

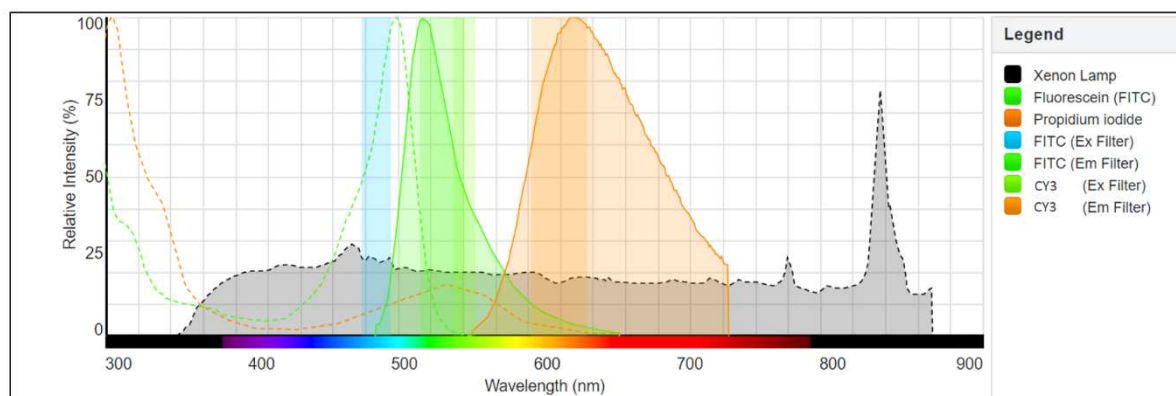


Figure 21: Excitation (dashed lines)/Emission (straight lines) spectra for two dyes: FDA (green) and PI (orange) for the optical configuration of the epi-fluorescence microscope used. Xenon lamp, fluorescence filters: Nikon FITC and Cy3.

This verification of the fluorescence bands was performed for all the dyes used for viability/permeability, lipid content and cell wall staining (see Chapter 2).

In conclusion, **viability (enzymatic activity) was measured with Fluorescein Diacetate (FDA)** while **membrane permeability was determined with either Propidium Iodide (PI) (microscopy) or Sytox Green (SG) (flow cytometry measurements).**

II3b) Determination of the optimal staining conditions

The **staining protocols** were optimized regarding the **amount of dye per cell** and the **incubation time** along with **optical parameters**, *i.e.* **fluorescence filter, lamp intensity, exposure duration and gain for microscopy, photomultiplier (PMT) gain and fluorescence threshold** in the case of flow cytometry.

The optimization of **PI and FDA protocols** is described hereafter.

PI staining conditions

The **PI stock solution** was prepared by diluting the molecule at a concentration of **1 g/L (1.5 mM)** in distilled water. PI concentrations within the range of 5 to 500 μM were tested on preheated *Chlamydomonas reinhardtii* at concentrations from **$3 \cdot 10^6$ to $1 \cdot 10^7$ cells/mL**.

From microscopic observations, the optimal conditions were found: PI concentration **100 μM** and incubation time **5 minutes**. Although PI stained DNA of permeabilized cells was efficiently observed at lower concentrations of PI, the visualization was better at 100 μM . At **higher PI concentrations, a significant fluorescence of the medium was observed**, with no improvement in the DNA staining. Confocal Laser Scanning Microscopy (CLSM) images showing PI stained DNA of a permeabilized *Chlamydomonas reinhardtii* cell are presented in Figure 22.

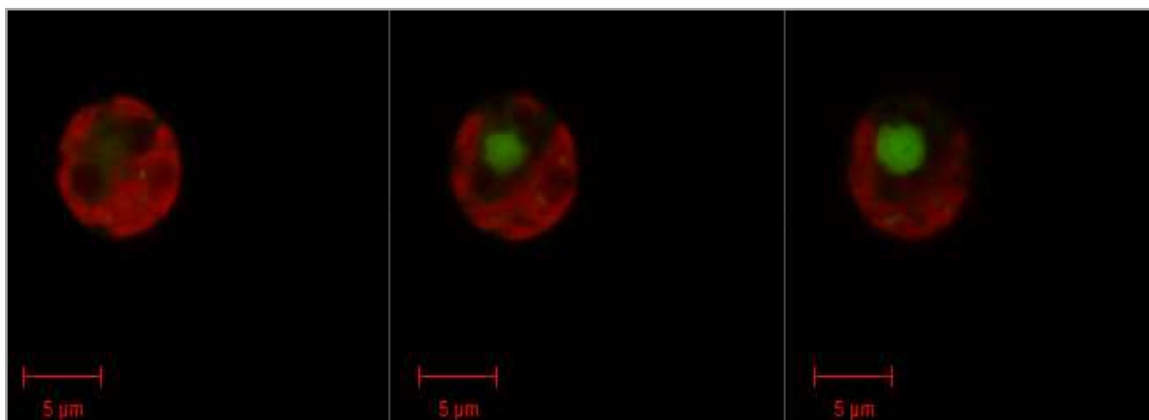


Figure 22 Depth stacks (from bottom to top) of a single permeabilized *Chlamydomonas reinhardtii* cell in growth phase stained with Propidium Iodide. Stained nucleus is shown in green, chlorophyll auto-fluorescence in red.

FDA staining conditions

FDA protocol optimization was performed using flow cytometry.

FDA was diluted in acetone at a concentration of 11 mM, as found in literature [66]. The FDA staining protocol was optimized on *Chlamydomonas reinhardtii* cells both in growth phase (Figure 23 a and b) and after seven days of lipid accumulation (Figure 23 c and d). The mean green fluorescence per cell was measured by flow cytometry for several incubation times and FDA concentrations.

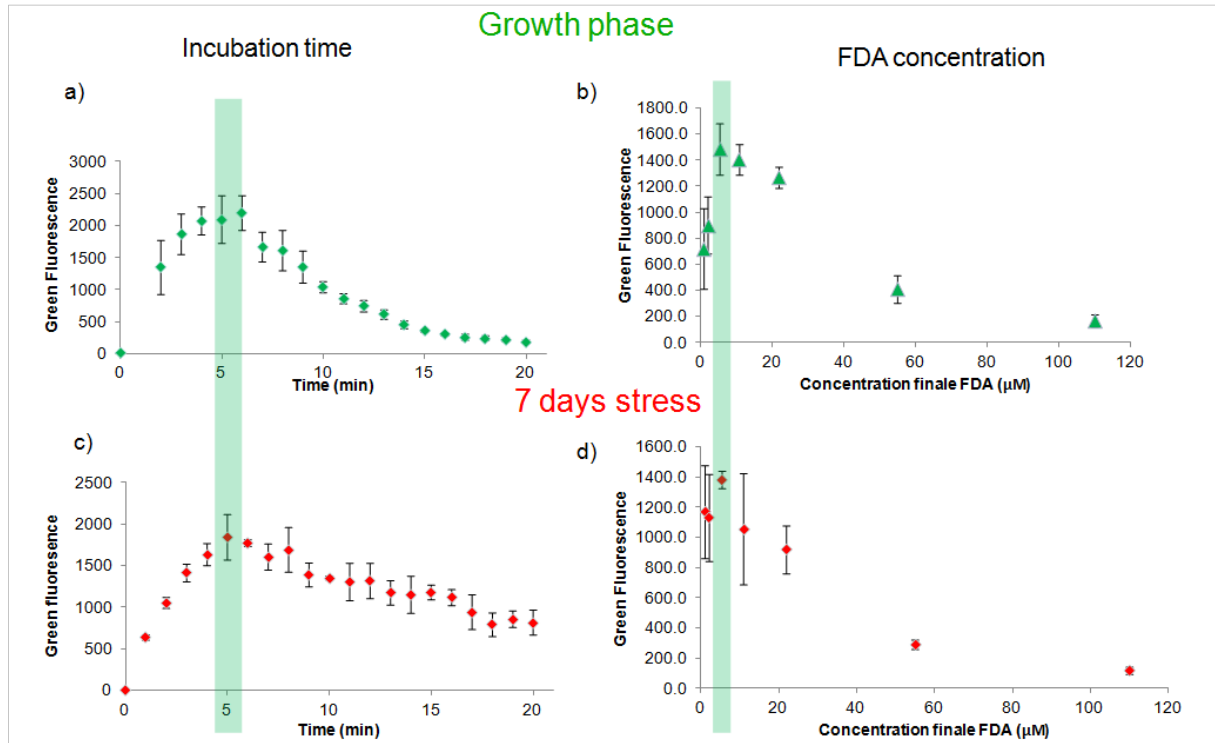


Figure 23 Optimization of the FDA staining protocol using flow cytometry regarding the green fluorescence per cell. Measurements were performed on *Chlamydomonas reinhardtii* cells in growth phase and stress conditions (7 days of nitrogen stress). Optimal conditions are indicated with the green rectangles. Growth phase a) incubation time: 5-6 minutes, b) FDA concentration: $5.5 \cdot 10^{-3} \mu\text{mol} \cdot \text{mL}^{-1}$ for a concentration of $1.5 \cdot 10^5 \text{ cells} \cdot \text{mL}^{-1}$. 7 days of stress c) incubation time: 5-6 minutes, d) FDA concentration: $5.5 \cdot 10^{-3} \mu\text{mol} \cdot \text{mL}^{-1}$ for a concentration of $1.5 \cdot 10^5 \text{ cells} \cdot \text{mL}^{-1}$

A decrease in the green fluorescence per cell is observed for FDA concentrations higher than $5.5 \mu\text{M}$ for both conditions. A significant **decrease in cell concentration after staining with FDA concentration higher than $55 \mu\text{M}$ was observed suggesting cell lysis**. Furthermore, cell disruption was confirmed to be due to **FDA and not to acetone** (FDA is indeed diluted in acetone).

Figure 23 also shows the impact of incubation time with a dye penetration in the first 5 minutes after staining and a slow release of the dye in the medium after this time [67]. The **optimal measurement time is thus 5 minutes after staining**.

In summary, the optimal incubation time was found within the range of 5 - 6 minutes and the optimal concentration is $5.5 \mu\text{M}$ for a cell concentration of $1.5 \cdot 10^5 \text{ cells} / \text{mL}$.

II3c) Validation of the PI and FDA optimal conditions

In order to validate the staining methods, samples treated with the optimized FDA and PI protocols were first observed by epi-fluorescence microscopy. Some cells were permeabilized and enzymes inactivated by heating the cells at 80°C during 10 minutes and a **mixture of non-treated and treated cells (equal proportion) was prepared**. Cells were successively stained with FDA and PI as previously described. Bright field, **green fluorescence (FDA)** and **red fluorescence (PI)** images observed with an objective 40x are presented in Figure 24. **Viable cells** detected with a **green** fluorescence are circled in green while the **dead cells** detected with a **red** fluorescence appear in red (detection with separated filters).

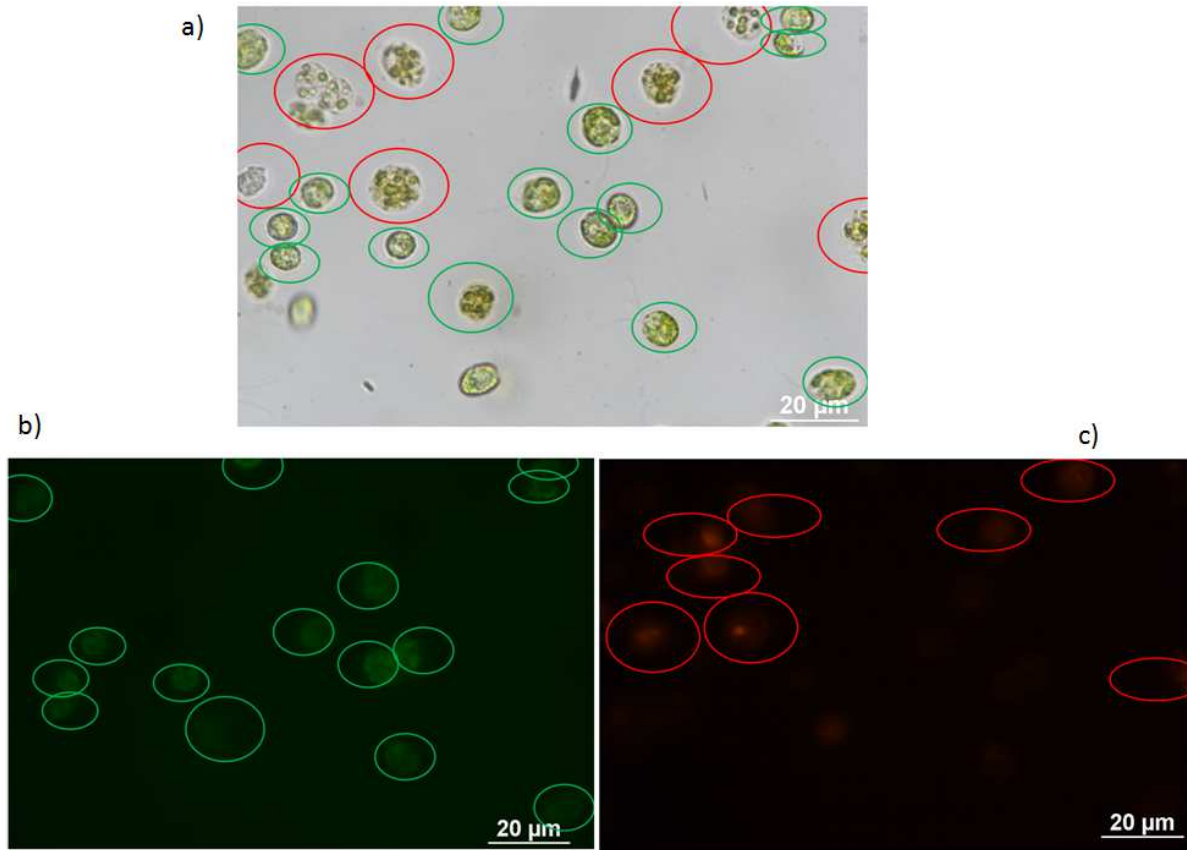


Figure 24: 50/50 mixture of *Chlamydomonas reinhardtii* dead /alive (cells in growth phase) stained with FDA and PI. a) Bright field, b) esterase enzymatic activity detected with the green fluorescence filter (FITC), c) Nucleus of permeabilized cells detected with the orange-red fluorescence filter (CY3). 13 living cells are detected for 8 dead.

As is can be seen in the bright field image (Figure 24.a), some cells (circled in red) appear less green and less structured than the others. Heat treated cells have indeed their photosynthetic apparatus and their cytoplasm membrane degraded, inducing a loss of structure, as it appears when they are stained with PI (Figure 24.c). The cells with a regular circular shape and bright green in the bright field image, circled in green, appear efficiently stained with FDA (Figure 24.b).

An observation of non-treated cells was also performed with an objective 20x on *Chlamydomonas reinhardtii* cells at 5 days of stress (Figure 25). In this sample, 19 cells are stained by PI and 120 with FDA, which indicates 86.33 % of viability.

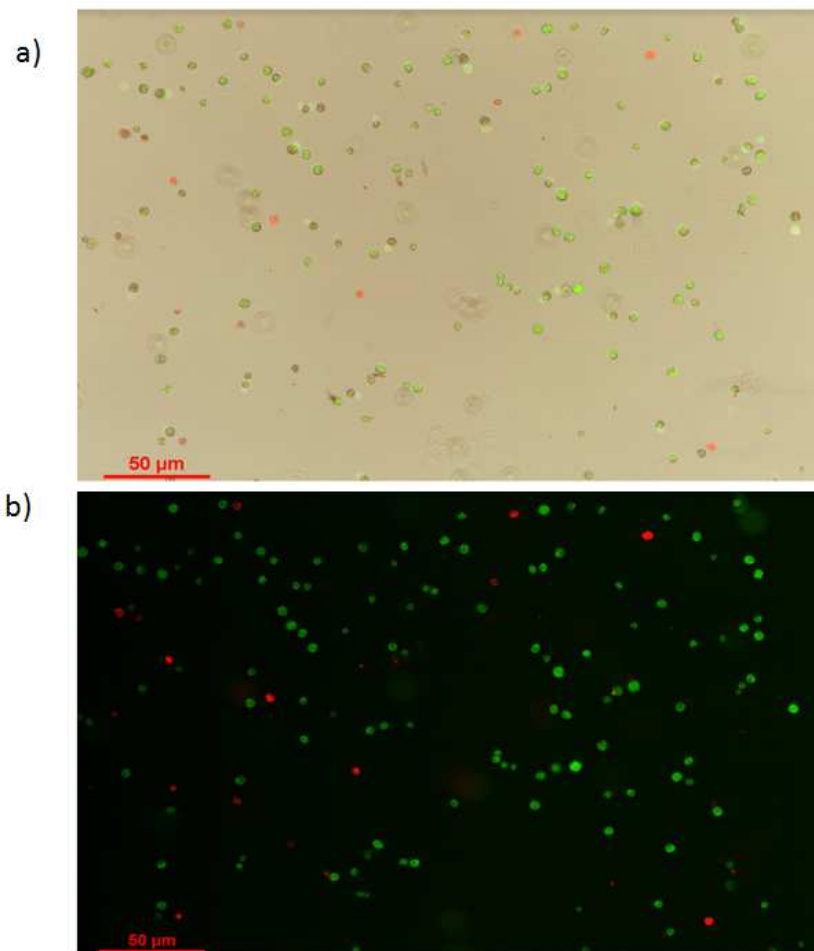


Figure 25: *Chlamydomonas reinhardtii* cells at 5 days of stress, stained with FDA and PI. a) bright field, green fluorescence and red fluorescence acquisitions merged in one image, b) green fluorescence and red fluorescence acquisitions merged in one image.

A manual counting of PI stained cells was used to estimate the permeabilization ratio of hundreds of PEF treated cells in micro-devices as reported later on. However, for rapid quantitative results on over thousands of cells, the flow cytometry method was preferred.

II3d) Development and validation of the staining methods by flow cytometry

As explained before, for FDA, in flow cytometry, the optimal incubation time was found within the range of 5 - 6 minutes and the optimal concentration is 5.5 µM for a cell concentration of $1.5 \cdot 10^5$ cells/mL.

The **Sytox Green protocol was also optimized using flow cytometry**. The commercial solution (5 mM in DMSO) is diluted in TAP medium to a concentration of 200 µM to prepare the stock solution. Finally, the **optimal concentration of SG was determined 0.5 µM for $2.5 \cdot 10^5$ cells/mL for an incubation time of 5 min.**

For the development of the methods in flow cytometry, both **viability and permeabilization fluorescence thresholds** (R4 Figure 27 for Sytox Green, R3 Figure 28 for FDA) were determined by mixing heat treated cells and non-treated cells at different ratios.

Unlike SG and PI which can be stained simultaneously on the same cell population (Figure 24), SG and FDA staining methods were performed separately in flow cytometry because both FDA and SG exhibit a fluorescence emission in the green and yellow fluorescence channels.

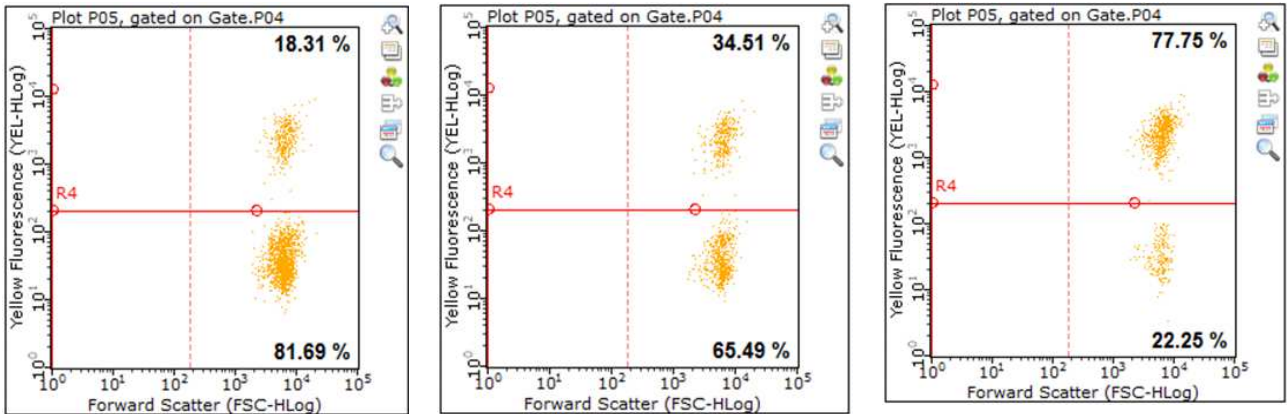


Figure 26: Mean yellow fluorescence (SG) of samples with different ratios of treated/non treated *Chlamydomonas reinhardtii* cells (7 days of stress) stained with SG. Permeabilized cells are stained by SG and their fluorescence is within the range of $8 \cdot 10^2$ to $1 \cdot 10^4$ a.u. while non stained cells have a fluorescence within the range of $1 \cdot 10^1$ to $1 \cdot 10^2$ a.u. A threshold R4 is fixed at $2 \cdot 10^2$ a.u. to discard non permeabilized cells on the bottom and permeabilized cells on the top of Plot 05. Theoretical permeability measured: 20 %, 30 %, 80 %.

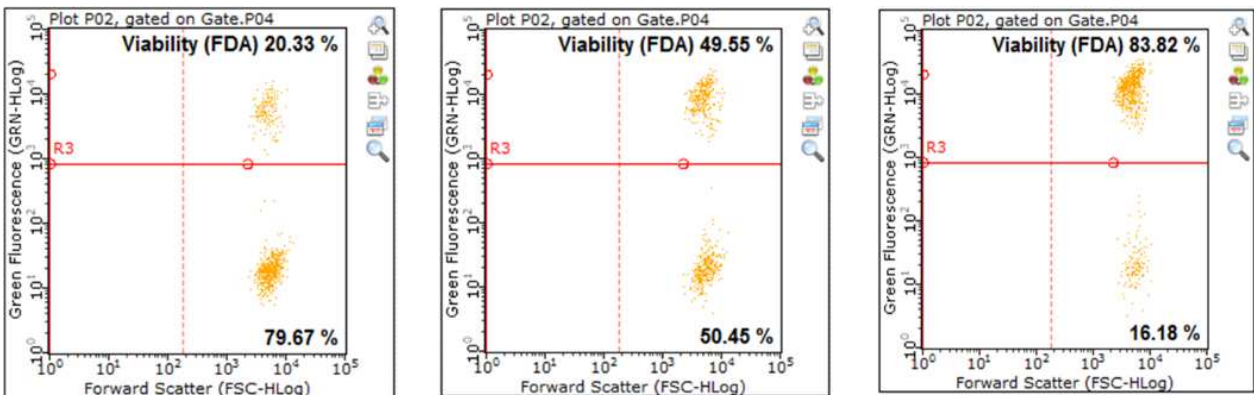


Figure 27: Mean green fluorescence (FDA) of samples with different ratios of treated/non treated *Chlamydomonas reinhardtii* cells (7 days of stress) stained with FDA. Cells with esterase enzyme activity and non permeable are stained by FDA, and their fluorescence increases within the range of $2 \cdot 10^3$ to $4 \cdot 10^4$ a.u. while non stained cells appear to have a fluorescence within the range of $5 \cdot 10^0$ to $1 \cdot 10^2$ a.u. A threshold R3 is fixed at $1 \cdot 10^3$ a.u. to discard non viable cells on the bottom from viable cells on the top of the Plot 02. Theoretical viability measured: 20 %, 50 %, 80 %.

It must be underlined that all these arbitrary fluorescence intensities and corresponding thresholds are highly dependent of the gains and sensitive optical settings that can vary over time: laser to detectors X/Y alignments, voltage of the 5 PMT detectors. Whether for FDA, SG or Bodipy staining, it is highly recommended to **verify the fluorescence in the different channels with calibrated beads** (Merck easy-check kit in the case of our device, even if beads of the size of algae would have been preferred) and adjust the optical settings if necessary.

The calibration curves correlating the measured and theoretical viability/permeability of samples at different ratios of heat-treated and non-treated cells are presented in Figure 28.

Accordingly, the viability and permeability measured with FDA and SG, respectively, fully correlate with the theoretical values.

All measurements were performed in triplicate. The average standard deviation for the triplicate is approximately 1% of viability/permeability.

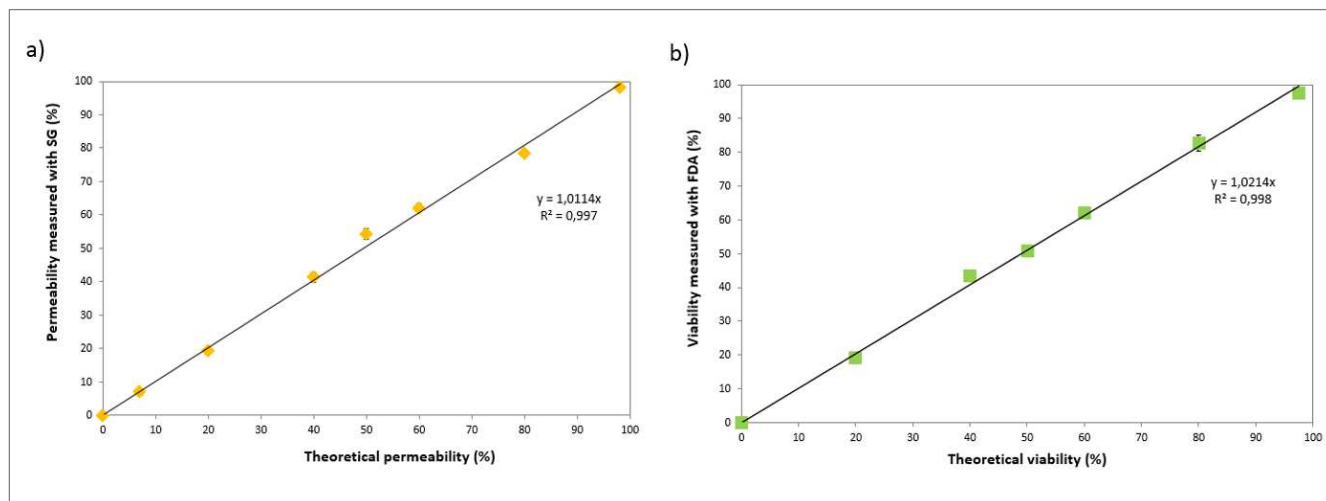


Figure 28 : Correlation curves permeability (a) and viability (b) measured/theory to validate flow cytometry methods for Sytox Green (SG) and Fluorescein Diacetate (FDA). Tested on *Chlamydomonas reinhardtii* wild type in 7 days of stress.

In conclusion, **viability (enzymatic activity)** was measured with **Fluorescein Diacetate (FDA)** while **membrane permeability** was determined with either **Propidium Iodide (PI)** (microscopy) or **Sytox Green (SG)** (flow cytometry measurements).

II3e) Measure of the permeabilization level in the micro-device

The effect of PEF on cell permeabilization was evaluated in the micro-device and was characterized using propidium iodide (PI) diluted in the sample of microalgae cells to a final concentration of 100 μM .

All experiments were performed in **TAP medium**, which **conductivity** is **0.213 $\text{S}\cdot\text{m}^{-1}$** at 20 °C.

15 μL of the microalgae solution, with a cell concentration in the range of **2 \cdot 10⁶ - 1 \cdot 10⁷ cells/mL** and containing PI were placed on the surface of the device. A glass cover-slide (24 x 30 mm, d = 1 mm) covered the algae solution in order to spread it and fill the multiple electroporation chambers with the sample. We assume that a variation of algae concentration would have no impact on the obtained results as algae cells represent less than 0.2 % v/v (*i.e.* less than 2 g/L) in the chamber. The **electrical shielding of the cells can thus be considered negligible** in our case. The use of a more concentrated sample may however affect the electrical treatment.

For microscopic observations, we used an inverted microscope Nikon eclipse Ti-U equipped with a 20x objective (Nikon Plan fluor x20 DIC N2 NA = 0.6) and a 40x objective (Nikon Achromat LWD x40 Ph1 ADL NA = 0.5).

In order to get quantitative data of cell PI uptake, each experiment was performed in three independent chambers and in duplicate.

First, the cells in the chambers were observed with the **x20 objective** and the images were recorded in **bright field** (Figure 29.a) (no fluorescence filter, exposure time of 10 ms and gain x1) **and afterwards with the CY3 filter** (Figure 29.b) (exposure time of 700 ms, and gain x4). **The number of stained cells n_{PI_0} and the total number of cells $ntot_0$ within each chamber were calculated, giving the natural permeabilization rate (before PEF).**

The PEF treatment was then applied. It was observed **that PI penetrated permeabilized cells within a few seconds after treatment.** Afterwards, **new bright field and fluorescence images** (Figure 29.c and d) were **recorded in the three chambers**, more than 30 s after the treatment, to let the cells settle down within the focus of the objective.

In the calculation of the PI uptake (equation 3.12), for each measurement, the total number of cells stained with PI before treatment (n_{PI_0} consisting of naturally permeabilized cells) was subtracted from the stained cell number after treatment (n_{PI_1}) and from the total cell number measured after treatment $ntot_1$ ($ntot_1$ and $ntot_0$, the cell number in the chamber after and before treatment, were always very close).

$$\text{PI uptake (\%)} = \frac{n_{PI_1} - n_{PI_0}}{ntot_1 - n_{PI_0}} \times 100 \quad (3.11)$$

The average number of cells per chamber was approximately 60. Algae permeabilization experiments are illustrated in Figure 29.

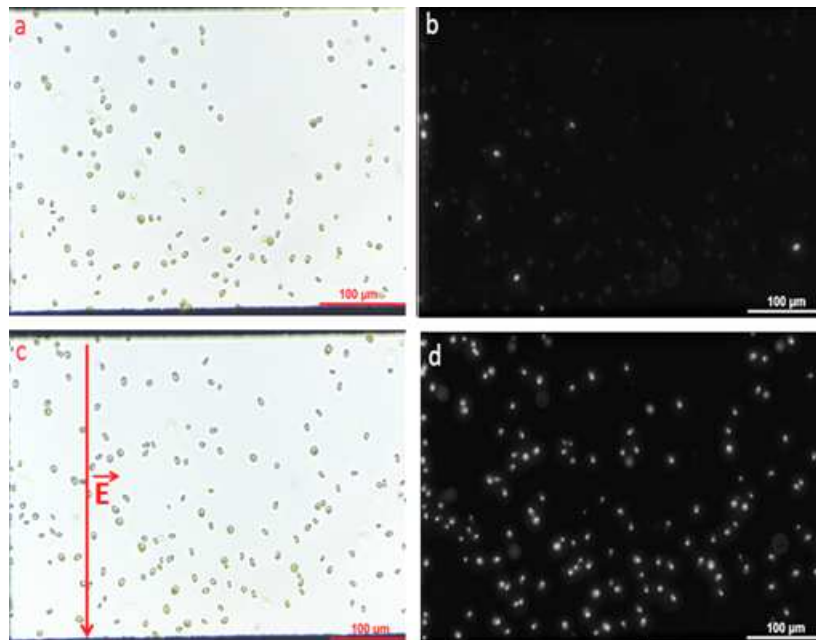


Figure 29: View in one of the large electroporation chamber (720 μm x 480 μm , electrode gap: 300 μm) with the x20 objective. Images recorded before and after PEF treatment (10 pulse of 5 μs , frequency 10 Hz, 180V corresponding to $E=6$ kV $\cdot\text{cm}^{-1}$). Bright field images (a) before and (c) after PEF; and fluorescence images (b) before and (d) after treatment. Scale bar: 100 μm .

A picture of the experimental set-up is presented in Figure 30.

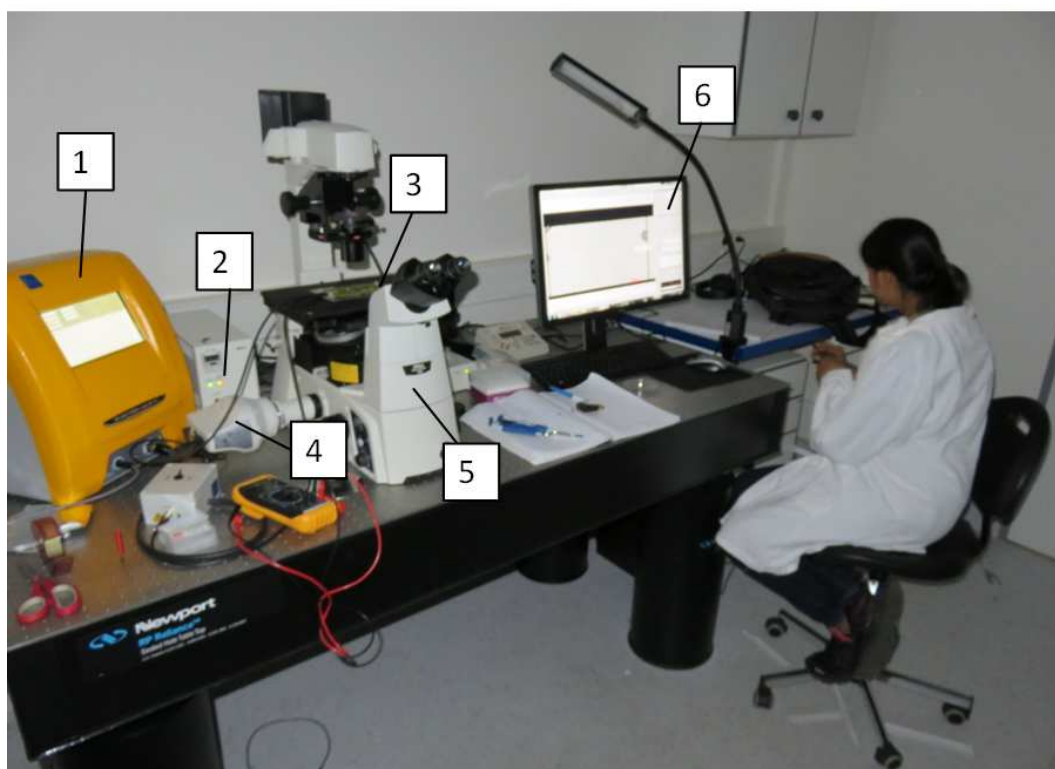


Figure 30: Experimental set-up to measure *in-situ* permeabilization with the micro-device. 1: Beta-tech generator electrocell B10 HVIV. 2: Fluorescence lamp (Xenon). 3: Electroporation device on the support plugged to the generator. 4: Camera color CMOS NIKON DS-RI2 5: Inverted microscope Nikon eclipse Ti-U equipped with several fluorescence filters and objectives 6: Cell permeabilization monitoring.

II3f) Measure of permeability (irreversible permeabilization (IP) and reversible permeabilization (RP)) and viability in the electroporation cuvettes

In the micro-device, the **cells are in contact with PI during permeabilization**. This means that the **dye stains both irreversible and reversible permeabilized cells** together with natural permeabilized cells (**cells before treatment**). It should be stressed that if staining is carried out 1h after PEF, the dye would stain only irreversibly and natural permeabilized cells as the literature reported that reversible pores may reseal a few seconds after treatment. Vernes *et. al* [68] mentioned 10 min as the time necessary for membrane recovery after PEF treatment.

To distinguish **natural permeabilization (NP)**, **reversible permeabilization (RP)** and **irreversible permeabilization (IP)**, three measurements must be performed: levels of permeabilization of **non-treated cells** (standing for NP), of **cells stained before PEF application** (SB includes NP+IP+RP) and of **cells PEF-treated and stained 1h after PEF application** (SA includes NP+IP).

These assays were carried out in the electroporation cuvettes illustrated in Figure 18 (see section II2).

The permeability levels were measured with Sytox Green (SG) by cytometry as presented previously in Figure 26. The SG uptake by the cell is determined according to the protocols described in Figure 31.

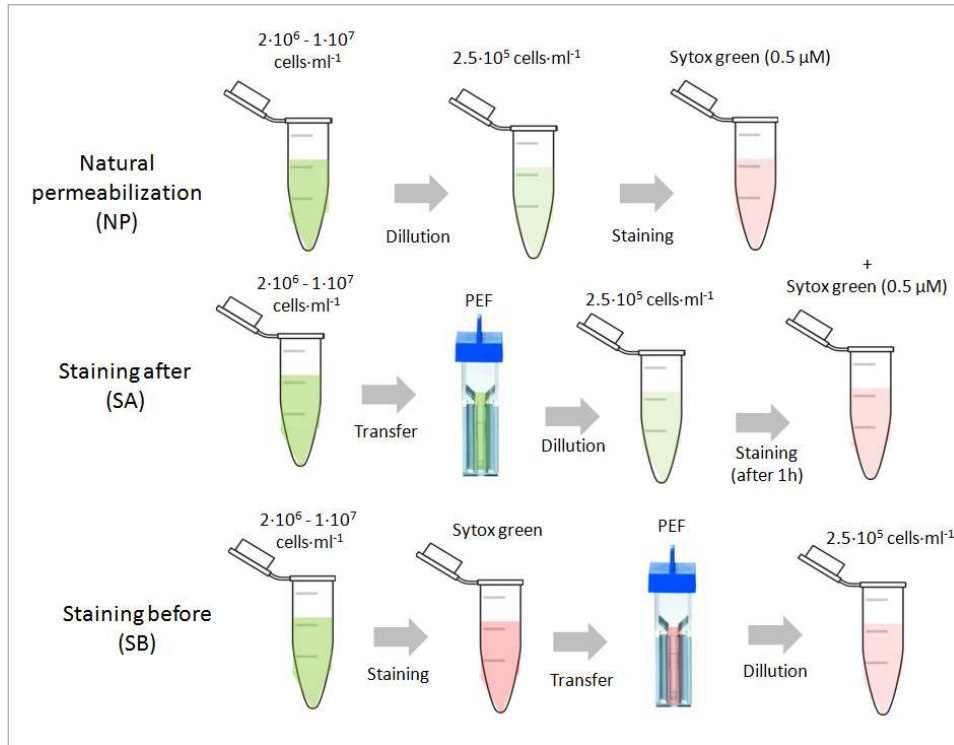


Figure 31: Sytox green staining protocols. Natural permeabilization (NP), Staining after (SA) measures NP+ irreversible permeabilization (IP), Staining before (SB) measures NP+IP+RP.

Additionally, viability tests were performed with fluorescein diacetate (FDA) 1h after the PEF treatment. The staining protocol was the one optimized before: 5.5 μM FDA for $1.5 \cdot 10^5$ cells/mL, 5-6 min incubation time.

114) Measurement of lipid extraction with/without PEF

To measure the impact of PEF pre-treatment on lipid extraction from *Chlamydomonas reinhardtii*, cells were either treated or not by a PEF treatment, and then mixed with a solvent. At first, the contact of algae with solvent during PEF treatment was tested in our electroporation system. However, the biphasic system (algae/water + organic solvent) requires a very efficient mixing in order to improve the transfer of lipids between both phases. Aqueous phase (water + algae) and/or solvent phase were then separated before being analyzed with the SPV method (Chapter 2). On the difference with the solvents used for lipid analysis, generally chloroform/methanol, **the solvents used for lipid extraction must be safe, eco-friendly and cheap to be scaled-up.**

114a) Characteristics of the solvent

To choose the solvent, several characteristics were taken into account.

The solubility of solvent in water (in mg/L) or hydrophobicity which is generally expressed by $\text{Log}(P_{\text{oct/wat}})$, $P_{\text{oct/wat}}$ being the partition coefficient of the solvent between 1-octanol and water. A high $\text{Log}P$ denotes a high hydrophobicity.

A high hydrophobicity of the solvent generally results in a strong affinity with neutral lipids. A low extraction yield is however expected because of the poor contact of the solvent with the cytoplasmic lipids in this biphasic system; the solvent is indeed scarcely soluble in the water phase and does not penetrate easily into the cell through the polar heads of the phospholipids of the membrane; besides the lipid droplets are protected in the cell by a hydrophilic layer. As a consequence, in these conditions, **algae viability** is usually slightly affected by hydrophobic solvents. Zheng *et. al.* [69] identified **the solvents with LogP < 5.5 as “toxic”** and the solvents with **LogP > 5.5 as “biocompatible”**. It was also observed by Mojaat *et. al* [70], which has plotted the photosynthetic activity in function of the log P and observed an effect on the activity below $\text{Log}(P) = 5$. They have also showed a linear correlation between the critical aqueous solvent concentration and the **LogP value of the solvent**: “the amount of solvent dissolved in water and in the cellular membrane decreases with increasing solvent hydrophobicity ($\text{log}P_{\text{oct}}$)”. The molecular weight has, together with the **LogP, a major impact on cell viability** [69,70]. **A molecular weight over $150 \text{ g}\cdot\text{mol}^{-1}$ has shown to be biocompatible whereas below, the solvent is toxic.**

In the lipids extraction process, apolar biocompatible solvents may be blended with polar chemicals which can penetrate into the cell and break the hydrogen bounds of neutral fatty acids with polar molecules of the cytoplasm [71]. Moreover, the extraction yield can be improved without negative effect on cell viability if the concentration of the toxic solvent in the aqueous phase is lower than the aqueous critical solvent concentration [70,72] (solvent concentration in the water which result in membrane denaturation). Accordingly, Marchal *et. al.*, [73] added 5 % v/v of dichloromethane to the biocompatible solvent decane to increase β -carotene solubility in the solvent without strongly affecting cell viability of *Dunaliella salina* (from 80 to 70 % of viable cells, solubility increased from 300 to $500 \text{ mg}\cdot\text{mL}^{-1}$).

A low boiling point was also preferred for facilities of evaporation.

The Sulpho-phospho-vanillin colorimetric method (SPV, see Chapter 2) was then used to quantify lipid extraction after solvent evaporation. Triolein (three 18:1 FA linked to glycerol molecule) was used as standard. The calibration curve obtained at different triolein concentrations dissolved in the chosen solvent was used for the calculations (see Appendix III3).

In the choice of the solvents tested, we took into account the ability to extract neutral lipids with a limited impact on glycolipids and phospholipids (polar lipids), and a low toxicity on the cells. The impact on the toxicity is evaluated in the prospect of re-use of the cells after extraction [74–76] (bio-milking), coupled with reversible electroporation (electroporation with an impact on the membrane but no impact on cell viability). If the extraction of intracellular lipids seems incompatible with the extraction of lipid droplets, we aimed to use a solvent which has no lysis effect in prospect of algae fractionation (separation of valuable compounds).

The solvents hexane and ethyl-acetate showed to have the ability to extract neutral lipids with limited effects on polar lipids in comparison with chloroform, methanol, and ethanol [77]. The lipid extraction is generally known to be more efficient when using a solvent mixture. In the article of Wu *et. al* [77], the extraction duration needed is of 2 hours, and it was shown that the temperature has a paramount impact on the extraction, especially over $60 \text{ }^\circ\text{C}$. Chen *et. al.*, [78], used a mix of hexane:ethanol 3:1 in subcritical state (1.4 MPa, 90°C). This ratio was also used by Li *et. al.*, [79]. Dodecane is shown to be the

more bio-compatible solvent by Zhang et.al [69] but the extraction could be very low because of the low affinity with the polar phase.

The protocol used to extract lipids from *Chlamydomonas reinhardtii* is presented hereafter.

II4b) Mixing protocol

Before being mixed with the solvent, the algae solution (*Chlamydomonas reinhardtii* wt at 7 days of stress) was first centrifuged to concentrate it in order to obtain a significant response of the SPV method. A volume of 100 μ L of $1 - 5 \cdot 10^7$ cells/mL (Figure 32) was placed in a 1 mm electroporation cuvette, subjected to PEF or not and transferred back in Eppendorf tubes.

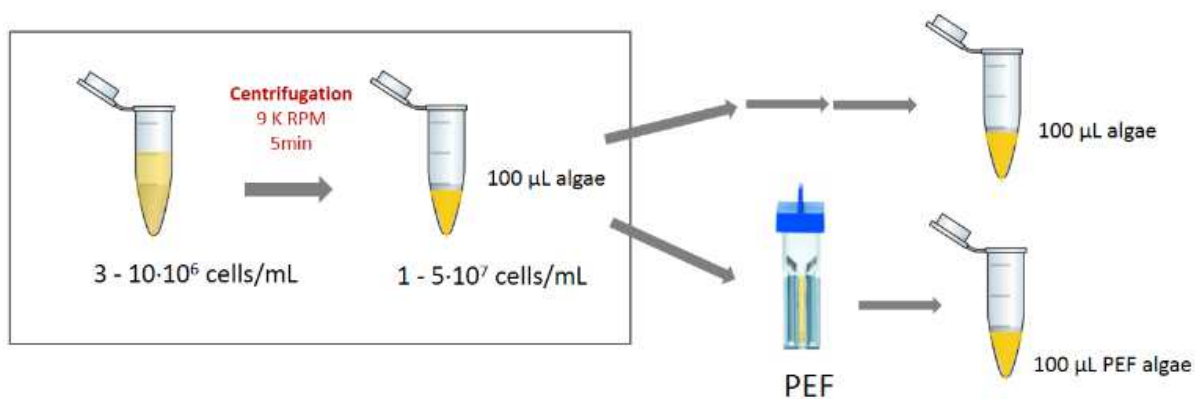


Figure 32 : Concentration and electroporation steps before mixing with solvent.

The solvent was added in a ratio 2:1 (2 volumes of solvent for 1 volume of algae solution). Samples were mixed with a mixing device: "intelli-Mixer RM-2l elmi", the program used is the F6 (alternation of rotation and oscillation) at 90 rpm (Figure 33). The time of mixing varies from 10 to 120 minutes depending on the experiment.



Figure 33 : Picture of the mixing device: intelli-Mixer RM-2l elmi.

Afterwards, the two phases are separated by a centrifugation step (Figure 34).

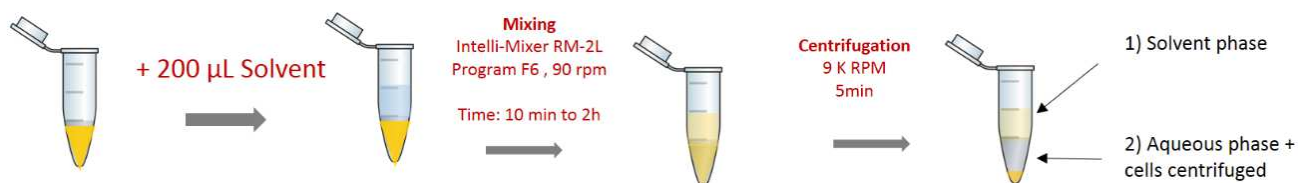


Figure 34 : Mixing step of algae with solvent and phase separation

II4c) SPV analysis after extraction

From the phases recovered after solvent extraction, **SPV colorimetric method was performed for the determination of the lipid extraction yield**. The upper solvent phase could be recovered and evaporated (90°C; 10 min) before completing the SPV analysis (addition of 100 µL of distilled water, 2 mL of sulfuric acid, heating, then 5 mL phosphor-vanillin solution). The 100 µL containing the algae extracted can be recovered and the SPV method is performed directly on it (2 mL of sulfuric acid, heating, then 5 mL phosphor-vanillin solution). The SPV response (Abs 530 nm) of the aqueous phase extracted SPV_{aq1} is compared with the SPV response measured from the aqueous phase before extraction SPV_{aq0} . The lipid extraction yield, referred as Y (%), is calculated as below:

$$Y(\%) = \left(1 - \frac{SPV_{aq1}}{SPV_{aq0}}\right) \times 100 \quad (3.12)$$

III. Results

First, the results on the effect of PEF on cell permeability in the micro-device and electroporation cuvettes set-ups are presented. Afterwards, data of lipid extraction with or without PEF pre-treatment is discussed. Results are presented as following:

Micro-device experiments:

- We first investigated the relation between **the PEF energy consumption**, for a given set of electrical conditions, and the efficiency of the treatment measured by the **propidium iodide uptake** by algae at 7 days of stress (high lipid content).
- Afterwards, the impact **of the stress duration on the sensitivity of *Chlamydomonas reinhardtii* to permeabilization** was investigated.
- **The effects of PEF on lipids and cell wall behavior during the PEF treatment were observed *in-situ*.**

Electroporation cuvettes assays:

- Conditions tested in the micro-device were further used in an **up-scaled system (electroporation cuvettes)**. Cell permeabilization was further characterized: the **distinction between reversible/irreversible permeability was assessed**. Finally, cells were harvested after PEF treatment to be **observed with CLSM imaging** to characterize the effects on lipid droplets and cell wall.

First lipid extraction results:

- Three solvents (ethyl-acetate, hexane, dodecane) of various toxicities were tested regarding their **effect on cell lysis**
- Thereafter the **effect of two solvents (ethyl-acetate, dodecane) on the cells (lipids and cell wall stained)** were qualitatively observed (CLSM)
- Finally, **lipid extraction performed by hexane with or without PEF** pre-treatment was evaluated.

III.1) Electroporation in the micro-device

The goal was to determine the optimal conditions of electroporation while minimizing the energy demand of the process.

In this context, the membrane charging time τ_m (time constant to lead 63 % of the maximal charge, see Figure 3), and the critical electrical field (E_{crit}), the electric field applied to trigger membrane permeabilization, were first calculated before performing the electroporation assays.

III1a) Calculation of the theoretical critical electrical field and charging time

The **minimum and maximum charging times** can be estimated with equations 3.3 (single shell model) and 3.4 (double shell model) presented in section I1b) of this chapter, using the minimal and maximal values of the radius r and the cytoplasm conductivity σ_{cyt} , as shown in equations 3.14 and 3.15. The equation taking into account the **cell wall** (double shell model) **tends to increase the value of the membrane charging time**.

$$\tau_{m \min} = r_{\min} \cdot Cm \left(\frac{1}{\sigma_{cyt_{\max}}} + \frac{1}{2 \sigma_{med}} \right) \text{ single shell model [15] (3.13)}$$

$$\tau_{m \max} = r_{\max} \cdot Cm \left(\frac{1}{\sigma_{cyt_{\min}}} + \frac{\sigma_{med} + \sigma_{cw}}{2 \sigma_{med} \sigma_{cw}} \right) \text{ double shell model [16] (3.14)}$$

with C_m equal to $0.01 \text{ F} \cdot \text{m}^{-2}$

The values presented in Table 2 were used to evaluate the charging time. Most of the values presented below come from the study of Bono *et. al* [15], or were determined in our work (cytoplasm radius = cell diameter/2 when considering the cell wall and membrane thicknesses negligible in comparison with the cytoplasm).

Table 2: Electric parameters for calculating the charging time of *Chlamydomonas reinhardtii*. Data collected from [15]. Bold: data measured.

	Conductivity (mS/m)	Relative permittivity	Radius/Thickness
cytoplasm	1200 (low lipid content) to 200 (high lipid content)	60	3.5 μm (low lipid content) 5 μm (high lipid content)
plasma membrane	0.01	2.3	4.5 nm
cell wall	50	60	165 nm
medium	213 (TAP N-)	80 (pure water)	(-)

From the two models presented above and the dielectric properties of *Chlamydomonas reinhardtii*, the **charging time was determined in the range of 0.12 – 0.88 μs** , *i.e.* below one micro-second. The **increase in cell radius** (from 3.5 μm up to 5 μm) and the **reduction of the cytoplasm conductivity** (from 1.2 to 0.2 S/m) **during stress due to lipid accumulation increase the charging time**: from 0.12 to 0.38 μs in the single shell model, and from 0.47 to 0.88 μs in the double shell model.

In this chapter, **the minimal pulse duration used is therefore 5 μs . We can thus consider that in any case, the full charge of the membrane is reached.**

III1b) Determination of the critical electric field for *Chlamydomonas reinhardtii* (membrane fully charged)

The critical electric field required to permeabilize the membrane E_{crit} can be calculated using the **Schwann equation** (equation 3.2), considering the full charge of the membrane and using the theoretical critical value required to induce membrane destabilization $\Delta\psi_{\text{crit}}$ (0.2 to 1.5 V for mammalian cells).

$$E_{crit} = \frac{2 \Delta\Psi_{crit}}{3r} \quad (3.15)$$

The minimal electric field can be evaluated using the $\Psi_{crit\ min}$ and r_{max} (5 μm , Table 2), while the maximal electric field is calculated with $\Psi_{crit\ max}$ and r_{min} . The critical electric field ranges from 0.3 to 3 kV/cm.

III1c) Experiments

Taking into account the theoretical critical electric field and membrane charging time, several electric field amplitudes in the range of 0.2 – 20 kV/cm adapted for five pulse durations Δt_{pu} regularly spaced in logarithmic scale (5, 16, 50, 158 and 500 μs) were applied to cells with a high lipid content. Different levels of energy (43, 135, 426, 1243 and 4260 $\text{kJ}\cdot\text{m}^{-3}$) were therefore obtained.

The temperature increase ΔT ($^{\circ}\text{C}$), due to Joule effect, corresponding to each condition, was estimated using equations 3.5. The simulation of the evolution of temperature in the chamber with space and time is presented in appendix III2: the results show that for any treatment, the pulses are sufficiently spaced out to enable efficient cooling between them. Indeed, a maximum duration of 100 mS (10 Hz treatment) is required to cool down to the initial temperature. For each treatment, the temperature increase was thus calculated for one single pulse.

All experiments were performed using a burst of 10 Hz monopolar pulses on *Chlamydomonas reinhardtii* SAG 34.89 (wild type) cells in 7-8 days of lipid accumulation. The PI uptake (equation 3.11), measured at the 5 energy levels tested for various pulse durations Δt_{pu} and electric fields E is presented in Table 3.

Table 3: PI uptake in *Chlamydomonas reinhardtii* in lipid accumulation phase (7-8 days of stress) for various PEF conditions (burst of 10 unipolar square pulses, with a frequency of 10 Hz).

		Energy levels					
		W1	W2	W3	W4	W5	
		W_{pu} ($\text{kJ}\cdot\text{m}^{-3}$)	43	135	426	1342	4260
		ΔT_{pu} ($^{\circ}\text{C}$)	0.010	0.032	0.119	0.32	1.019
Pulse duration/Electric field	$\Delta t_{pu1} = 500 \mu\text{s}$	$E(\text{kV}\cdot\text{cm}^{-1})$	0.20	0.36	0.63	1.12	2.00
		PI uptake (%)	-1.85 ± 0.05	-2.01 ± 0.98	2.19 ± 0.48	76.93 ± 1.81	78.53 ± 14.46
	$\Delta t_{pu2} = 158 \mu\text{s}$	$E(\text{kV}\cdot\text{cm}^{-1})$	0.36	0.63	1.13	2.00	3.56
		PI uptake (%)	-0.34 ± 0.48	-0.49 ± 0.69	12.73 ± 2.09	90.85 ± 2.17	92.24 ± 3.46
	$\Delta t_{pu3} = 50 \mu\text{s}$	$E(\text{kV}\cdot\text{cm}^{-1})$	0.63	1.12	2.00	3.55	6.32
		PI uptake (%)	0.86 ± 0.49	0.35 ± 1.33	89.34 ± 5.06	90.91 ± 0.98	95.81 ± 3.10
	$\Delta t_{pu4} = 16 \mu\text{s}$	$E(\text{kV}\cdot\text{cm}^{-1})$	1.13	2.00	3.56	6.31	11.25
		PI uptake (%)	0.91 ± 1.29	54.87 ± 3.13	93.36 ± 1.39	93.68 ± 0.10	98.98 ± 0.96
	$\Delta t_{pu5} = 5 \mu\text{s}$	$E(\text{kV}\cdot\text{cm}^{-1})$	2.00	3.56	6.32	11.22	20.00
		PI uptake (%)	3.03 ± 1.23	97.40 ± 0.19	97.57 ± 1.55	98.64 ± 1.51	99.35 ± 0.93

The results of permeabilization for several treatment durations at four levels of electric fields are presented in Figure 35, while those for several levels of energy W ($W2$, $W3$ and $W4$) are presented in Figure 36.

The Schwan equation (equation 3.2), neglects the impact of pulse duration as soon as the membrane is fully charged (after 5 μs).

However, results show that for a given electric field, pulse duration has a paramount impact on permeability. An electric field of 3.56 kV/cm leads to cell permeabilization whatever the pulse duration tested (from 5 to 158 μs). On the other hand, an electric field of 2 kV/cm does not permeabilize cells when associated with 5 μs pulses, leads to 55 % of PI uptake when associated with 16 μs pulses and above 90 % of PI uptake for longer pulses. The lower electric field 1.13 kV/cm leads to cell permeabilization only with 500 μs pulses.

Regarding the energy spent, conditions leading to 1342 $\text{kJ}\cdot\text{m}^{-3}$ per pulse (W4) permeabilize cells for any pulse duration (low pulse durations have a high electric field associated, long pulse durations have a lower electric field associated). On the other hand, at lower levels of energy, cells are permeabilized only when using short pulses (coupled with high electric field): 426 $\text{kJ}\cdot\text{m}^{-3}$ per pulse (W3) requires a maximum pulse duration of 50 μs and 135 $\text{kJ}\cdot\text{m}^{-3}$ per pulse (W2) required a maximum pulse duration of 5 μs .

Moreover, data demonstrate that, for similar cell permeabilization, short pulse durations are more energy efficient than long pulses (e.g, lower energy is spent when using 5 μs compared to 158 μs at 3.56 kV/cm while attaining cell permeability higher than 91%).

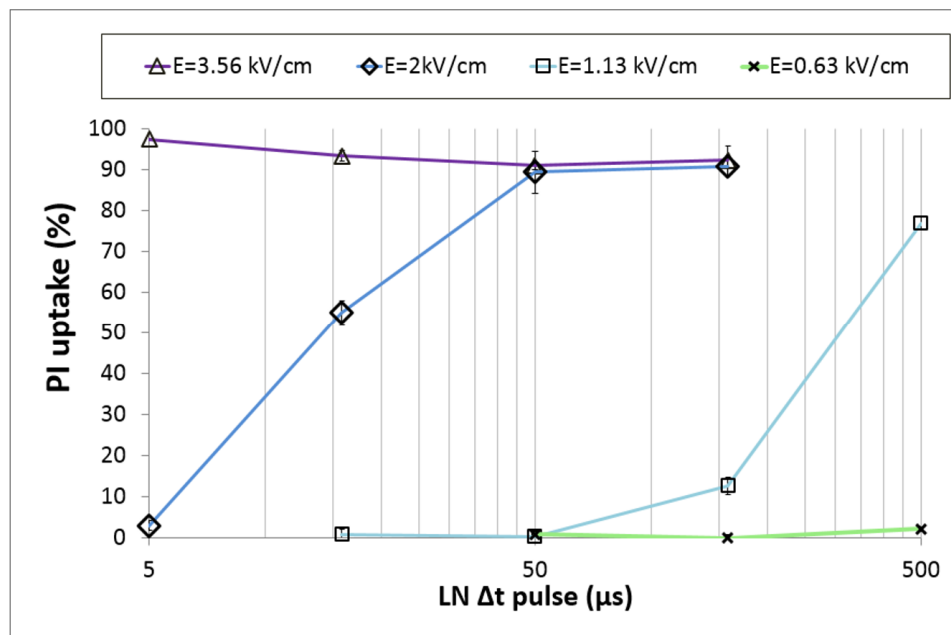


Figure 35: PI uptake (%) resulting from several treatments with different electric fields E (0.63, 1.13, 2 and 3.56 $\text{kV}\cdot\text{cm}^{-1}$) and pulse durations Δt_{pu} (5, 16, 50, 158 and 500 μs). Experiments performed with *Chlamydomonas reinhardtii* cells at 7-8 days of lipid accumulation

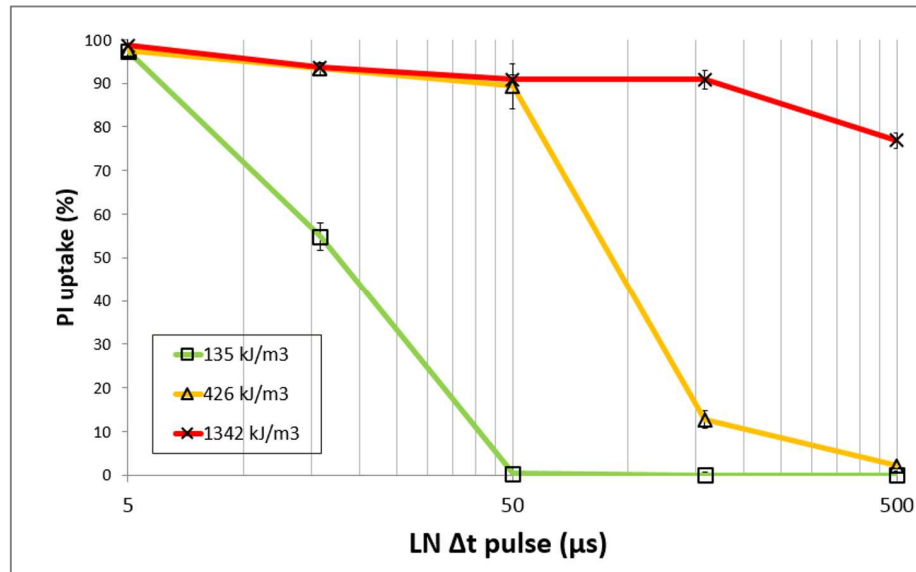


Figure 36: PI uptake (%) resulting from several treatments with varying electric field E (from 0.36 to 20 $\text{kV}\cdot\text{cm}^{-1}$) and pulse duration Δt_{pu} (5, 16, 50, 158 and 500 μs) corresponding to 3 levels of energy: 135, 426 and 1342 $\text{kJ}\cdot\text{cm}^{-3}$. Experiments performed with *Chlamydomonas reinhardtii* cells at 7-8 days of lipid accumulation.

The parameter E_{50} (kV/cm) is used to indicate the minimal electric field required to obtain at least 50 % of PI uptake for a given pulse duration. The values of E_{50} corresponding to 500, 50 and 5 μs pulses are presented in Table 4.

Table 4: Pulse duration and the corresponding electric field inducing at least 50% of cell permeabilisation (E_{50}) determined for *Chlamydomonas reinhardtii* (in 7-8 days of lipid accumulation phase).

Pulse duration Δt_{pu} (μs)	500	50	5
E_{50} ($\text{kV}\cdot\text{cm}^{-1}$)	1.12	2	3.56
Energy per pulse W ($\text{kJ}\cdot\text{m}^{-3}$)	1342	426	135
Increase in temperature ΔT_{pu} ($^{\circ}\text{C}$)	0.32	0.12	0.03

The obtained electric fields (Table 4) were lower than those reported in the literature, regardless of the applied pulse duration (Table 2). Indeed, for $\Delta t_{pu} > 5 \mu\text{s}$, values of 10 - 20 $\text{kV}\cdot\text{cm}^{-1}$ have been reported [22,47] for *Chlorella vulgaris* and *Nannochloropsis species*. Moreover, cell electroporation has been reported at 2.7 $\text{kV}\cdot\text{cm}^{-1}$ for $\Delta t_{pu}=100 \mu\text{s}$ [48] for *Chlorella vulgaris*, while our results demonstrate at least 50% cell permeabilization for pulse duration between 50 - 500 μs at 1 - 2 $\text{kV}\cdot\text{cm}^{-1}$ for *Chlamydomonas reinhardtii* at 7-8 days of stress. Finally, by extrapolating our results, approximately 5 - 6 $\text{kV}\cdot\text{cm}^{-1}$ for 1 μs pulse (instead of 23 -43 $\text{kV}\cdot\text{cm}^{-1}$ [20]) and 0.8 - 0.9 $\text{kV}\cdot\text{cm}^{-1}$ for 2 ms pulses (instead of 3 $\text{kV}\cdot\text{cm}^{-1}$ [23]) would be required to induce cell electroporation

We can easily explain those differences by at least two reasons: (i) *Chlamydomonas reinhardtii* cells are 3 to 4 fold larger than *Chlorella vulgaris* and *Nannochloropsis*. This increase in cell diameter contributes to the reduction of the critical electric field (E_{crit}) by a factor of 3 - 4 according to the Schwan equation (eq. 3.2, section I1b)) and (ii), in most cases, including references [20] and [23], the intensity of the field actually applied for algae electroporation is set much higher (2 - 3 times) than the critical value, ensuring the permeabilization of 100 % of the cells.

III1d) Relation between energy consumption and permeabilization

As mentioned before, the use of **short pulses associated with optimal electric fields is more energy efficient than that with long pulses**. When considering the E_{50} (Table 4), **reducing the pulse duration by 10 times requires an increase of the electric field by a factor slightly less than two**. Under this condition, **the corresponding energy is drastically reduced by a factor of 3.15** (Table 4). Moreover, since the temperature increase is proportional to energy (equation 3.5), **less heat is generated when using shorter pulses** (Table 4).

Additional simulations which take into account the heat transfer within the chamber and throughout the electrodes and the glass of the system showed **that the temperature cools down to its initial level between two pulses in any condition tested** (Appendix III2). This is linked to the natural cooling that occurs between pulses under our frequency conditions and large surface to volume ratio [60] (Small volume of the electroporation chamber in comparison to the surfaces of cooling).

Nevertheless, **the approximation obtained when using equation 3.5 should be reconsidered when using frequencies higher than 10 Hz, higher energies than those presented in Table 3, higher medium conductivity, or using a larger chamber possessing a reduced surface to volume ratio**. Moreover, the conductivity of the medium may increase during PEF treatment because of the leakage of ions from the biomass, further impacting the calculation [80].

Moreover, it should be noted that for conditions associated to **high energy delivered per pulse** ($W \geq 1342 \text{ kJ}\cdot\text{m}^{-3}$), **gas appeared at the vicinity of electrodes**, probably due to **water electrolysis**. These mechanisms can impact negatively the distribution of the electric field or change the medium conductivity as previously stated. **Reducing the energy used during the PEF treatment is thus a way to avoid such effects**. In some conditions, algae can precipitate at the vicinity of the electrodes, probably because of electrophoretic forces [81]. In accordance with our results, Straessner *et. al.* showed that short pulses reduce these effects [81].

Under our conditions, the best result in terms of PI uptake to energy delivered was found when using a burst of 10 unipolar pulses at 10 Hz with 5 μs of pulse duration and a field amplitude of 3.5 $\text{kV}\cdot\text{cm}^{-1}$.

It must be noted that the energy consumption should not be the only criterion to select pulse width and electric field intensity. It was indeed shown in the literature that the **pulse width impacts the size of the pores created by the treatment; short pulses result in a multiplicity of small pores while long pulses result in a few large pores** [32]. Moreover, the use of micro-pulses, with a duration lower than 100 μs , remains quite unexplored and may have **unexpected intracellular effects impacting probably cells viability** [11].

III1e) Sensitivity of *Chlamydomonas reinhardtii* to PEF at various stages of lipid accumulation

Chlamydomonas reinhardtii at different stages of lipid accumulation (after 4, 7 and 14 days of nitrogen stress conditions) and in exponential growth phase has been subjected to PEF treatment (burst of 10 unipolar pulses of 5 μs with a frequency of 10 Hz, amplitude ranging from 0 to 5 $\text{kV}\cdot\text{cm}^{-1}$). The results showed that *Chlamydomonas reinhardtii* cell permeabilization occurred at electric field intensities ranging from 2 to 5 $\text{kV}\cdot\text{cm}^{-1}$ (Figure 37).

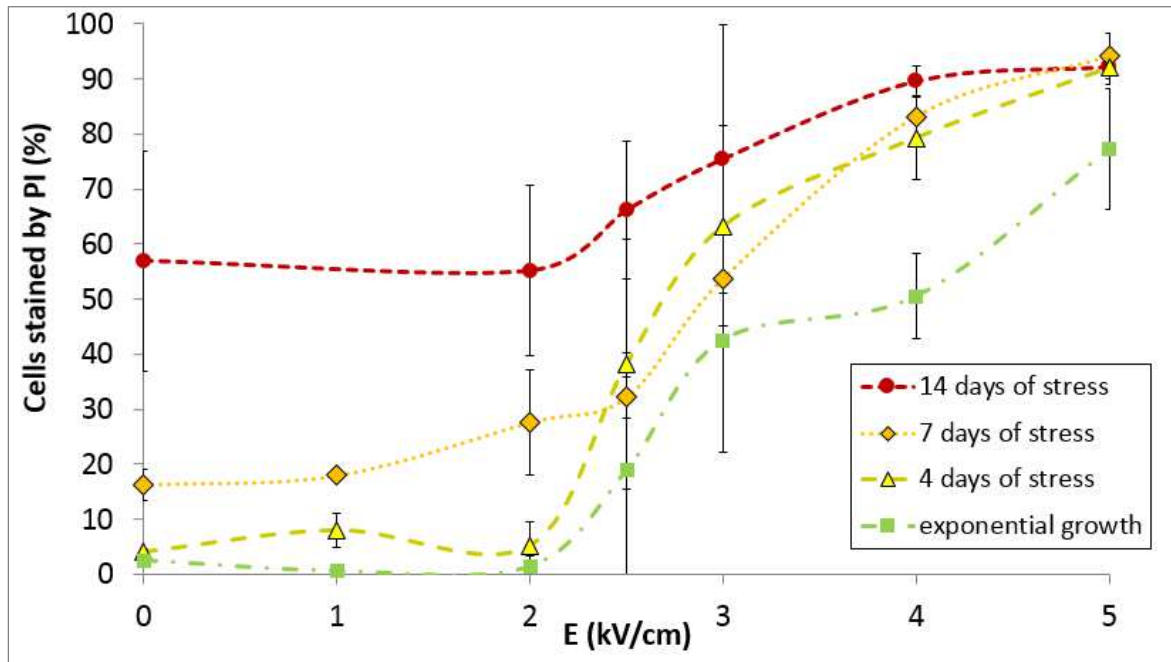


Figure 37 Permeabilization efficiency of *Chlamydomonas reinhardtii* cells (wild type) over electrical field intensity (PEF treatment conditions: 10 unipolar pulses, 5 μs long, 10 Hz). The efficiency is expressed as the total number of stained cells by PI after treatment (this includes the PI stained cells prior to PEF) over the total number of cells in the sample. The colors correspond to different conditions: exponential growth phase (green square), 4 days of stress (yellow triangle), 7 days of stress (orange diamond) and 14 days of stress (red circle).

Without PEF treatment (0 kV/cm), the percentage of cells stained by PI is below 5 % for the cells at exponential growth and after 4 days of stress. Permeability achieves values in the range of 10 to 20 % after 7 days of stress and **dramatically increases above 50 % after 14 days of stress. These results show that the duration of the starvation stress affects *Chlamydomonas reinhardtii* cell permeability.**

Besides, **lipid accumulation does not seem to affect the permeabilization behavior.** Indeed, whether after 4, 7 or 14 days of stress, cell permeabilization is observed in the range of 2 to 4 kV/cm .

We found that **the cells in exponential growth seem to be slightly less sensitive to the treatment.** This result may be explained by the **smaller diameter** of the *Chlamydomonas reinhardtii* cells in division in comparison with the one of the cells in stress (see Chapter 2: during stress, the mean diameter increases from 7 to 10 μm). In addition, cells in growth phase have a **particular ovoid shape** for which, according to the orientation of the cells with the electric field, a higher electric field may be required to ensure permeabilization. The measurement was repeated several times (two populations of cells

measured in duplicate for each cell condition). Moreover, two **permeabilization patterns seem to be observed**, one between 2 and 3 kV/cm, and a second between 3 and 4 kV/cm (certainly due to the orientation of the ovoidal shape with the field which has an impact in the Schwan equation, eq. 3.2).

III1f) Qualitative observations by optical and epifluorescence microscopy

In order to get a better insight into PEF effects on cell structure/morphology, in particular lipid droplets, cells were observed by optical/epifluorescence microscopy during PEF treatment. PEF experiments were carried out at $6 \text{ kV}\cdot\text{cm}^{-1}$, burst of $5 \mu\text{s}$ and 10 Hz unipolar pulses. A significant membrane permeabilization of *Chlamydomonas reinhardtii* cells is detected with PI penetration (Figure 38.b). However, the cell structure was maintained as suggested by the bright field observation (Figure 38.a). In addition, Bodipy fluorescence showed that the lipid droplets remain in the cytoplasm (Figure 38.c). The cell wall may prevent both lipid release from the cytoplasm and cell disintegration, even after electrical treatment.

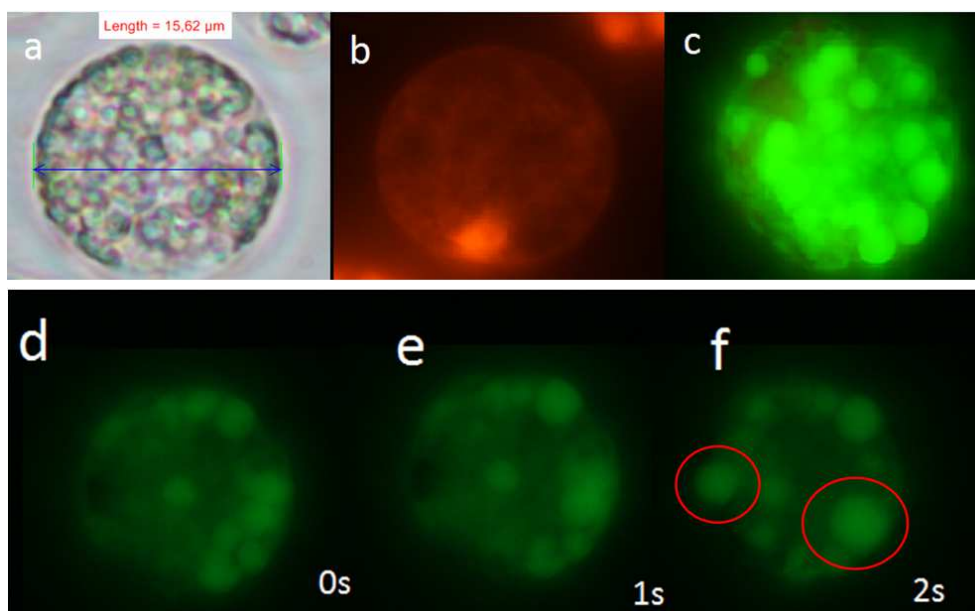


Figure 38: *Chlamydomonas reinhardtii* (wild type) permeabilized by a PEF treatment of $6 \text{ kV}\cdot\text{cm}^{-1}$, $5 \mu\text{s}$ pulses and 10 HZ (a) bright field, (b) PI detected using CY3 fluorescence filter, (c) lipid droplets stained with bodipy 505/515 using B2A fluorescence filter. Observation at the beginning of the treatment (d), 1s after (e) and 2s after (f). Displacement and appearance of large droplets are observed (red circles).

However, a **rearrangement of lipid droplets in the cytoplasm was observed a few seconds after the PEF treatment** (Figure 38, 0s, 1s, 2s after treatment corresponding to d, e and f images, respectively); some droplets were merged 2s after treatment (red circles). **Lipid displacement and coalescence of lipid droplets within the cytoplasm can be observed in real time during the PEF treatment in a video provided in supplementary data in Bodénes *et. al.* (2016) [82].**

On the whole, from observations performed at repeated times in bright and fluorescence fields, the data show that very short pulses ($5 \mu\text{s}$) permeabilize the cytoplasm membrane (shown by PI penetration) with limited effects on the cell wall (Figure 38.a), **but with clear additional effects on the intracellular lipids.**

Additional observations of PEF treated *Chlamydomonas reinhardtii* cells at 7 days of stress (6 kV/cm, 5 μ s, burst of 10 pulses, few minutes after treatment) is illustrated in Figure 40. In this figure, the observation is performed with bright field and fluorescence. The fluorescence filter (Nikon B2A) enables to excite and observe the simultaneous fluorescence of the lipid droplets stained with Bodipy (in green) and the autofluorescence of the chlorophyll (in red). As it can be seen, **all the lipid droplets and chlorophyll remain in the cytoplasm of the PEF treated cells.**

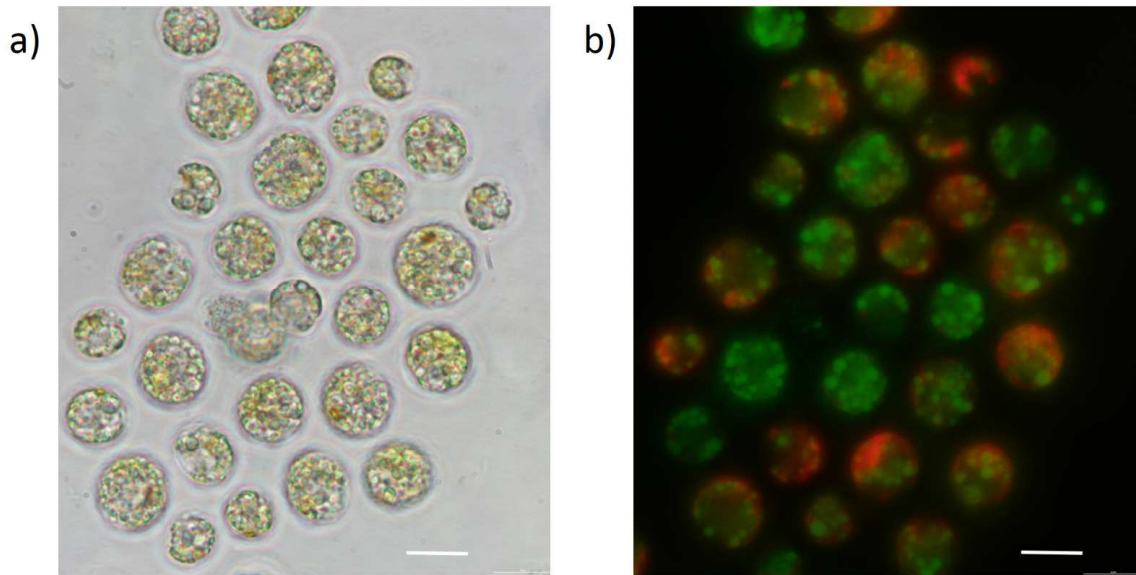


Figure 39 : *Chlamydomonas reinhardtii* wild type (7 days of stress) cells few minutes after PEF treatment (6 kV/cm, 5 μ s, burst of 10 pulses). a) Bright field, b) B2A fluorescence filter which shows lipid droplets stained by bodipy (green) and chlorophyll autofluorescence (red). Scale bar: 10 μ m.

In addition, the effects of PEF were also tested on the *Chlamydomonas reinhardtii* cell wall deficient strain cw15 (SAG 34.98) (Figure 40).

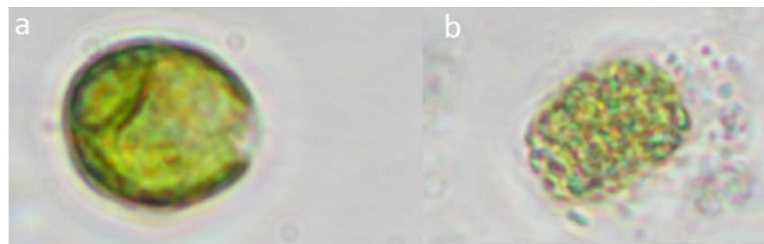


Figure 40: *Chlamydomonas reinhardtii* cell wall deficient mutant in exponential growth conditions (a) before and (b) 2 minutes after 6 KV \cdot cm $^{-1}$, 5 μ s, 10 Hz treatment.

A strong effect on cell integrity was observed in the mutant compared with the wild type strain. This experiment underlines the fact that **when a wild type cell is permeabilized, the cell wall maintains the cell integrity** (Figure 39), **while a cell wall deficient strain, as *Chlamydomonas reinhardtii* cw15, is destructured, as expected, in such fields (6 kV/cm, 5 μ s) [83].** The Figure 41 shows the **destabilization of the membrane of the cell wall deficient strain cw15** (in growth phase) observed a few seconds after PEF.

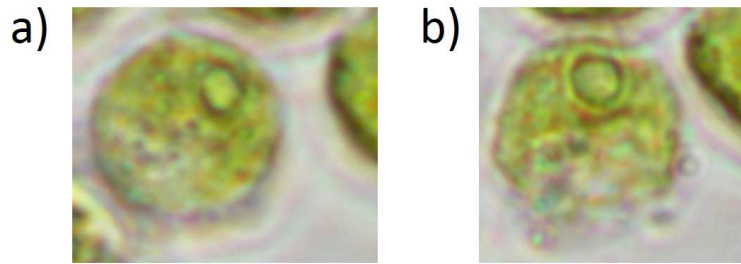


Figure 41 : Destabilization of the membrane of the cw15 strain: a) at the beginning of treatment ($6 \text{ kV}\cdot\text{cm}^{-1}$, $5 \mu\text{s}$, 10 Hz , 10 pulses), b) 15 seconds after.

III2) Electroporation in cuvettes

The effect of electrical parameters on reversible et irreversible permeability was evaluated in an upper scale system, the electroporation cuvettes. All experiments were performed at least in duplicate on two algae populations, measurements were performed in duplicate.

III2a) Measurement of viability and irreversible permeability after PEF treatment

Chlamydomonas reinhardtii cells after 7 days of stress were electroporated in cuvettes and stained 1h after treatment with either FDA (viability) or Sytox Green (permeability). Electroporation was performed with various electric fields ranging from 2 to 7 kV/cm with a burst of 10 pulses of $5 \mu\text{s}$ with a 10 Hz frequency. Results are presented in Figure 42.

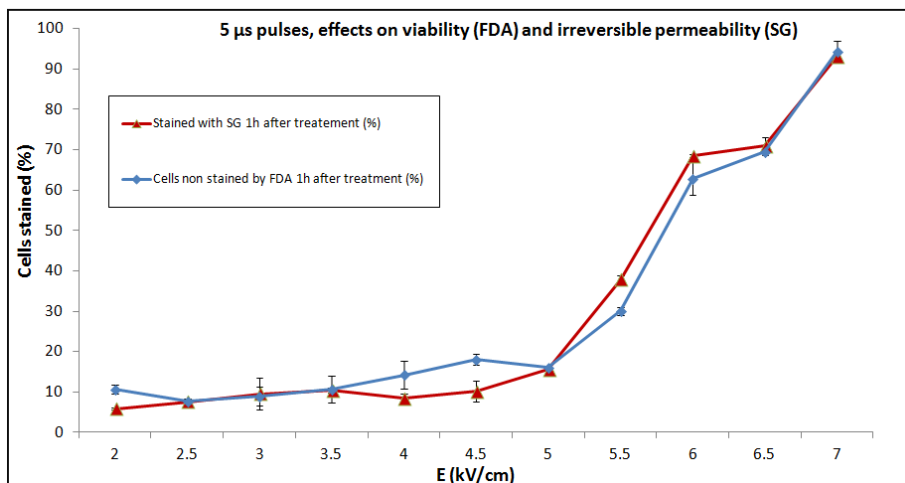


Figure 42: SG uptake and FDA negative cells 1h after PEF treatment (E ranging from 2 to 7 kV/cm with a burst of 10 pulses of $5 \mu\text{s}$, 10 Hz)

Similar trends are observed for the SG stained cells (membrane permeabilized) and cells non-stained with FDA (FDA stains cells with an enzymatic activity and an intact cytoplasmic membrane) (Figure 42). There is therefore a good correlation between these two staining methods as expected. In this case, staining both with FDA and SG may be unnecessary. The choice of SG was preferred as the fluorescence of the dye is much more stable than the one of FDA (see FDA: Figure 23).

III2b) Reversible and irreversible permeabilization for different pulse durations

The distribution of reversibly, irreversibly, naturally and non permeabilized cells for various PEF treatments is presented in Figure 43 (5 μ s pulses), Figure 44 (50 μ s pulses) and Figure 45 (500 μ s pulses). Data were estimated by staining the cells with SG before PEF (naturally permeabilized cells), immediately (naturally together with reversible and irreversible permeabilized cells) and 1h (naturally together with irreversible permeabilized cells) after PEF treatment as described in Figure 31. *Chlamydomonas reinhardtii* in 7-8 days of stress showed an average natural permeabilization of 5.7 ± 0.6 %.

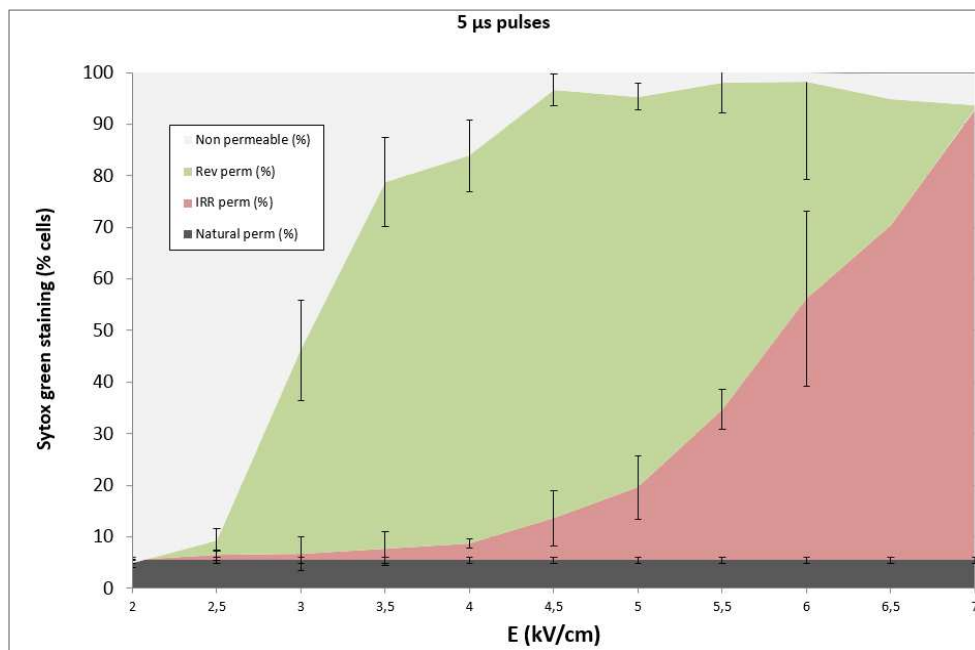


Figure 43: Non permeabilized, reversibly permeabilized (Rev), irreversibly permeabilized and naturally permeabilized *Chlamydomonas reinhardtii* cells (7-8 d of stress) measured by staining with SG before and after PEF treatment and expressed as a percentage of SG uptake in the cells, measured by flow cytometry. PEF treatment: E ranging from 2 to 7 kV/cm with a burst of 10 pulses of 5 μ s, 10 Hz.

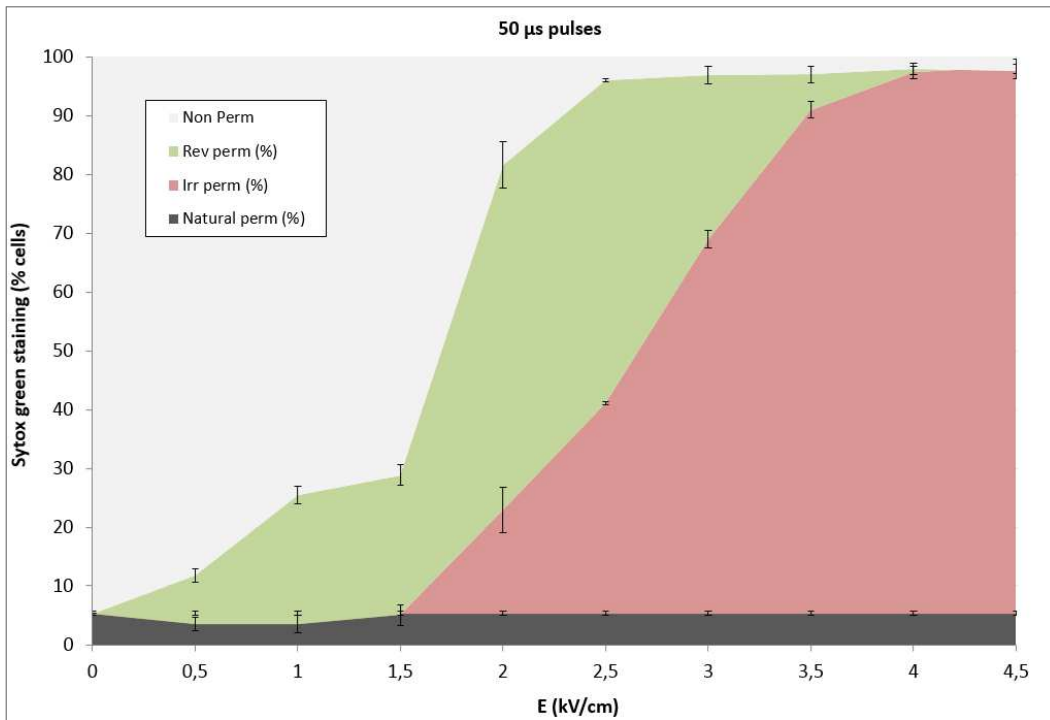


Figure 44: Non permeabilized, reversibly permeabilized (Rev), irreversibly permeabilized and naturally permeabilized *Chlamydomonas reinhardtii* cells (7-8 d of stress) measured by staining with SG before and after PEF treatment and expressed as a percentage of SG uptake in the cells, measured by flow cytometry. PEF treatment: E ranging from 2 to 7 kV/cm with a burst of 10 pulses of 5 μs, 10 Hz.

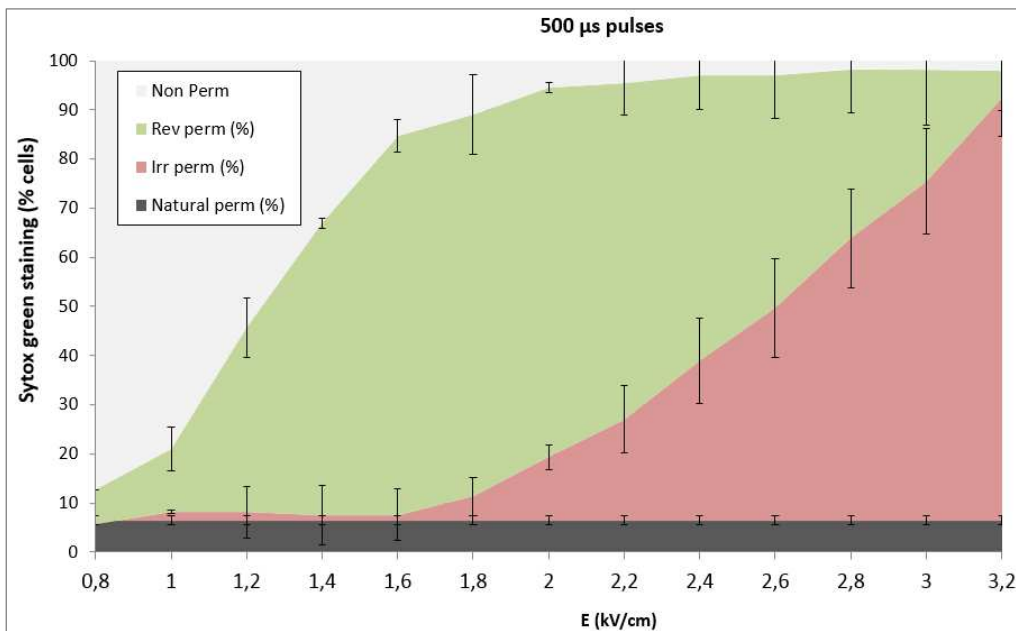


Figure 45: Non permeabilized, reversibly permeabilized (Rev), irreversibly permeabilized and naturally permeabilized *Chlamydomonas reinhardtii* cells (7-8 d of stress) measured by staining with SG before and after PEF treatment and expressed as a percentage of SG uptake in the cells, measured by flow cytometry. PEF treatment: E ranging from 2 to 7 kV/cm with a burst of 10 pulses of 500 μs, 10 Hz.

The figures show two permeabilization patterns: first the reversible permeabilization (in green) and the irreversible permeabilization (in red): reversible permeabilization concerns cells that are stained

by SG during treatment but not stained after treatment because the membrane has resealed. **These results are in agreement with those obtained in the micro-device**, presented in Table 4. In the latter case, total permeabilization (reversible + irreversible + natural permeabilization) was evaluated by PI staining before PEF treatment (the dye is in the medium during PEF treatment).

III2c) Reversible/irreversible permeabilization parameters, energy and temperature increase

The **maximum ratio of reversibly permeabilized cells is observed at an electric field of 4.5 kV/cm, 2.2 kV/cm and 1.7 kV/cm for 5, 50 and 500 μ s pulses, respectively** (Figure 46 and Figure 47). Note that for the 50 μ s pulses, the ratio of reversibly permeabilized cells is surprisingly lower than that of 5 μ s and 500 μ s but this difference is certainly due to experimental errors.

Irreversible permeabilization (minimum of 90% of SG uptake 1h after treatment) is **obtained for an electric field of 7 kV/cm, 4.5 kV/cm and 3.2 kV/cm for 5, 50 and 500 μ s pulses, respectively** (Figure 46).

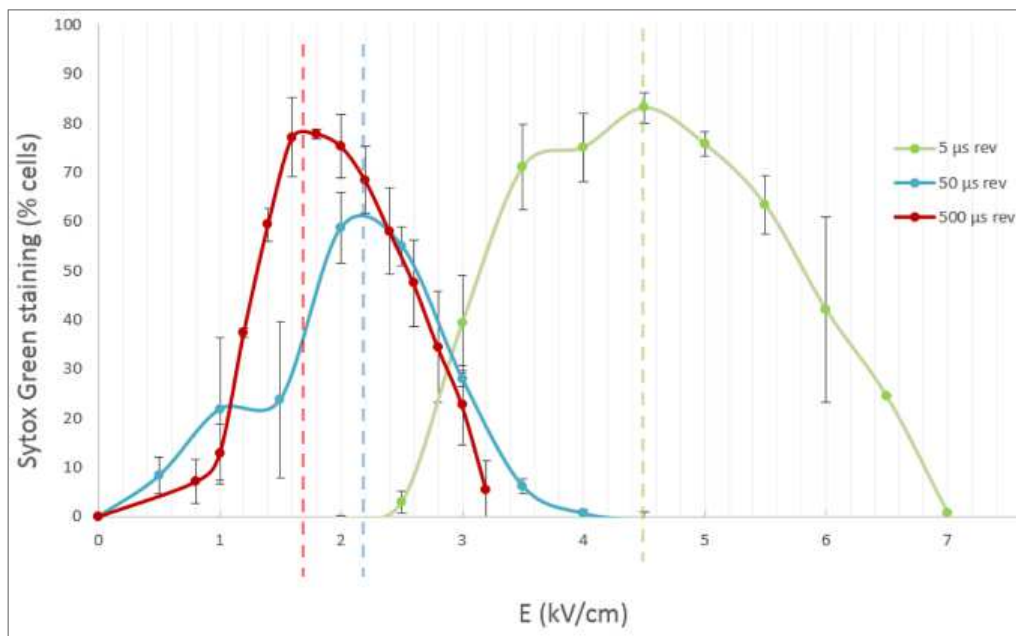


Figure 46: Reversible permeabilization (reversibly permeabilized cells over total cells) for 5, 50 and 500 μ s pulses (burst of 10 pulses, 10 Hz) on *Chlamydomonas reinhardtii* cells in 7-8d of stress.

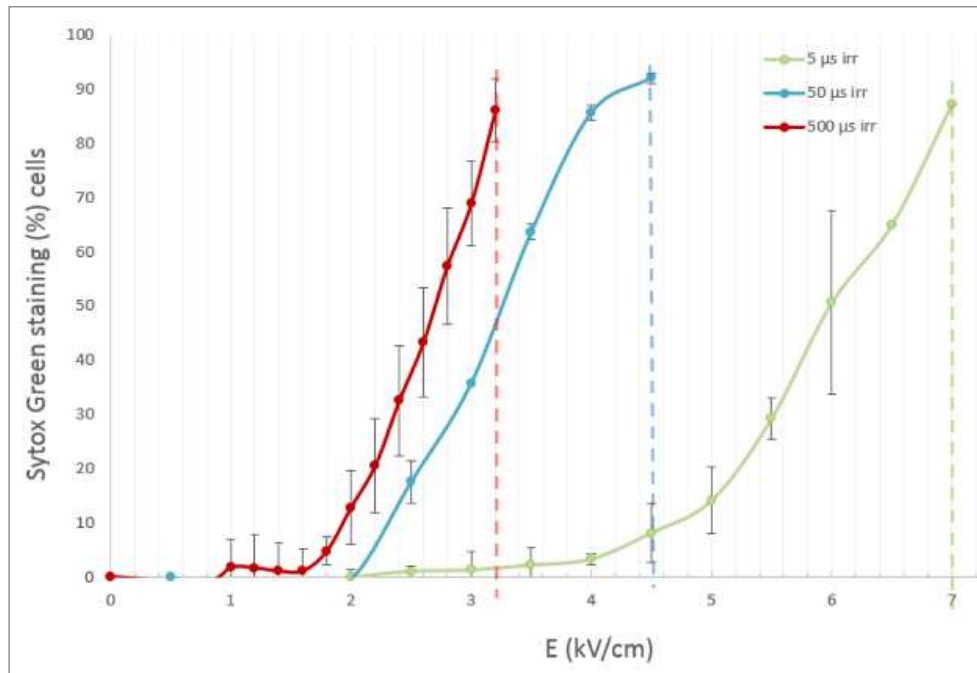


Figure 47 : Irreversible permeabilization (irreversibly permeabilized cells over total cells) for 5, 50 and 500 μs pulses (burst of 10 pulses, 10 Hz) on *Chlamydomonas reinhardtii* cells in 7-8d of stress

The electric fields required for obtaining the maximal percentage of reversibly permeabilized cells and 90% of irreversible permeabilization for 5, 50 and 500 μs pulses are summarized in Table 5. The energy of the complete treatment (10 pulses delivered in one second with a frequency of 10 Hz) and the potential temperature increase (min: considering cooling to the initial temperature between each pulse, max: no cooling considered) are also presented in Table 5 (calculations were carried out using equation 3.5 with a medium conductivity evaluated at 0.213 S/m).

Table 5: Electric fields E required to obtain maximal % of reversibly permeabilized cells or irreversible permeabilization (90% Sytox green uptake) with 5, 50 and 500 μs pulses and corresponding treatment energy W and potential temperature increase ΔT.

E (kV/cm) <i>Electric field required</i>	W_{treat} (kJ/m³) <i>Total energy of the treatment</i>	ΔT_{treat} (°C) <i>Potential temperature increase of the treatment (min –max)</i>
5 μs pulses		
Rev Perm : 4.5	2.1·10 ³	< 0.05 - 0.52
Irr Perm : 7	5.2·10 ³	< 0.12 - 1.24
50 μs pulses		
Rev Perm : 2.2	5.1·10 ³	< 0.12 - 1.23
Irr Perm : 4.5	2.2·10 ⁴	< 0.51 - 5.15
500 μs pulses		
Rev Perm : 1.7	3.1·10 ⁴	< 0.73 - 7.36
Irr Perm : 3.2	1.1·10 ⁵	< 2.61 - 26.08

As shown in Table 5, the potential temperature increase is moderate for all the conditions proposed, except for the case of irreversible permeabilization with 500 μs pulses which may lead to a high temperature increase (+26°C). But the actual value may however be lower because of the heat dissipation into the environment. Our experiments suggest that permeabilization is not linked to temperature increase as low pulse durations permeabilize the cells with a moderated temperature increase.

In our optimized pulse duration (5 μs), the energy consumption is in the range of 2 - 5 kJ/L (or kW/L as the treatment duration is one second) for 80 % of reversibly and 90% of irreversibly permeabilized cells, respectively. According to complementary experiments, it could also be possible to reduce the number of pulses of the treatment to less than 5 without significant change in permeabilization. To compare with the energy levels found in the literature: 7 - 28 kJ/L [48], 42 kJ/L [25], 100 kJ/L [20], we obtain lower energy consumptions thanks to our optimized conditions of electric field/pulse duration. As mentioned before, the higher values of energy found in literature may be related to parameters other than ours such as (1) cell size, (2) cell density (high cell density may require an increased electric field because of cell shielding), and also (3) size of the pores aimed: the extraction of large molecules may require a stronger treatment (discussed thereafter).

Additional experiments should however be performed with more concentrated cell cultures to see the impact of the biomass concentration on the treatment efficiency. In our conditions the biomass concentration was approximately 1 g/L (0.1 % volumetric), far from the conditions used by Goettel *et. al* [20] (36-167 g dry weight per kg suspension, 3-15 % volumetric). The cell suspension may indeed interfere with the propagation of the electric field within the electroporation chamber.

III2d) Life cycle of reversible pores

To estimate the life duration of reversible pores obtained with pulses of 5, 50 and 500 μs , electroporated cells under reversible conditions were recovered and immediately stained with SG at 20 s, 40 s, 1 min, 2 min, 3 min, 4 min, 5 min or 6 min after treatment (Figure 48).

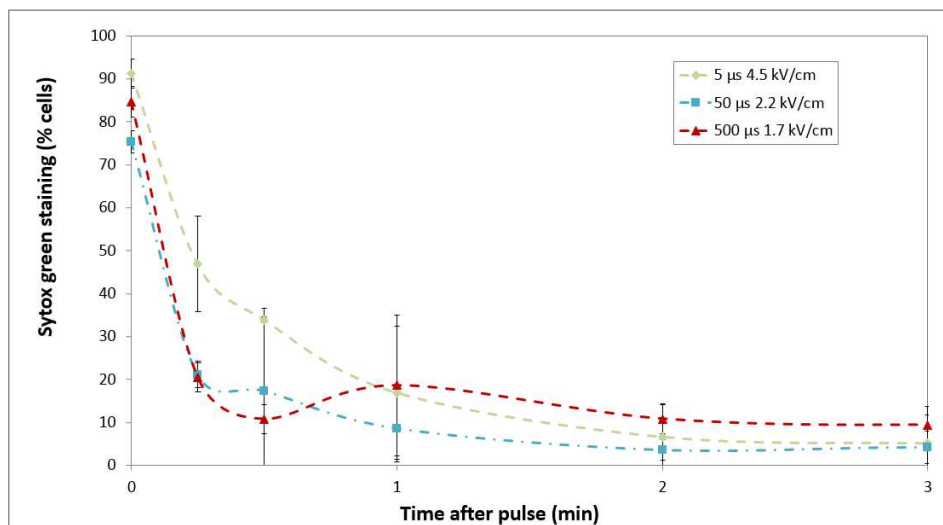


Figure 48: Dynamics of pore releasing of *Chlamydomonas reinhardtii* after reversible PEF treatments at 21.5°C Reversible PEF conditions were those presented in Table 5. SG staining was performed after reversible PEF conditions treatment ($t=0$) or 20s, 40s, 1 min, 2 min, 3 min, 4 min, 5 min and 6 min after treatment. Because the pores were stable after 3 min, the figure is focused between 0 and 3 min.

Interestingly, the results show that at room temperature, **the reversible pores last for a maximum of one minute and the majority reseals in the first 20 s after the PEF treatment**. Experiments could not be performed with shorter durations, from 0 to 20 s.

The PEF treated cells showed 60 to 80% of reversible permeabilization (reversible permeabilization obtained with 50 μ s pulses was higher in the experiment of the Figure 48 than the experiment of the Figure 44). **Various pore resealing durations, ranging from a hundred of milliseconds to several hours, are reported in the literature**. Saulis *et. al.* [84] reported various stages in the membrane recovery: a rapid decrease of pore size (in less than one second), then a slow decrease (a few minutes), and a complete pore closing (in dozens of minutes). The memory effect of an increased membrane viscoelasticity and mechanical effects on cytoskeletal networks [6] are also reported. The dynamics of pore resealing is also highly dependent on temperature. Working at temperatures around 0°C might greatly increase the resealing duration of reversible pores.

III2e) Transport of various molecules through the pores

Permeabilization effects were monitored both with Propidium Iodide (micro-device) and Sytox Green (cuvettes) which have similar molecular weights of 668 and 600 Da, respectively and are able to enter into the cells. The uptake of molecules of other sizes was obtained at other electric fields as reported by Saulis and Saulé [32]. Small particles/ions (K^+ : $r = 0.16 - 0.22$ nm, Mannitol 182 Da: $r = 0.36 - 0.42$ nm, Sucrose 342 Da: $r = 0.44 - 0.52$ nm) penetrate at lower electric field strength and short pulse durations (micro-second pulses), while large molecules (Bleomycin 1500 Da: $r = 0.8$ nm) require higher electric field strength and pulse durations (millisecond pulses). However, in these conditions, large pores are created and cell lysis occurs as pores are not able to reseal, as observed with mammalian cells in the case of the penetration of large molecules such as bleomycin.

The **molecular weight of TAG molecules is less than 900 Da**. Indeed, the molecular weight of a triacylglycerol molecule is equal to the weight of the central glycerol backbone (38 Da) and three times the weight of the FA chain. For example, in the case of three 18:1 oleic acid (282 Da), one of the main neutral FA present at 7 days of stress (see chapter 2), the molecular weight is 884 Da. **This means that the TAG molecule radius is probably similar to that of SG and PI and thus a single TAG molecule is, regarding the size, probably able to be transported across the created pores.**

From the experiments performed, it is shown that a molecule such as PI or SG can penetrate through reversible pores, created on very specific electrical conditions. However, these pores reseal themselves very fast, within a minute, and the molecules could not penetrate any longer.

III2f) Observations of the cell structure and lipid droplets by CLSM

From previous data, it was observed *in situ* that the cell wall of *Chlamydomonas reinhardtii* was poorly or not affected at all during the PEF treatment in our conditions in the microdevice (optical/epifluorescence microscopy). Further experiments were carried out in which confocal observations of PEF treated cells, stained with bodipy (neutral lipids) and with Concanavalin a (cell wall carbohydrate-binding protein) were performed.

The observation of the cells before and after PEF treatment (irreversible conditions of 7 kV/cm, 5 μ s, burst of 10 pulses with a frequency of 10 Hz were applied) suggest **that the cell wall** (in yellow) is not

affected by the treatment. No wall destructuration is detected (Figure 49). Multiple cells observed before treatment however exhibited various wall appearances: from a hundred of nanometers to several micrometers of thickness, multiple layers, with sometimes empty layers.

Regarding the lipid droplets (stained in bright green), no neutral lipid leakage seems to occur, as previously reported (see section III1f)). **Lipid droplet coalescence is once more confirmed. But we could go further on their morphology and demonstrate that at first, they presented a circular shape and were deconstructed after treatment.** Instead of multiple small droplets, only a few lipid patches are seen. **We could hypothesize that the phospholipid layer surrounding oil bodies was affected by the PEF treatment.**

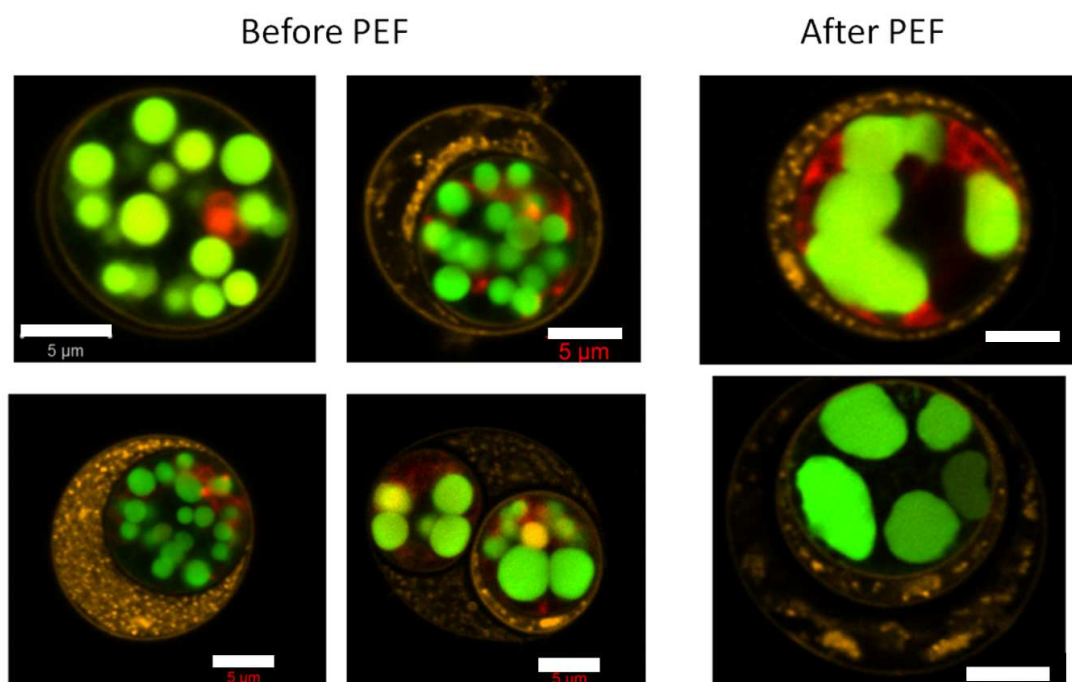


Figure 49: CLSM observation of *Chlamydomonas reinhardtii* cells (7 days of stress) before and after PEF treatment (7 kV/cm, 5 μ s, burst of 10 pulses with a frequency of 10 Hz). Cell wall stained with Concanavalin A (yellow), neutral lipids stained with Bodipy (green), Chlorophyll autofluorescence (red). Scale bar: 5 μ m.

III3) Association of PEF to solvent for lipid extraction

III3a) Cell lysis

In order to extract lipid from *Chlamydomonas reinhardtii* three solvents were tested: ethyl acetate (LogP = 0.73), hexane (LogP = 4.00) and dodecane (LogP = 6.6). As explained in the section II4a), a high LogP indicates a high biocompatibility of the solvent to algae, but its extraction capability can also be reduced because of its low affinity with the aqueous phase. Ethyl-acetate and hexane are known to be able to extract a majority of neutral lipids [77], dodecane is a solvent with a high biocompatibility for the algae [76].

First, the impact of those solvents on cell lysis was evaluated.

The mixing step was performed as described in Figure 34, except that the ratio of solvent to aqueous phase was different: ethyl acetate (Figure 50) was added at low volumes (7.5 μL , 10 μL and 20 μL for 100 μL of algae solution), hexane (Figure 51) was added at a ratio of 2:1, and dodecane (Figure 52) at a ratio 1:1 (experiments were performed at various stages of the project).

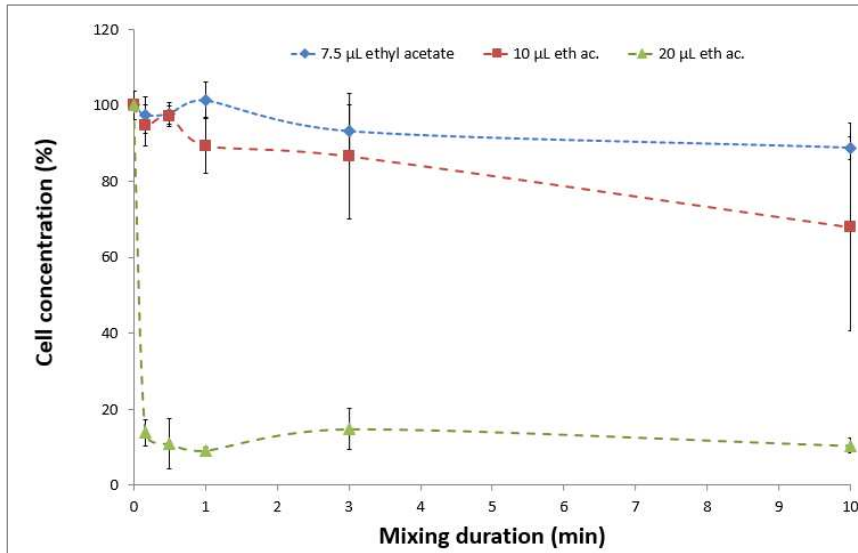


Figure 50 : Cell concentration* (%) over mixing time when mixing *Chlamydomonas reinhardtii* wt (7d of stress) with ethyl acetate. *Cell concentration relative to the cell concentration before mixing.

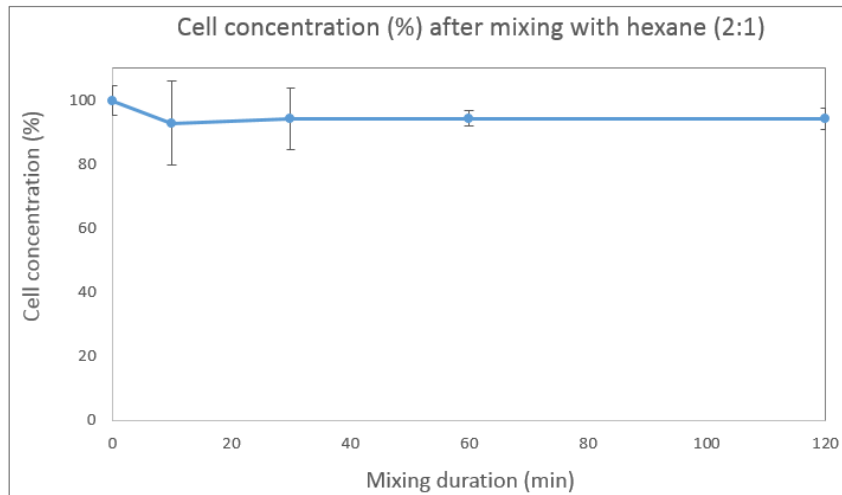


Figure 51: Cell concentration* (%) over time when mixing *Chlamydomonas reinhardtii* wt (7d of stress) with hexane. *Cell concentration relative to the cell concentration before mixing.

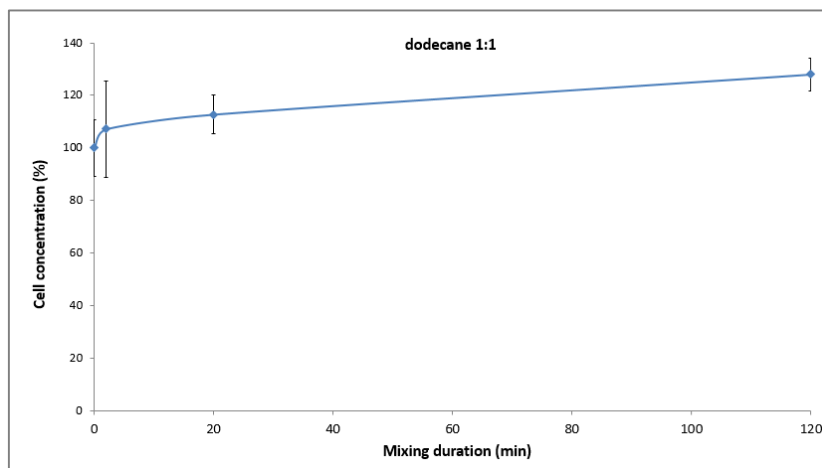


Figure 52 : Cell concentration* over time when mixing *Chlamydomonas reinhardtii* wt (7d of stress) with dodecane. *Cell concentration relative to the cell concentration before mixing.

As it can be observed in Figure 50, **ethyl-acetate has a very strong impact on cell lysis as a high reduction of the cell number is measured after a few seconds of contact** when using a solvent ratio of 0.1:1 (20 μ L of solvent of 200 μ L of algae). When using a lower volume of solvent, cell lysis is reduced. This is in accordance with the **aqueous critical solvent concentration** mentioned previously in the report [70], where solvent with a low LogP can have major impact on the cells. **For the other solvents, hexane and dodecane, the impact on cell lysis is negligible**, even when using a high volume of solvent and longer mixing times (up to 2 hours). From the previous data, ethyl acetate was no further studied.

III3b) CLSM imaging of cells after solvent extraction

Chlamydomonas reinhardtii wt cells (7 days of stress) treated with ethyl acetate (10 μ L in 100 μ L of algae, mixing duration: 10 minutes) were observed by CLSM (Figure 53). Lipids are stained by Bodipy (in green) and the cell wall is stained with concanavalin TRITC (in yellow). **As it can be observed, cells are still intact after contact with ethyl acetate. Moreover, bodipy staining is found in the cytoplasm and in between the cell wall layers, suggesting that part of the lipids is trapped in the cell wall and that others left the cytoplasm under solvent action.**

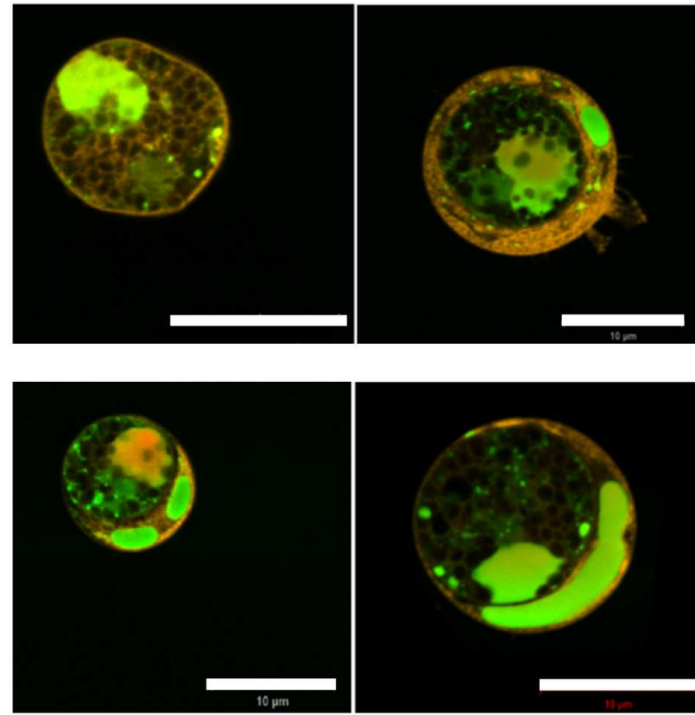


Figure 53 : CLSM imaging of *Chlamydomonas reinhardtii* wt cells after 10 min mixing with ethyl acetate (7.5 μL of ethyl acetate added to 100 μL of algal solution). Lipid droplets stained by bodipy (green), cell wall stained by concanavalin TRITC (yellow). Scale bar: 10 μm .

The effect of dodecane on *Chlamydomonas reinhardtii* wt cells (7 days of stress) is shown in Figure 54 (2 h mixing time solvent/algae ratio of 1:1). Observations confirmed that **a part of the cells was totally unaffected by the solvent. Indeed**, due to the high hydrophobicity of the solvent, the contact between cells and dodecane was quite reduced despite the used mixing conditions. In Figure 54, only cells affected by the solvent are shown. **The lipid droplets are destructured in the cytoplasm, but most of them seem to remain in the cytoplasm.** Also, **Bodipy fluorescence seems to be bleached by the solvent.**

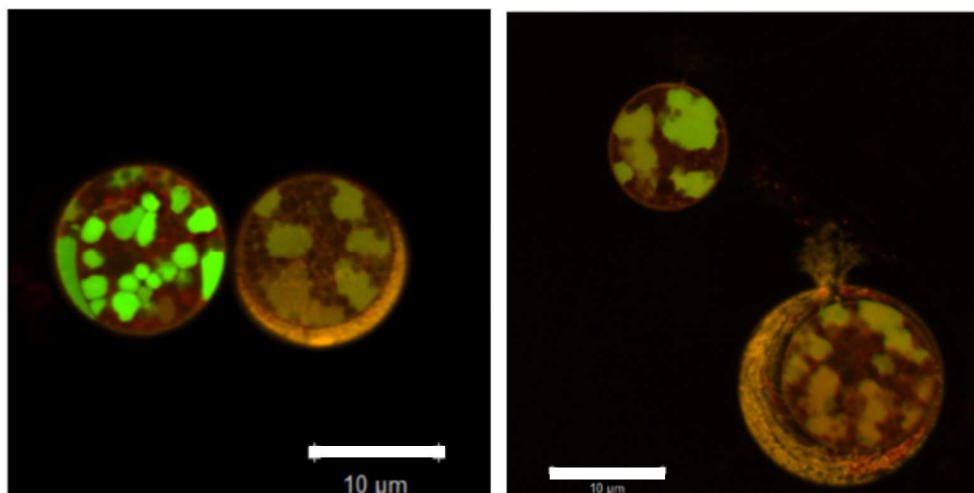


Figure 54 : CLSM imaging of *Chlamydomonas reinhardtii* wt cells after 2 h mixing with dodecane (ratio 1:1). Lipid droplets stained by bodipy (green), cell wall stained by concanavalin TRITC (yellow). Scale bar: 10 μm .

III3c) Lipid extraction

After evaluating cell lysis and solvent effect on lipid droplets behavior by CLSM imaging, lipid extraction is quantified.

Because of Bodipy bleaching when cells are in contact with solvents and loss of lipid droplets structure under these conditions (see Figure 54), **Bodipy was not used for quantitative analyzes of lipid extraction**. Indeed, the measurement of the mean bodipy fluorescence per cell before and after solvent extraction is not a suitable method in these conditions.

SPV colorimetric method was therefore used to evaluate lipid extraction from the cells. Lipid amounts in the solvent and aqueous phases before and after extraction were measured (section II4c))

For further experiments, **hexane was chosen as the model solvent because of its very low impact on cell lysis** (Figure 51), and its **LogP of 4** (intermediate between dodecane and ethyl acetate) **is expected to allow a rather good contact of the solvent with the cells and then a significant lipid extraction**. In addition, **its boiling point is low (68°C)** which enables an easy solvent evaporation required for the SPV method.

First, similar **calibration curves of triolein dissolved in hexane and chloroform**, the solvent commonly used in the SPV method, were obtained (Figure 59). The former (see appendix III3) was used for the calculations.

After mixing the algal solution and hexane and centrifugation of the mixture, the system split into three phases with a yellowish layer between hexane (upper layer) and the aqueous phase (bottom layer) as illustrated below (Figure 55):

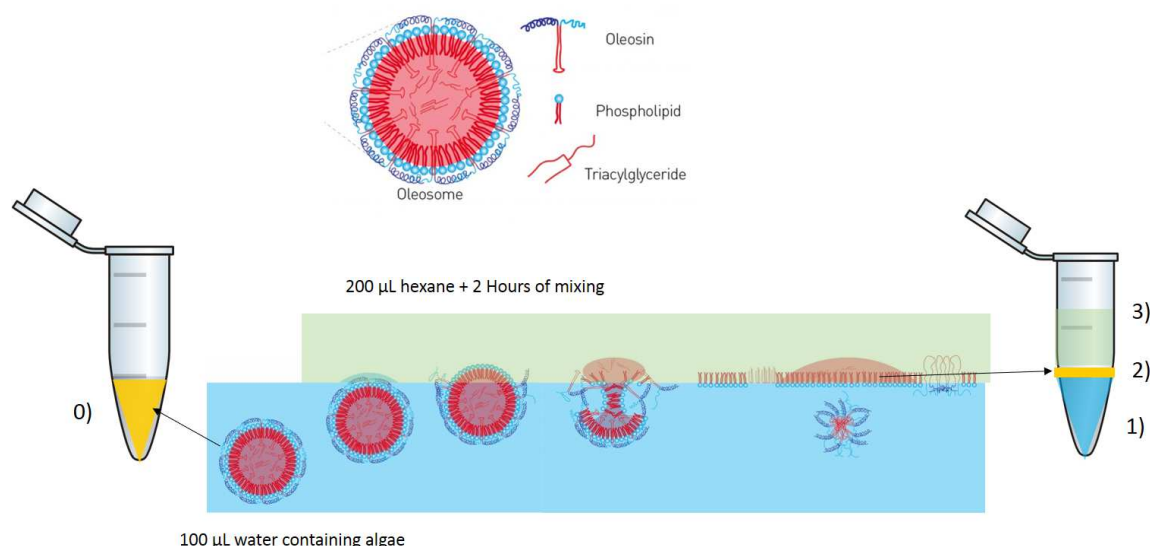


Figure 55 : Lipid extraction performed with 200 µL of hexane on 100 µL of aqueous phase containing algae. Oleosome (neutral lipids as Triacylglycerides surrounded by a mono-layer of phospho-lipids and proteins) are contained in the cytoplasm of algae in the aqueous phase (0). Lipids extracted remains as an interphase (2) between the aqueous phase (1) and the hexane phase (3). Modified from [85].

The yellowish layer probably consists of **neutral and/or polar lipids extracted, but not dissolved in the hexane upper phase**; this yellow layer **indeed entirely dissolves into hexane after addition of a low quantity of Isopropanol (IPA), resulting in only two phases (aqueous and organic containing hexane, IPA and lipids)**. The mixture of high polar IPA and low polar hexane could thus be used to dissolve the fatty acids in the upper phase.

However, further experiments showed that **IPA is not suitable for SPV analyzes**. Indeed, after its addition, the absorbance measured in the aqueous and solvent phases was much higher (absorbance above 10) than determined in the algal solution before extraction (in the range of 0.4). Consequently, experiments were further performed without IPA, and the yellowish interface was considered as an independent phase.

The extraction rate in the aqueous phase is presented in Figure 56.

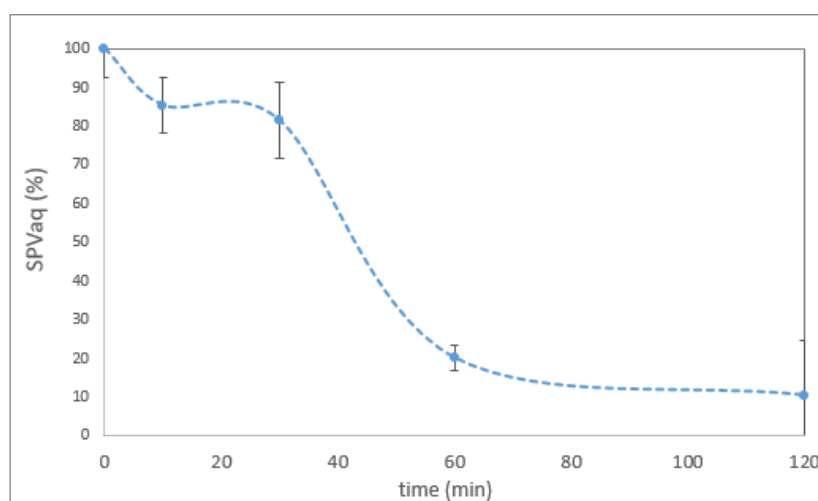


Figure 56 : SPV signal measured in the aqueous phase after mixing with hexane. The value is expressed as a percentage, relative to the initial value before extraction.

The figure presenting the evolution of SPV signal of the aqueous phase with time shows that most of the lipids are extracted during the first hour of extraction. After two hours of extraction, about 10 % of the signal remain in the aqueous phase, 90 % is in the interface, no signal is measured in the hexane phase.

In the following experiment, **algae solutions were mixed with hexane during 10 minutes** with or without PEF pre-treatment. **PEF conditions used were those leading to irreversible permeabilization of *Chlamydomonas reinhardtii* wt cells while minimizing energy consumption, i.e. 7 kV/cm, 5 μ s and a burst of 10 pulse (10 Hz).**

SPV data of the different phases under the tested conditions are presented in Figure 57. Results (in absorbance) are converted into triolein equivalent with the equation of the calibration curve presented before. The medium and upper phases are analyzed together.

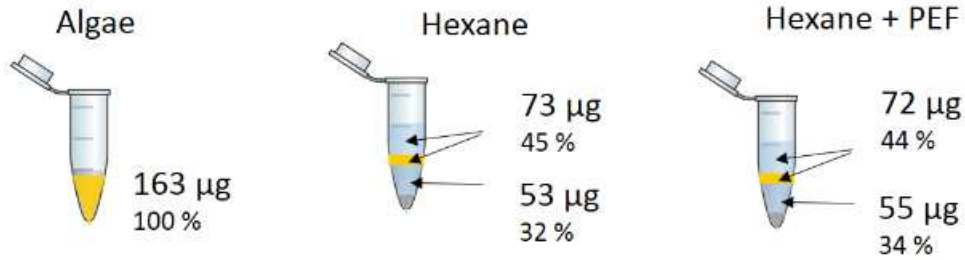


Figure 57 : Lipid extraction after 10 minutes of mixing with hexane with or without PEF pre-treatment (5 µs, 7 kV/cm).. Analyzes of the phases by the SPV method. Measurements are given in triolein equivalent.

The results show that part of the lipids is efficiently extracted after 10 minutes of mixing of the algae solution with hexane (which is not in accordance with the extraction rate presented Figure 56). The mass balances of triolein equivalents are not satisfied due to the difficulty of volume precise measures. As a consequence, assuming that the aqueous response would be more precise, the extracted lipid mass, expressed in triolein equivalent, (in both medium and upper phases), was calculated by difference between the initial lipid mass and the aqueous remaining value.

Nevertheless, up to this point with our experiment, we couldn't distinguish the **extraction obtained with or without PEF pre-treatment** (66-68%). We could not demonstrate the improvement brought by the PEF treatment to the lipid extraction.

In addition, the majority of the SPV response of both medium and upper phases is obtained in the medium phase and not in hexane, due to the poor solubility of lipids in pure hexane. Moreover, no cell lysis was detected under these conditions.

Finally, **stronger PEF conditions were used in order to check if lipid extraction could be improved with PEF pre-treatment** (50 and 500 µs pulses with an electric field of 7 kV/cm). The lipid content of the aqueous phase was measured and the extraction yield was calculated by difference as before.

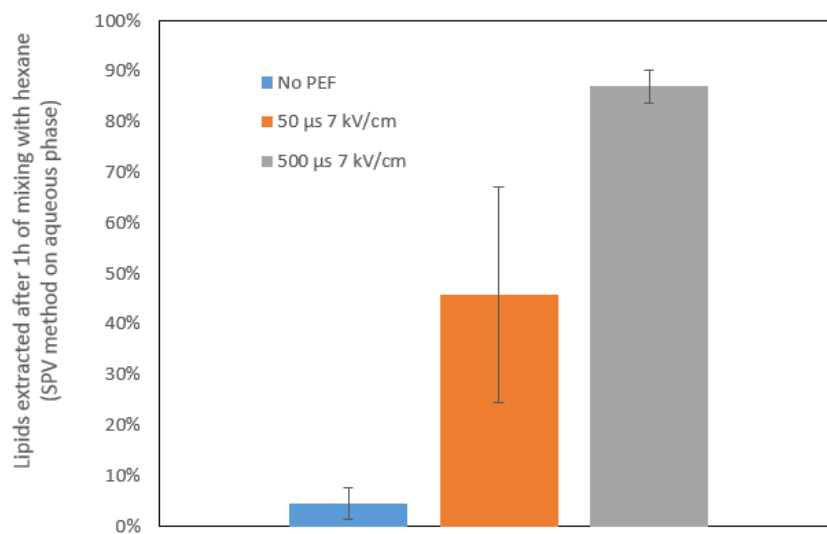


Figure 58 : Lipid extraction after 1h of mixing with hexane with or without PEF pre-treatment (50 µs, 7 kV/cm and 500 µs 7 kV/cm). Analyzes of the phases by SPV method. Calculation: equation 3.13.

An improvement of lipid extraction after treating the cells with these stronger conditions of PEF is clearly observed. However, this positive result must be carefully evaluated: (1) the **energy spent in this PEF pre-treatment is huge** in comparison with the optimal conditions determined before. This leads to a **high temperature increase in the cuvette which can melt the cell wall leading to cell lysis and foster the release of lipids**. In comparison with 5 μ s pulses and 7 kV/cm, **the energy spent for 50 μ s and 500 pulses with an electric field of 7 kV/cm is 10 and 100 times higher, respectively**. (2) the lipid extraction obtained here without PEF (reference), of 4.5 ± 3.1 %, is much lower than the extraction of 66% obtained after 1 hour in the experiment performed with 5 μ s pulses (Figure 57) and than the extraction rate presented in Figure 56. **Results must be carefully evaluated**. A question still remains on the non reproductibility of lipid extraction with solvent; this must be further examined.

III3d) Conclusion on lipid extraction

A **good compromise must be found when choosing the PEF pre-treatment conditions in order to obtain an improvement of lipid extraction with a limited energy use**. In our tested conditions (7KV/cm, 5 μ s), the opening of **irreversible pores on the cell membrane does not improve clearly lipid extraction with solvent**. Two hypothesis can be drawn from this observation (1) either **the size of the pores opened is not sufficient** for a rapid lipid transfer across the membrane or (2) lipid diffusion across the membrane is improved with PEF but the **cell wall hinders further lipid extraction**.

We could verify that an irreversible permeabilization followed by several hours of incubation (to let irreversible pores expand) allows efficient lipid extraction.

If it is verified that the cell wall is the limiting interface which prevents lipids extraction, **the use of PEF as a pre-treatment must be accompanied by other complementary treatments (mechanical compression) to improve lipid extraction. This strategy is evaluated in the laboratory (with promising preliminary results)**. Anyway, the use of PEF for the extraction of soluble compounds such as proteins and pigments remains reasonable. More studied on the use of the cell wall deficient algae *Chlamydomonas reinhardtii* cw15 could be performed to trigger the release of the cytoplasm content by non-thermal electroporation.

Chapter 3 conclusion

The use of pulsed electric fields has an increasing interest in various fields: biomedical, food, environment. PEF is also a candidate as a novel downstream process in algal biotechnology as it can be used as a low-energy demanding pre-treatment process to facilitate the extraction of intracellular compounds from algae. Because of the multiplicity of **(1) PEF parameters** (pulse duration, electric field intensity, pulse frequency and shape), **(2) algae strain and cultures** features (cell size, cell wall thickness, medium conductivity etc...) and **(3) the various applications** (cell lysis, extraction of soluble compounds as well as lipids), it is difficult to have a **clear overview of the effects of such a process** in algae and therefore its application as an innovative downstream process. Studies aiming at understanding **the impact of PEF on microalgae membrane and cell wall must therefore be undertaken**. Moreover, in contrast to biomedical applications, **the energy demand is a paramount criterion for the economic viability and environmental footprint of this innovative process at industrial scale**.

The study was performed on *Chlamydomonas reinhardtii* wild type. PEF main parameters, **electric field and pulse durations, were optimized (considering the energy consumption, the permeabilization of cells as well as their viability after permeabilization)** and a burst of 10 monopolar square pulses delivered with a frequency of 10 Hz was set constant. Membrane permeability, measured with two dyes: Propidium Iodide and Sytox Green, was determined at different electric fields (0.2 to 20 kV/cm) and various pulse durations within the range of **5 μ s to 500 μ s**.

We designed and built a dedicated micro-device to study the impact of PEF on algae cells *in situ*. With this new approach, cell structure and, in particular, the behavior of special features (lipids, membrane, cell wall) could be observed *in situ* and, in some cases, *in real time* when applying a PEF treatment. PEF conditions allowing high permeability were optimized while minimizing the process energy demand. In this context, an experimental method based on the penetration of Propidium Iodide in permeabilized cells was developed. **The results obtained by a visual counting in the micro-device were then verified in an up-scaled system** (micro-cuvettes) by automatic counting using a flow cytometry method.

Electric fields required to trigger reversible and irreversible electroporation of *Chlamydomonas reinhardtii* cells in accumulating lipids conditions, were, respectively, for 5 μ s pulses, 4.5 kV/cm and 7 kV/cm. Electric fields required for 50 and 500 μ s pulses are lower, but the overall energy spent is higher. The energy consumptions to perform electroporation are though lower than those reported by other authors. It is thus very interesting **to use short pulses with high electric field from an economic point of view**. However, it is not so trivial to scale up the process to large volumes, due to the high voltage required to achieve the desired electric field.

The effects of sub-microsecond pulses were not investigated because our generator was not able to deliver nano-pulses. Nanopulses, which consist in the application of very high electric field (tens – hundreds of kV/cm during few nano-seconds) may lead to very different results, such as internal effects without affecting the cytoplasmic membrane. In term of energy spent per pulse, these pulses may

result in a very economical treatment. However, the effects on membrane permeability, cell viability, cell wall effects are totally unknown.

The optimal parameters determined in this study could be used, as a starting point, for another algae strain by a simple adaptation of the electric field to the algae size (see the importance of cell radius in Schwan equation, eq. 3.2). Although, PEF inducing permeability does not seem to be related to Joule effect, in our optimized conditions. However, temperature increases, which highly depend on electric field and pulse duration, and on the medium conductivity, must be carefully evaluated to distinguish electroporation effects with other side effects when using long pulses.

The resealing of reversible pores using short (5 μ s) or long pulses (500 μ s) was shown to be very fast: within one minute.

In situ qualitative observations using lipid droplets staining demonstrated lipids displacement and coalescence during the application of pulses in bright field and fluorescence. Moreover, our treatment conditions, leading to membrane permeabilization with low thermal effects, showed **no impact on the thick wall of *Chlamydomonas reinhardtii* wild type**. Despite an effect of PEF on lipid droplets, the **low affinity of lipids with the external medium and the presence of the unaffected cell wall may prevent natural lipid leakage**. Consequently, and as expected, in the case of a strain with a resistant cell wall, **PEF must be associated with a secondary treatment, e.g. the use of organic solvents**.

Additional experiments performed with solvents have shown that the **polar affinity of the solvent is a paramount parameter** to consider in order **to find the compromise between biocompatibility with algae and lipid extraction**. Based on the effect of the solvents on **cell lysis and qualitative observations, pure hexane was finally chosen** for lipid extraction in a purpose of algae fractionation in an aqueous extraction (valorization of the remaining biomass, reduction of the energy spent during water separation). The goal was to check if PEF pre-treatment could improve lipid extraction with hexane. Our preliminary results showed that irreversible electroporation can increase the lipid extraction with solvents. **In the case of reversible electroporation, complementary treatment must be applied prior to the solvent assisted lipid extraction. Promising preliminary experiments are currently held in the laboratory.**

Chapter 3 references

- [1] R. Slade, A. Bauen, Micro-algae cultivation for biofuels: Cost, energy balance, environmental impacts and future prospects, *Biomass and Bioenergy*. 53 (2013) 29–38. doi:10.1016/j.biombioe.2012.12.019.
- [2] C.P. Bravo-Fritz, C.A. Sáez-Navarrete, L.A. Herrera-Zepelin, F. Varas-Concha, Multi-scenario energy-economic evaluation for a biorefinery based on microalgae biomass with application of anaerobic digestion, *Algal Res.* 16 (2016) 292–307. doi:10.1016/j.algal.2016.03.028.
- [3] T. Kotnik, P. Kramar, G. Pucihar, D. Miklavcic, M. Tarek, Cell membrane electroporation- Part 1: The phenomenon, *IEEE Electr. Insul. Mag.* 28 (2012) 14–23. doi:10.1109/MEI.2012.6268438.
- [4] J. Teissie, M. Golzio, M.P. Rols, Mechanisms of cell membrane electroporation: a minireview of our present (lack of ?) knowledge., *Biochim. Biophys. Acta.* 1724 (2005) 270–80. doi:10.1016/j.bbagen.2005.05.006.
- [5] E.C. Neyts, M. Yusupov, C.C. Verlackt, A. Bogaerts, Computer Simulations of Plasma-Biomolecule and Plasma- Tissue Interactions for a Better Insight in Plasma Medicine, *J. Phys. D. Appl. Phys.* XX (2014) 29. doi:10.1088/0022-3727/47/29/293001.
- [6] W. Sung, P.J. Park, Dynamics of pore growth in membranes and membrane stability., *Biophys. J.* 73 (1997) 1797–804. doi:10.1016/S0006-3495(97)78210-9.
- [7] L. Chopinet, C. Roudit, M.-P. Rols, E. Dague, Destabilization induced by electroporation analyzed by atomic force microscopy., *Biochim. Biophys. Acta.* 1828 (2013) 2223–9. doi:10.1016/j.bbame.2013.05.035.
- [8] M. Kanduser, M. Sentjerc, D. Miklavcic, The temperature effect during pulse application on cell membrane fluidity and permeabilization., *Bioelectrochemistry.* 74 (2008) 52–7. doi:10.1016/j.bioelechem.2008.04.012.
- [9] L. Barr, Membrane Potential Profiles and the Goldman Equation, (1965) 351–356.
- [10] S. Abe, J. Takeda, M. Senda, Resting membrane potential and action potential of *Nitella expansa* protoplasts, 21 (1980) 537–546.
- [11] J.C. Weaver, K.C. Smith, A.T. Esser, R.S. Son, T.R. Gowrishankar, A brief overview of electroporation pulse strength-duration space: a region where additional intracellular effects are expected., *Bioelectrochemistry.* 87 (2012) 236–43. doi:10.1016/j.bioelechem.2012.02.007.
- [12] P. Marszalek, Schwan equation and transmembrane potential induced by, 58 (1990) 1053–1058.
- [13] C.M. Electroporation, An Experimental Evaluation of the Critical Potential Difference, 65 (1993) 409–413.
- [14] D. Grund, D. Zellmembranen, B. Anlegen, D. Zellinnere, D. Auf, D. Ladungsverteilung, Über die Im pedanz einer Suspension von kugelförmigen Teilchen mit einer Schale, (1959) 125–131.
- [15] M.S. Bono, B. a Ahner, B.J. Kirby, Detection of algal lipid accumulation due to nitrogen limitation via dielectric spectroscopy of *Chlamydomonas reinhardtii* suspensions in a coaxial transmission line sample cell., *Bioresour. Technol.* 143 (2013) 623–31. doi:10.1016/j.biortech.2013.06.040.
- [16] Y. Polevaya, I. Ermolina, M. Schlesinger, B.Z. Ginzburg, Y. Feldman, Time domain dielectric spectroscopy study of human cells. II. Normal and malignant white blood cells., *Biochim. Biophys. Acta.* 1419 (1999) 257–271. doi:10.1007/BF00188038.
- [17] W.M. Arnold, U. Zimmermann, Rotating-field-induced rotation and measurement of the membrane capacitance of single mesophyll cells of *avena sativa*, *Zeitschrift Fur Naturforsch. - Sect. C J. Biosci.* 37 (1982) 908–915. doi:10.1515/znc-1982-1010.
- [18] B.G. Frank S. Barnes, Biological and Medical Aspects of Electromagnetic Fields (Handbook of Biological Effects of Electromagnetic Fields) 3Ed, 2006.
- [19] http://www.electronics-tutorials.ws/rc/rc_1.html.
- [20] M. Goettel, C. Eing, C. Gusbeth, R. Straessner, W. Frey, Pulsed electric field assisted extraction of intracellular valuables from microalgae, *Algal Res.* 2 (2013) 401–408. doi:10.1016/j.algal.2013.07.004.
- [21] C. Dalmay, M. a De Menorval, O. Français, L.M. Mir, B. Le Pioufle, A microfluidic device with removable packaging for the real time visualisation of intracellular effects of nanosecond electrical pulses on adherent cells., *Lab Chip.* 12 (2012) 4709–15. doi:10.1039/c2lc40857k.
- [22] E. Luengo, S. Condón-Abanto, I. Alvarez, J. Raso, Effect of Pulsed Electric Field Treatments on Permeabilization and Extraction of Pigments from *Chlorella vulgaris*., *J. Membr. Biol.* 247 (2014) 1269–77. doi:10.1007/s00232-014-9688-2.
- [23] M. Coustets, N. Al-Karablieh, C. Thomsen, J. Teissie, Flow process for electroextraction of total proteins from microalgae., *J. Membr. Biol.* 246 (2013) 751–60. doi:10.1007/s00232-013-9542-y.
- [24] J. Sheng, R. Vannela, B.E. Rittmann, Evaluation of cell-disruption effects of pulsed-electric-field treatment of *Synechocystis* PCC 6803., *Environ. Sci. Technol.* 45 (2011) 3795–802. doi:10.1021/es103339x.
- [25] M.D.A. Zbinden, B.S.M. Sturm, R.D. Nord, W.J. Carey, D. Moore, H. Shinogle, S.M. Stagg-Williams, Pulsed electric field (PEF) as an intensification pretreatment for greener solvent lipid extraction from microalgae., *Biotechnol. Bioeng.* 110 (2013) 1605–15. doi:10.1002/bit.24829.
- [26] S. Tristram-Nagle, J.F. Nagle, Lipid bilayers: Thermodynamics, structure, fluctuations, and interactions, *Chem. Phys. Lipids.* 127 (2004) 3–14. doi:10.1016/j.chemphyslip.2003.09.002.
- [27] C.E. Nebel, D. Shin, B. Rezek, N. Tokuda, Diamond and biology, (2007) 439–461. doi:10.1098/rsif.2006.0196.
- [28] M. Kanduser, M. Sentjerc, D. Miklavcic, The temperature effect during pulse application on cell membrane fluidity and permeabilization., *Bioelectrochemistry.* 74 (2008) 52–7. doi:10.1016/j.bioelechem.2008.04.012.
- [29] P.T. Vernier, Z. a Levine, Y.-H. Wu, V. Joubert, M.J. Ziegler, L.M. Mir, D.P. Tieleman, Electroporating fields target oxidatively damaged areas in the cell membrane., *PLoS One.* 4 (2009) e7966. doi:10.1371/journal.pone.0007966.
- [30] M.L. Yarmush, A. Golberg, G. Serša, T. Kotnik, D. Miklavčič, Electroporation-based technologies for medicine: principles, applications, and challenges., *Annu. Rev. Biomed. Eng.* 16 (2014) 295–320. doi:10.1146/annurev-bioeng-071813-104622.
- [31] S.J. Beebe, N.M. Sain, W. Ren, Induction of Cell Death Mechanisms and Apoptosis by Nanosecond Pulsed Electric Fields (nsPEFs), *Cells.* 2 (2013) 136–62. doi:10.3390/cells2010136.
- [32] G. Saulis, R. Saulė, Size of the pores created by an electric pulse: microsecond vs millisecond pulses., *Biochim. Biophys. Acta.* 1818 (2012) 3032–9. doi:10.1016/j.bbame.2012.06.018.
- [33] M.G. Moisesescu, M. Radu, E. Kovacs, L.M. Mir, T. Savopol, Changes of cell electrical parameters induced by electroporation. A

Chapter 3: The use of Pulsed Electric Fields for the extraction of lipids from *Chlamydomonas reinhardtii*: study in microdevice and electroporation cuvettes

- dielectrophoresis study., *Biochim. Biophys. Acta.* 1828 (2013) 365–72. doi:10.1016/j.bbamem.2012.08.030.
- [34] M.M. Sadik, J. Li, J.W. Shan, D.I. Shreiber, H. Lin, Quantification of propidium iodide delivery using millisecond electric pulses: experiments., *Biochim. Biophys. Acta.* 1828 (2013) 1322–8. doi:10.1016/j.bbamem.2013.01.002.
- [35] S. Guo, D.L. Jackson, N.I. Burcus, Y.-J. Chen, S. Xiao, R. Heller, Gene electrotransfer enhanced by nanosecond pulsed electric fields, *Mol. Ther. — Methods Clin. Dev.* 1 (2014) 14043. doi:10.1038/mtm.2014.43.
- [36] S. Haberl, D. Miklavcic, G. Sersa, W. Frey, B. Rubinsky, Cell membrane electroporation-Part 2: the applications, *IEEE Electr. Insul. Mag.* 29 (2013) 29–37. doi:10.1109/MEI.2013.6410537.
- [37] T.S. Santra, P. Wang, *Electroporation Based Drug Delivery and Its Applications*, (2013).
- [38] R. Buckow, S. Ng, S. Toepfl, Pulsed Electric Field Processing of Orange Juice: A Review on Microbial, Enzymatic, Nutritional, and Sensory Quality and Stability, *Compr. Rev. Food Sci. Food Saf.* 12 (2013) 455–467. doi:10.1111/1541-4337.12026.
- [39] M.F. Turk, C. Billaud, E. Vorobiev, A. Baron, Continuous pulsed electric field treatment of French cider apple and juice expression on the pilot scale belt press, *Innov. Food Sci. Emerg. Technol.* 14 (2012) 61–69. doi:10.1016/j.ifset.2012.02.001.
- [40] L. Schrive, G. Lumia, F. Pujol, N. Boussetta, Liquid food pasteurization by pulsed electric fields: dimensionless analysis via Sherwood number for a comprehensive understanding, *Eur. Food Res. Technol.* 239 (2014) 707–718. doi:10.1007/s00217-014-2268-y.
- [41] G. Saldaña, I. Álvarez, S. Condón, J. Raso, Microbiological aspects related to the feasibility of PEF technology for food pasteurization., *Crit. Rev. Food Sci. Nutr.* 54 (2014) 1415–26. doi:10.1080/10408398.2011.638995.
- [42] K. Loginova, M. Loginov, E. Vorobiev, N.I. Lebovka, Better lime purification of sugar beet juice obtained by low temperature aqueous extraction assisted by pulsed electric field, *LWT - Food Sci. Technol.* 46 (2012) 371–374. doi:10.1016/j.lwt.2011.10.005.
- [43] E. Puértolas, O. Cregenzán, E. Luengo, I. Alvarez, J. Raso, Pulsed-electric-field-assisted extraction of anthocyanins from purple-fleshed potato., *Food Chem.* 136 (2013) 1330–6. doi:10.1016/j.foodchem.2012.09.080.
- [44] D. Miklavc, *Electrotechnologies for Extraction from Food Plants and Biomaterials*, Springer New York, New York, NY, 2009. doi:10.1007/978-0-387-79374-0.
- [45] <http://hpbandgisurgery.com/irreversible-electroporation/>.
- [46] T. Kotnik, W. Frey, M. Sack, S. Haberl Meglič, M. Peterka, D. Miklavčič, Electroporation-based applications in biotechnology, *Trends Biotechnol.* 33 (2015) 480–488. doi:10.1016/j.tibtech.2015.06.002.
- [47] O. Parniakov, F.J. Barba, N. Grimi, L. Marchal, S. Jubeau, N. Lebovka, E. Vorobiev, Pulsed electric field and pH assisted selective extraction of intracellular components from microalgae *Nannochloropsis*, *Algal Res.* 8 (2015) 128–134. doi:10.1016/j.algal.2015.01.014.
- [48] K. Flisar, S.H. Meglic, J. Morelj, J. Golob, D. Miklavcic, Testing a prototype pulse generator for a continuous flow system and its use for *E. coli* inactivation and microalgae lipid extraction., *Bioelectrochemistry.* 100 (2014) 44–51. doi:10.1016/j.bioelechem.2014.03.008.
- [49] M.U. Khan, K. Mitchell, Chlorophylls Carotenoids, *Methods.* 148 (1987) 350–382.
- [50] K. Matsumura, T. Yagi, A. Hattori, M. Soloviev, K. Yasuda, Using single cell cultivation system for on-chip monitoring of the interdivision timer in *Chlamydomonas reinhardtii* cell cycle., *J. Nanobiotechnology.* 8 (2010) 23. doi:10.1186/1477-3155-8-23.
- [51] S.K. Min, G.H. Yoon, J.H. Joo, S.J. Sim, H.S. Shin, Mechanosensitive physiology of *Chlamydomonas reinhardtii* under direct membrane distortion., *Sci. Rep.* 4 (2014) 4675. doi:10.1038/srep04675.
- [52] H.S. Kwak, J.Y.H. Kim, S.C. Na, N.L. Jeon, S.J. Sim, Multiplex microfluidic system integrating sequential operations of microalgal lipid production, *Analyst.* 141 (2016) 1218–1225. doi:10.1039/C5AN02409A.
- [53] Olivier Français and Bruno Le Pioufle, *Single Cell Electrical Characterization Techniques*, 2016. doi:10.1007/978-3-319-26779-1_15-1.
- [54] Y.-L. Deng, J.-S. Chang, Y.-J. Juang, Separation of microalgae with different lipid contents by dielectrophoresis., *Bioresour. Technol.* 135 (2013) 137–41. doi:10.1016/j.biortech.2012.11.046.
- [55] K. a. Michael, S.R. Hiibel, E.J. Geiger, Dependence of the dielectrophoretic upper crossover frequency on the lipid content of microalgal cells, *Algal Res.* 6 (2014) 17–21. doi:10.1016/j.algal.2014.08.004.
- [56] T. Mu, *Dielectric single cell spectra in snow algae*, (1998) 303–310.
- [57] C.I. Trainito, E. Bayart, F. Subra, O. Français, B. Le Pioufle, The Electrorotation as a Tool to Monitor the Dielectric Properties of Spheroid During the Permeabilization, *J. Membr. Biol.* (2016). doi:10.1007/s00232-016-9880-7.
- [58] M.M. Bahi, M.-N. Tsaloglou, M. Mowlem, H. Morgan, Electroporation and lysis of marine microalga *Karenia brevis* for RNA extraction and amplification., *J. R. Soc. Interface.* 8 (2011) 601–8. doi:10.1098/rsif.2010.0445.
- [59] C.I. Trainito, O. Français, B. Le Pioufle, E.N. Supérieure, L. Satie, C.I. Trainito, E.N. Supérieure, L. Satie, Monitoring the permeabilization of a single cell in a microfluidic device , through the estimation of its dielectric properties based on combined dielectrophoresis and electrorotation in-situ experiments . Abbreviation : PEF : Pulsed Electric Field , ROT , (n.d.) 1–18. doi:10.1002/elps.201400482.This.
- [60] M.B. Fox, D.C. Esveld, a Valero, R. Lutgje, H.C. Mastwijk, P. V Bartels, a van den Berg, R.M. Boom, Electroporation of cells in microfluidic devices: a review., *Anal. Bioanal. Chem.* 385 (2006) 474–85. doi:10.1007/s00216-006-0327-3.
- [61] M. Sato, Y. Murata, M. Mizusawa, A Simple and Rapid Dual fluorescence Viability Assay, 20 (2004).
- [62] P. Hyka, S. Lickova, P. Přibyl, K. Melzoch, K. Kovar, Flow cytometry for the development of biotechnological processes with microalgae., *Biotechnol. Adv.* 31 (2012) 2–16. doi:10.1016/j.biotechadv.2012.04.007.
- [63] F.C. Mortimer, D.J. Mason, V. a Gant, Flow Cytometric Monitoring of Antibiotic-Induced Injury in *Escherichia coli* Using Cell-Impermeant Fluorescent Probes Flow Cytometric Monitoring of Antibiotic-Induced Injury in *Escherichia coli* Using Cell-Impermeant Fluorescent Probes, 44 (2000) 676–681. doi:10.1128/AAC.44.3.676-681.2000.Updated.
- [64] K.-S. Kan, J.P. Thornber, The light-harvesting chlorophyll a/b-protein complex of *Chlamydomonas reinhardtii*, *Plant Physiol.* 57 (1976) 47–52. doi:10.1104/pp.57.1.47.
- [65] G. Bonente, S. Pippa, S. Castellano, R. Bassi, M. Ballottari, Acclimation of *Chlamydomonas reinhardtii* to different growth irradiances, *J. Biol. Chem.* 287 (2012) 5833–5847. doi:10.1074/jbc.M111.304279.
- [66] M.H.A. Michels, A.J. Van Der Goot, N.H. Norsker, R.H. Wijffels, Effects of shear stress on the microalgae *Chaetoceros muelleri*, *Bioprocess Biosyst. Eng.* 33 (2010) 921–927. doi:10.1007/s00449-010-0415-9.
- [67] P. Hyka, S. Lickova, P. Přibyl, K. Melzoch, K. Kovar, Flow cytometry for the development of biotechnological processes with microalgae., *Biotechnol. Adv.* 31 (2012) 2–16. doi:10.1016/j.biotechadv.2012.04.007.
- [68] M.C. Vernhes, P. a. Cabanes, J. Teissie, Chinese hamster ovary cells sensitivity to localized electrical stresses, *Bioelectrochemistry Bioenerg.* 48 (1999) 17–25. doi:10.1016/S0302-4598(98)00239-6.

Chapter 3: The use of Pulsed Electric Fields for the extraction of lipids from *Chlamydomonas reinhardtii*: study in microdevice and electroporation cuvettes

- [69] F. Zhang, L.-H. Cheng, X.-H. Xu, L. Zhang, H.-L. Chen, Screening of biocompatible organic solvents for enhancement of lipid milking from *Nannochloropsis* sp., *Process Biochem.* 46 (2011) 1934–1941. doi:10.1016/j.procbio.2011.06.024.
- [70] M. Mojaat, A. Foucault, J. Pruvost, J. Legrand, Optimal selection of organic solvents for biocompatible extraction of β -carotene from *Dunaliella salina*, *J. Biotechnol.* 133 (2008) 433–441. doi:10.1016/j.jbiotec.2007.11.003.
- [71] R. Halim, M.K. Danquah, P. a Webley, Extraction of oil from microalgae for biodiesel production: A review., *Biotechnol. Adv.* 30 (2012) 709–32. doi:10.1016/j.biotechadv.2012.01.001.
- [72] M. Vermu??, J. Sikkema, A. Verheul, R. Bakker, J. Tramper, Toxicity of homologous series of organic solvents for the gram???positive bacteria *Arthrobacter* and *Nocardia* Sp. and the gram???negative bacteria *Acinetobacter* and *Pseudomonas* Sp., *Biotechnol. Bioeng.* 42 (1993) 747–758. doi:10.1002/bit.260420610.
- [73] L. Marchal, M. Mojaat-Guemir, A. Foucault, J. Pruvost, Centrifugal partition extraction of β -carotene from *Dunaliella salina* for efficient and biocompatible recovery of metabolites., *Bioresour. Technol.* 134 (2013) 396–400. doi:10.1016/j.biortech.2013.02.019.
- [74] M.A. Hejazi, R.H. Wijffels, Milking of microalgae., *Trends Biotechnol.* 22 (2004) 189–94. doi:10.1016/j.tibtech.2004.02.009.
- [75] D.M.M. Kleinegris, M.A. van Es, M. Janssen, W.A. Brandenburg, R.H. Wijffels, Phase toxicity of dodecane on the microalga *Dunaliella salina*, *J. Appl. Phycol.* 23 (2011) 949–958. doi:10.1007/s10811-010-9615-6.
- [76] F. Zhang, L.-H. Cheng, X.-H. Xu, L. Zhang, H.-L. Chen, Application of memberane dispersion for enhanced lipid milking from *Botryococcus braunii* FACHB 357., *J. Biotechnol.* 165 (2013) 22–9. doi:10.1016/j.jbiotec.2013.02.010.
- [77] J. Wu, M.A. Alam, Y. Pan, D. Huang, Z. Wang, T. Wang, Enhanced extraction of lipids from microalgae with eco-friendly mixture of methanol and ethyl acetate for biodiesel production, *J. Taiwan Inst. Chem. Eng.* 71 (2017) 323–329. doi:10.1016/j.jtice.2016.12.039.
- [78] M. Chen, T. Liu, X. Chen, L. Chen, W. Zhang, J. Wang, L. Gao, Y. Chen, X. Peng, Subcritical co-solvents extraction of lipid from wet microalgae pastes of *Nannochloropsis* sp., *Eur. J. Lipid Sci. Technol.* 114 (2012) 205–212. doi:10.1002/ejlt.201100120.
- [79] Y. Li, F. Ghasemi Naghdi, S. Garg, T.C. Adarme-Vega, K.J. Thurecht, W.A. Ghafor, S. Tannock, P.M. Schenk, A comparative study: the impact of different lipid extraction methods on current microalgal lipid research., *Microb. Cell Fact.* 13 (2014) 14. doi:10.1186/1475-2859-13-14.
- [80] M. Goettel, C. Eing, C. Gusbeth, R. Straessner, W. Frey, Pulsed electric field assisted extraction of intracellular valuables from microalgae, *Algal Res.* 2 (2013) 401–408. doi:10.1016/j.algal.2013.07.004.
- [81] R. Straessner, A. Silve, C. Eing, S. Rocke, R. Wuestner, K. Leber, G. Mueller, W. Frey, Microalgae precipitation in treatment chambers during pulsed electric field (PEF) processing, *Innov. Food Sci. Emerg. Technol.* (2016). doi:10.1016/j.ifset.2016.07.008.
- [82] P. Bodénès, F. Lopes, D. Pareau, O. Français, B. Le Pioufle, Microdevice for studying the in situ permeabilization and characterization of *Chlamydomonas reinhardtii* in lipid accumulation phase, *Algal Res.* 16 (2016) 357–367. doi:10.1016/j.algal.2016.03.023.
- [83] R.J. Thompson, J.P. Davies, G. Mosig, ‘Dark-Lethality’ of Certain *Chlamydomonas reinhardtii* Strains Is Prevented by Dim Blue Light’, (1985) 903–907.
- [84] G. Saulis, M.S. Venslauskas, J. Naktinis, Kinetics of pore resealing in cell-membranes after electroporation, *Bioelectrochemistry Bioenerg.* 26 (1991) 1–13.
- [85] <http://www.int.laborundmore.com/archive/936206/From-fat-droplets-in-plant-cells-to-novel-foods.html>.

III1.Appendix III.1: Lipid production strategies in literature. List of viability related dyes, from [62]. Dyes can be classified according to their application: (1) permeability dyes, (2) membrane potential dyes, and (3) cellular enzyme activity dyes [62].

Permeability			
Dye	Target	Fluorescence	
		Excitation (nm)	Emission (nm)
DAPI	DNA	358 (UV)	461
Hoeschst 33342	DNA	536	617
PI (Propidium Iodide)	Nucleic acid content	536	617
PicoGreen	DNA	480	520
SYBR Green I	Nucleic acid content	497	520
SYTO 9	Nucleic acid content	483	503
SYTO 13	Nucleic acid content	488	509
SYTO RNaselect	RNA	490	530
SYTOX Green I (SG)	Nucleic acid content	504	523
SYTOX Green II	Nucleic acid content	504	523
Membrane potential			
CTC	Electron transport	450	630
DHR	ROS (Reactive Oxygen species)	505	534
DiOC6	Membrane potential, respiration rate	484	501
TMRM	Membrane potential and integrity	555	580
Cellular enzyme activity			
Calcein-AM	Non-specific esterase activity, membrane integrity	494	517
Carboxy-H ₂ DFFDA	ROS	478	519
CFDA-SE	Non-specific esterase activity	492	517
CMFDA	Non-specific esterase activity	485	538
ELF 97 - phosphate	Alkaline phosphatase activity	345	530
FDA (fluorescein diacetate)	Non-specific esterase activity	492	519
H ₂ DCFDA	ROS, respiration activity	505	535
HE (hydroethidine, dihydroethidium)	Peroxidase activity	510	595
Rhodamine 123	Mitochondrial membrane potential	507	529

III.2. Appendix III.2: Temperature profiles in the microdevice simulated in COMSOL

Pulse of 5 μ s, 620V (20 kV/cm)

A single 5 μ s pulse of 620V leads to a temperature elevation of 2°C on the edge of the electrode, dissipated in 100 ms.

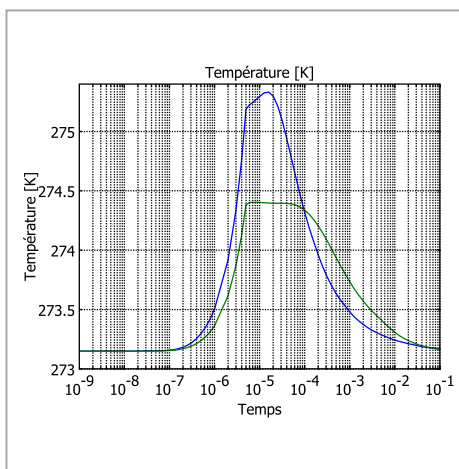


Figure 1: Evolution of the temperature (y, in °K) with time (x, in second) after a single pulse near the electrode (green) and at the center of the electroporation chamber (blue) LOG Scale.

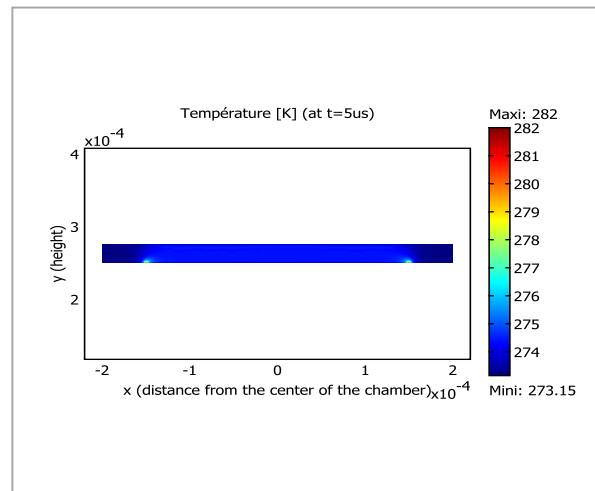


Figure 2: Mapping of the temperature distribution among the chamber (x, distance from the center of the chamber in m) after pulse application (5 μ s, 620 V). Temperature elevation of 2 °C near the electrodes)

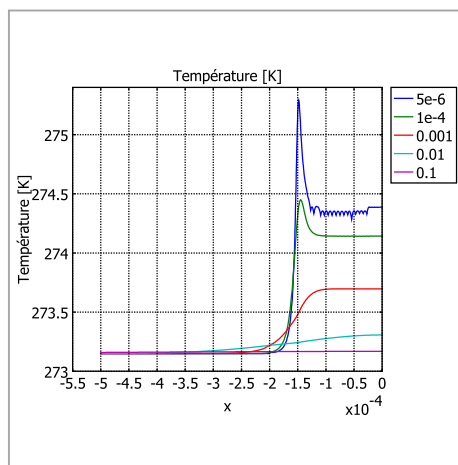


Figure 3: Temperature profile from the center of the chamber ($x=0$) to the electrode ($x=-1.5 \cdot 10^{-4}$) for $t = 5 \mu$ s , $t=10 \mu$ s, $t=1$ ms, $t=10$ ms, $t=0.1$ s. $E = 20$ kV/cm

Pulse of 500 μ s, 62V (2 kV/cm)

A single 500 μ s pulse of 62V leads to a progressive temperature elevation of 1°K homogeneous among the whole chamber at the end of the pulse, dissipated after 100 ms.

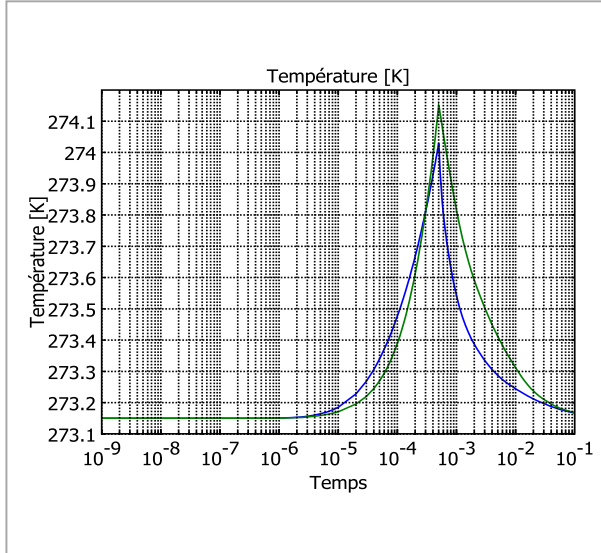


Figure 4: Evolution of the temperature (y, in °K) with time (x, in second) after a single pulse near the electrode (green) and at the center of the electroporation chamber (blue) LOG Scale.

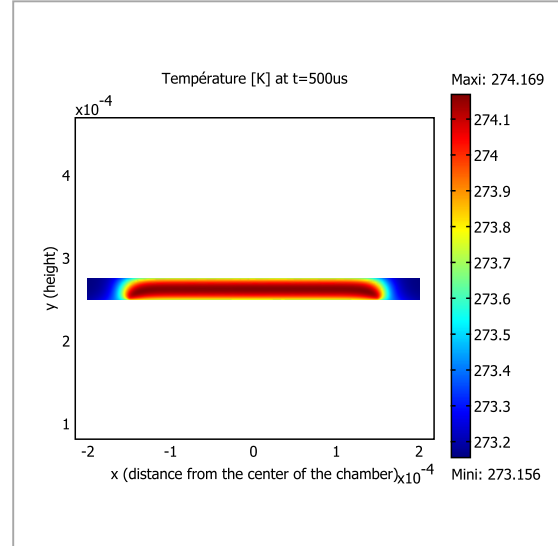


Figure 5: Mapping of the temperature distribution among the chamber (x, distance from the center of the chamber in m) after pulse application (500 μ s, 62 V). Temperature elevation of 1°C.

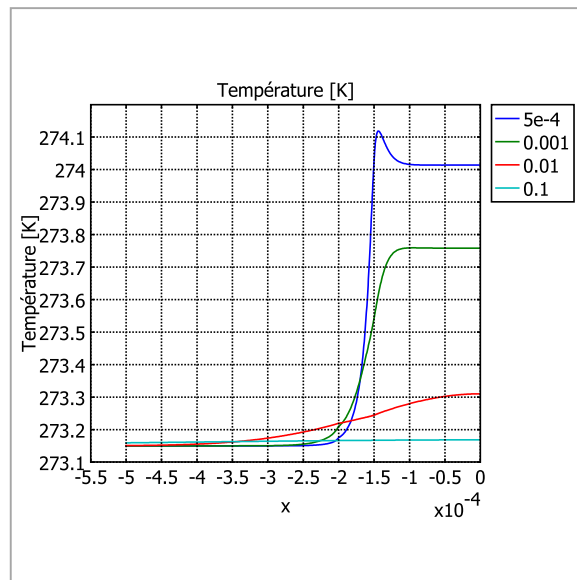


Figure 6: Temperature profile from the center of the chamber ($x=0$) to the electrode ($x=-1.5 \cdot 10^{-4}$) for $t = 5 \mu$ s , $t=10 \mu$ s, $t=1$ ms, $t=10$ ms, $t=0.1$ s. $E = 2$ kV/cm

III3.Appendix III.3: Calibration curves of triolein dissolved in hexane

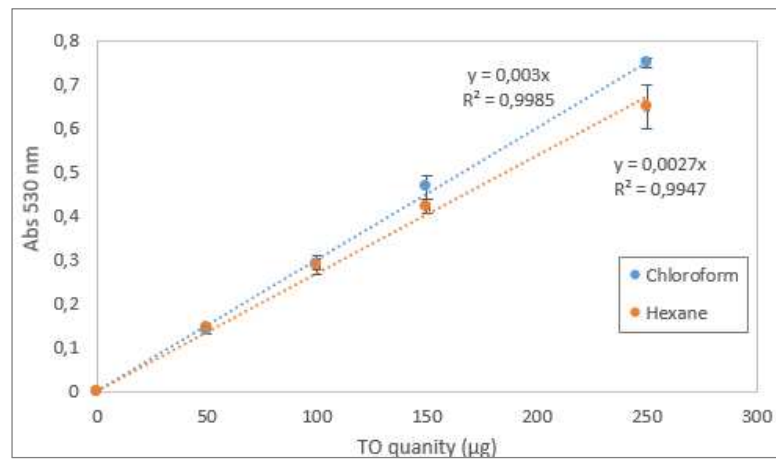


Figure 59 : Calibration curves of triolein dissolved in chloroform and hexane

Discussion

This work takes part in the research of innovative solutions which can be implemented to overcome the challenge of **producing biofuels with microalgae at a favorable energy efficiency**. Here, the effect of **Pulsed Electric Fields (PEF)**, which are already of primary interest in various domains such as oncology, biotechnology, food processes, **on microalgae cells and on lipid extraction** from these organisms is evaluated. Studies are first performed in a micro-system. This is required before upscaling the PEF process.

First, we chose a microalgae specie as a model to our study. Among various strains cultivated for this project, such as *Dunaliella Salina*, *Parachlorella Kessleri* and *Acutodesmus obliquus*, ***Chlamydomonas reinhardtii* wild type and its cell wall deficient mutant were finally chosen as the final candidates** for the following reasons: (i) **the high number of** data already existing in literature about this strain, (ii) *Chlamydomonas reinhardtii* is known to accumulate a **high lipid content** during stress, (iii) the cell has a **larger diameter in comparison with *Chlorella vulgaris*** (preliminary assays were performed with this specie). This increases its sensitivity to the electric field applied according to Schwan equation, (iv) **its relative circular shape which leads to a homogeneous effect** of the electric field on the cell and (v) this freshwater strain is cultivated in a relative **low conductivity medium** which limits the Joule effect of the PEF treatment. The only strong disadvantage of *Chlamydomonas reinhardtii* is its **motility** conferred by two flagella, which does not facilitate the observation of the cells during the treatment; motility is however highly reduced when the cells are in lipid accumulation conditions.

Concerning the cell culture, the system was kept as simple as possible. The batch cultures **required to rapidly fix a certain stress duration** to obtain reproducible lipid content in the cells subjected to PEF treatment. After visual observations and first analyses of lipid content with Bodipy by flow cytometry, **the stress duration of seven days was finally chosen.**

Concerning cell characterization, the evaluation of **lipid content** was however challenging in our conditions (very low amount of biomass) as the conventional methods of gravimetric quantification together with gas chromatography require a high sample volume. **We developed then a simple analytical method that uses low biomass amounts.**

The Bodipy staining of cells permits to localize the lipid droplet within the cytoplasm but is not adequate to quantify precisely. There are many interferences indeed; the application of PEF on algae cells before Bodipy staining increases the bodipy fluorescence intensity and the contact of algae with organic solvents also affects the results. **Finally, the colorimetric SPV method** was implemented showing a high robustness and a fast and simple protocol of analysis; in addition, this method can be applied on both raw algae solutions and solvent extracts. **The SPV response is however not specific to neutral lipids and GC analysis is then required to determine the exact composition of lipids accumulated. But the SPV method can be a precious tool for estimating the evolution of the cell lipid content. Additional correlations between SPV responses and fatty acid contents (determined by GC analysis) might be performed.**

Innovative, fast and accurate methods of lipid quantification are required. In this context, the determination of lipid content by 3D reconstruction of bodipy stained lipid droplets recorded by LCSM could be further studied. But a high quality software of deconvolution must be used and an automatic image processing method must be developed, as well as a cell fixation method.

Lipid and **cell wall staining** with bodipy and concanavalin respectively was used to record cell images before and after PEF or solvent treatments.

Cell viability/permeability were evaluated by microscopy and flow cytometry. These methods were first optimized. Manual counting of stained permeable cells in electroporation chambers, used in the first part of the project, is a very long process in comparison with analysis with flow cytometry. But the counted could be automated with image analysis software. In our case, flow cytometry was chosen to evaluate cell viability/permeability.

The interest of using an electroporation micro-device from the very beginning of the project was to **visualize *in situ* the phenomena at the cell scale**. This approach enabled to observe, for the first time, the coalescence of lipid droplets during PEF treatment. We also measured, in direct, the rapid penetration of the propidium iodide into permeabilized cells during/after PEF treatment. Reversibly permeabilized cells showed to be stained with PI, but still able to swim with their flagella. We also observed no effect on the cell wall due to PEF treatment, though, the cell walls deficient mutant of *Chlamydomonas reinhardtii* showed to be strongly affected by the PEF treatment: a complete destructuration of the cell is observed. Also, we observed in dedicated fluidic system the mixing of algae with solvent, showing the necessity of an efficient mixing system during lipid extraction. Following a single cell during PEF treatment was tested but rapidly replaced by the monitoring of several cells for two important reasons: (1) a very high disparity of the cells was observed: it seemed then be more relevant to observe a sample of several different cells which present variable sizes, lipid contents, cell wall sizes, etc... These differences are not important when considering the scale of the process but they are critical at the scale of cell engineering. (2) Secondly, the cell motility and mobility (due to hydrodynamics) strongly reduced the possibility to follow a single cell during the treatment with a high magnification objective. Most of the single cell monitoring studies found in literature are realized on adherent mammal cells.

The mobility of the cells is then a problem for their observation. A specific method was tested to fix the cells on glass coverslips for their observation during PEF; Poly-L-lysine was used but the adhesion obtained on *Chlorella vulgaris* (preliminary assays performed in this thesis) was inconclusive. The attachment of an algae cell may indeed greatly vary with the composition of the cell wall of the strain tested; the coating of a glass substrate with a thin layer of a gel containing proteins and sucrose could be tested in order to improve adhesion. Cell immobilization may also be necessary when using LCSM imaging to quantify the cell lipid content, as previously reported.

The contact of algae with solvent during PEF treatment was first tested in the electroporation system. However, the biphasic system (algae/water + organic solvent) requires a very efficient mixing in order to improve the transfer of lipids between both phases. **The process of associating electroporation and solvent mixing extraction may could also be miniaturized and is under consideration in our group.**

The work was performed with the goal of recycling algae cells after lipid extraction. **The optimal conditions to perform a reversible electroporation treatment were found in our study. However, in our first experiments, cells electroporated with low PEF energy (5 μ s, 7 kV/cm) did not exhibit a higher lipid extraction in comparison with non electroporated cells. This may be due to the absence of effect on the cell wall though the membrane is permeabilized. But more results must be obtained to confirm the hypothesis.**

In contrast, very energetic treatments leading to an important thermal effect in the electroporation chamber showed to improve lipid extraction by solvent, but the cell wall may be highly affected by temperature.

Anyway, we worked to combine other effects (like mechanical solicitations) with moderate PEF conditions to enhance solvent assisted extraction of lipids.

Assays performed with lower solvent volume (lower solvent to algae ratio) should be performed in cells subjected or not to PEF treatment. PEF may improve lipid extraction while reducing the solvent volume required for the extraction. Moreover, the process developed is also interesting regarding the energy consumption as extraction is performed on wet algae: water removal is not necessary, leading to high energy savings. The influence of other PEF parameters should be also have been investigated: pulse number, bipolar pulses, lower frequency, temperature in the electroporation cuvette (electroporation in ice...).

PEF treatment can be an interesting pre-treatment process before solvent extraction compared to other highly energy demanding processes that disrupt the cells and thus unease further downstream/purification processes. But, more experiments are required to confirm this statement.

PEF should be also used to extract high-valuable compounds from microalgae. The extraction of carotenoids such as astaxanthin in a pigment accumulating freshwater strain could also be tested: the measure of pigment content could be very easy using the flow cytometry, thanks to the pigment auto-fluorescence. Also, the market of natural pigments is very promising because of their high price (see Chapter 1).

Finally, this project had an important part of experimental work: set-up of the lipid accumulation device, optimization of several methods for cell characterization by flow cytometer and microscopy, set-up of a new Pulsed Electric Field generator, design and mounting of the electroporation set-up (reception of a new color camera, fabrication of connections...), choice of dye, development of staining protocols, development of SPV method, development of solvent extraction method, *etc...* The major part of this work was then devoted to design, install, optimize experimental devices and to develop characterization and analytical methods; without this preliminary but important work, no experiment could have been performed. Very interesting results were already obtained and many questions are raised. From now with these optimized tools it will be rather easy for future students and researchers to perform the necessary experiments to answer the questions raised by this study: **can we show that PEF improves solvent extraction at low energy expense?** Additional experiments are required. **What is the state of the algae after the extraction (membrane, enzymatic activity, cell wall, valorization of other compounds)?** Additional analyzes such as electronic microscopy, use of fluorescent dyes, and analysis of chemicals are required.

Titre : Etude de l'application de champs électriques pulsés sur des microalgues en vue de l'extraction de lipides neutres.

Mots clés : microalgues, biodiesel, champs électriques pulsés, microsystèmes

Résumé : Les microalgues, de par leur diversité, peuvent offrir une multiplicité de molécules bio-sourcées pour des applications variées (alimentation, énergie, santé *etc.*). Cependant, la production de biodiesel à partir de microalgues, désignée comme la 3^e génération de biocarburant, nécessite encore une optimisation lors de l'étape de culture de la biomasse ou lors de l'extraction de l'huile pour que le procédé soit énergétiquement viable. Parmi les voies d'amélioration, l'application de champs électriques pulsés (PEF) en prétraitement à la biomasse pourrait améliorer la rentabilité énergétique du procédé d'extraction de lipides.

Ce procédé appliqué aux microalgues est étudié dans le contexte d'une collaboration entre le laboratoire SATIE de l'ENS Cachan Paris Saclay et le laboratoire LGPM de Paris Saclay.

Un microsysteme d'électroporation a été conçu afin d'étudier *in situ* l'impact des champs électriques pulsés sur les cellules de microalgue, *Chlamydomonas reinhardtii* chargées en lipides.

Parmi les principaux résultats du projet, l'étude énergétique du procédé a montré que les impulsions de très courte durée (5 μ s) sont les moins énergivores. Associées à un champ électrique de 4.5 kV/cm, ces impulsions entraînent une perméabilisation réversible (80 % de cellules atteintes) de quelques secondes tandis qu'un champ de 7 kV/cm entraîne un effet irréversible. Après ce prétraitement, les algues sont ensuite mélangées à de l'hexane afin d'évaluer si les lipides sont extraits plus facilement de la cellule.

Title: Study of the application of pulsed electric fields (PEF) on microalgae for the extraction of neutral lipids.

Keywords: microalgae, biodiesel, PEF, micro-systems

Abstract: Microalgae offer a multiplicity of applications for the production of bio-sourced compounds such as proteins, pigments, sugar and oils. However, the energy spent for algae culture and lipid extraction hinder the energetic viability of the process for the production of biofuel derived from algae oils. Among possible improvements, pulsed electric fields (PEF) may be used as a pre-treatment to extract valuable compounds from microalgae and making the process less energy demanding.

This project started with a collaboration between the team of bio-micro-systems Biomis, laboratory SATIE, with the team of bio-process engineering laboratory LGPM to study *in situ* the effects of PEF on microalgae.

First, a energetic study is performed in a

micro-system specially built for this project to characterize *in situ*, the effect of various treatment parameters (pulse duration / electric field) on *Chlamydomonas reinhardtii* cells with high lipid content.

Among the outputs of this study, an energetic optimization of PEF conditions shows that a high level of permeability and low energy consumption are obtained when using short pulses of 5 μ s. Associated with an electric field of 4.5 kV/cm, the pores are reversible (80 % of the cells reached) during few seconds, and with a field of 7 kV/cm or higher, the permeabilization is irreversible. Afterwards, the pre-treatment is associated with solvent mixing (hexane) to evaluated if the lipid extraction is improved.